PHOTOIONIZATION OF DIATOMIC MOLECULES

by

J.L. Bahr B.Sc. (Hons.)

Department of Physics

A thesis
submitted for the degree of
Doctor of Philosophy
in the
University of Adelaide

January, 1970

CONTENTS

Chapter I. Review of Photoionization Processes

Chapter II. The Photoelectron Spectrometer

Chapter III. Partial Photoionization Cross-Sections

Chapter IV. Photoelectron Spectroscopy and Preionization in Nitrogen, Carbon Monoxide and Nitric Oxide

Chapter V. Photoelectron Spectroscopy for some Preionized States of Molecular Oxygen

SUMMARY

This thesis describes measurements of partial photoionization cross-sections for processes leading to the formation of particular ionic states. The partial cross-sections for nitric oxide and carbon monoxide as a function of the incident wavelength are presented. The effects of autoionization states of the neutral molecule on the photoelectron spectra of the gases molecular oxygen, molecular nitrogen, carbon monoxide and nitric oxide have been investigated and the results are discussed along with theoretical considerations of the mechanisms involved.

The partial photoionization cross-sections have been measured by recording the photoelectron energy spectra at 5Å intervals from 600Å to the first ionization potential with an incident beam resolution of 8Å. The photoelectron spectrometer used the retarding potential technique and was of quasi-spherical construction. It consisted of two concentric hemi-spherical grids about a "point" source of photoelectrons, a plane collecting grid and a channel-electron-multiplier as a detector. The best resolution obtainable from the spectrometer was 0.1eV (full width at half maximum) at an energy of 5eV. The light source consisted of a one-metre near normal incidence monochromator equipped with a helium capillary discharge lamp. The

relative area associated with each electronic state in a spectrum was measured and this was combined with the total photoionization cross-section data for the gas to produce the partial photoionization cross-sections for the various states at that particular wavelength.

The partial cross-sections of carbon monoxide show the thresholds for the $B^2\Sigma^+$ and $A^2\Pi$ states of CO^+, the $A^2\Pi$ continuum having a maximum just above threshold. In the wavelength region 580Å to 600Å structure was observed in the spectra which has been attributed to dissociation.

The thresholds of the $A^1\Pi$ and $a^3\Sigma^+$ states of NO^+ are evident in the partial photoionization cross-section curves for nitric oxide, and photoelectron groups corresponding to transitions to the $X^1\Sigma^+$ and $b^3\Pi$ states were resolved in spectra where they were energetically possible. Unresolved states were included in the analysis as combinations of states. The $b^3\Pi$ and $a^3\Sigma^+$ states contributed almost 50% of the cross-section between 600Å and 700Å, this value rising to a maximum of 70% at 740Å.

Photoelectron spectra have also been recorded for the gases molecular oxygen, molecular nitrogen, carbon monoxide and nitric oxide using an incident beam resolution of 1.6Å. These spectra have been recorded at wavelengths corresponding to autoionization resonances in the photoionization cross-section curve of each gas, and also at neighbouring off-resonance wavelengths. Marked differences in the intensity distribution of the vibrational states have been observed between the on and off-resonance spectra and between different on-resonance spectra. It has been possible to determine, at certain wavelengths, the contribution by the different vibrational states to the total photoionization cross-section. In some cases it has been possible to compare the results with theoretical calculations of Franck-Condon factors and thereby determine the internuclear equilibrium distance of some of the autoionization states of the molecule.

PREFACE

This thesis contains no material which has been accepted for the award of any other degree or diploma in any University. To the best of the author's knowledge and belief it contains no material previously published or written by another person, except where due reference is made in the text.

J.L. Bahr,

January, 1970.

ACKNOWLEDGEMENTS

The experiments described in this thesis were carried out in association with Dr. V. Kumar, Dr. A.J. Blake and Mr. J.L. Gardner. The author would like to thank them for their co-operation during this work.

Thanks are due to the Workshop and Technical Staff of the Physics Department for their assistance in the construction of the apparatus.

The author would like to thank most sincerely Dr. A.J. Blake and Professor J.H. Carver for their enthusiasm, help, and encouragement during the experiments and the writing of this thesis.

Finally, the author wishes to thank his supervisors, Dr. K.H. Lokan and Dr. D.G. McCoy for their guidance throughout the course of this work.

CHAPTER I

REVIEW OF PHOTOIONIZATION PROCESSES

I.1 Introduction

The interaction of photons with gases, especially in the ionization region, is important to the understanding of topics such as upper atmospheric aeronomy, astrophysics and plasma physics.

The photoionization of an atomic or molecular system occurs when a photon is absorbed by the system causing an electron to be ejected, consequently leaving the system in an ionic state. Since photoionization occurs over a continuous range of photon energies above the ionization potential of the system, information can be obtained about the discrete energy states of the atomic or molecular ion by measuring the cross-section for the photoionization process as a function of the incident wavelength.

The photoionization cross-sections for many atoms, and a few molecules, have been calculated theoretically. These calculations usually involve many approximations. Comparison of the theoretical calculations with the experimental measurements makes it possible to distinguish between the various approximations.

During the last two decades the photoionization of gases has been experimentally studied in some detail. The photoionization cross-sections for many gases have been measured as a function of the incident photon wavelength by several investigators (see reviews by WEISSLER 1956, SAMSON 1966, MARR 1967 and SCHOEN 1968). For molecular gases there is the added complication of dissociative ionization which has been investigated by identifying the dissociative products using a mass spectrometer, (HURZELER 1957, WEISSLER 1959, COMES 1964, DIBELER 1966-67 and SCHOEN 1968). Information about the nature of the photoionization process has also been gained by studying the threshold behaviour of the cross-section, (MORRISON 1962, VILLAREJO 1968).

The photoionization of the upper atmosphere by solar radiation makes an important contribution to the formation of the ionosphere (HINTEREGGER 1964), but although total photoionization cross-sections are sufficient to account for the production rates of the electrons in the ionosphere, their subsequent behaviour can only be predicted through a knowledge of the initial energy distribution (DALGARNO 1963). In order to predict the initial energy distribution of electrons in the ionosphere, the distribution of the photoionization cross-section of a gas among its ionic states must be known. The <u>partial</u> photoionization cross-sections of a gas are thus defined as the cross-sections corresponding to transitions to particular ionic states of the gas. As well as the initial ionospheric electron energy distribution, the partial cross-sections of a gas can be used to predict the intensity and spectral distribution of the fluorescent radiation emitted when ions in an excited state decay to a lower state (DALGARNO 1965).

Conversely, both the fluorescent decay of excited ions and the energy distribution of the ejected electrons are methods by which the partial photoionization cross-sections may be measured in the laboratory. Thus by measuring the spectral distribution of fluorescent radiation Judge and Weissler (JUDGE 1963, 1965, 1968) have been able to determine the number of ions produced in the higher of the two states involved in the transition, and hence the partial cross-section for this state.

The measurement of the energy distribution of photoelectrons (photoelectron spectroscopy), has been used to determine the relative probabilities for exciting various electronic and vibrational ionic states at 584 Å (21.21 eV) for many gases (AL-JOBOURY 1963, 1964, 1965, BAKER 1968, BERKOWITZ 1967, BRUNDLE 1969, COLLIN 1968, 1969, ELAND 1968, EDQVIST 1969, FROST 1965-1967, LEMPKA 1968, NATALIS 1968-1969, RADWAN 1966, SPOHR 1967, TURNER 1962-1966-1967-1968, PRICE 1968). Several of these groups have also extended their measurements to a few other wavelengths (304 Å, 736-744 Å, and 1048-1067 Å), but these do not of course give any information about the variation of the relative probabilities with the energy of the exciting photon.

Samson and Cairns (SAMSON 1968b) have used a photoelectron spectrometer to measure the partial photoionization cross-sections for the rare gases Ne, Ar, Kr and Xe from the $^2P_{\frac{1}{2}}$ ionization limit threshold to 400 Å. Schoen (SCHOEN 1964) has determined the partial cross-sections for three diatomic molecules (N_2, O_2, CO) at 22 discrete wavelengths in the region 500-700 Å by measuring the energies of the photoelectrons. Blake and Carver (BLAKE 1965-1967) have obtained partial photoionization cross-sections at 5 Å intervals in the continuous wavelength range from threshold to 600 Å for N_2, O_2 and H_2O by also using photoelectron spectroscopy.

Both molecular measurements were made at relatively poor resolution and thus may not have observed effects due to preionized levels which are evident in the total cross-section curves of many diatomic gases (see Section I.7). However, Schoen has reported that part of the excitation of vibrational states may have been due to preionization phenomena, and Blake and Carver have also reported anomalous structure in the spectra of O_2 at incident wavelengths above 680 Å which they have attributed to "fluorescent autoionization".

The object of the present work was to obtain partial photoionization cross-sections for the diatomic gases nitric oxide and carbon monoxide using a photoelectron spectrometer of higher resolution and greater sensitivity than previously used for determination of partial cross-sections for molecules. The photoelectron spectrometer was also used to investigate the variation of the electron energy spectrum in the neighbourhood of preionized regions for the gases oxygen, nitrogen, nitric oxide and carbon monoxide.

I.2 Diatomic molecules and their spectra.

The absorption of ultra-violet light by molecules leads to a considerably more complex reaction than does the similar case for atoms. For molecules, the interaction can lead to dissociation into neutral or ion fragments. As well as being competing processes, these reactions are further complicated by predissociation and preionization (Section I.7).

For diatomic molecules two additional modes of freedom which do not occur for atoms are possible, viz:

a) the atoms can vibrate relative to each other along the internuclear axis, and

b) the molecule can rotate about the axis passing through the centre of gravity and perpendicular to the internuclear axis.

The total energy of a diatomic molecule consists of the potential energy and kinetic energy of the electrons and the nuclei. Potential energy curves, such as those shown in Fig. I.1. for a hypothetical molecule M_2 show the variation with internuclear distance of the effective potential energy of the nuclei (i.e. the electronic energy plus the Coulomb energy of the nuclei). As the two atoms are separated so that $r \rightarrow \infty$ (dissociation) the potential energy tends to a constant value called the dissociation energy, D_o.

For diatomic molecules the potential energy for many

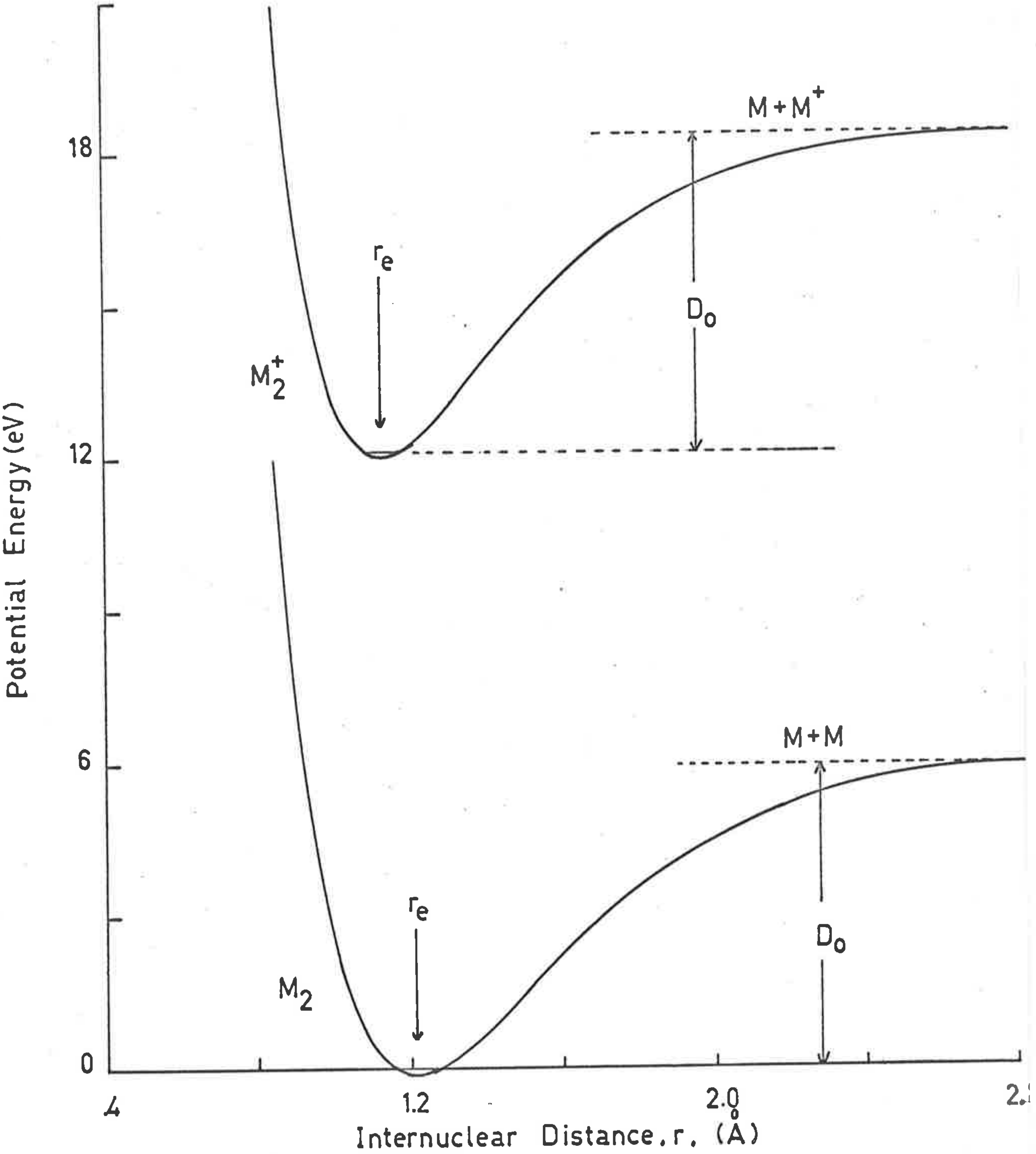

Fig.I.1. Morse potential curves for a hypothetical diatomic molecule M_2.

electronic states can be represented fairly accurately by the Morse potential function (MORSE 1929):

$$U(r) = D_e \, (1 - \exp(-\beta(r-r_e)))^2 \tag{1}$$

where r_e is the equilibrium internuclear distance and β is a constant. The curves of Fig. I.1. are examples of this potential function. Gilmore (GILMORE 1965) has reviewed the potential energy curves of several diatomic molecules, and the curves for some of the states of molecular oxygen given by him are shown in Fig. I.2.

I.2.1. Resolution of the total eigenfunction.

The Schrödinger equation for a diatomic molecule can be written (HERZBERG 1950):

$$\frac{1}{m} \sum_i \nabla_i^2 \Psi + \sum_j \frac{1}{M_j} \nabla_j^2 \Psi + \frac{8\pi^2}{h^2} (E-V)\Psi = 0 \tag{2}$$

where $\nabla_k^2 = \frac{\partial^2}{\partial x_k^2} + \frac{\partial^2}{\partial y_k^2} + \frac{\partial^2}{\partial z_k^2}$,

x_i, y_i, z_i are the coordinates of the electron of mass m, and x_j, y_j, z_j are the coordinates of the nuclei of mass M_j. Born and Oppenheimer (BORN 1927) have shown that for most cases Ψ can be resolved as:

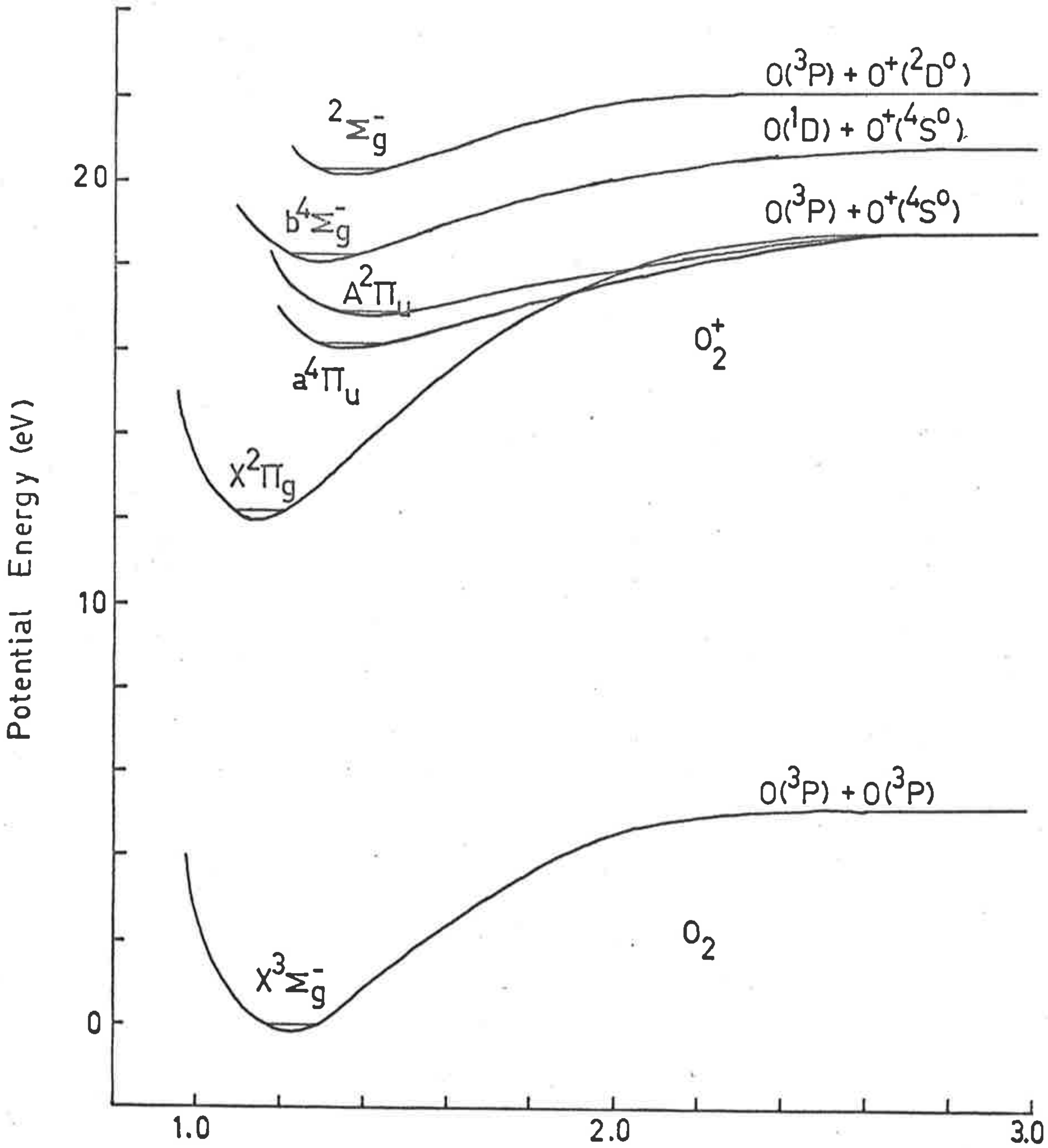

Fig. I.2. Potential energy curves for O_2 and O_2^+. (GILMORE 1965).

$$\Psi = \Psi_e\ (\ldots.x_i,y_i,z_i\ldots.).\ \ \Psi_{vr}\ (\ldots.\ x_j,y_j,z_j\ldots.) \tag{3}$$

where Ψ_e and Ψ_{vr} are the solutions to the equations

$$\frac{1}{m}\sum_i \nabla_i^2\Psi_e + \frac{8\pi^2}{h^2}\,(E_{el} - V_e)\,\Psi_e = 0 \tag{4}$$

and

$$\sum_i \frac{1}{M_j}\ \nabla_j^2\,\Psi_{vr} + \frac{8\pi^2}{h^2}\ (E - E_{el} - V_n)\,\Psi_{vr} = 0 \tag{5}$$

(4) represents the Schrödinger equation for the electrons moving in the field of the fixed nuclei with potential energy V_e and as r, the internuclear distance varies, V_e, and therefore the eigenfunctions Ψ_e and the eigenvalues E_{el}, also vary. (5) is the Schrödinger equation for the nuclei moving under the potential $(V_n + E_{el})$ where V_n is the Coulomb potential of the nuclei. Born and Oppenheimer have shown that (2) is only satisfied if

$$\sum_j \frac{2}{M_j}\quad \frac{\partial\Psi_e}{\partial x_j}\frac{\partial\Psi_{vr}}{\partial x_j} + \frac{\partial\Psi_e}{\partial y_j}\ \frac{\partial\Psi_{vr}}{\partial y_j} + \frac{\partial\Psi_e}{\partial z_j}\ \frac{\partial\Psi_{vr}}{\partial z_j} + \Psi_{vr}\ \nabla_j^2\ \Psi_e \tag{6}$$

can be neglected. This implies that the variation of Ψ_e with r is sufficiently slow that the differential terms in (6) can be ignored.

Thus the use of $(E_{el} + V_n)$ as the potential energy for the motion of the nuclei is justified and equation (3) is valid to the above approximation.

The eigenfunction of a vibrating rotator can be expressed as (SCHIFF 1955):

$$\Psi_{vr} = \frac{1}{r}.\Psi_v.\Psi_r \tag{7}$$

to a first approximation, where Ψ_v is the vibrational eigenfunction of a linear oscillator which depends only on the change in r and Ψ_r is the rotational eigenfunction depending only on the orientation of the molecule. Thus a good approximation to the total wavefunction of a diatomic molecule is given by:

$$\Psi = \Psi_e.\frac{1}{r}.\Psi_v.\Psi_r \tag{8}$$

I.2.2 Resolution of the total energy

The minimum value of the potential energy function $(E_{el} + V_n)$ of a given stable electronic state is usually considered as the electronic energy of the state and is symbolized by E_e. If the vibrational energy E_v and the rotational energy E_r are added to E_e, the total energy, E, of the molecule may be written as

$$E = E_e + E_v + E_r \tag{9}$$

This equation is usually expressed in wave-number units (the reciprocal of wavelength in cm^{-1}) and the quantities are called term values giving,

$$T = T_e + G + F \tag{10}$$

Using the model of the vibrating rotator (HERZBERG 1950),

$$G = \omega_e(v+\tfrac{1}{2}) - \omega_e x_e(v+\tfrac{1}{2})^2 + \omega_e y_e(v+\tfrac{1}{2})^3 + \ldots. \tag{11}$$

and

$$F = B_v J(J+1) - D_v J^2(J+1)^2 + \ldots. \tag{12}$$

ω_e, $\omega_e x_e$, and $\omega_e y_e$ are vibrational constants, B_v and D_v are rotational constants and v and J are respectively the vibrational and rotational quantum numbers. In general $F \ll G$ so that when considering vibrational transitions F can be neglected.

Thus two electronic states with their vibrational and rotational levels can be shown schematically as in Fig. I.3. The energy of a pure vibrational transition is typically about 0.1 eV and a rotational transition is characterized by an energy of about 0.001 eV.

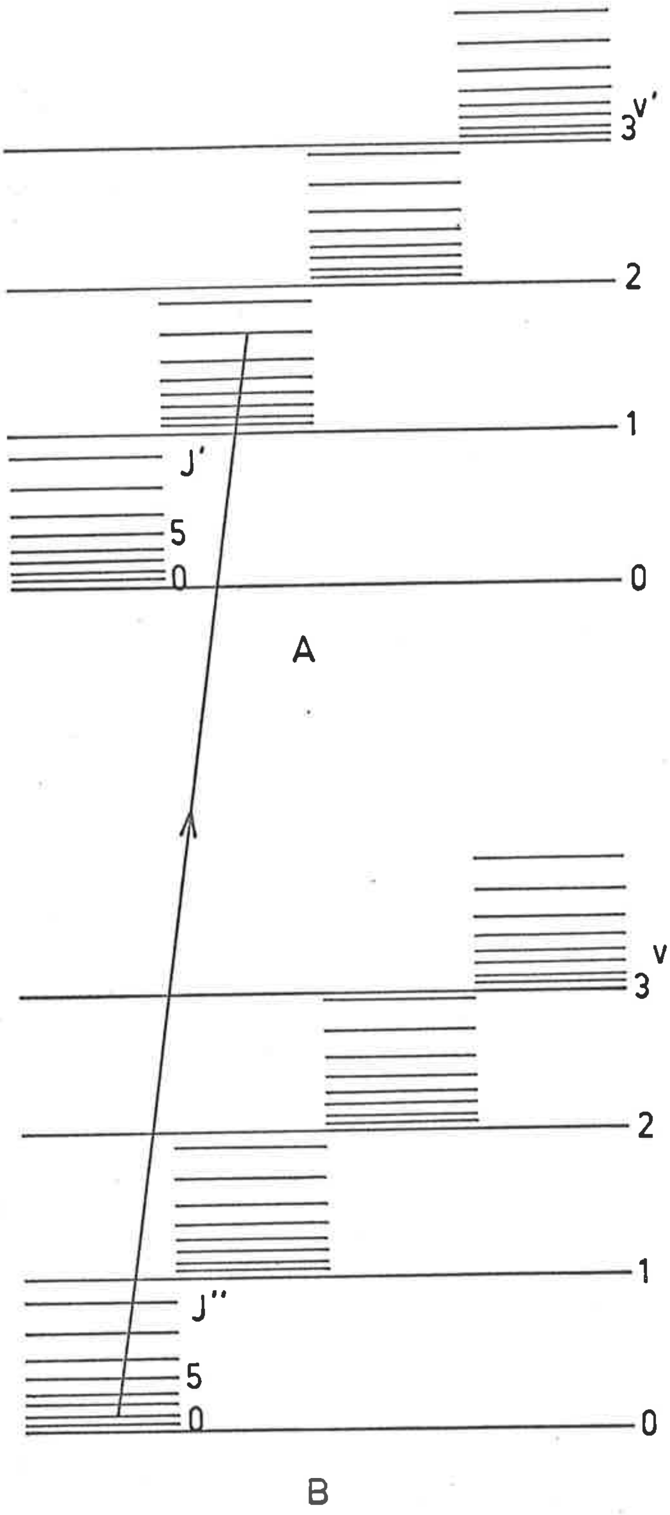

Fig.I.3. Vibrational and rotational levels of two electronic states A and B of a diatomic molecule (schematic), showing a typical vacuum ultraviolet transition.

I.2.3 The vibrational structure of electronic transitions.

For a transition between two electronic states the wave numbers of the spectral lines are given by

$$\nu = T'-T'' = (T_e'-T_e'') + (G'-G'') + (F'-F'') \tag{13}$$

where ' refers to the upper state and " to the lower state. Since F<<G, in considering the vibrational structure of the transitions the last term can be neglected and rotationless transitions ($F'=F''=0$) considered.

For a given electronic transition $(T_e'-T_e'')$ is constant and $(G'-G'')$ is the only variable, so that all possible transitions between the different vibrational levels of the two electronic states are represented by

$$\begin{aligned}\nu = (T_e'-T_e'') + \quad & \omega_e'(v'+\tfrac{1}{2})-\omega_e x_e'(v'+\tfrac{1}{2})^2+\omega_e y_e'(v'+\tfrac{1}{2})^3+ \ldots \\ - \quad & \omega_e''(v''+\tfrac{1}{2})-\omega_e x_e''(v''+\tfrac{1}{2})^2+\omega_e y_e''(v''+\tfrac{1}{2})^3+ \ldots\end{aligned} \tag{14}$$

For electronic transitions there is no strict selection rule for v (HERZBERG 1950) and so each v' can combine with each v" leading to a large number of bands in the spectrum. However, in photoabsorption at room temperature, in general, only a single v' progression (that with $v''=0$) need be considered. (Fig. I.4 shows a typical v' progression

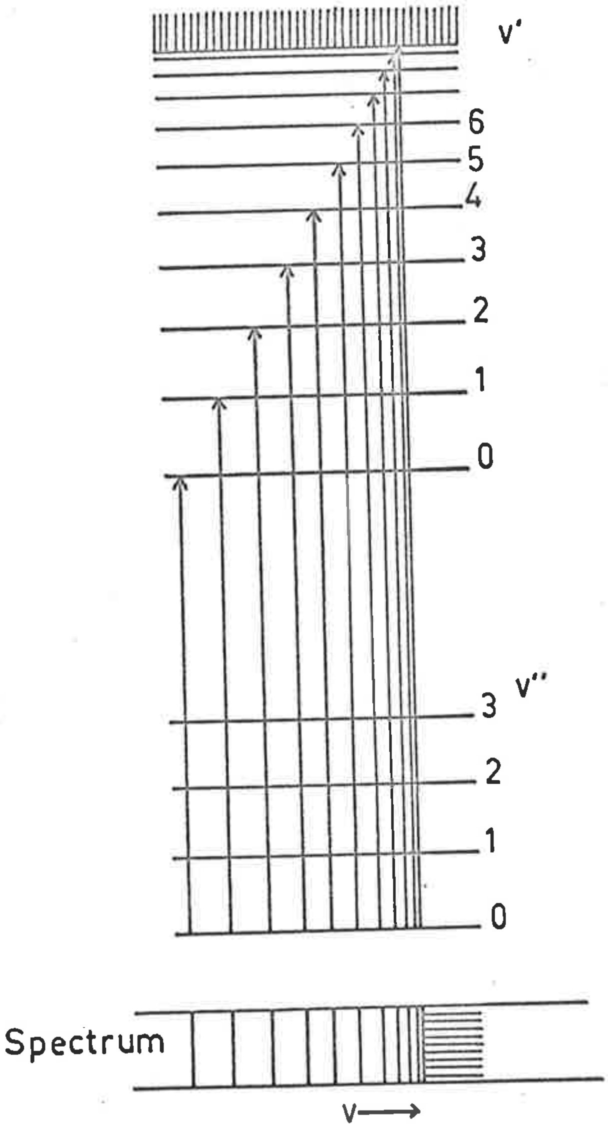

Fig.I.4. A typical v' progression (schematic) in a diatomic molecule.

(schematic)). The formula for all possible transitions thus reduces to

$$\nu = (T_e{}' - T_e{}'') + \omega_e{}'(v'+\tfrac{1}{2}) - \omega_e x_e{}'(v'+\tfrac{1}{2})^2 + \omega_e y_e{}'(v'+\tfrac{1}{2})^3 \;\ldots\; - \tfrac{1}{2}\omega_e{}'' + \tfrac{1}{4}\omega_e x_e{}'' - \tfrac{1}{8}\,\omega_e y_e{}'' \;\ldots \qquad (15)$$

I.2.4 The Franck-Condon Principle.

If a transition occurs in a diatomic molecule between the v=0 levels of two electronic states which have different equilibrium internuclear distances (r_e), the relative positions of the nuclei must change during the transition. According to the Franck-Condon principle (FRANCK 1925 and CONDON 1928) such a transition is unlikely to occur since electronic transitions take place so rapidly in comparison to the vibrational motion that immediately after the transition the nuclei have nearly the same relative position and velocity as before the transition. Thus the most probable transition is the one which is shown by the vertical line on the diagram in Fig.I.5; i.e. the transition is to the vibrational level closest to the point of intersection of the vertical line and the upper potential curve.

The intensity of a band depends on the following:

1) the probability of the electronic transition

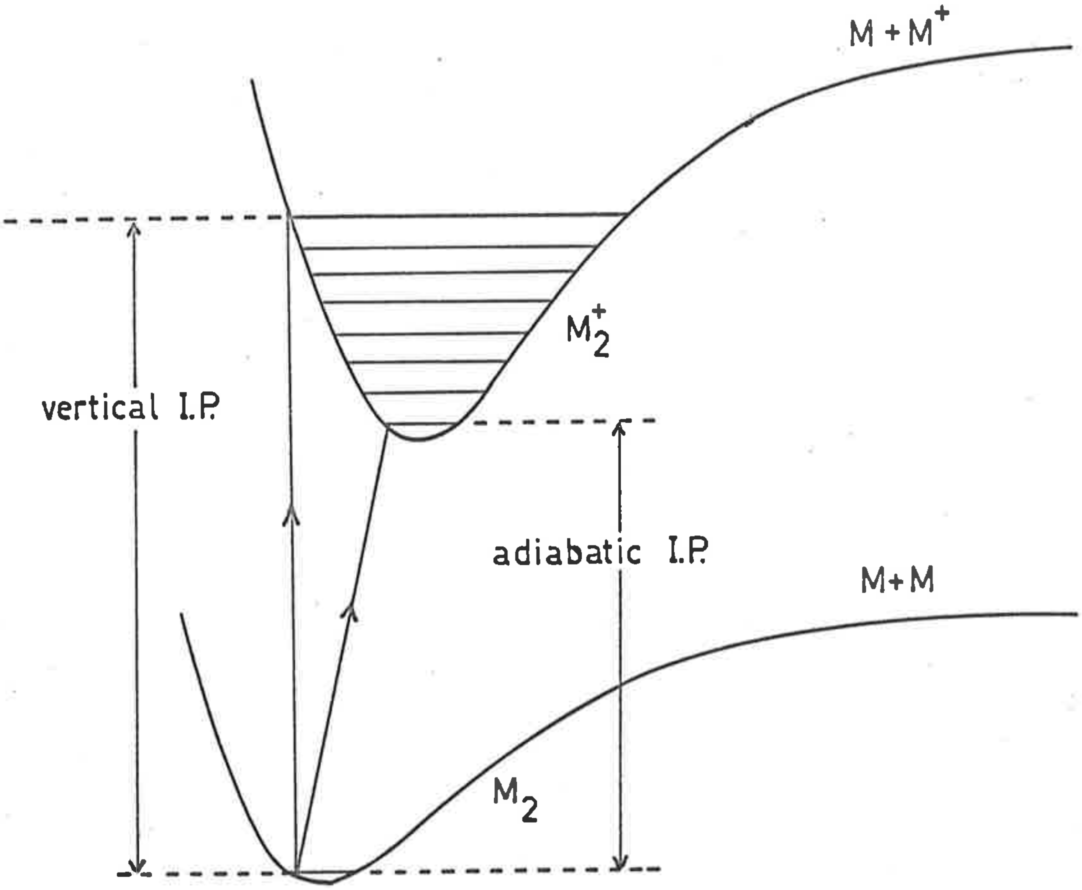

Fig.I.5. Potential energy diagram showing a vertical transition, and the vertical and adiabatic ionization potentials.

2) the vibrational intensity distribution and,

3) the population of molecules in the initial state.

Thus for absorption,

$$I_{v'v''} = I_o \frac{8\pi^3}{3hc} \Delta x \, N_{v''} \, \nu \, |R_{v'v''}|^2 \qquad (16)$$

where I_o and $I_{v'v''}$ are the incident and absorbed intensities, Δx is the absorption path length, $N_{v''}$ is the population of the lower state, ν is the wave-number of the incident light and $R_{v'v''}$ is the matrix element of the electronic dipole moment. Thus the probability of a transition between two states characterized by the total eigenfunctions ψ' and ψ'' is proportional to $|R_{v'v''}|^2$, and

$$R_{v'v''} = \int \psi'^{*} \, \underline{p} \psi'' \, d\tau \qquad (17)$$

where $\underline{p}$ is a vector with components $\sum e_i \underline{r}_i$. If Ψ is separated as in (8), and the integrated rotational wavefunctions which depend only on angular coordinates are ignored, then

$$\Psi = \Psi_e \cdot \Psi_{vr} \qquad (18)$$

and $\underline{p}$ is resolved into two components

$$\underline{p} = \underline{p}_e + \underline{p}_n \qquad (19)$$

where $\underline{p}_e$ depends on the electrons and $\underline{p}_n$ on the nuclei.
Since $\Psi_v^* = \Psi_v$

$$R_{v'v''} = \int \underline{p}_e \, \Psi_e'^* \, \Psi_v' \, \Psi_e'' \, \Psi_v'' \, d\tau + \int \underline{p}_n \, \Psi_e'^* \, \Psi_v' \, \Psi_e'' \, \Psi_v'' \, d\tau \tag{20}$$

Now $\underline{p}_n$ is independent of the electron coordinates and so the second term can be written

$$\int \underline{p}_n \, \Psi_v' \, \Psi_v'' \, d\tau_v \quad \int \Psi_e'^* \, \Psi_e'' \, d\tau_e$$

and

$$\int \Psi_e'^* \, \Psi_e'' \, d\tau_e = 0 \tag{21}$$

since electronic eigenfunctions belonging to different electronic states are orthogonal, and thus

$$R_{v'v''} = \int \Psi_v' \quad \Psi_v'' \, dr \int \underline{p}_e \Psi_e'^* \quad \Psi_e'' \, d\tau_e \tag{22}$$

as Ψ_v depends only on r.
The second term in (22)

$\underline{R}_e = \int \underline{p}_e \, \Psi_e'^* \, \Psi_e'' \, d\tau_e$ is called the electronic transition moment, and the Franck-Condon principle rests on the assumption that $\underline{R}_e$ varies slowly with r and can be replaced by $\bar{\underline{R}}_e$, an average value for all the bands. Thus

$$R_{v'v''} = \overline{R}_e \int \Psi'_v \, \Psi''_v \, dr \tag{23}$$

and

$$q_{v'v''} = \left[\int \Psi'_v \, \Psi''_v \, dr \right]^2 \tag{24}$$

is called the square of the "overlap integral", or the Franck-Condon factor for the transition.

Therefore the most probable transition is the one which corresponds to two states whose eigenfunctions have the maximum "overlap". The calculation of $q_{v'v''}$ values therefore gives an estimate of the distribution of intensity among the vibrational levels.

Franck-Condon factors have been calculated for many diatomic molecules, usually by employing the Morse potential function and its wavefunctions (MORSE 1929) to calculate the overlap integral. More recently, numerical methods have been used to obtain more accurate potential curves and wavefunctions (ZARE 1963, SHARMA 1967, GARDNER 1969).

In chapter V of the present work, Franck-Condon factors have been calculated, using a Morse potential, for transitions from pre-ionized states to an ionic state in molecular oxygen.

I.3 Calculation of photoionization cross-sections.

Until recently, theoretical work on photoionization has been limited to atoms or at the most to quasi-atomic systems such as H_2^+ (BATES 1953) and CH_4 (DALGARNO 1952). The calculation of photoionization cross-sections has been reviewed by Ditchburn and Opik (DITCHBURN 1962), Marr (MARR 1967) and Stewart (STEWART 1967).

I.3.1 General considerations.

Above the ionization threshold absorption of a photon leads to a final state which lies in the continuum, and thus the photoionization cross-section is continuously variable with the wavelength of the incident light. Generally, the photoionization cross-section is given by:

$$\sigma(\nu) = \frac{8\pi^3\nu e^2}{3cw_i} \quad |R^L_{if}|^2 \tag{25}$$

where ν is the photon frequency and w_i is the statistical weight of the initial bound state of the system. R^L_{if} is the dipole length matrix element defined by:

$$|R^L_{if}|^2 = \sum_i \sum_f \left| \int \Psi^*_f \sum_k r_k \Psi_i \, d\tau \right|^2 \tag{26}$$

where Ψ_i and Ψ_f are the initial and final state wave functions of the system and r_k is the position of the k^{th} electron. The integration is over the configuration space of all the electrons and includes summation over the spin coordinates. The Ψ_i are, as usual, normalised to unity, but the Ψ_f being continuous are normalised to

$$\int \Psi_f^*(\varepsilon') \, \Psi_f(\varepsilon) \, d\tau = \delta(\varepsilon - \varepsilon') \tag{27}$$

where ε is the kinetic energy of the electron in the continuum and δ is the Dirac delta function. To obtain the total cross-section the equation must be summed over all possible values of l and m for the electron.

The dipole length matrix element

$$R_{if}^{L} = \int \Psi_f^* \left(\sum_k r_k\right) \Psi_i \, d\tau \tag{28}$$

may also be formulated as the dipole velocity and dipole acceleration matrix elements respectively:

$$R_{if}^{V} = \frac{\hbar^2}{mE} \int \Psi_f^* \left(\sum_k \nabla_k\right) \Psi_i \, d\tau \tag{29}$$

and

$$R_{if}^{A} = \frac{\hbar^2}{mE^2} \int \Psi_f^* \left(\sum_k \nabla_k V\right) \Psi_i \, d\tau \tag{30}$$

where if Z is the nuclear charge

$$\sum_k \nabla_k V = \sum_k \frac{Z}{r_k^2} \tag{31}$$

If the wave functions Ψ_i and Ψ_f are exact, the three forms are exactly equivalent, but in practice they are different because they depend on different parts of the radial wavefunction. Thus approximations to the wavefunctions which are based on one-electron orbitals are expected to create differences, (STEWART 1954) and the quality of agreement between cross-sections calculated using the three forms indicates the accuracy of the wavefunctions used (COOPER 1962).

I.3.2 Approximations to the Wavefunctions.

For the hydrogen atom, and for a few hydrogen-like ions, the initial and final state wavefunctions can be obtained explicitly and hence the matrix elements can be exactly calculated (GORDON 1929, BETHE 1957). For non-hydrogen-like systems the equation for the wavefunctions required in the calculations of photoionization cross-sections cannot be solved, thus approximations to the wavefunctions must be made.

Most simple calculations are based on the central field approximation (BATES 1946) where the electrons are considered to move in a central potential. Other approximations have been devised. The separable wavefunction approximation assumes that each electron moves in a stationary state in the field due to the nucleus and the other electrons, so that the wavefunctions can be separated and the approximation expressed as a product of one-electron orbitals of the various electrons.

More sophisticated wavefunctions have been obtained by allowing for the correlation between the active electron and the other electrons (core polarization) e.g. (BATES 1943). The central potential can also be modified by using semi-empirical methods, such as the quantum defect method (BURGESS 1960, PEACH 1962). This method allows the radial wavefunctions for large r to be obtained without knowledge of the form of the potential for small r values.

I.3.3 Atomic photoionization cross-sections.

Samson and Marr (SAMSON 1966, MARR 1967) have recently reviewed atomic photoionization cross-sections. A number of atomic systems have been investigated experimentally and some of the results agree well with the theoretical values (e.g. helium). In many cases experimental data are unavailable and the theoretical values must be relied upon.

For the rare gases, although detailed gaps still exist, an almost complete picture of the continuum absorption of these gases is available. The alkali elements have only been studied experimentally down to 1000 Å but are being extended progressively below this wavelength (SAMSON 1966).

The cross-sections of atomic nitrogen, oxygen and hydrogen are of considerable importance to ionospheric physics (DALGARNO 1963). There are many experimental difficulties in these measurements because the atomic gases must be first isolated from the "parent" molecule by dissociation in order to measure their cross-section. Approximate values can be obtained in the soft X-ray region by considering the molecule to be equivalent to two atoms. In this way atomic cross-sections have been estimated from the molecular data from 0.01-68 Å and 200-500 Å.

I.3.4 Molecular photoionization cross-sections.

Calculations of theoretical cross-sections for molecules present much more difficult problems than do calculations for atomic systems. The main difficulty has been the lack of accurate one-electron wavefunctions for bound and free molecular orbitals, except for the H_2^+ ion.

Bates, Opik and Poots (BATES 1953) have calculated the photoionization cross-section for H_2^+ using numerically solved electronic wavefunctions. There are no experimental results for H_2^+ which can be compared with these calculations.

Dalgarno (DALGARNO 1952) has calculated the approximate photoionization cross-section for CH_4. The molecule was reduced to a "quasi-atomic" system by considering the motion of the electrons and protons of the H atoms in the tetrahedral CH_4 structure to be averaged, thus giving a central potential. This method gave results which are in reasonable agreement with the experimental results of Cook et al (COOK 1965) and Ditchburn (DITCHBURN 1955); see Fig. I.6.

H_2 has been investigated by two methods. Shimizu (SHIMIZU 1960) represented the orbital of the ejected electron by a plane wave

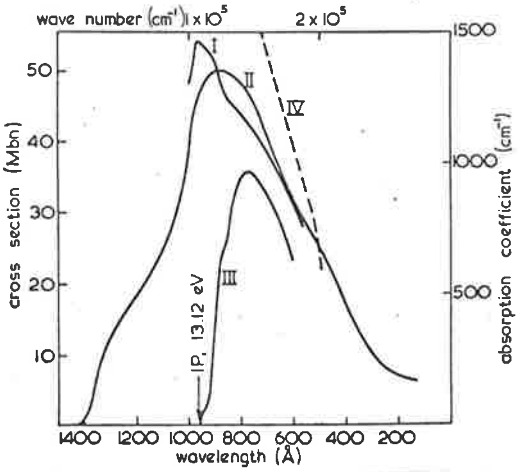

Fig.I.6. Absorption cross-section curves for methane. I - COOK 1965 - total absorption; II - DITCHBURN 1955 and RUSTGI 1964 - total absorption; III - COOK 1965 - photoionization; IV - DALGARNO - 1952 - theory.

and assumed that the nuclei were fixed at their equilibrium positions. In this way the ratio of the concentrations of H^+ and H_2^+ produced from the photon-molecule reaction was determined, but no absolute cross-section values were obtained.

In a more refined calculation, Flannery and Opik (FLANNERY 1965) used the bound state wavefunctions of Weinbaum (WEINBAUM 1933) and took the final state of H_2^+ to consist of the $1s\sigma_g$ ground electronic state and a free electron moving in a field which incorporated an ionic quadrupole moment contribution. Their results agreed very well with the experimental results of Cook et al (COOK 1965) and Wainfain (WAINFAIN 1955). At a photon wavelength of 700 Å the total photoionization cross-section, representing the sum of the cross-sections due to 12 vibrational levels, was calculated to be 11.474 Mbn. ($1\text{Mbn} = 10^{-18}\ \text{cm}^2$). The experimental value is 10.05 Mbn (COOK 1965).

More recently Tuckwell (TUCKWELL 1969) has calculated the photoionization cross-sections for the diatomic gases N_2 and O_2 from 50 Å to threshold. Approximate methods were used for both the initial and final states; S.C.F.-L.C.A.O.-M.O.* wavefunctions were used for the initial state, and Flannery and Opik's H_2^+ model for the final state wavefunctions. The vibrational eigenstates were included in the

---

* Self-Consistent-Field -- Linear-Combination-of-Atomic-Orbitals -- Molecular-Orbital.

calculations by making use of the Franck-Condon principle (see Sec. I. 2.4) which was found to be valid to a few percent.

The calculated partial cross-sections for the $1\pi_g$, $1\pi_u$ and $3\sigma_g$ (see HERZBERG 1950 for nomenclature of molecular states and orbitals) electrons of N_2 and O_2 were in fair agreement with the experimental values of Blake and Carver (BLAKE 1967). The values for theory and experiment for the total cross-section are compared in Fig. I.7 for O_2. The agreement was very good near threshold for the transitions to O_2^+ ($X^2\Pi_g$, $b^4\Sigma_g^-$) and N_2^+ ($A^2\Pi_u$), fair for the transition to N_2^+ ($X^2\Sigma_g^+$) and uncertain due to insufficient experimental data for O_2^+ ($^2\Sigma_g^-$). The calculated values for the transitions to O_2^+ ($a^4\Pi_u$, $A^2\Pi_u$) were somewhat lower than the experimental values.

The model, however, was found to be unsatisfactory for $2\sigma_u$ and $2\sigma_g$ electrons in N_2 and O_2, the failure being most probably due to the form of the final state wavefunctions. It has been suggested (TUCKWELL 1969) that the inner electrons that are not ejected may have a repulsive effect on the free electron, therefore diminishing the continuum waves in the region where the initial bound state functions for $2\sigma_u$ and $2\sigma_g$ are appreciable. This effect would lower the values of the transition integrals and hence the cross-section for these orbitals.

For the heteronuclear molecule NO, only the transition to the ground state of NO^+ ($X^1\Sigma^+$) was investigated. An approximate

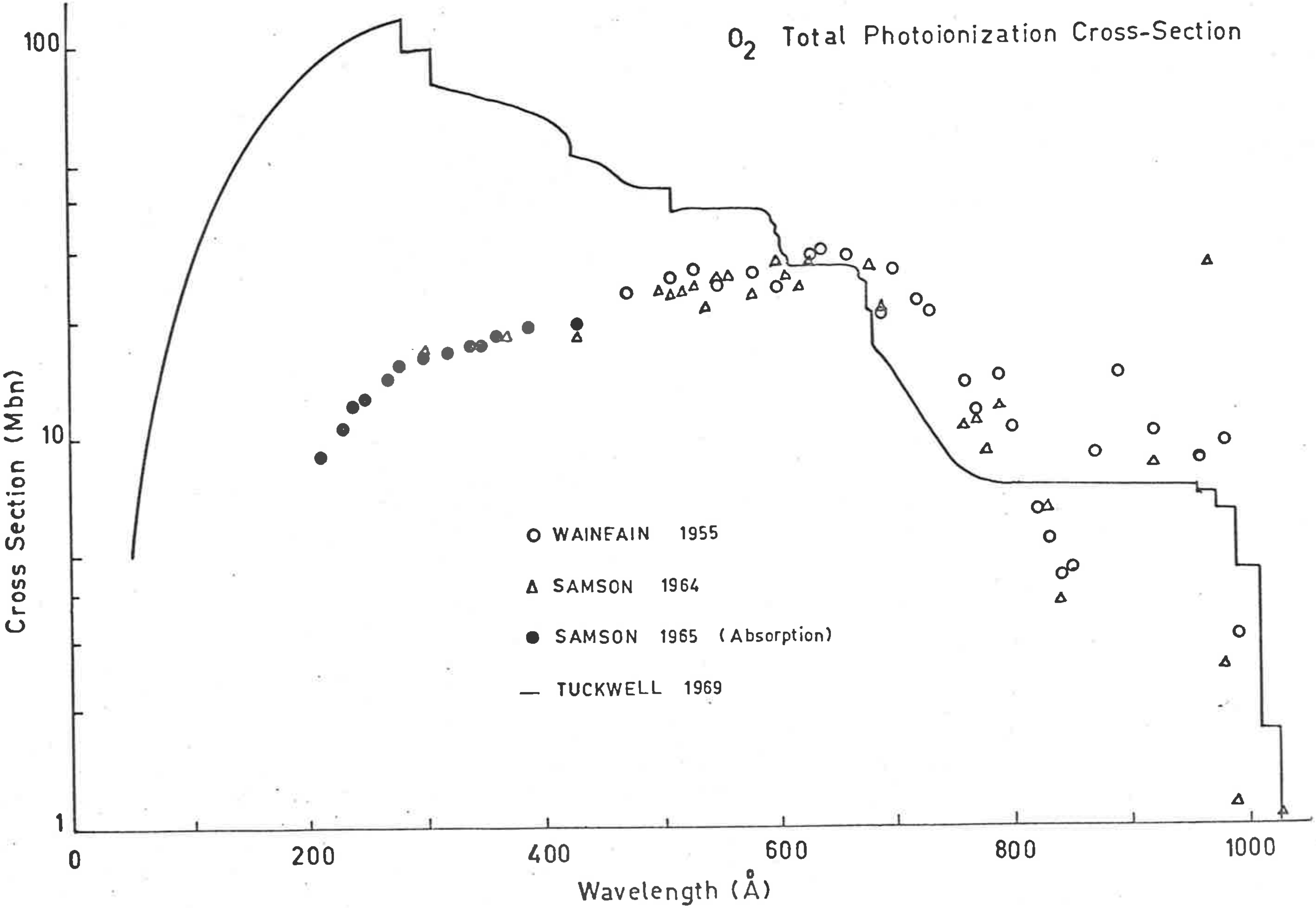

O_2 Total Photoionization Cross-Section
Cross Section (Mbn)
100
10
1
0
200
400
600
800
1000
Wavelength (Å)
○ WAINFAIN 1955
△ SAMSON 1964
● SAMSON 1965 (Absorption)
— TUCKWELL 1969

Fig. I.7.

treatment was used whereby the NO molecule was replaced by a homonuclear molecule composed of two atoms whose properties were the "average" of the properties of N and O.

I.4 Molecular ionization potentials.

The ionization potentials of an atomic gas are usually relatively easy to measure since Rydberg series are generally found which converge to a limit which constitutes the "edge" of the ionization continuum. However, in molecular spectra only a few Rydberg series have been found.

Another method for determining molecular ionization potentials is by varying the incident photon wavelength and detecting the onset of ionization by measuring the ion current. Observations of this onset as the wavelength varies are prone to difficulties caused by Franck-Condon distribution effects. There is often considerable difficulty in relating the measurement to a particular vibrational transition in the molecule, since the maximum in the related Franck-Condon distribution may occur at a high vibrational level of the upper state. Thus if the equilibrium internuclear distances of the two electronic states are very different there will be a difference between the "vertical" and "adiabatic" ionization potentials (see Fig. I.5). Therefore in using the total cross-section method for finding the ionization potential the shape of the curve near threshold is of great importance. Hurzeler and Morrison (HURZELER 1957) attempted to improve the measurements by taking the first derivative of the photoionization cross-section curve near its threshold and using this as the probability distribution among the vibrational levels. The vertical ionization potential could then be associated with the peak of the distribution and the adiabatic ionization potential with the sharp cutoff in the distribution. Nevertheless, the most reliable values are obtained via this method when the vertical and adiabatic ionization potentials are nearly the same.

I.4.1 Ionization potentials by photoelectron spectroscopy.

More recently, ionization potentials have been measured using photoelectron spectroscopy, where, for a given incident photon energy, the energies of the ejected photoelectrons are analysed. Providing that the vibrational levels of an ionic state can be resolved sufficiently, the vertical and adiabatic ionization potentials can be found readily to an accuracy of 0.005 eV. (EDQVIST 1969). Fig. I.8 shows an example of the photoelectron spectrum of molecular oxygen using an incident beam energy of 21.21 eV (584 Å) (TURNER 1968b). The vibrational levels of the states are clearly resolved in this spectrum and the adiabatic ionization potential can be associated with the $v' = 0$ level of each state by reference to the energy scale of the electrons. Similarly the vertical ionization potential can be taken to be at the v' level which has the maximum probability in the distribution of each electronic state. Thus for the ground state of

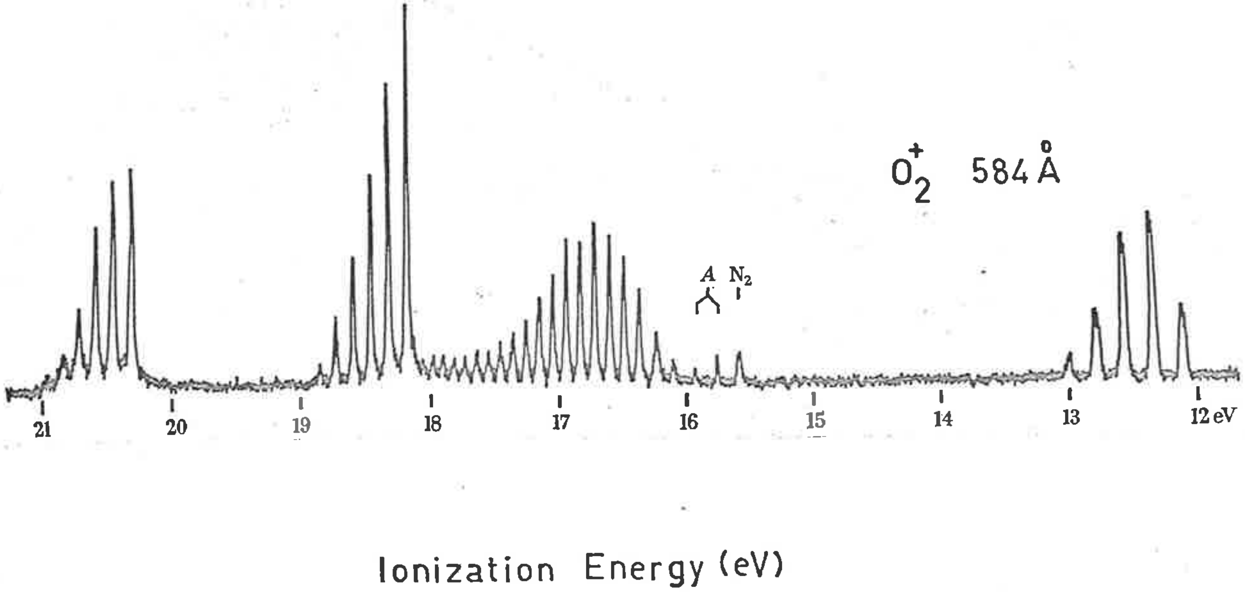

Fig. I. 8. Photoelectron spectrum from molecular oxygen at 584 Å (TURNER 1968).

O_2^+ ($X^2\Pi_g$) the adiabatic potential is 12.07 eV (v' = 0) and the vertical ionization potential is 12.31 eV (v' = 1).

Most of the work using photoelectron spectroscopy which has been done over the last few years has been in determining the ionization potentials of molecules. Table I.1 shows a comparison of adiabatic ionization potentials for the gases oxygen and nitrogen as obtained by several groups using photoelectron spectroscopy.

TABLE I.1a

IONIZATION POTENTIALS OF O_2 (eV)

Ionic State	v'	(Collin 1969)	(Vroom 1966)	(Turner 1966)	
$X^2\Pi_g$	0	12.075	12.08	(12.07*)	12.08
	1	12.31	12.31		12.32
	2	12.54	12.54		12.54
	3	12.75	12.76		12.73
	4	12.96	12.97		-
$a^4\Pi_u$	0	16.11			16.12
	1	16.23			16.26
	2	16.35			16.37
	3	16.47			16.49
	4	16.58			16.60
	5	16.69			16.72
	6	16.80			16.83
	7	16.90			16.93
	8	17.00			17.04

TABLE I.1a (cont)

IONIZATION POTENTIALS OF O_2 (eV)

Ionic State	v'	(Collin 1969)	(Vroom 1966)	(Turner 1966)
	9	17.10		17.14
	10	17.19		17.23
	11	17.29		17.33
	12	17.39		17.43
	13	17.49		-
$b^4\Sigma_g^-$	0	18.19		18.17
	1	18.33		18.33
	2	18.46		18.45
	3	18.59		18.58
	4	18.71		18.71
$^2\Sigma_g^-$	0	20.33		20.29
	1	20.47		20.42
	2	20.60		20.55
	3	20.72		20.67
	4	20.84		20.78
	5	20.95		20.88
	6	-		20.96

* Turner 1968b.

TABLE I.1b (cont)

IONIZATION POTENTIALS FOR N_2 (eV)

Ionic State	v'	(Collin 1969)	(Vroom 1966)	(Turner 1966)
$X^2\Sigma_g^+$	0	15.61	15.58	15.59

TABLE I.1b (cont)

IONIZATION POTENTIALS FOR N_2 (eV)

Ionic State	v'	(Collin 1969)	(Vroom 1966)	(Turner 1966)
	1	15.88	15.91	-
	2	16.13	-	-
	3	16.39	-	-
$A^2\Pi_u$	0	16.73	16.70	16.73
	1	16.96	16.93	16.96
	2	17.18	17.16	17.19
	3	17.40	17.38	17.41
	4	17.61	17.59	17.61
	5	17.81	17.79	17.82
	6	18.00	17.98	18.02
$B^2\Sigma_u^+$	0	18.81	18.80	18.78
	1	19.11	-	19.05
	2	19.36	-	-
	3	19.62	-	-

I.5 Partial photoionization cross-sections.

If, in a photon-gas reaction, the energy of the absorbed photon is sufficient, the residual ion may be left in any one of a number of final states, the energy balance being determined by the kinetic energy of the emitted electron. For a molecular gas there is the additional complication of dissociative ionization.

The partial photoionization cross-sections of a gas are defined (Sec. I.1) as the cross-sections for transitions to a particular ionic state of the gas. Judge and Weissler (JUDGE 1963, 1968) succeeded in dispersing the fluorescent radiation from O_2, N_2 and CO, and have calculated, from these results, the cross-section for the transition $N_2(X^1\Sigma_g^+, v''=0) \rightarrow N_2^+(B^2\Sigma_u^+, v'=0,1)$ in the region 550-650 Å. However, the technique of using fluorescent radiation as a means of determining partial cross-sections suffers from the disadvantage of being experimentally difficult owing to the low light intensities, the presence of metastable states, and the inability to measure the number of ions which are formed in the ground ionic state.

Photoelectron spectroscopy has been used as a means of determining partial cross-sections by observing the competition between the various electron groups as a function of the incident photon energy. The energy of the final ionic state is in each case uniquely determined by the difference between the incident photon energy and the electron energy and thus the relative transition probabilities to the ionic states can be determined.

Various workers have recorded photoelectron energy spectra for numerous gases at the incident wavelengths of 584 Å and 736-744 Å (Sec. I.1) but these results do not give any detailed information about the variation of the relative transition probabilities, and hence the partial cross-sections, with the incident photon energy.

A few groups (VILESOV 1961, SCHOEN 1964, BLAKE 1967, SAMSON 1968b) have extended the measurements to other wavelengths. The partial photoionization cross-sections for the rare gases Ne, Ar, Kr, and Xe have been measured by Samson and Cairns from the $^2P_{\frac{1}{2}}$ ionization limit to 400 Å. The ratio of the number of ions produced in the ground $^2P_{\frac{3}{2}}$ state to the number produced in the excited $^2P_{\frac{1}{2}}$ state was found to be constant with respect to wavelength with the values 2.18, 1.98, 1.79, and 1.60 for Ne, Ar, Kr, and Xe respectively. They also measured the partial cross-section for the formation of s electrons in Ar, Kr, and Xe.

Schoen used as a light source the emission lines from gas discharges to measure the partial cross-sections of O_2, N_2 and CO at ∿22 wavelengths. Blake and Carver used a helium continuum light source and were able to measure the partial cross-sections for the gases O_2, N_2 and H_2O as a function of the incident wavelength from 584 Å to the threshold of the first excited ionic state. In Fig. I.9 the partial photoionization cross-sections for N_2 by Doolittle and Schoen (SCHOEN 1968), Weissler and Judge (JUDGE 1968) and Blake and Carver are compared. While Doolittle and Schoen's results cover a greater range of wavelengths than those of Blake and Carver, the latter's contain more detail in the 640-700 Å range. It is interesting to note that even though Doolittle and Schoen's results are normalised to the total cross-sections of Samson and Cairns (SAMSON 1964c) and Blake and Carver's

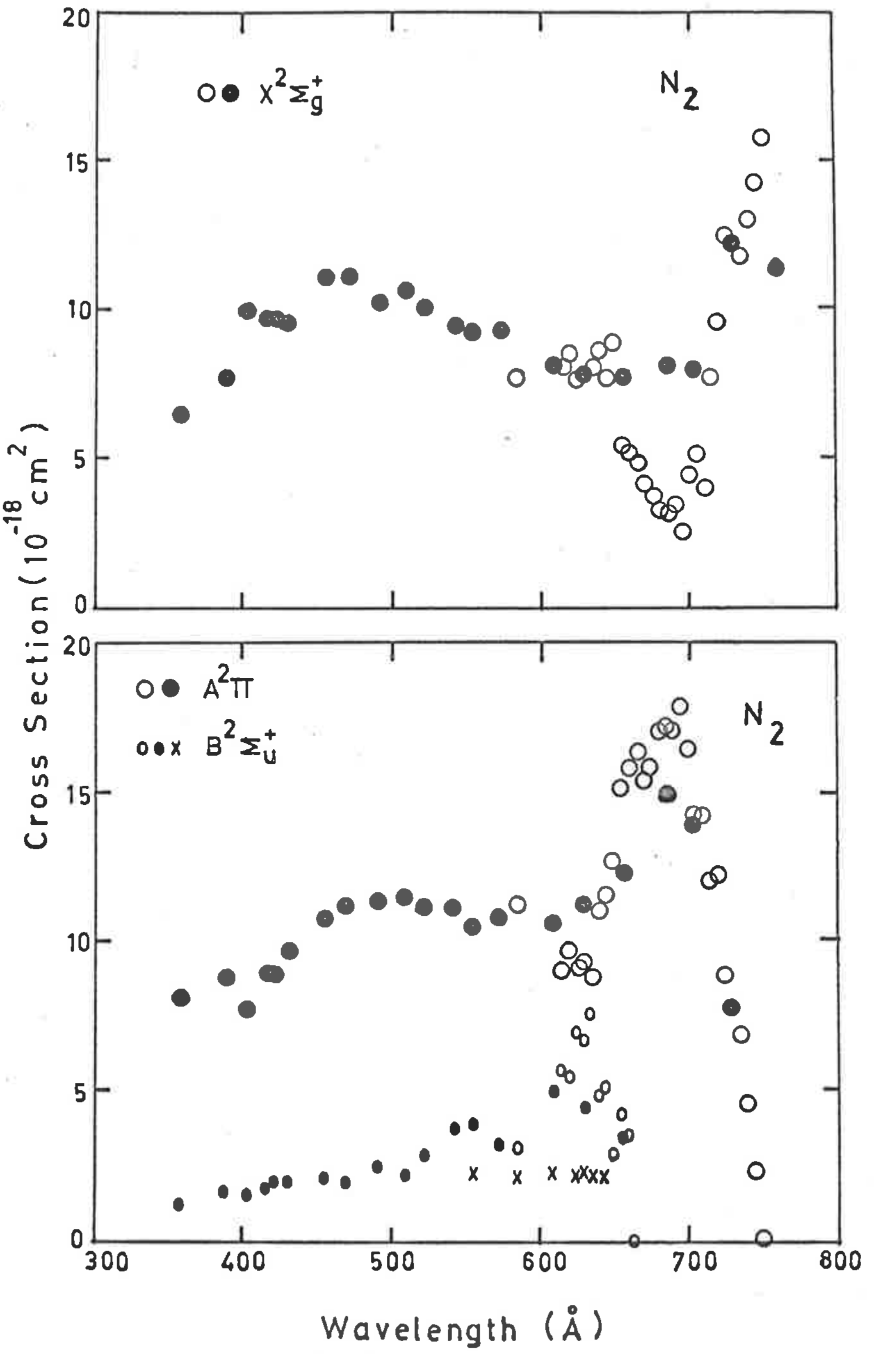

Fig.I.9. Partial photoioization cross-sections for N_2; o- BLAKE 1967; ●- SCHOEN 1968; x- JUDGE 1968.

are normalised to the data of Cook et al (COOK 1965), the two total cross-section results are in reasonable agreement between 600 Å and 700 Å where the partial cross-sections differ the most, especially for the $X^2\Sigma_g^+$ ground state.

I.6 Autoionization.

Excitation of an electron other than the most loosely bound one, or simultaneous excitation of two electrons, may result in a set of discrete states which extend above the normal ionization threshold. Two different states of an atom may thus have the same energy, and so a mixing of the eigenfunctions takes place; i.e. an oscillation between the two "states", one of which is continuous. However, once the atom goes from the discrete state to the continuous state it cannot return since it will have emitted an electron and ionized, and thus a radiationless transition takes place from the discrete state to the continuous state. This process is called autoionization; the transitions involved are shown schematically in Fig. I.10.

In the photoionization cross-section this effect is seen as a set of "lines" superimposed on the photoionization continuum. Beutler (BEUTLER 1935) identified members of two Rydberg series between the $^2P_{\frac{3}{2},\frac{1}{2}}$ limits of argon, krypton and xenon in their respective absorption spectra. The lines were very broad and asymmetrical in shape, trailing off towards shorter wavelengths. The broadness of these lines indicated that the intermediate autoionization states had very short lifetimes.

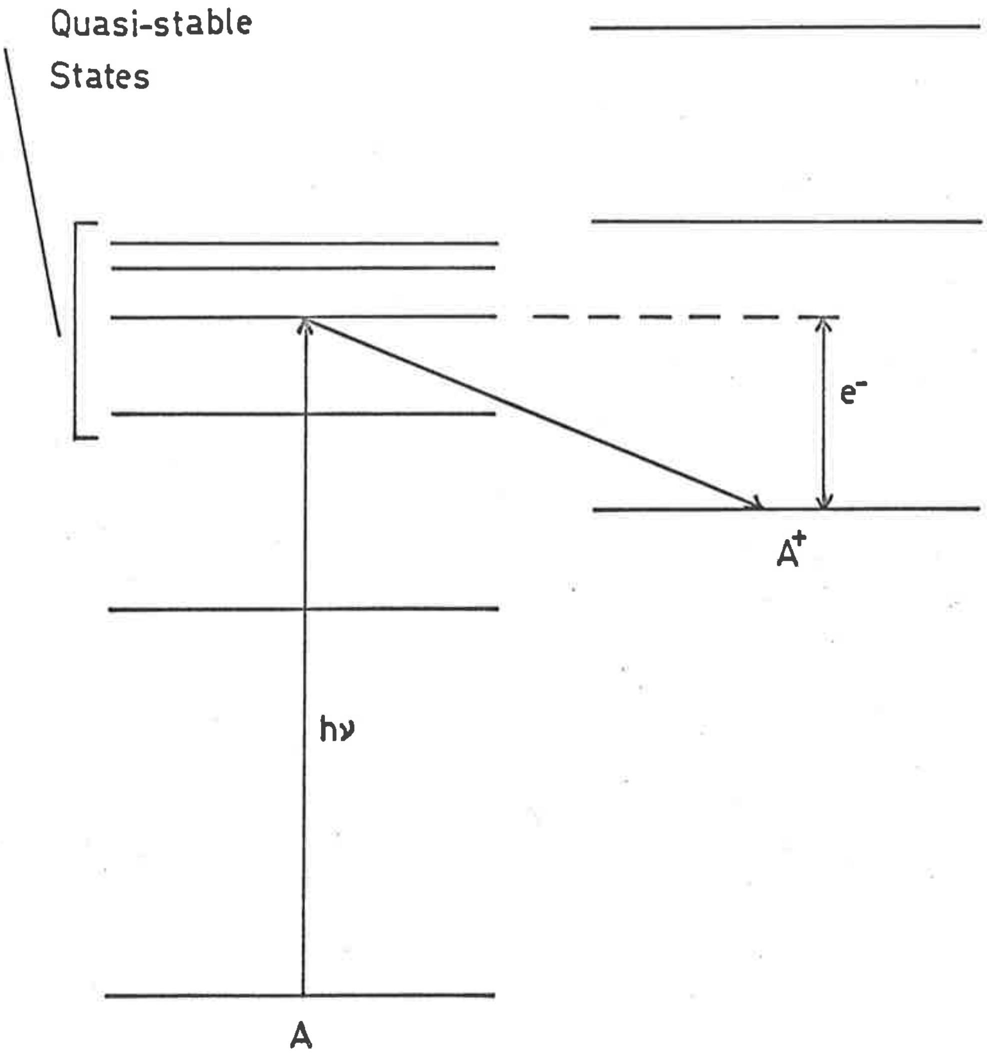

Fig.I.10. Energy levels of an atom A and the ion A^+ showing an autoionizing transition.

Fig. I.11 shows an example of these lines in the absorption spectrum of xenon.

A comprehensive analysis of the profiles of autoionized absorption lines has been given by Fano and Cooper (FANO 1961-65). They considered the problem of the configuration interaction between a discrete state and an overlapping continuum and arrived at an expression for the overall absorption cross-section:

$$\sigma(E) = \sigma_a \frac{(q+\varepsilon)^2}{1+\varepsilon^2} + \sigma_b \tag{31}$$

where σ_a and σ_b represent respectively those parts of the continuum which do and do not interact with the discrete state, and

$$\varepsilon = 2(E-E_r)/\Gamma \tag{32}$$

E_r is the unperturbed energy of the discrete state (represented by the peak of the resonance profile), E is the photon energy, Γ is the half-width of the resonance and q is a parameter called the "line-profile index" and is a function of the eigenfunctions of the discrete state and the continuum. Fig. I.12 shows profiles for several values of q as a function of E. A notable feature of these profiles is that the absorption cross-section for the interaction part goes to zero at one point viz: $q=-\varepsilon$ which accounts for the transmission windows which were

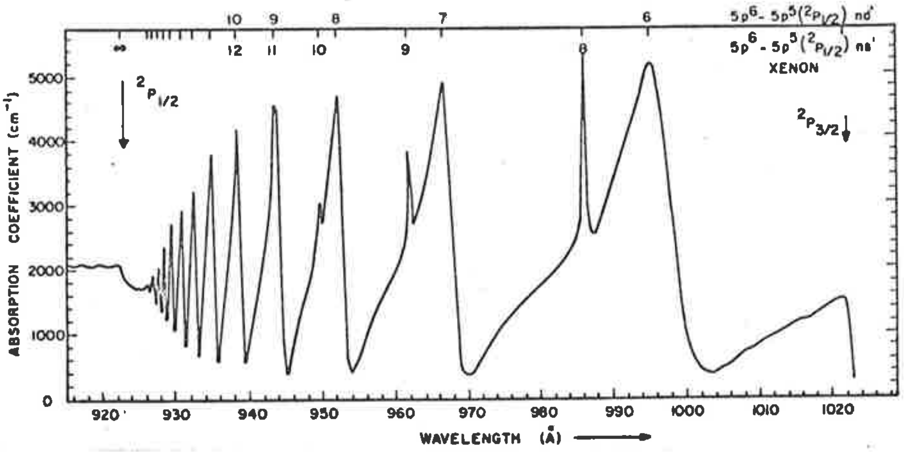

Fig.I.11. Beutler autoionized lines in xenon as measured by HUFFMAN 1963 (after SAMSON 1966)

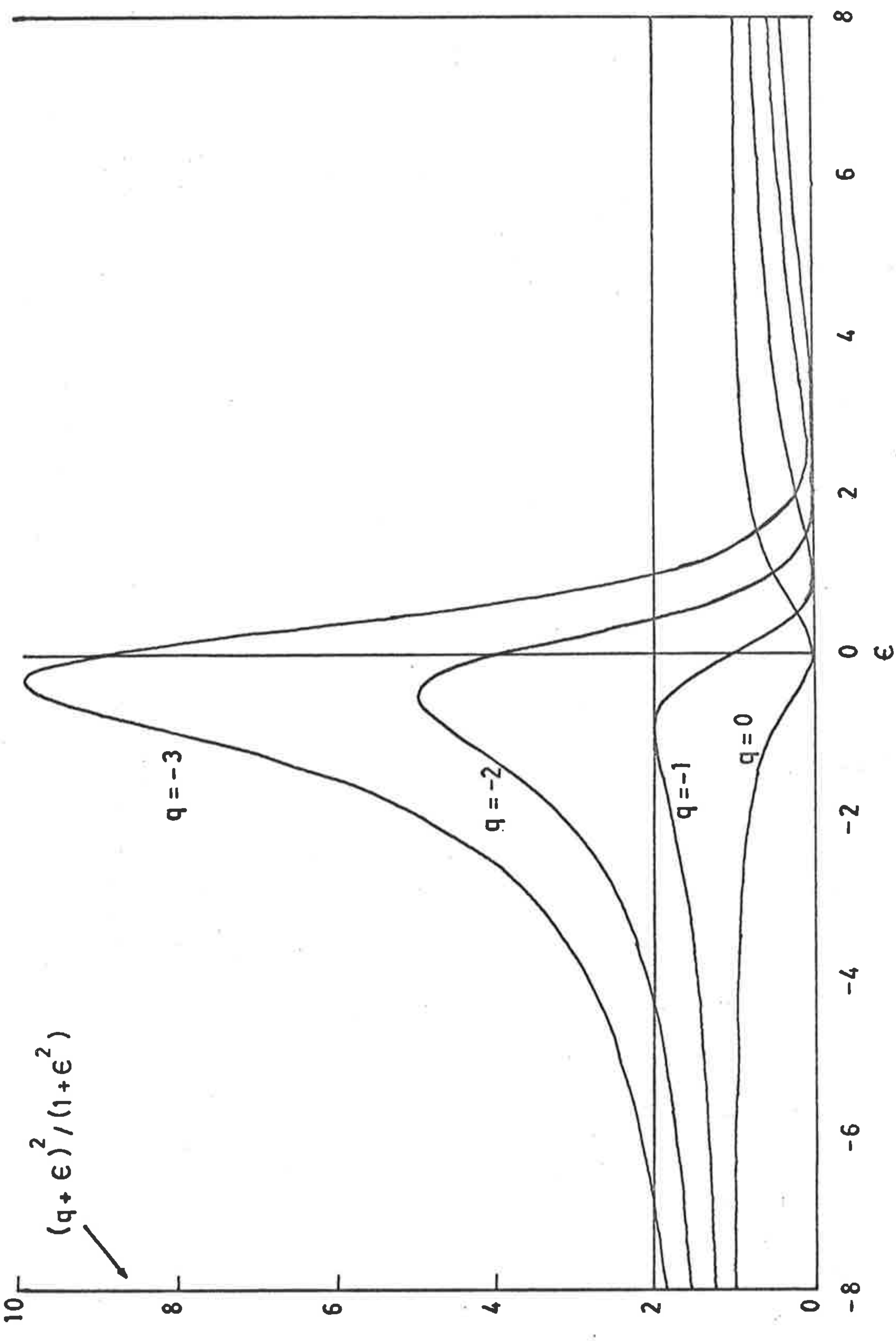

Fig.I.12. Autoionized line profiles for several values of q.

observed in the original spectra (BEUTLER 1935).

I.6.1 Rydberg series in autoionization.

In absorption studies in the vacuum ultra-violet, discrete lines superimposed on a continuum and converging to a series limit at one of the ionic states are often encountered. These Rydberg series can be treated as a set of discrete states which experience configuration interaction with the continuum.

Fano and Cooper showed that in the interval between successive resonances the same line shapes occur as for the single discrete level and single continuum. They were able to predict the behaviour of the resonances for a series provided that the Rydberg approximation,

$$E_\nu = \frac{Z'^2\ R}{(n-\mu_{nl})^2} \tag{33}$$

holds, where μ_{nl} is the quantum defect. They also found that the half-width, Γ_ν, decreases rapidly in proportion to the spacing between the resonances, and thus the intensity changes would remain uniformly sharp throughout the series in proportion to their line spacing. Fig. I.11 shows this effect in xenon.

I.6.2 Experimental results for autoionization.

The photoionization cross-sections of the inert gases have been measured by a number of workers in the regions of autoionization.

In argon, krypton, and xenon a series of diffuse absorption lines are observed between the ${}^{2}P_{\frac{3}{2}}$ and ${}^{2}P_{\frac{1}{2}}$ edges (BEUTLER 1935, HUFFMAN 1963a and b, COOK 1965). Measurements of the ionization efficiencies in these regions have shown the value to be 100% (SAMSON 1966). Madden and Codling (MADDEN 1963), using the continuum radiation from a synchrotron, observed the absorption spectra of the rare gases below 600 Å, which revealed another range of autoionization structure for helium, neon, argon, krypton and xenon. Some of these observed autoionized levels have been identified with levels obtained in electron-scattering experiments by Simpson et al (SIMPSON 1964). Samson (SAMSON 1963-64) has used the continuum provided by a flash tube to study these same levels and his singularities are in agreement with the higher resolution results of Madden and Codling.

Garton et al (GARTON 1969) have recently developed a new continuum light source (B.R.V. source) for use in the 100-600 Å range. With this source they have also managed to observe the autoionized absorption resonances in the rare gases below 600 Å.

Autoionization structure has also been observed in many alkali metals and alkali earth metals. One of the most interesting of these has been the absorption spectrum of aluminium, where a line-pair (1932.25-1936.45 Å) has been identified as due to autoionization transitions of the element in the solar spectrum (DETWEILER 1961). The laboratory measurements were made by Selvyn (SELVYN 1929) and Garton (GARTON 1950) who identified the transition as $3s^{2}3p\,{}^{2}P^{0}_{\frac{1}{2}}$, ${}^{2}P^{0}_{\frac{3}{2}}$ ..... $3s^{3}p^{2}\ {}^{2}S_{\frac{1}{2}}$. Garton (GARTON 1964) has also used a shock tube experiment to obtain quantitative measurements on the doublet by comparing the aluminium lines with the measured lines of calcium at 1850 Å.

I.7 Molecular autoionization (preionization).

Molecular autoionization (usually known as pre-ionization), while similar to the atomic case, is complicated by the additional process of pre-dissociation.

The two processes are distinguished by the products of the radiationless transition. For predissociation the transition takes place into either an unstable state or a stable state above the dissociation limit and hence the molecule disintegrates into atomic or molecular fragments (if the number of atoms in the molecule is greater than two). In preionization the end product consists of the molecular ion and an ejected electron and is thus directly analogous to the atomic case. Since the radiationless transition in the latter case must end in the ionic state, the process of preionization is only observed in the far ultra-violet region of the spectrum (<1000 Å).

I.7.1 Selection rules.

As in autoionization, the fact that a discrete level and a continuum of states have the same energy does not necessarily imply that the discrete level is effected. The radiationless transition has a finite probability only if there is mixing of the wavefunctions of the states concerned. Thus one must take account of the selection rules which govern such transitions.

The selection rules for preionization were derived by Kronig (KRONIG 1928) and for permitted transitions are: (HERZBERG 1950)

(1) $\Delta J=0$ i.e. both states must have the same total angular momentum.

(2) $\Delta S=0$ i.e. both states must have the same multiplicity.

(3) $\Delta\Lambda=0$ or ± 1.

(4) $+ \nleftrightarrow -$, $+ \leftrightarrow +$, $- \leftrightarrow -$. i.e. both states must be positive or both must be negative.

(5) for homonuclear molecules,
$s \nleftrightarrow a$, $s \leftrightarrow s$, $a \leftrightarrow a$. i.e. both states must have the same nuclear symmetry.

While (1), (4) and (5) are rigorous, (2) and (3) hold only approximately, especially as (3) is only appropriate when Λ is well defined.

In the ionization continuum the system is considered as an ion plus an electron and the vectorial sum of the J and K values of both particles must be found to give the required angular momentum of the preionizing molecule (see HERZBERG 1950).

I.7.2 Preionization in total absorption.

In 1932 Henning (HENNING 1932) observed diffuse bands in the absorption spectra of carbon dioxide between 750 Å and 780 Å which he associated with preionization. Similar bands were reported in molecular hydrogen by Beutler and Junger (BEUTLER 1936) in the far ultra-violet region.

For wavelengths shorter than 1000 Å preionization is very evident in the absorption data of molecular oxygen presented by Huffman, Larrabee and Tanaka (HUFFMAN 1964), by Cook et al (COOK 1965) and by Matsunaga and Watanabe (MATSUNAGA 1967). Rydberg series converging to three excited states of O_2^+ ($a^4\Pi_u$, $A^2\Pi_u$ and $b^4\Sigma_g^-$) have been identified in the region 680-1000 Å as well as many vibrational progressions. Fig. I.13 shows the photoionization cross-section curve for O_2 between 800 Å and 900 Å by Matsunaga and Watanabe in which 5 vibrational progressions have been denoted by the letters I, I', J, N and P. Codling and Madden (CODLING 1965) have observed complex preionized bands in O_2 in the 500 Å region utilizing the radiation from a synchrotron.

Below 800 Å, ionization continua with superimposed Rydberg bands are seen in the photoionization cross-section curve for nitrogen. Worley (WORLEY 1953) identified Rydberg series converging to the $A^2\Pi_u$ state of N_2^+, which have also been reported by Tanaka and Ogawa (TANAKA 1962) and Cook et al (COOK 1965) who also observed two progressions in the region 780 Å to 730 Å. The latter authors also report diffuse structure in the region 650-725 Å which they attribute to preionization or predissociation of N_2 (Hopfield Rydberg bands).

Preionization structure can be seen in the photoionization cross-section curve of nitric oxide (COOK 1965, WATANABE 1967) between 1000 Å and 680 Å where Tanaka (TANAKA 1942) originally identified Rydberg series leading to three excited electronic states of NO^+

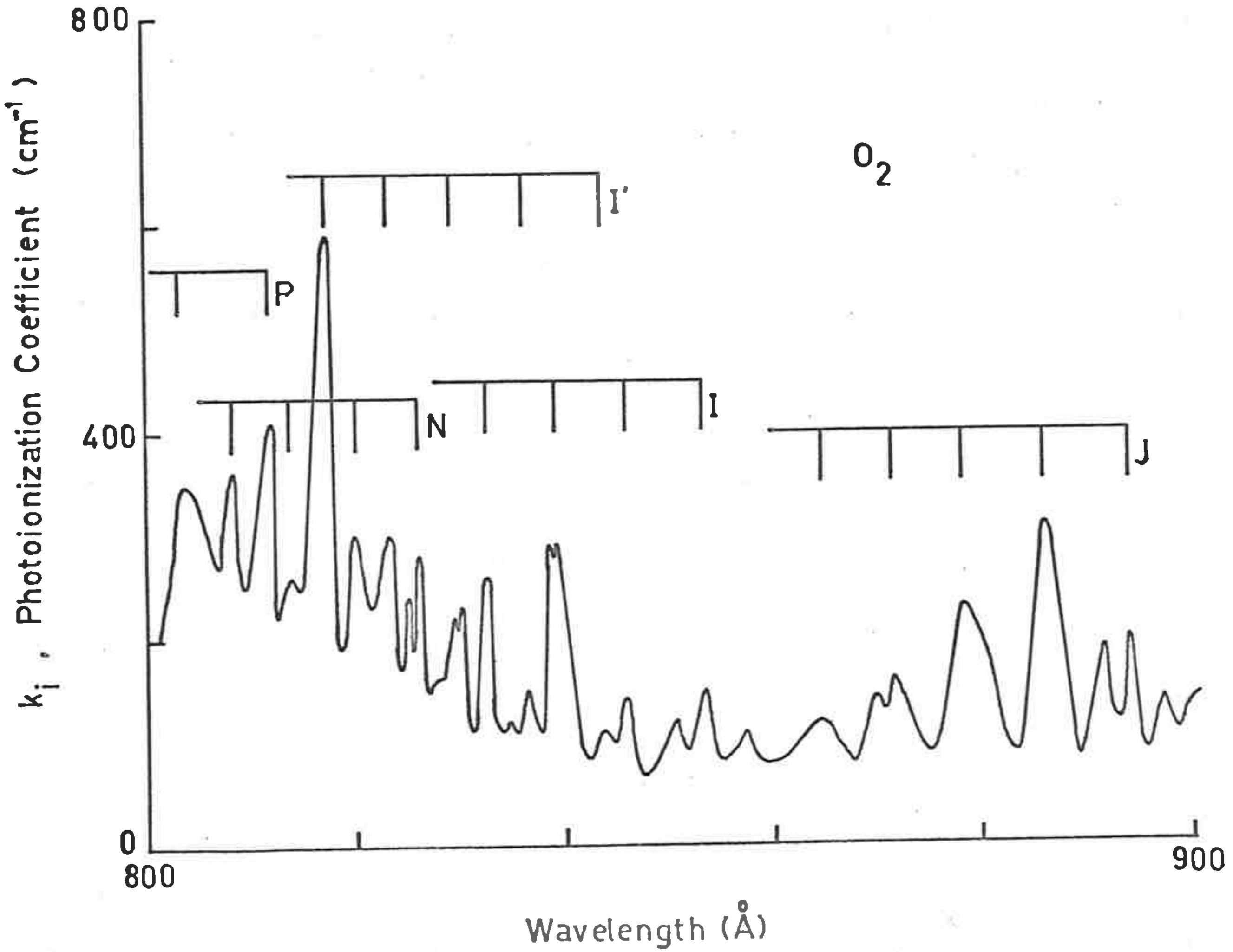

Fig. I.13. Total photoionization cross-section for molecular oxygen from 800-900 Å. (MATSUNAGA 1967).

(these have been reclassified by Huber (HUBER 1961)). Cook et al also noted several progressions in the region 700-900 Å.

Rydberg series converging to higher electronic states of CO^+ ($A^2\Pi$ and $B^2\Sigma^+$) have been reported by Tanaka et al (TANAKA 1958). Two vibrational progressions were reported by Henning (HENNING 1932), and also three other progressions by Tanaka. Cook et al (COOK 1965) report all of these series and progressions in their photoionization cross-section data.

I.7.3 Preionization and photoelectron spectra.

There are few results of photoelectron spectra which have been recorded at wavelengths corresponding to autoionized resonances in atoms or molecules.

Samson and Cairns (SAMSON 1968b) have recorded photoelectron spectra at wavelengths corresponding to resonances in the total photoionization cross-section of Xe and have noted changes in the partial cross-sections for the $^2P_{\frac{1}{2}}$ and $^2P_{\frac{3}{2}}$ states at these wavelengths. Doolittle and Schoen (DOOLITTLE 1965) have observed changes in the photoelectron spectra of H_2 at wavelengths of 772 Å, 780 Å and 790 Å. Price (PRICE 1968) has observed marked changes in the vibrational distribution of the $X^2\Pi_g$ state of O_2^+ between photoelectron spectra recorded at 584 Å and 744 Å. This effect in O_2 has also been observed by Collin and Natalis (COLLIN 1968). Price, and Collin and Natalis, have also observed similar effects in the photoelectron spectra of

NO, CO and N_2. These results will be discussed in more detail in Sec. IV.1.

It is evident that there is a need for a detailed investigation of the photoelectron energy spectrum of the above gases in regions of preionization. In Chapters IV and V of this thesis, photoelectron spectra recorded at wavelengths corresponding to preionized levels in diatomic molecules are presented which show marked changes from spectra recorded in regions of no preionization. These spectra have been recorded for the gases O_2, N_2, CO and NO.

CHAPTER II

THE PHOTOELECTRON SPECTROMETER

II.1 Introduction

It was pointed out in Chapter I that the measurement of the energy distribution of photoelectrons as a function of the incident wavelength was a method by which partial photoionization cross-sections of a gas could be obtained. Since the energy of the final state of the ion is determined to a high degree of accuracy by the difference between the photon energy and the photoelectron energy, a photoelectron spectrometer is also a very useful tool for accurately measuring the ionization potentials of the ionic states of a molecule (see Sec. I.4.1). With sufficient resolution the vibrational levels of a molecule can be resolved by a photoelectron spectrometer, and this provides a useful method for determining the relative vibrational transition probabilities or Franck-Condon factors for the photoionization process (TURNER 1966, BLAKE 1969, EDQVIST 1969).

II.2 Requirements of the photoelectron spectrometer.

There are three essential features of any photoelectron energy analyzing system, viz.:

(1) an ionization region,

(2) a method for collecting the electrons and measuring their energies, and

(3) an electron detector.

For the experiments envisaged in this thesis it was desirable that the spectrometer should have a resolution of at least 0.1 eV as this is the order of the separation of the vibrational levels of the diatomic molecules that were to be studied. As well, it was essential that the energy scale of the spectrometer should be known to sufficient accuracy to enable identification of the ionic states, eg. to 0.1 volts for analysis of the vibrational structure.

Since it was proposed to use the Hopfield helium continuum with a monochromator, as a light source, implying a small light flux for reasonably high beam resolution (eg. 1 Å), it was necessary that the spectrometer should employ a sensitive electron detector incorporating low background noise, and preferably sensitive to single electrons. Because of the sensitivity needed at low light levels, a compromise between resolution and sensitivity at some wavelengths was also anticipated.

II.3 Choice of photoelectron spectrometer.

There are three main types of photoelectron spectrometer which have been used in the past:-

(1) cylindrical retarding potential (eg. SCHOEN 1964, BLAKE 1965-67, and PRICE 1968),

(2) magnetic or electrostatic focusing (eg. TURNER 1966-67, SPOHR 1967), and

(3) spherical retarding potential (eg. FROST 1965, SAMSON 1966b).

These three types will be considered together with their relevant advantages and disadvantages.

There are two experimental limitations which are common to all types of spectrometer; they are the maximum gas pressure which can be used and the available intensity of the incident ultraviolet light. The electron flux from a column of gas is given by:

$$n_e = YI_o \ (1 - \exp(-kx)) \tag{34}$$

where I_o is the incident beam intensity, Y is the photoionization yield, k is the absorption coefficient (in cms^{-1}), and x is the path length through the gas. Thus ideally, the higher the gas pressure the more electrons that can be produced, but the maximum pressure allowable in the ionization region is limited by the mean free path of the electrons which must be sufficiently long to allow electrons to travel to the detector without colliding with other particles. This restriction limits the pressure in a spectrometer to $\sim 10^{-2}$ Torr. However, in the present experiment, the pressure was even more strictly limited by the detector, a channel electron multiplier, which allowed a maximum working pressure of only 10^{-3} Torr (Sec. II.4.3).

The maximum beam intensity available from the monochromator used in the present work was of the order 10^9 photons/sec and thus, for a typical gas at a pressure of 10^{-3} Torr with $k = 500\ \mathrm{cm}^{-1}$, the number of photoelectrons produced per centimetre path length along the beam is $\sim 10^6$ electrons/sec.

The number of electrons detected from the ionization region is also affected by the angular distribution of the electrons if they are not collected over 4π steradians of solid angle. Thus the danger in using a cylindrical or focusing type of spectrometer is that the measured electron flux depends on the angular distributions of the electrons, which in turn depends on the final states of the ions.

The direction of emission of the electrons is defined by the angles θ and ϕ as shown in Fig. II.1. For electric dipole transitions the probability of an electron being emitted in a direction (θ,ϕ) is independent of ϕ but depends on θ according to:
(SOMMERFELD 1930, BETHE 1956),

$$f(\theta) = A + B\sin^2\theta \qquad (35)$$

where A and B are constants depending on ℓ, the electron quantum number. Two measurements have been attempted on the angular distribution of photoelectrons from gases, viz; Berkowitz et al (BERKOWITZ 1967), and Vilesov et al (VILESOV 1967). Vilesov measured the angular distribution of the total electron flux at 584 Å. Berkowitz measured the angular distribution of electrons which left the ions in different states for a number of gases, including O_2, N_2 and NO, and found it to be

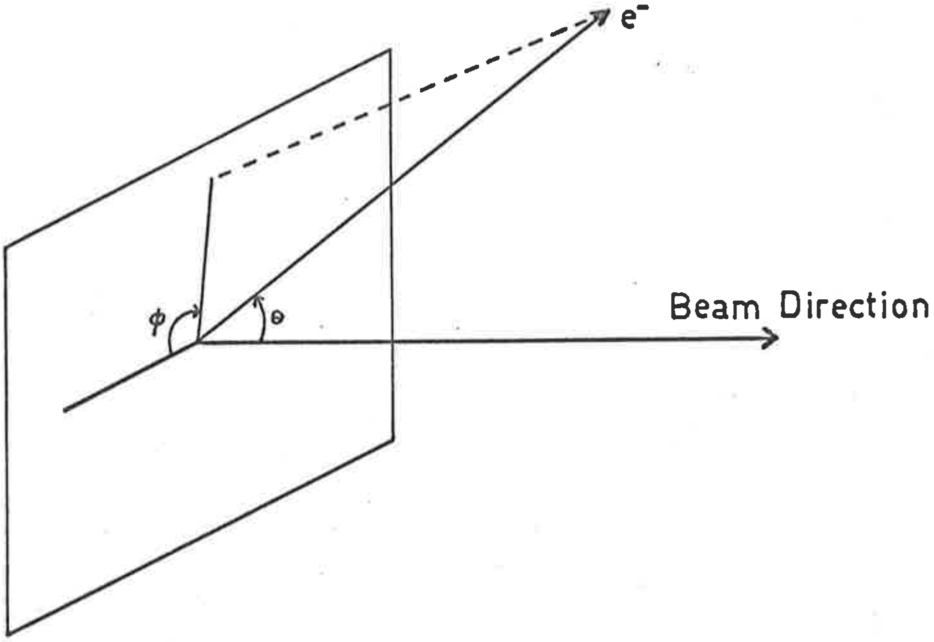

Fig.II.1. Diagram defining the angles θ and ϕ which describe the direction of emission of a photoelectron.

spherically symmetric except for the O_2^+ ($X^2\Pi_g$) and NO^+ ($X^1\Sigma^+$) states where the distribution tended to favour the θ = 0° and θ = 180° directions. Thus an angular discriminating system could give misleading results for the relative transition probabilities of these states.

For sensitivity, a system which uses an electron multiplier is to be preferred, but this, however, creates difficulty in using a system with cylindrical geometry. A cylindrical system must also be collimated in both θ and ϕ directions, which considerably reduces the available electron flux.

A magnetic or electrostatic analyzer with focusing of the electrons is capable of better resolution (TURNER 1968), but an analyzer of this type necessarily accepts electrons from only a small solid angle, implying angular discrimination.

An analyzer of spherical geometry requires no collimation and is independent of angular distribution effects. Frost et al (FROST 1965) and more recently Samson (SAMSON 1966b) have used spherically symmetric systems with a retarding potential to analyze photoelectron energies. The spectrometer chosen for the present work was based on a modification of the system used by Frost (Samson has adopted a similar procedure).

II.4 Construction of the spectrometer.

The photoelectron spectrometer was of quasi-spherical construction. It consisted of two concentric hemispherical grids mounted about a "point" source of photoelectrons, with a plane grid to "pull" the electrons into a channel-electron-multiplier detector.

II.4.1 The analyzing grid system.

The spherical grids were formed by cutting an appropriate section from a copper hemi-sphere of the required diameter and replacing the removed copper with a bronze wire mesh. The mesh consisted of 0.01 inches diameter woven wire at a spacing of 20 lines per inch. This rather coarse mesh was ∿ 70% transparent and was used to maintain spherical rigidity across the opening. A finer copper mesh was then placed over the coarse mesh so that the potential across the surface of the grid would be more uniform. The fine mesh was electroformed mesh obtained from Buckbee and Mears Company, Minnesota, U.S.A. The wire diameter was 0.00095 inches and was spaced at 70 lines per inch with a transparency of 90%.

The first grid (G_1, Fig. II.2), had a radius of 2¼ inches and was kept at earth potential (0 volts) to ensure that photoelectrons were formed in a field-free region. This grid also had a cone fixed to it as in Fig. II.2, which ensured that electrons outside a 60° cone, centred on the vertical axis, were not scattered into the analyzer, but reflected to the bottom of the spectrometer.

The second spherical grid (G_2) had a radius of 3 inches and was mounted concentric to G_1 and the electron source. The retarding

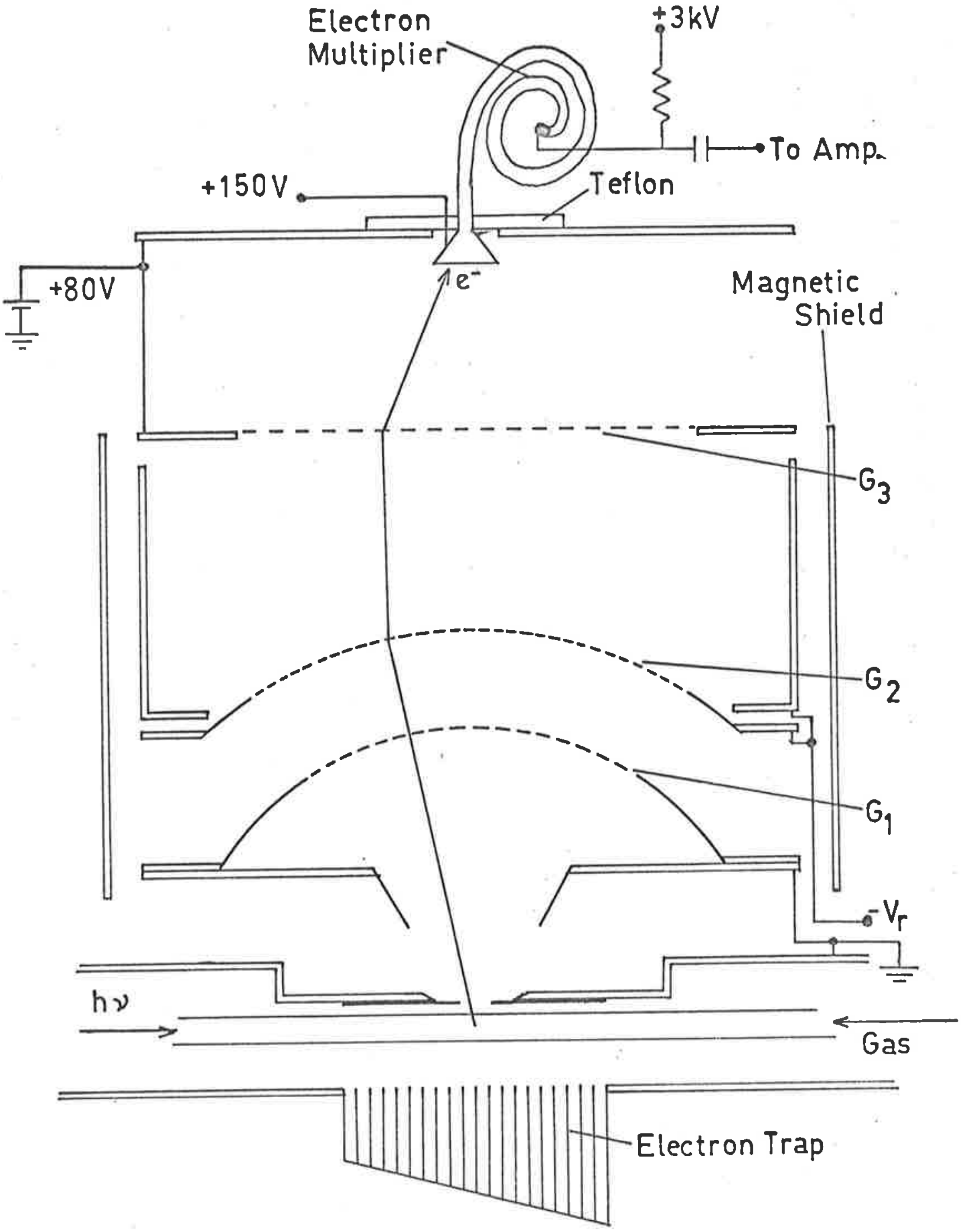

Fig. II. 2. The grid assembly and electron source of the photoelctron spectrometer.

potential was applied to this grid, and in future it will be referred to as the "analyzing grid".

At a distance of ∼ 1 inch from the top of G_2 was a plane grid, consisting of tungsten woven wire mesh (80% transparent) mounted on a copper annulus (G_3, Fig. II.2). This grid served as a collecter grid for the electrons and also shielded the analyzing grid from the relatively high potential (150 V) on the detector. A potential of 80 V was maintained on G_3.

A cylinder of 5 inches diameter and 2 inches long was placed between G_2 and G_3. This cylinder was kept at the same potential as G_2 so that a more uniform field existed in the region between the two grids.

The entire grid system was fixed by four brass rods and two brass brackets to the bottom flange of the vacuum chamber. The metal surfaces of the assembly were coated with Aquadag to minimise scattered electrons.

II.4.2 The photoelectron source.

Ideally, for a spherical retarding potential system, the photoelectrons should emerge from a point source coincident with the common centre of the spheres. In practice a finite volume must be used where the centre of the volume is the concentric centre of the spheres. This was achieved by using part of the gas-photon interaction region as the source-volume.

A 1 inch diameter brass tube was placed so that its axis passed through the spherical centre of the grids and was parallel to the photon beam. Thus it was fixed between the monochromator adaptor flange and the light flux monitor flange (Fig. II.3). A section of the tube near its centre was removed and replaced with a $\frac{1}{8}$ inch copper plate. A cone-shaped hole was machined into this plate and a sheet of 0.001 inch thick brass with a 0.5 inch diameter hole was fixed under it as shown in Fig. II.3. In this way a hole was produced as close as possible to the photon beam, which was collimated by two $\frac{1}{4}$ inch circular collimators in the tube.

The target gas was introduced by means of a $\frac{1}{16}$ inch hole drilled in the monitor flange, to which the electron source tube was permanently attached (Fig. II.3).

The photoelectron source thus consisted of a volume defined by the photon beam cross-section, and the diameter of the hole in the shim brass. The photoelectrons produced at the centre of the spherical system moved outwards along radii (i.e. normal to the retarding potential). An electron produced away from the centre moved at an angle to a radius and was retarded by a lower voltage. The resolving power of the spectrometer was thus limited by the relative diameters of the source volume element and the analyzing sphere. With a source volume diameter of effectively 0.5 inches and an analyzing grid of 6 inches diameter, the resolution, defined as $\Delta E/E$ for electrons of energy E, was expected to be at best 0.7%, or a spread of 0.035 eV at an energy of 5 eV.

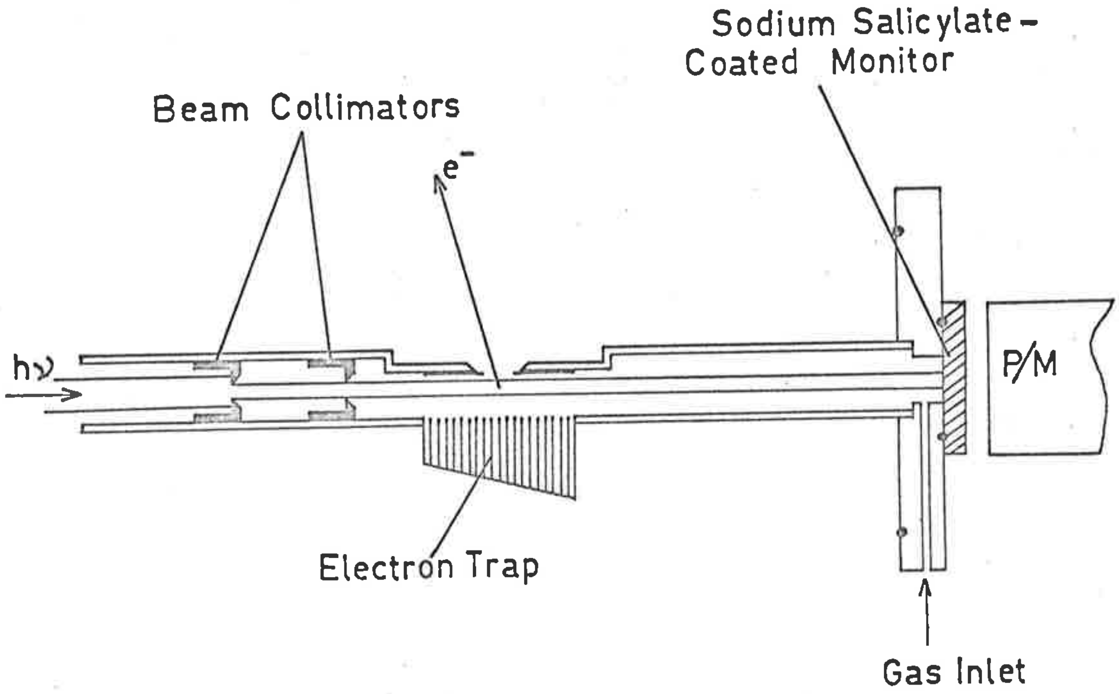

Fig.II.3. The photoelectron source, the beam monitor, and the electron trap.

The source volume determined, in part, the sensitivity of the instrument. Under typical operating conditions (10^9 photons/sec, 10^{-3} Torr pressure, and $k=500$ cm^{-1}) a volume of $1cm^3$ would produce $\sim 10^6$ electrons per second. Since the collecting area was effectively reduced to a 60° cone and the total transparency of the grids was ∿50% the expected number of electrons arriving at the detector per second was estimated to be $\sim 10^5$.

Under operation it was found that electrons scattered from the sides of the tube near the source hole contributed a large low-energy background to the photoelectron spectrum. This effect was reduced considerably by the use of an "electron trap" which is shown in Fig. II.3. The trap consisted of a piece of hexagonal aluminium honeycomb of $\frac{1}{8}$ inch cross-section and tapered in depth as shown. The honeycomb presented a number of channels to electrons moving in the general direction away from the grid. These channels acted as traps to the electrons by repeatedly reflecting them from the walls. The effectiveness of the trap was increased by coating the surfaces with Aquadag.

II.4.3 The photoelectron detector.

It was mentioned in Sec. II.4.2 that the electron production rate was expected to be $\sim 10^5$/sec, i.e. a current of $\sim 10^{-14}$ amps. Since the direct measurement of such a current was difficult, the electrons had to be detected by some other means.

The most convenient method of detecting single electrons is with an electron multiplier. These may be categorized in two groups:

(a) those with separate dynodes (i.e. a windowless photomultiplier) and

(b) those employing a high resistance strip as a continuous dynode.

The photoelectron spectrometer required a multiplier with the following characteristics:

(1) sensitive to electrons of energy >50 eV,

(2) high gain with good signal-to-noise ratio,

(3) electrode surfaces able to withstand repeated exposure to the atmosphere,

(4) fast time response,

(5) narrow pulse-height distribution,

(6) no pressure dependance of the charge-multiplication factor.

The discrete dynode type of multiplier has a relatively poor signal-to-noise ratio, and also suffers deterioration of the cathode and dynode material upon repeated exposure to the air.

The magnetic electron multiplier (GOODRICH 1961), which uses crossed electric and magnetic fields along two high resistance dynode strips to achieve the charge gain, has a good noise level (0.1/sec) and can be safely exposed to the atmosphere without degradation in performance, but the high magnetic field ($\sim$400 gauss) prevents detection of low energy electrons.

Goodrich and Wiley (GOODRICH 1962) developed a multiplier consisting of a glass tube whose inner surface was coated with a high resistance material. This device has been developed commercially and is known as a "channel electron multiplier" or CEM. In general, a CEM is a small curved glass tube whose inner wall is coated with a high resistance material, usually vanadium or lead. A potential is applied between the ends of the tube, thus causing the resistance strip to become a continuous dynode, analagous to the separate dynodes of the conventional electron multiplier.

When an electron enters the low potential end of a CEM it generates secondary electrons on collision with the wall of the tube. These are accelerated along the tube until they strike the wall again, generating further secondary electrons. This avalanching process produces a large number of electrons at the high potential end of the CEM, so that the final pulse of charge may contain up to 10^8 electrons and have a duration of up to 10^{-8} secs. Thus the gain of a CEM is approximately 10^8.

The tube is curved to prevent ionic feedback by residual gas ions, formed at the output end, from drifting back to the input end. If the tube is curved, these ions strike the wall of the tube before they have acquired sufficient energy to release secondary electrons. Thus the output of a curved CEM is independent of the surrounding pressure, provided it is less than 5×10^{-4} Torr. Above this pressure, the background noise, which is about 1 pulse per second, may increase. This type of detector, then, meets requirements 1 to 5 and also 6 providing that the pressure limit is not exceeded.

The detector chosen was a Mullard channel electron multiplier - type B419BL (type B318BL was used for some of the earlier results and has almost identical electrical characteristics, the only difference being in the input cone area).

The characteristics of the B419BL are listed in Table II.1.

TABLE II.1

Characteristics of Mullard CEM - B419BL

Maximum Operating Voltage	3.5 kV
Nominal Resistance	5×10^{9} ohm
Gain	1.1×10^{8} @ 2.5 kV
Noise (@ 2.5 kV)	2.0 p.p.s.
Pulse Height Distribution Resolution (@ 10^{8} gain and 1000 p.p.s.)	0.6
Minimum effective cone diameter	9 mm

Fig.II.4 shows a schematic diagram of the detector with the gain-voltage characteristics; the flared input increased the effective area presented to incoming electrons from less than 1 mm^2 to about

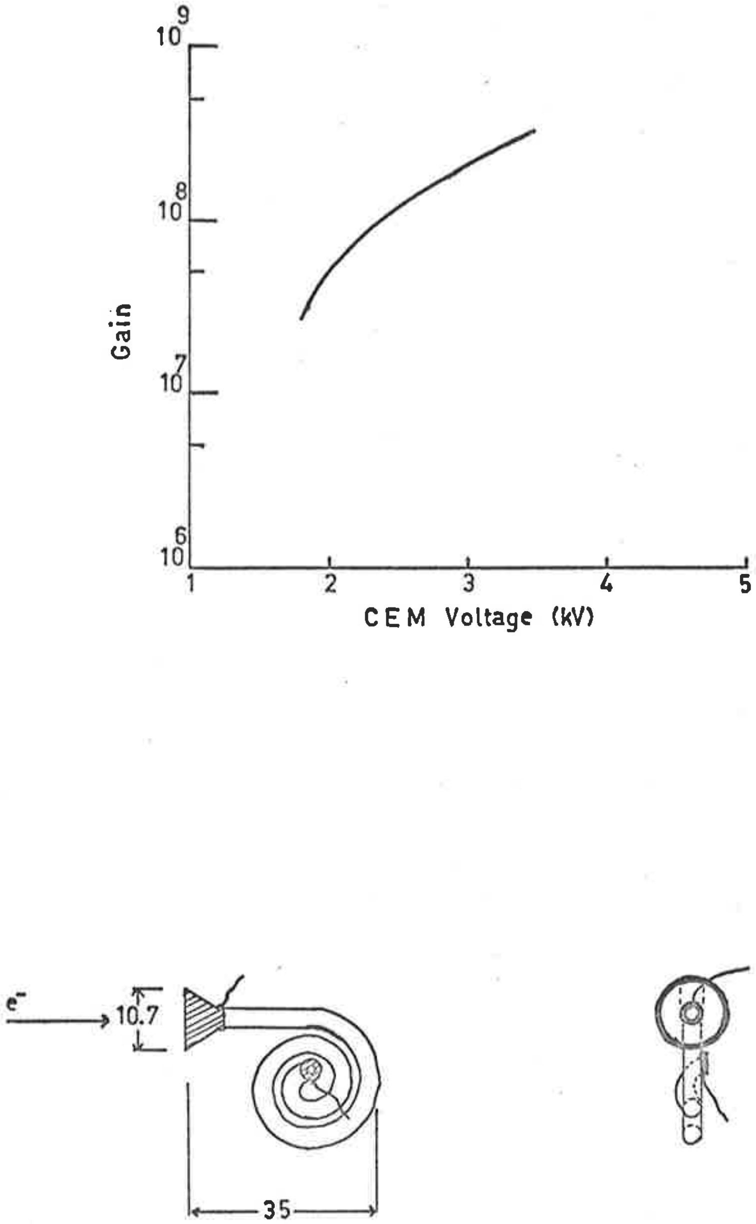

Fig.II.4. Mullard channel electron multiplier, model B419BL. Dimensions are in mm.

64 mm^2. However, because of the small aperture of the detector, compared with the area of the collecting grid (G_3), i.e. 64 mm^2 to $\sim$6400 mm^2, the input end of the CEM was maintained at a potential of 150 V in order to "focus" electrons to it, and to give the electrons sufficient energy for direct detection. The output from the detector was AC coupled to a linear pulse amplifier (Franklin, model 358) whose inbuilt discriminator had a pulse output compatible with the input to the 400 channel analyzer, (see Sec. II.5).

The detector was mounted by means of a small teflon clamp (Fig. II.2) to the centre of a 5½ inch diameter brass disc so that its flared end emerged through a small hole in the centre of the disc. This disc was maintained at the same potential as G_3 and served the purpose of shielding the high voltage end (3 kV) of the CEM from the low energy electrons. The disc was mounted using teflon insulators connected to two brass supports which were in turn fixed to the upper flange of the vacuum chamber.

II.4.4 The vacuum chamber.

The vacuum tank was constructed of 6 inch diameter copper tubing and is drawn schematically in Fig. II.5 and shown photographically in Fig. II.6.

The grids and detector were supported from the bottom and top flanges respectively of the main vacuum chamber, while the electron source tube was fixed to the beam monitor flange, its other end fitting

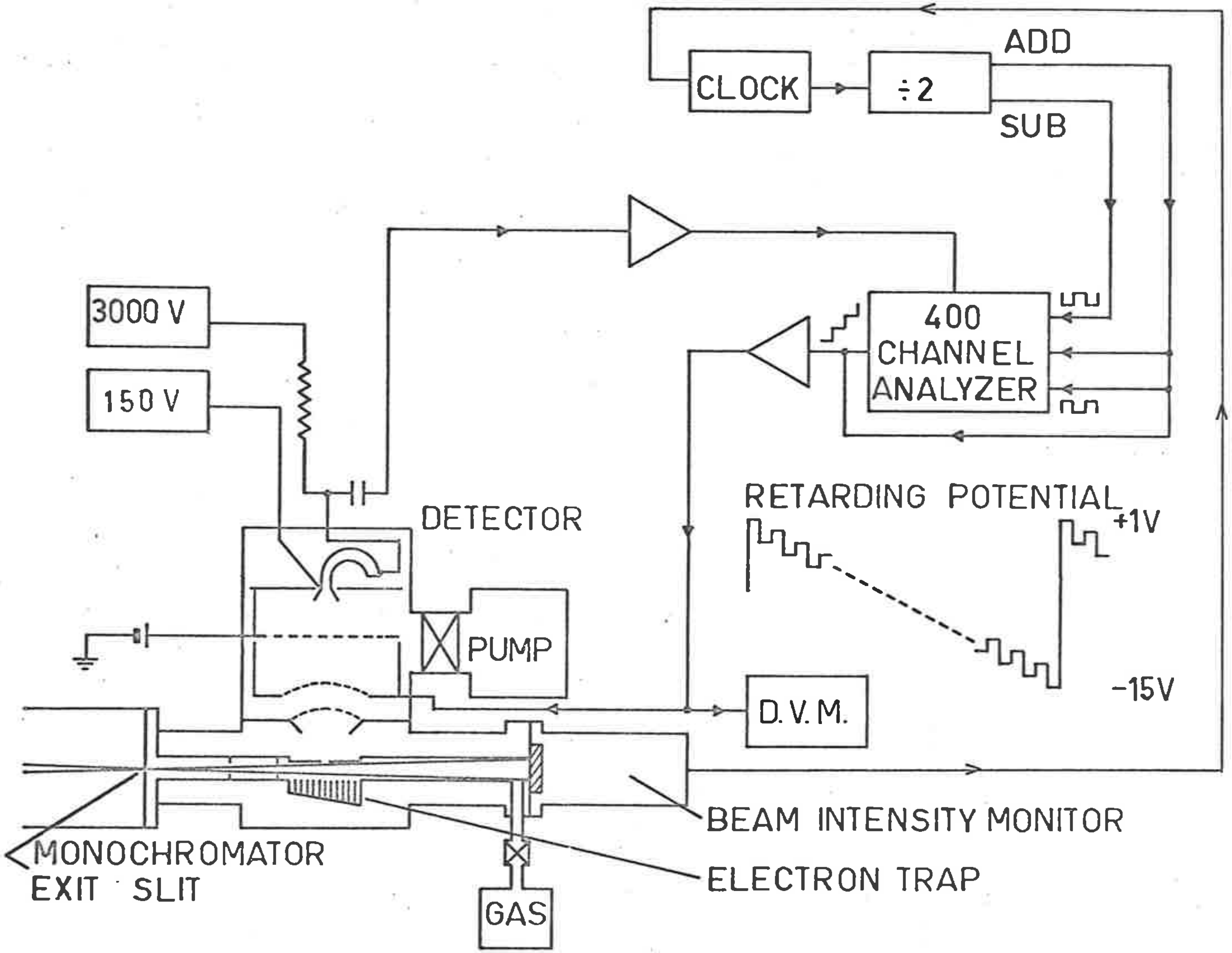

Fig.II.5. Experimental arrangement, showing the photoelectron spectrometer and the associated apparatus for recording photoelectron spectra.

Fig.II.6. The spectrometer vacuum chamber and light source mounted on the 1-metre monochromator. The large tube in the background is part of the differential pumping system.


DO NOT
SCAN MANUALLY BELOW [illegible] Å OR ABOVE [illegible] Å

a groove in the flange which mated the system to the monochromator.

The light flux was monitored by using a sodium salicylate coated perspex plate and a photomultiplier. The salicylate coating was on the vacuum side of the perspex window and acted as a wavelength converter for the photomultiplier (Fig. II.3).

Electrical connections were made through glass-cover seals in the top and bottom flanges of the main chamber.

The whole system was pumped through a 4 inch diameter tube from a position near the detector. The 4 inch tube was connected via a 6 inch tube and a valve to a 2 inch oil diffusion pump. The latter tube contained a liquid nitrogen cooled trap for removing condensable impurities. The diffusion pump was capable of evacuating the chamber to a pressure of less than 10^{-5} Torr.

The vacuum chamber was windowless to the monochromator and the photon beam entered through the exit slit of the latter, enabling a pressure of less than 10^{-4} Torr to be maintained in the monochromator with a gas pressure of 10^{-2} Torr in the electron source tube. (This pressure was measured by recording the amount of light at a given wavelength that was absorbed by a gas of known cross-section over the known length of the tube).

The target gas entered the source tube through a $\frac{1}{16}$ inch hole in the monitor flange via a needle valve, which was adjusted to maintain a constant pressure in the chamber. Facilities were provided for attaching an ionization vacuum gauge and a Pirani type gauge to the chamber. The ionization gauge was used to set the initial pressure in the chamber to $\sim 10^{-3}$ Torr, the Pirani gauge being used thereafter to monitor the chamber pressure.

II.5 The monochromator.

A near normal incidence, 1-metre scanning monochromator was used with a Bausch and Lomb replica grating as a source of ultraviolet photons. This grating had a ruling of 1200 lines per mm and was blazed for 1200 Å in the first order. The dispersive power was 8.3 Å per mm.

The light source employed in these experiments consisted of a high-voltage condensed discharge in helium through a water-cooled quartz capillary tube (Fig. II.7). In the earlier experiments, the discharge was initiated by an air-stabilized spark across two tungsten electrodes, but this was later replaced by a more efficient and reliable triggered thyratron circuit. It was also possible to excite the helium resonance line at 584 Å by using the high voltage in either A.C. or D.C. mode through a current limiting resistance. The circuits for obtaining the various modes of discharge are shown in Fig. II.8.

The Hopfield continuum of helium has a useful intensity in the wavelength range 600 Å to 1000 Å and was obtained with about 50 Torr of helium in the capillary tube. The helium continuum used in the present work is shown in Fig. II.9.

The light source was isolated from the monochromator by a

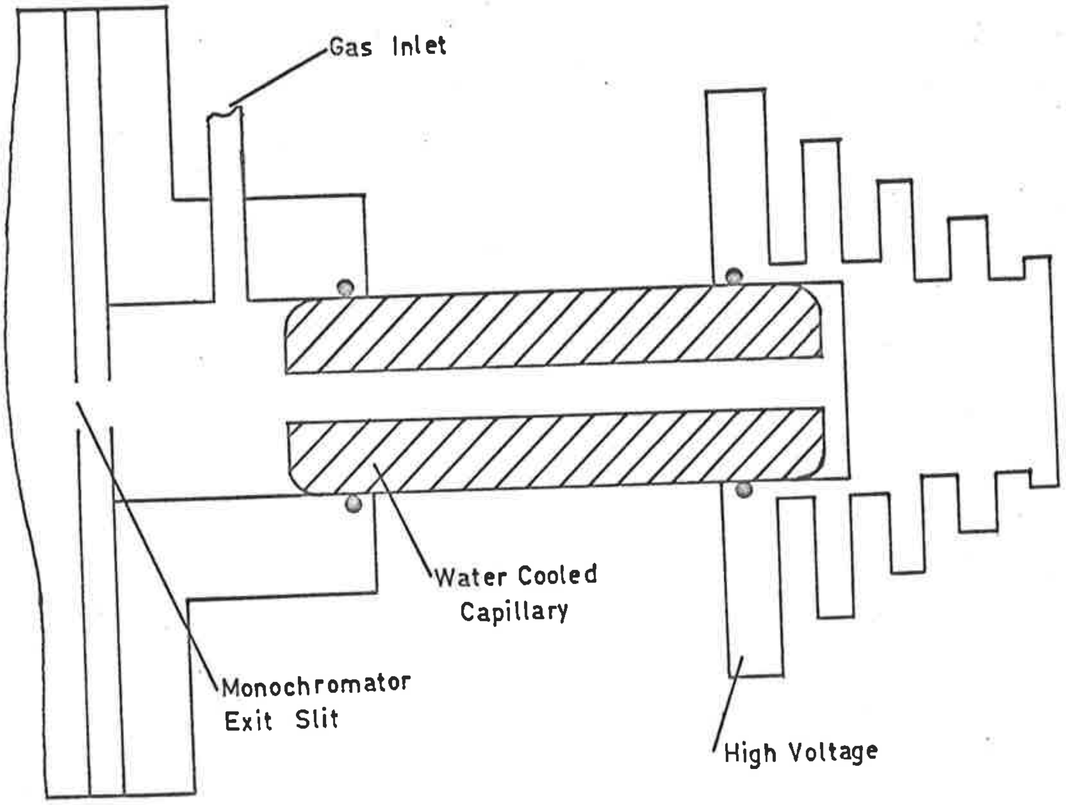

Fig.II.7. The water-cooled capillary discharge light source.

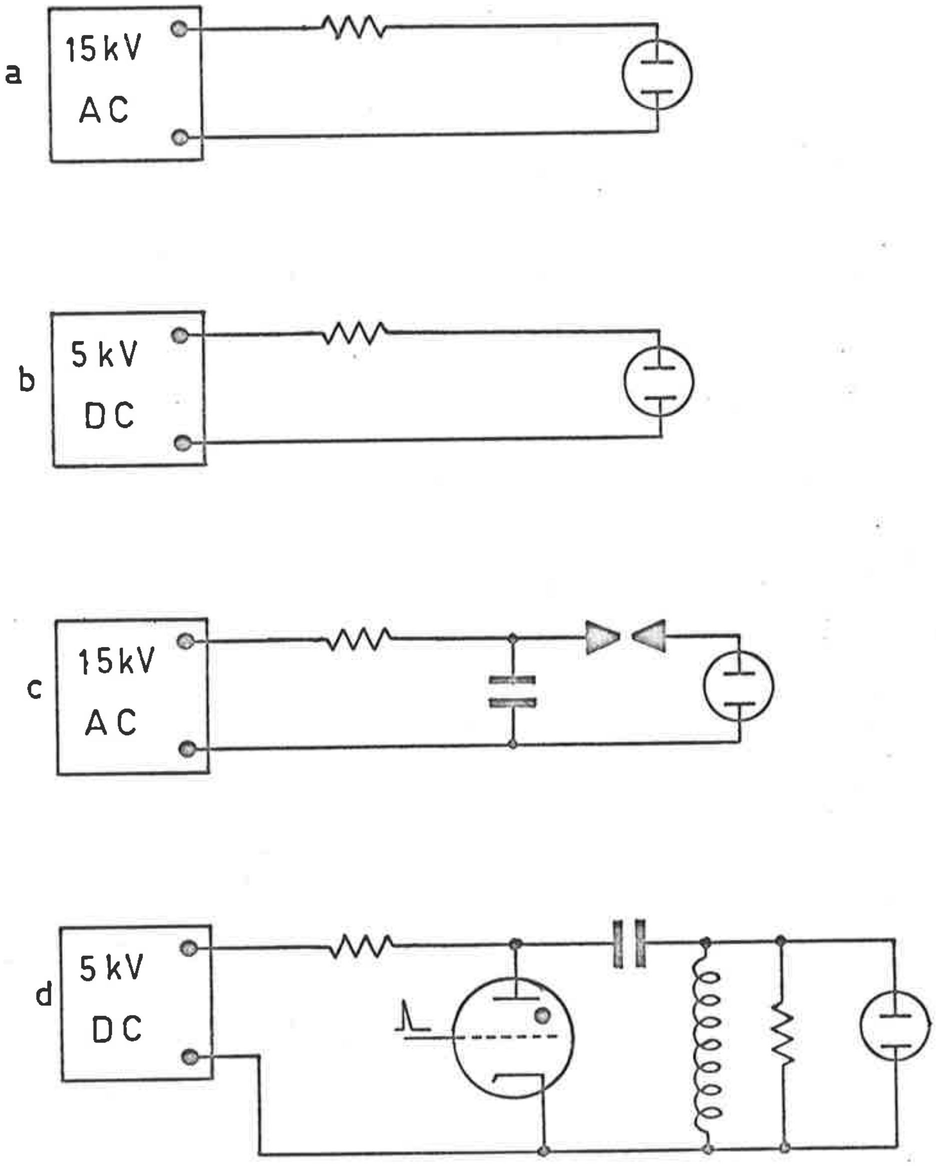

Fig.II.8. The circuits for supplying power to the capillary discharge lamp.

a A.C. mode

b D.C. mode

c condensed spark discharge mode

d thyratron triggered discharge mode

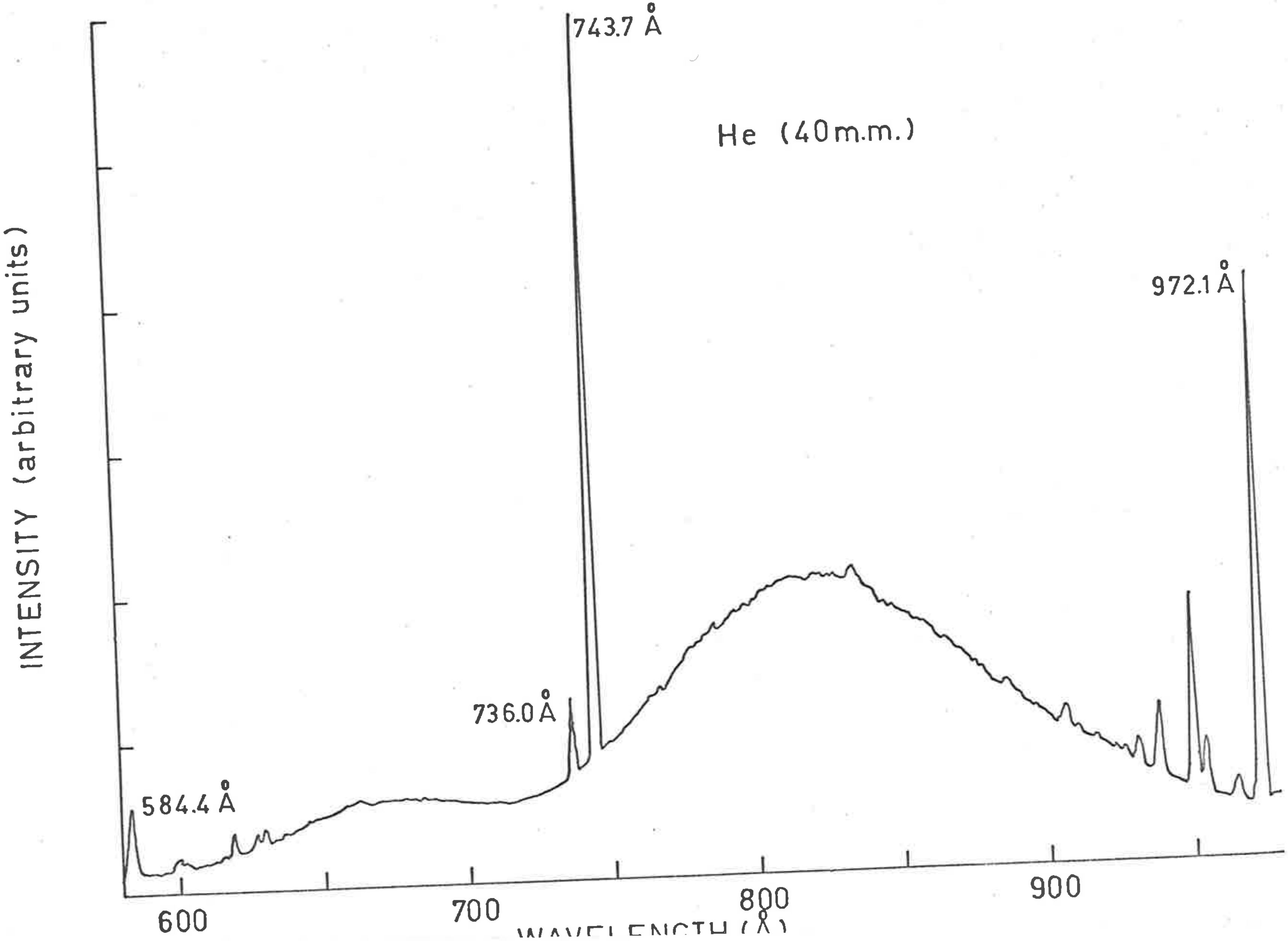

Fig. II.9. Hopfield continuum excited in helium.

two-stage differential pumping system. The first stage was pumped by a mechanical booster pump (Godfrey KB/V400/28) and backing pump, while the second stage was pumped by an oil booster pump (Dynavac OB1500) and backing pump. This differential pumping assembly allowed a maximum entrance slit width of 100μ, which, with the lamp at a pressure of 50 Torr, kept the pressure of the main chamber of the monochromator at less than 10^{-4} Torr.

II.6 Operation of the spectrometer.

The spectrometer was operated in a digital manner as this was more appropriate to single electron counting than an analog method.

II.6.1 The grid voltages.

The first spherical grid (G_1) was maintained at earth potential to ensure that electrons were formed in a field free region. The retarding potential, V_R, was applied to the analyzing grid (G_2), and the range covered by this voltage sweep could be varied from about 1 volt to over 60 volts. V_R began from a slightly positive voltage (∿0.2 volts) so that zero voltage effects could be observed.

The third grid (G_3) was supplied with a positive potential to collect all electrons which overcame the potential barrier on G_2, thus ensuring that all these electrons were accelerated towards the detector. This same potential was applied to the detector shield, S.

The voltage on the input cone of the CEM was adjusted until maximum count rate was obtained from the detector, thus ensuring optimum efficiency of the system.

The collecting-voltage characteristics of G_3 were investigated by observing the variation in the count rate (with zero volts on G_2) while the voltage on G_3 and S was changed. This variation is shown in Fig. II.10, and from this curve the best operating voltage for the collector and the shield was found to be 80 volts (a higher voltage was found to spoil the resolution).

The retarding potential applied to G_2 was in the form of a negative going staircase with either 100, 200, or 400 steps. This potential was obtained by amplifying the analog output voltage of the channel number of a 400-channel pulse height analyzer (RIDL model 34-12 B). Thus each step of the staircase corresponded to a channel of the analyzer and as the grid was held at some potential by the staircase voltage, the number of electrons detected was stored in the corresponding channel of the analyzer.

II.6.2 Photon beam monitor.

In Sec. II.4.4 it was shown how the photon beam was monitored by using a sodium salicylate coated window and a photomultiplier, Fig. II.3. The output from this photomultiplier was monitored by a micro-micro-ammeter which had, as an output facility, a voltage proportional to the input current (0- 3V). This voltage was converted to a train of pulses by an analog-to-digital converter, and these pulses, after having been reduced in frequency by a dividing network,

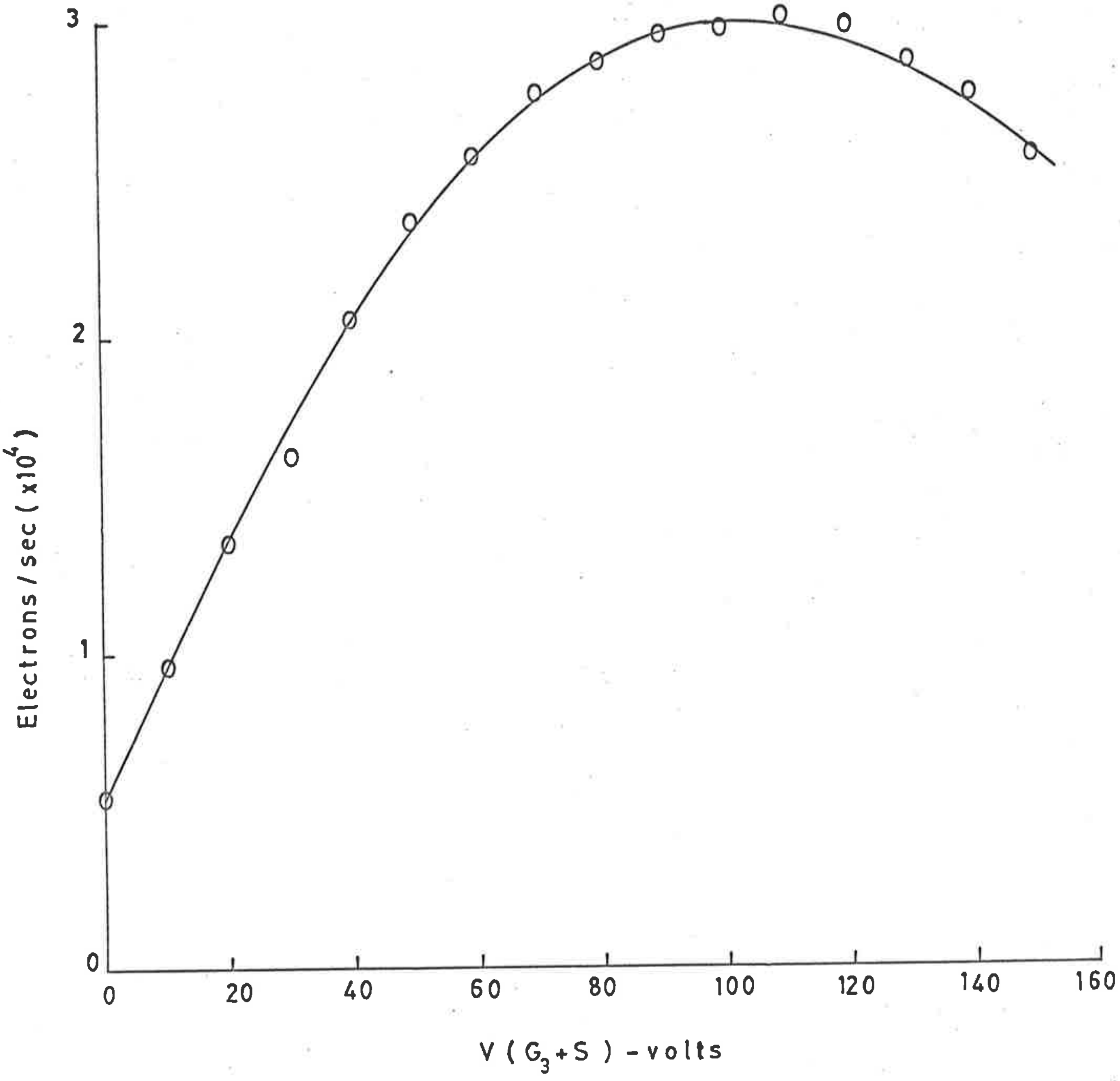

Fig.II.10. Collecting voltage characteristic of the photoelectron spectrometer.

were used to advance the channel number of the 400 channel analyzer. Thus any fluctuations in the light intensity, and hence in the electron flux, were counteracted by the amount of time spent in that channel; i.e. for constant pressure, the time spent in each channel was inversely proportional to the light beam intensity.

The circuit for converting the voltage to frequency is shown in Fig. II.11.

II.6.3 The integral spectrum.

The result of measuring the electron count rate as the retarding voltage was changed with time was a step-like function, each step corresponding to different electron energy groups being stopped by the retarding voltage. This electron stopping curve will be called an "integral spectrum" in the present work for reasons that will become apparent below. An example of an integral spectrum for the gas xenon at a wavelength of 584 Å is shown in Fig. II.12. The two steps in the spectrum correspond to the $^2P_{\frac{1}{2}}$ - $^2P_{\frac{3}{2}}$ levels of xenon at 13.44 eV and 12.08 eV respectively.

II.6.4 The differential spectrum.

In more complex spectra it was desirable to obtain the derivative of the electron stopping curve, so that each electron energy group was represented by a peak in the "differential" spectrum. Previously the electron current has been differentiated electronically by an R-C network (BLAKE 1967), but due to the digital nature of the

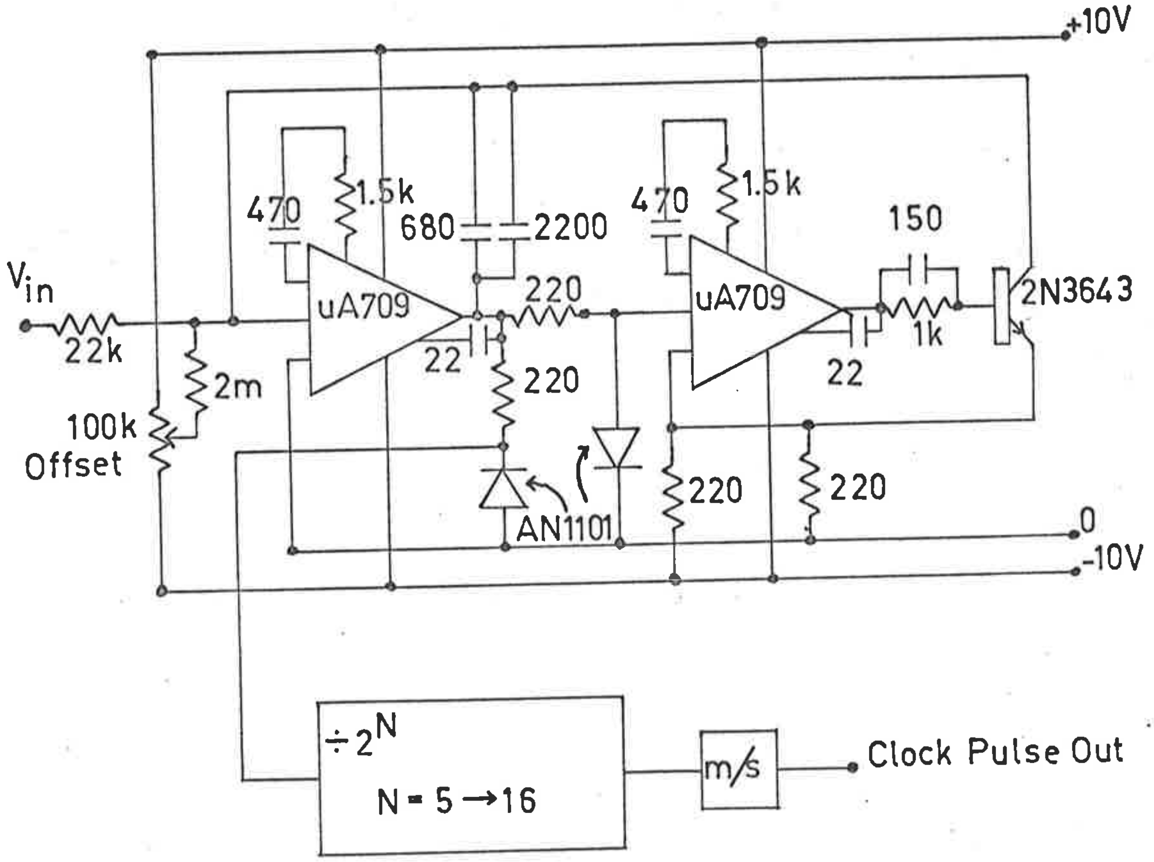

All Capacitors in pf

Fig. II.11. Analog-to-Digital converter used with the photon beam monitor.

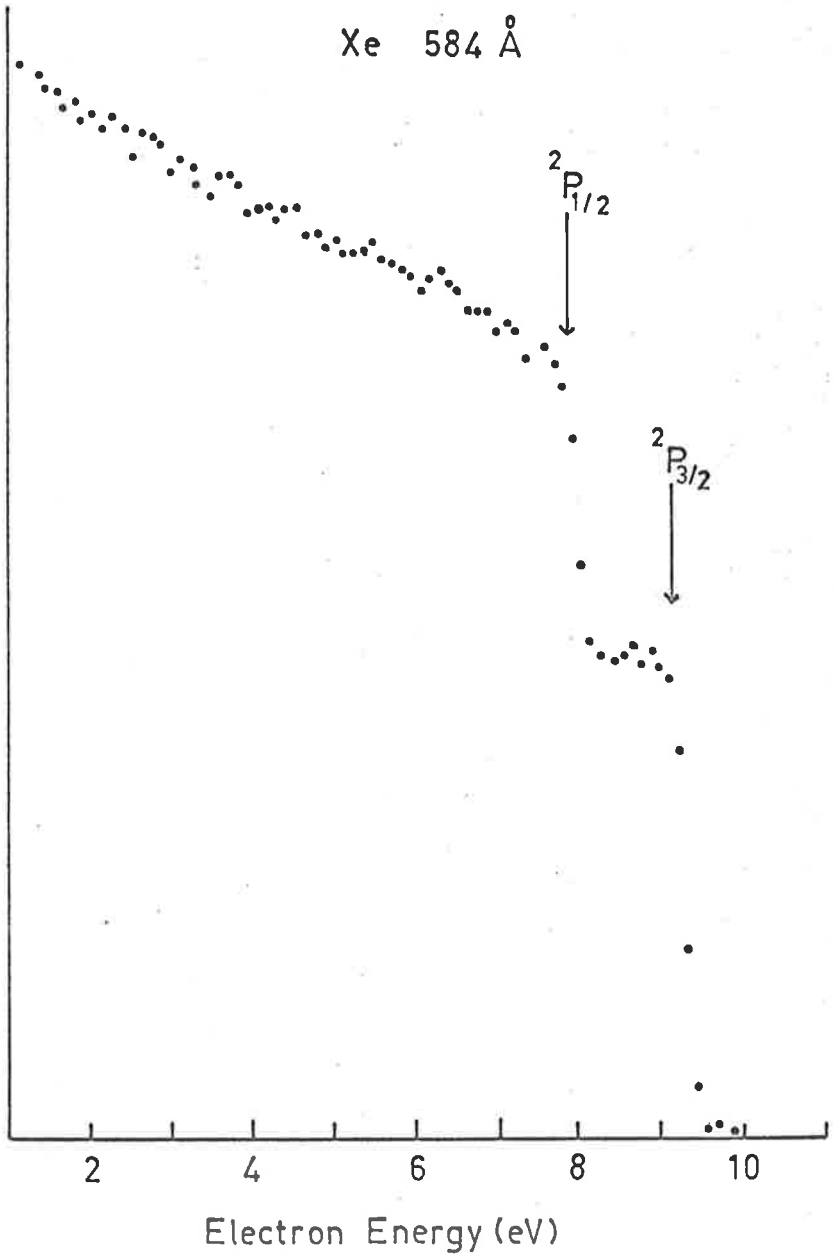

Fig.II.12. Integral photoelectron spectrum for xenon at 584 Å.

present experiment this technique could not be used. Because of the discrete nature of the electron "current" the differentiation had to be carried out numerically. This could be done on the existing integral spectrum by computer, but apart from being rather expensive this was found to be cumbersome, so a finite-difference technique was evolved for electronically differentiating the spectra.

The negative going staircase was modulated with a square-wave having twice the frequency of the staircase and an amplitude of $\sim$0.1-0.2 volts. For example, if the voltage on the staircase at any one time was -v volts, then the retarding potential was (-v+0.1) volts and (-v-0.1) volts respectively on each half cycle of the square-wave. On the positive half of the square-wave the electrons detected were <u>added</u> into the corresponding channel and on the negative half they were <u>subtracted</u> from the same channel. In this manner, the difference between the number of electrons retarded by (-v+0.1) volts and the number retarded by (-v-0.1) volts was stored in the channel corresponding to -v volts. This method of sweeping a voltage "window" across the electron energy spectrum enabled the differential spectrum to be obtained directly.

A block diagram of the electronic controls used to record a differential spectrum is shown in Fig. II.13. The detector input of the 400 channel analyzer had to be blocked while changing the mode of operation of the analyzer from addition to subtraction (or vice-

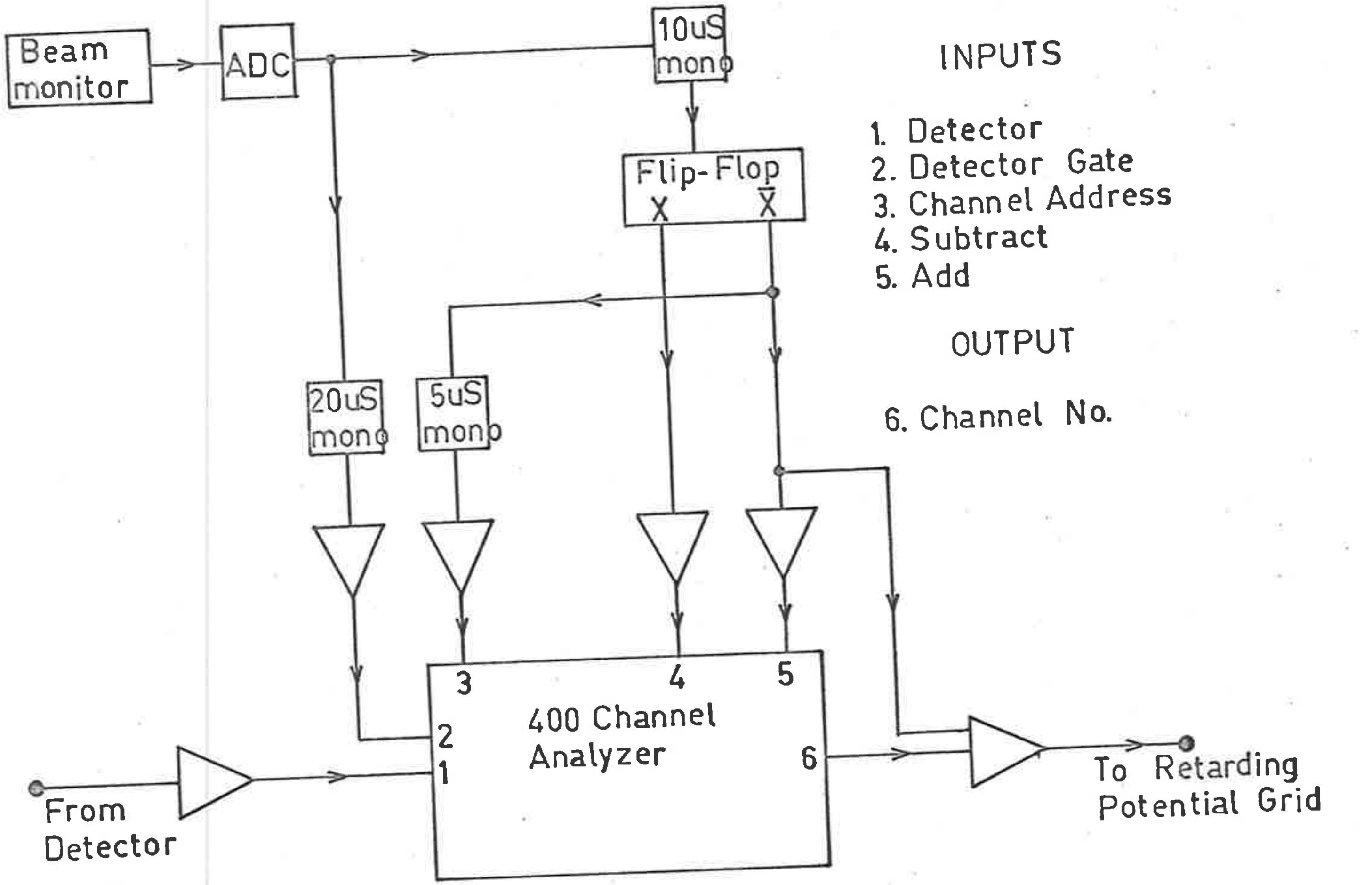

Fig.II.13. Block diagram of the electronic controls used to record a differential spectrum.

versa), in order to prevent spurious pulses from being stored in the memory. To do this, a monostable of 20 μS duration was triggered 10 μS before the add-subtract change and this pulse was used to gate the detector during a change from add to subtract mode or from subtract to add mode. The circuits involved in the operation of the logic control are shown in Fig. II.14. Monostables were constructed by using an integrated circuit dual "NAND" gate (Fairchild μL914) with two discrete components as the time constant elements. The add-enable and subtract-enable waveforms were obtained from the opposite outputs of an integrated circuit binary (Fairchild μL923) thus ensuring that they were completely opposite in phase. All the waveforms were amplified to the required voltage levels by conventional means. The waveforms associated with the operation of the spectrometer are shown in Fig. II.15.

The analog output of the channel number from the pulse height analyzer (∿15mV/400 channels) was fed through a potential divider to the inverting input of an operational amplifier (Fairchild μA709) which was connected to operate as a linear amplifier of constant gain, Fig. II.16. The square-wave modulation was obtained from the add-enable circuit and fed into the non-inverting input of the operational amplifier (also through a potential divider). In this way the magnitude of both the staircase and the square-wave could be varied independently. The balance control on the amplifier was used to set

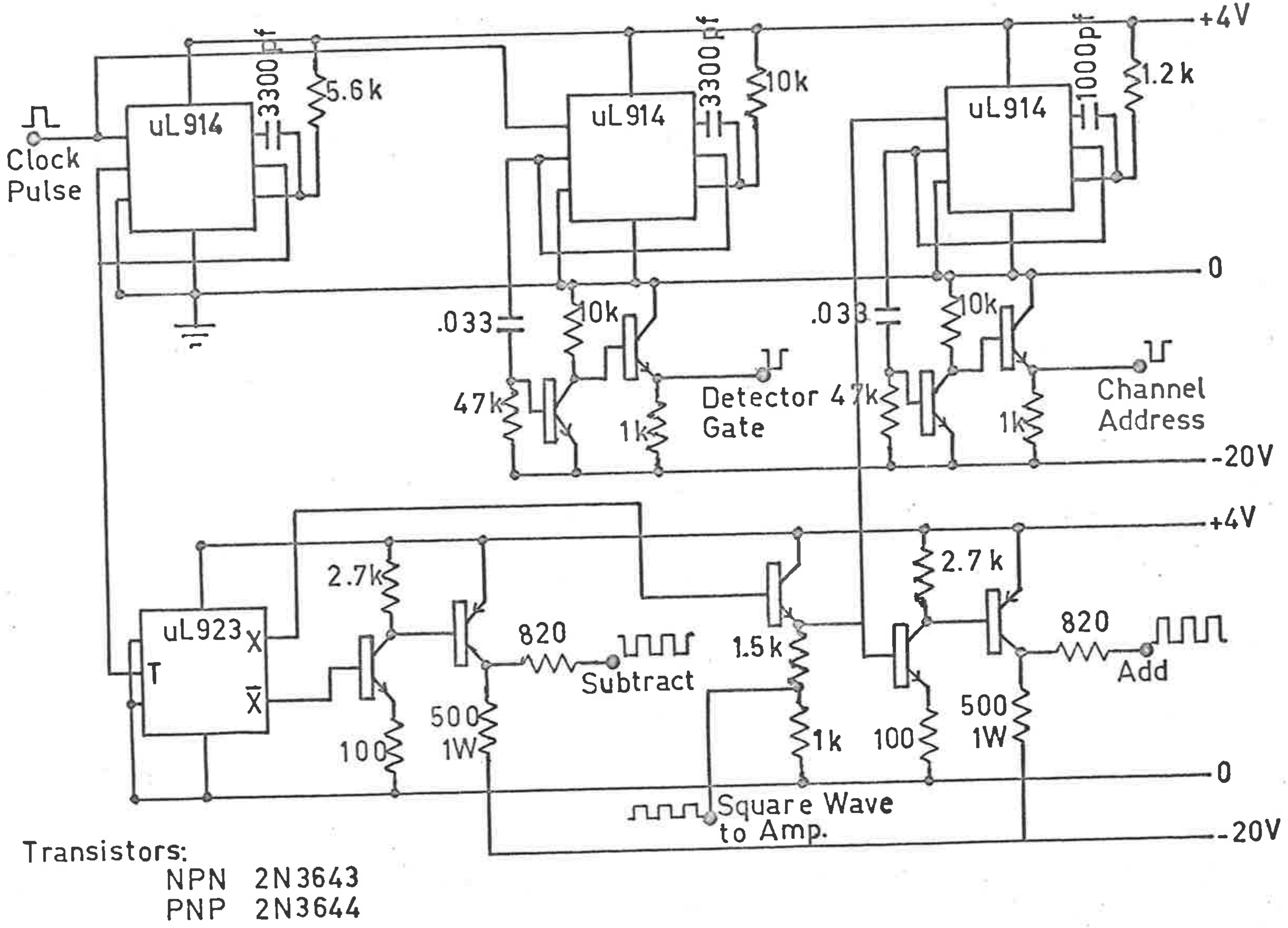

Fig.II.14. Circuits for the logic control of the spectrometer

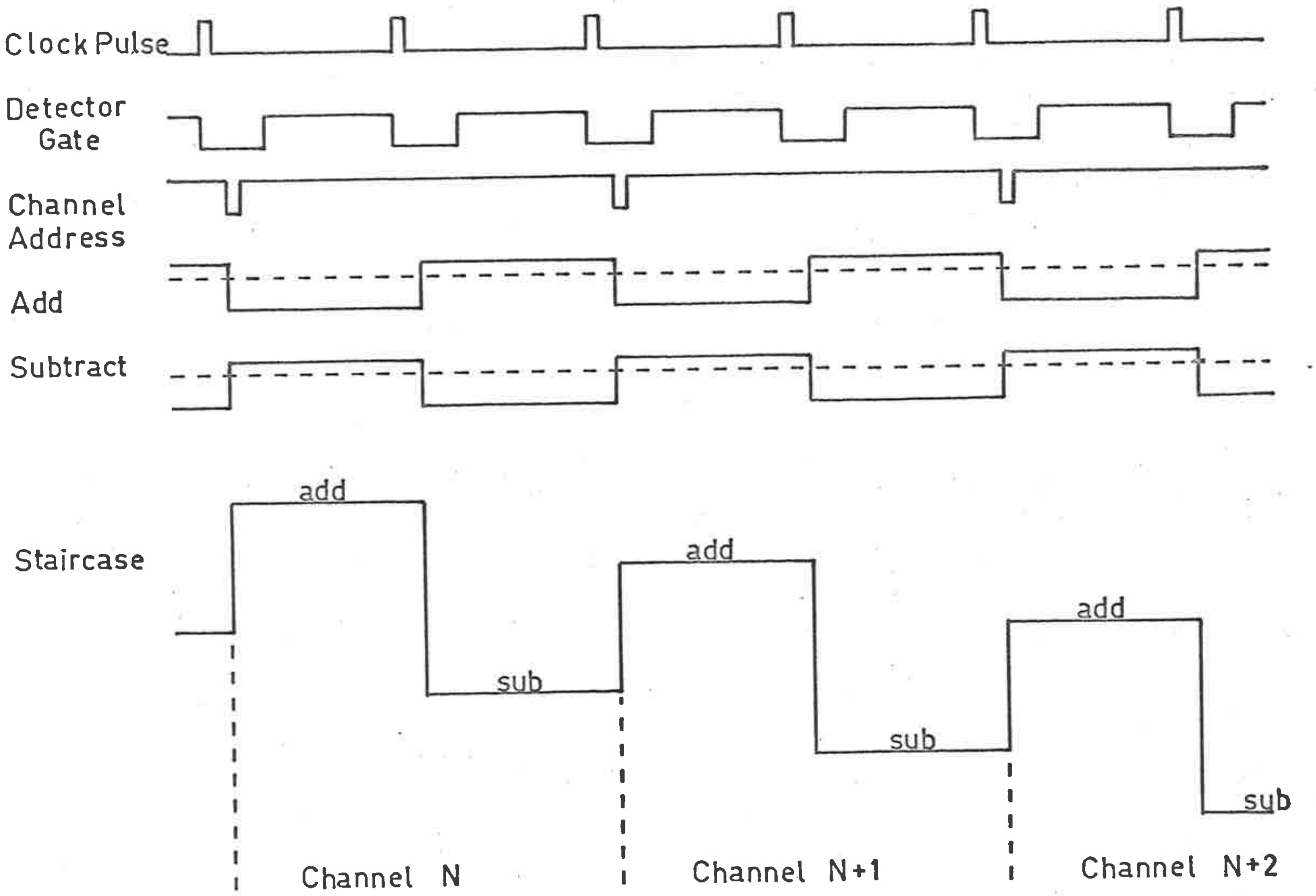

Fig. II.15. Waveforms associated with the operation of the spectrometer.

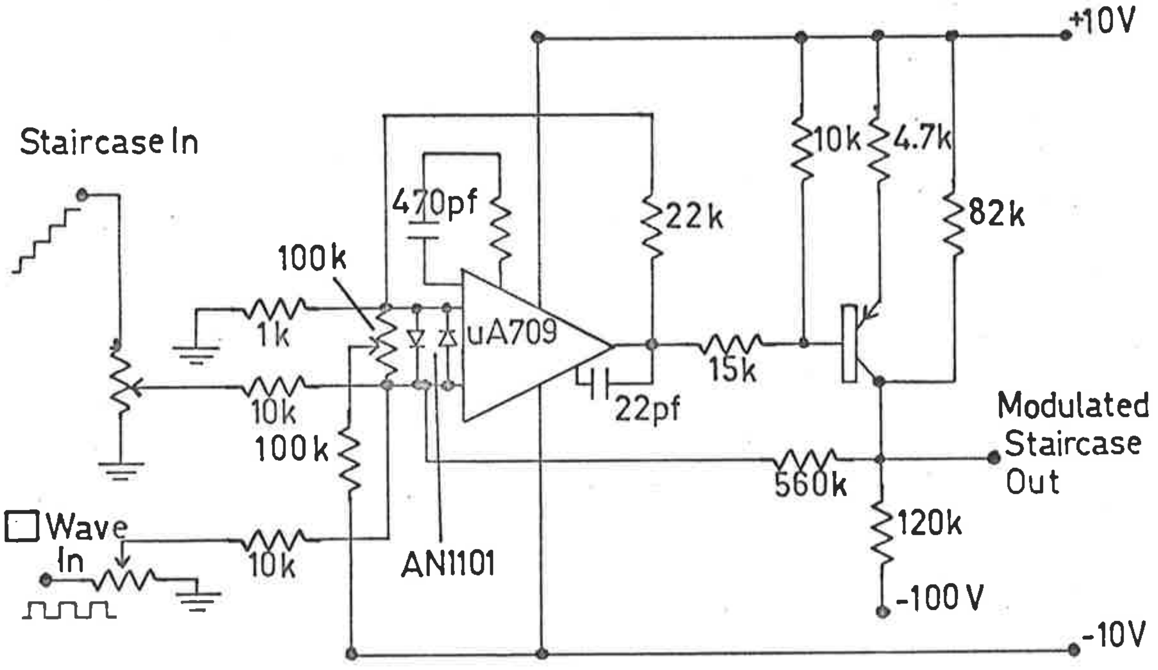

Fig.II.16. The staircase amplifier.

the beginning of the retarding sweep to a slightly positive voltage (0.2 volt).

A photo-copy of a recorder trace of the modulated staircase is shown in Fig. II.17. It can be seen from this trace that the staircase was automatically reset by the analyzer after each scan, thus allowing multiple scans at one wavelength, a facility which was invaluable for reducing statistical fluctuations when the light level was low. The voltage on the staircase was found to be repeatable to better than 0.01 volts over many scans.

Fig. II.18 shows a photograph of the experimental arrangement for recording photoelectron spectra.

II.6.5 Collection of data.

The data for each spectrum was collected in two ways; first a point plot of the spectrum was obtained on an X-Y plotter for use as a rough copy of the spectrum, and secondly the data was put directly onto punch cards for future use on a CDC 6400 computer. This latter method proved useful in reducing the data to a more usable form (Sec. II.7.2). The voltage scale for the spectra was obtained by reading the voltage on the analyzing grid in both add and subtract modes for each spectrum. The voltage was read for at least four points, and the actual value of each point was taken to be the mean of the values for the add and subtract modes; i.e. if the subtract-mode voltage was read as -3.86 V and the add-mode voltage as -3.76 V then the actual

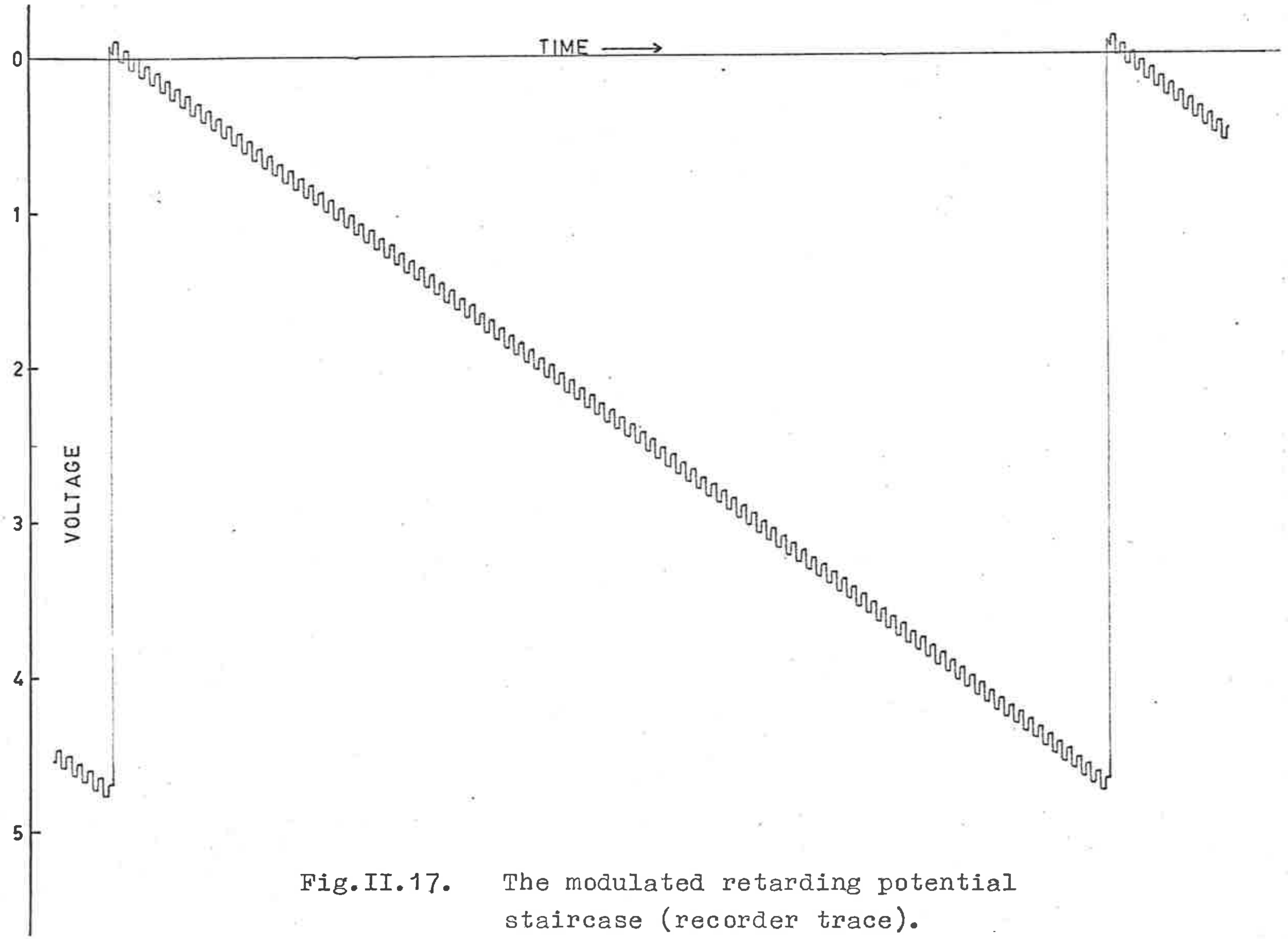

Fig.II.17. The modulated retarding potential staircase (recorder trace).

Fig.II.18. General view of the apparatus used to record photoelectron energy spectra.

voltage for this channel was -3.81 V. The voltages were measured with a digital voltmeter (DYNAMCO Model D2).

II.7 Performance of the spectrometer.

Before using the spectra in any way to determine partial cross-sections of a gas, several characteristics of the spectrometer and the spectra produced by it had to be determined; namely the resolution of the spectrometer, the calibration of the energy scale, the efficiency of the spectrometer at collecting electrons of different energy, and the shape of peaks produced in the spectra.

II.7.1 The atomic spectrum.

A spectrum of argon taken at 584 Å is shown in Fig. II.19. The square-wave amplitude was 0.05 V and the exit slit of the monochromator was set at 100 μ, representing a beam resolution of 0.8 Å (i.e. 0.03 eV at 584 Å). The resolution measured from this spectrum is 1.8% or 0.1 eV full width at half maximum for an electron energy of 5.5 eV. This value was measured on the $^2P_{\frac{3}{2}}$ peak and it must be noted that this resolution was obtained under the best operating conditions of the experiment. Many of the spectra recorded in this work were obtained under less favourable conditions than the above, due mainly to the low light levels which existed in the region below 700 Å in the helium continuum, and also sometimes to small values of the total cross-section.

Fig. II.20 shows a spectrum of xenon at 584 Å where the

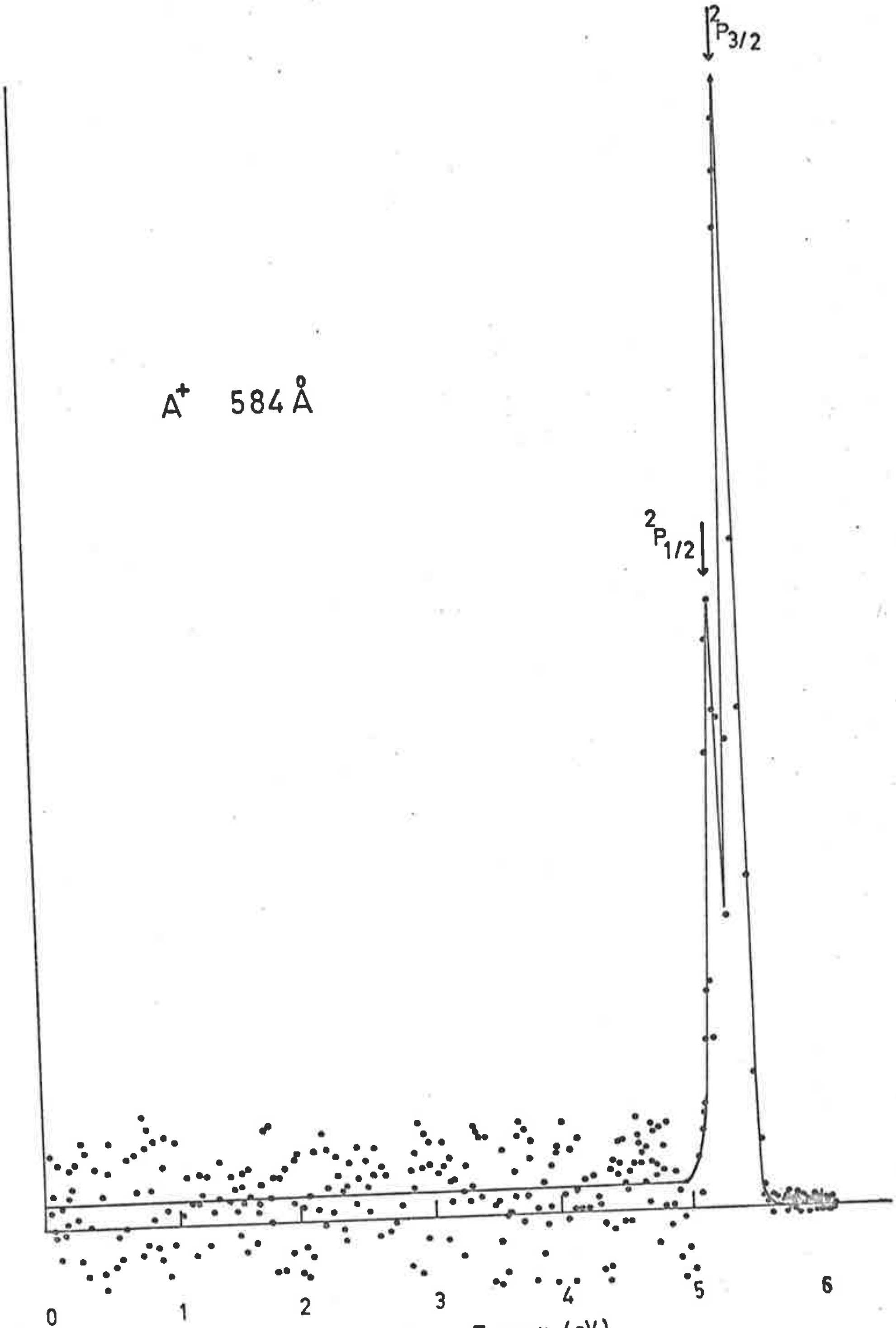

Fig.II.19. Photoelectron energy spectrum for argon at 584 Å.

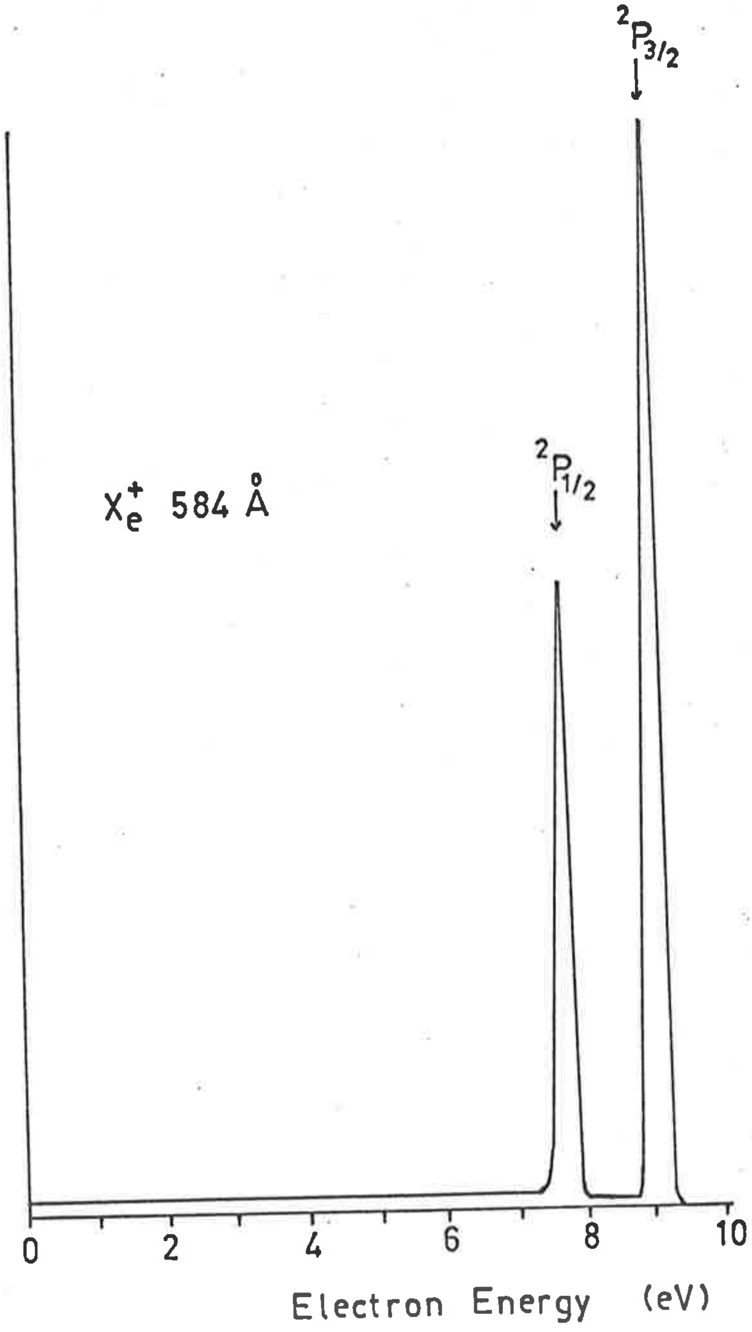

Fig.II.20. Photoelectron spectrum for xenon at 584 Å.

$^2P_{\frac{1}{2}}$ and $^2P_{\frac{3}{2}}$ levels are completely separated.

II.7.2 The molecular spectrum.

Fig. II.21 shows a spectrum for nitrogen at 584 Å in which some of the states of the ion appear as broad peaks containing partially resolved vibrational structure. From this spectrum it can be seen that there was much more difficulty in associating a peak in a molecular spectrum with its corresponding state in the molecule than was the case for atomic spectra. If a peak was very narrow, as in the ground state of N_2^+ $(X^2\Sigma_g^+)$, it was treated as virtually monoenergetic, and was therefore analyzed with direct reference to the argon and xenon spectra.

To assist in analyzing the more complicated peaks, argon and xenon spectra were recorded at a number of wavelengths, and these atomic spectra were divided into two parts. The first was a symmetrical peak, marked A_1 in Fig. II.22, and the second was the remaining low energy part, marked A_2 in Fig. II.22, which was due to electron reflection and secondary emission from the electrode surfaces. Assuming that the peak shape depended only on the peak energy, the ratio of the areas A_1 and A_2 was measured with a planimeter as a function of the peak energy over a range of wavelengths. The curve obtained is shown in Fig. II.23. This was used to unfold the more complicated spectra, by obtaining the low energy contribution to a peak which was otherwise lost under the lower energy peaks. Previously published spectra were

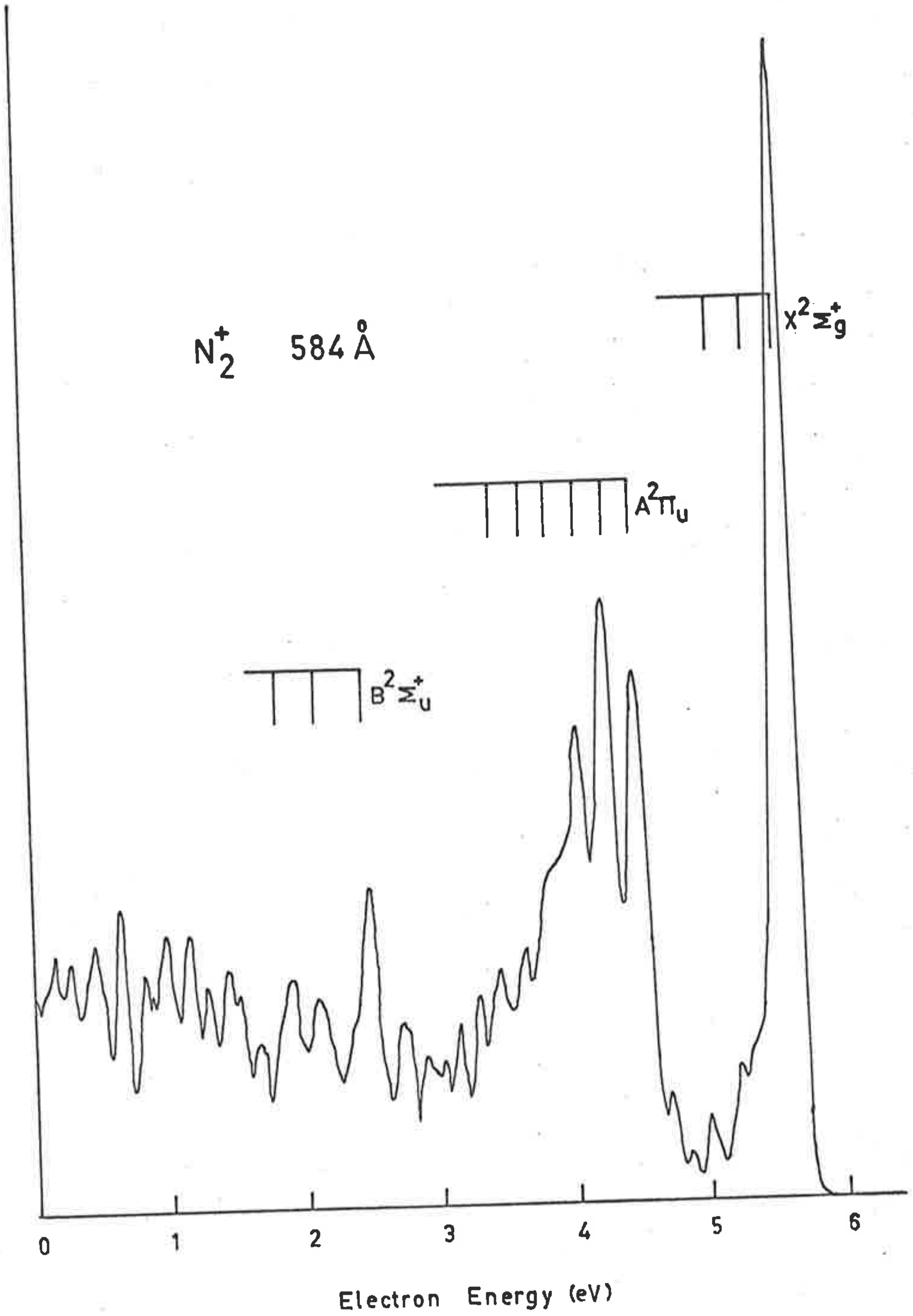

Fig.II.21. Photoelectron spectrum for molecular nitrogen at 584 Å.

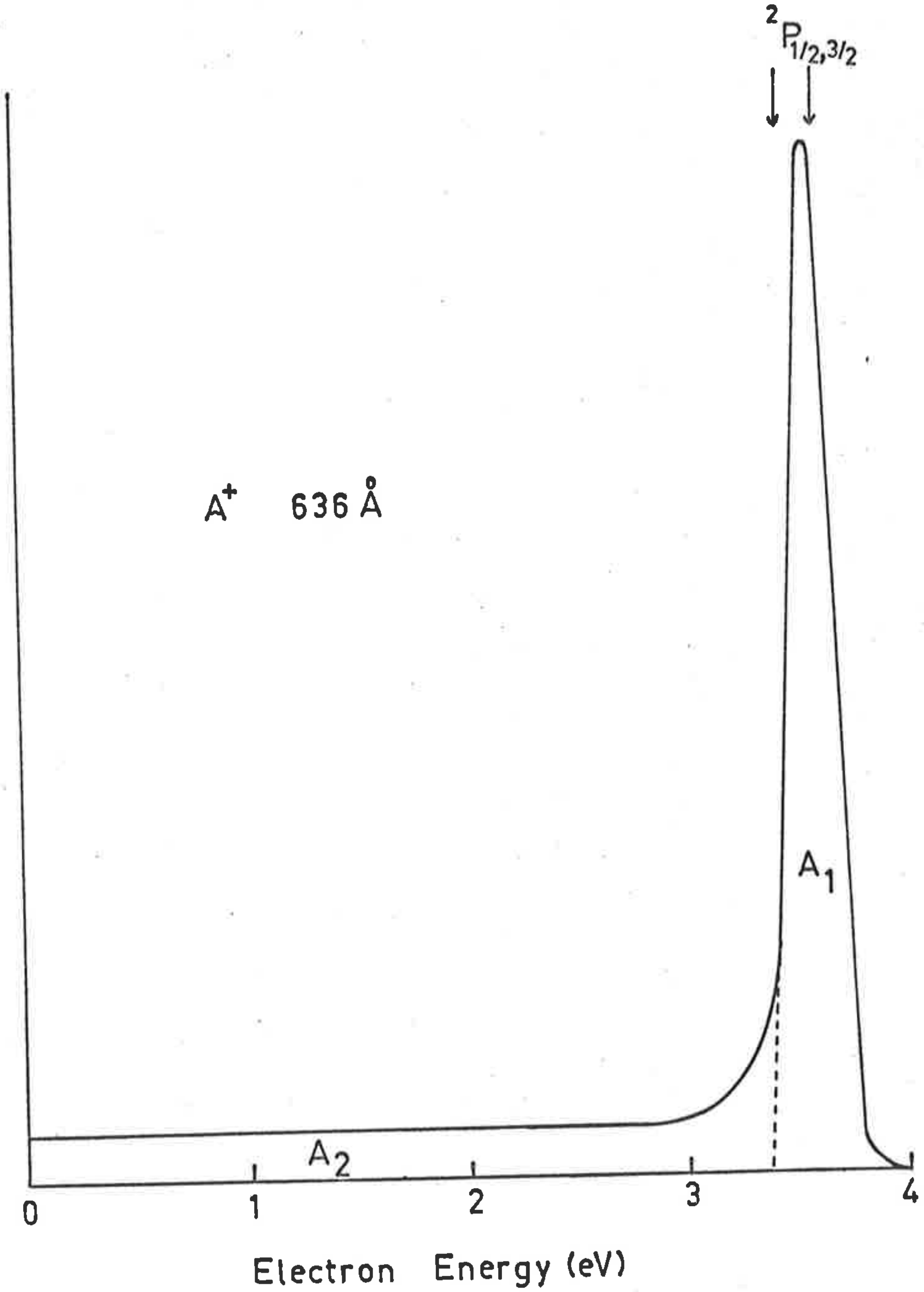

Fig.II.22. Photoelectron spectrum for argon at 636 Å.

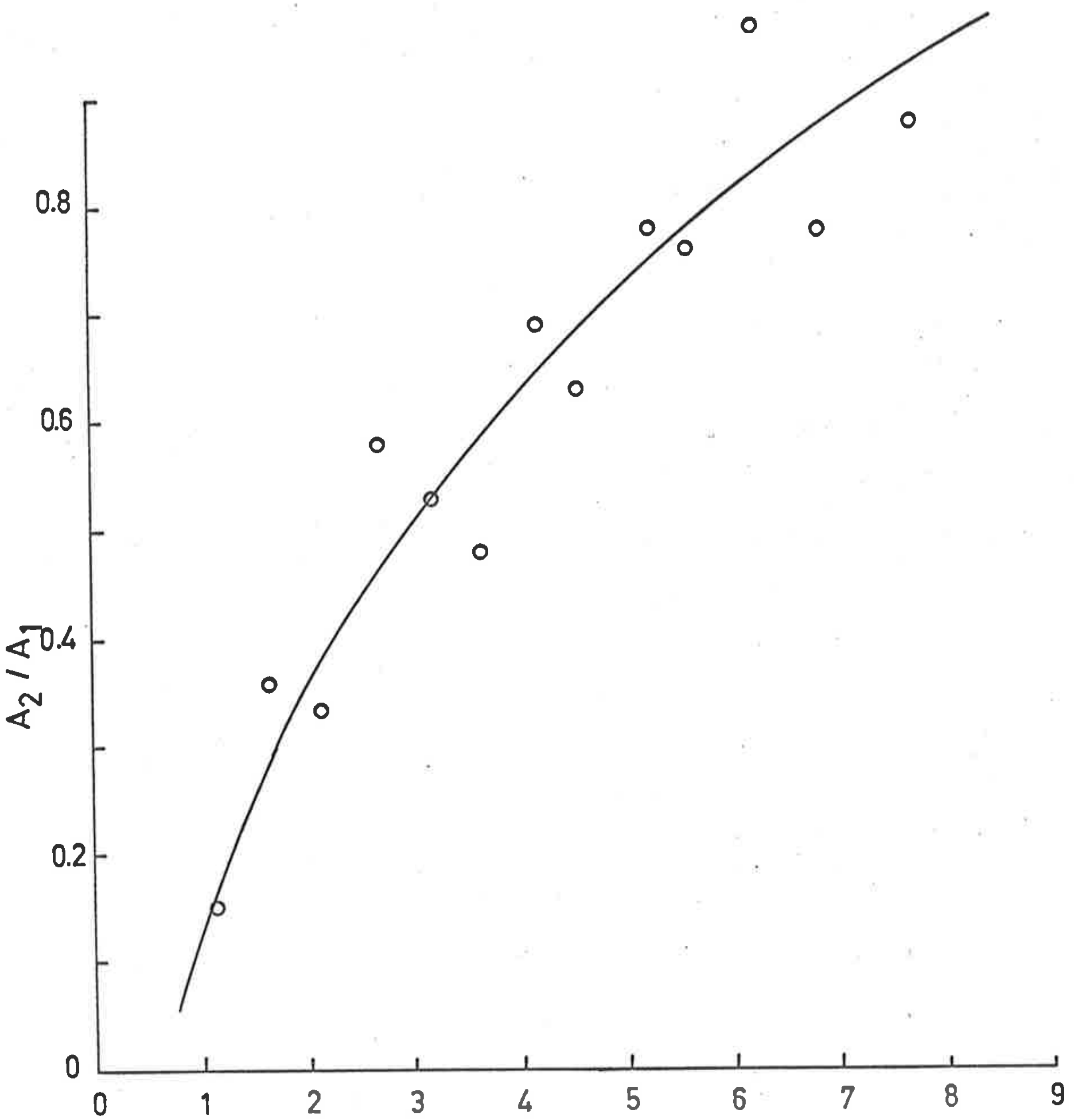

Fig.II.23. Argon and xenon peak shape as a function of peak position.

also used to assist the analysis of complicated spectra.

Many of the spectra which were recorded under adverse conditions (i.e. low light levels and/or small total cross-section) contained data with a considerable amount of scatter, even though recorded for two or three hours, and hence many scans of the retarding potential. These spectra were obtained in a more usable form for analysis, by fitting the data to a polynomial function of degree four. The polynomial was fitted to 15 or 21 points at a time, depending on the amount of scatter in the data. The data fitting process was carried out on the CDC 6400 computer mentioned in Sec. II.6.5. The resulting spectra were plotted by the computer onto a ten inch square graph, and these plots were used directly for the analysis. Fig. II.24 shows an example of the curve fitting for a spectrum of oxygen recorded at 947.7 Å, using a beam resolution of 1.6 Å. The polynomial in this case was fitted over 15 points and was of degree four.

II.7.3 Factors affecting the resolution.

Several factors may affect the resolution of a photoelectron spectrometer. There are the experimental limitations which are introduced by the spectrometer design and its mode of operation, and also more fundamental limits to the resolving power, which are, to a certain extent, independent of the spectrometer.

Turner (TURNER 1968) and Samson (SAMSON 1969) have discussed the fundamental factors involved in the resolving power of photo-

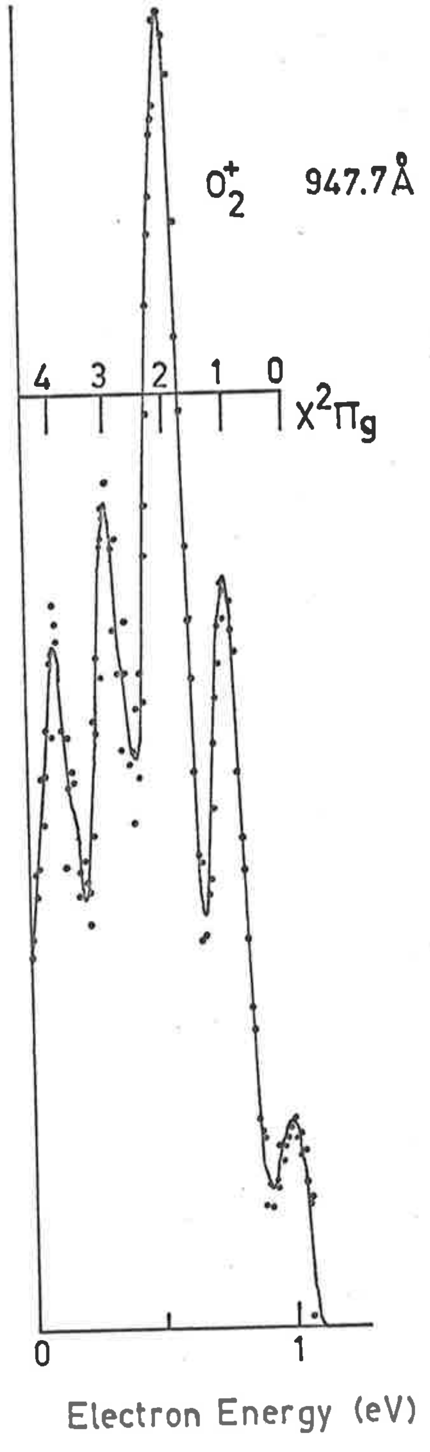

Fig.II.24. Photoelectron spectrum for O_2^+ at 947.7 Å, showing how the polynomial curve (line) was fitted to the data points.

electron spectrometers. A spread in the energy of a photoelectron can be caused by

(1) velocity of the target molecule,

(2) linewidth of the ionizing flux, and

(3) lifetimes of excited ionic states.

Theoretical considerations of (1) show that the spread in energy due to the thermal motion of the molecules is of the order of 10^{-2} eV, for some gases; for example, a photoelectron from N_2 at room temperature with an energy of 20 eV has an energy spread of $\sim$0.01 eV (SAMSON 1969). This problem could be reduced by using a molecular beam.

Samson has measured the linewidths of the He I 584 Å line for several types of light source (DC glow in an uncooled and a water-cooled capillary, aircooled microwave discharge, and a water-cooled condensed spark discharge) at various gas pressures. The half-widths were found to be of the order of 10^{-3} to 10^{-2} eV, the microwave discharge producing the sharpest line. The broadening depended strongly on the lengths of the discharge column, the shorter discharge producing a narrower line.

In the present work, the factors mentioned above were outweighed by less fundamental limits to the resolution which were caused by the design and operation of the spectrometer. The resolution relied upon the accurate alignment of the spherical grids with the point source of electrons. It must also be remembered that the point source actually consisted of a volume of electrons which in itself contributed to the spread in the electron energy. The voltage width of the scanning window also determined to a large extent the limit to the resolution.

One of the biggest factors affecting the resolution was the spacing between the grid wires; i.e. the variation of the potential in the space between the grid wires from the potential of the wires. If a grid consisting of parallel wires is considered, it can be shown (BUNEMANN 1949, BLAKE 1966) that the potential midway between two grid wires is

$$V = V_g - \frac{\Delta\varepsilon}{2\pi} d \ln (\pi r/d) \tag{36}$$

where V_g is the wire potential, $\Delta\varepsilon$ is the difference in the field strengths on either side of the grid, r is the radius of the grid wire and d is their separation. The grids used in the present spectrometer were of wire mesh, and so the potential fluctuations across the surface of the grids were substantially less than for a parallel wire grid with the same dimensions. Thus the above equation provides an upper limit to the potential barrier spread in this case.

For a parallel wire grid of 20 lines per inch and with wire of diameter 0.01 inches the grid factor $(d/2\pi \ln(\pi r/d))$ is 0.0092 inches. If the grid is at a potential of -10V with respect to the cathode, the anode is at 80 V, and both anode and cathode are 1 inch from the grid, then $V - V_g = 0.74$ V. For the fine mesh used which was of 70 lines per inch and of 0.00095 inch diameter wire, the grid factor is 0.0051 inches, giving, for the dimensions of Fig. II.2 and a grid voltage of 10 V, a maximum potential variation of $V - V_g = 0.24$ V. Fig. II.25 shows the potential variation through a plane grid and the ideal curve due to a solid conducting surface.

It was mentioned in Sec. II.4.1 that the initial grids were of 20 lines per inch mesh with a wire diameter of 0.01 inches. The improvement to the resolving power caused by overlaying these grids with the finer electroformed mesh is shown in Fig. II.26 which is a spectrum of argon at 584 Å, recorded with the fine mesh removed. The doublet was not resolved in this spectrum, and the measured energy spread at half height of the combined peak is 0.4 eV, compared to the 0.1 eV obtained in Fig. II.19.

Thus the resolution could be improved by placing the grid wires closer together, but a compromise must be reached between the resolution required and the transparency of the grids to electrons, where a high sensitivity is required.

Another cause of loss of resolution is the influence of stray electric and magnetic fields on the electron paths in a spectrometer. To counteract any such fields, the outside of the spectrometer was wrapped in a layer of Netic, and a cylinder of Conetic was placed

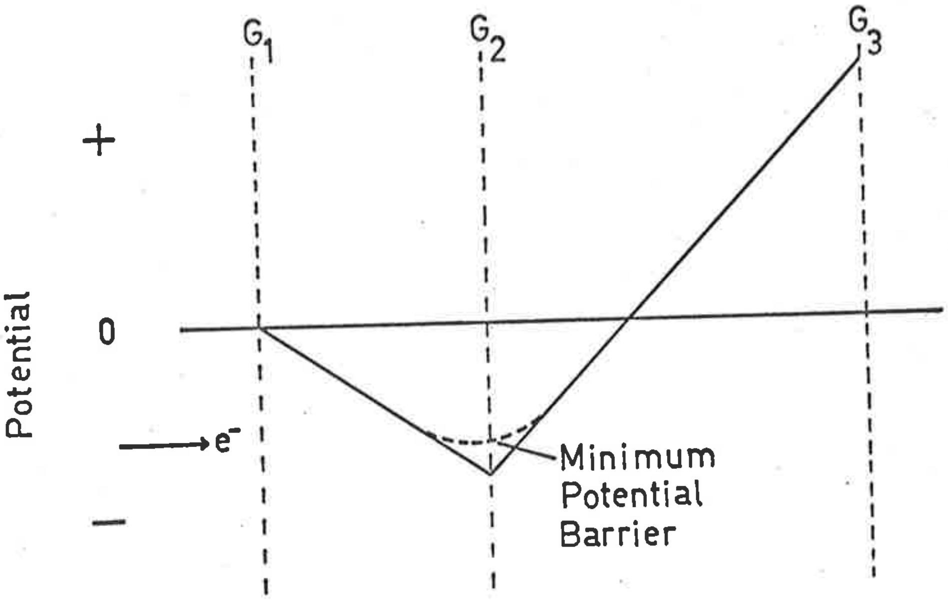

Fig.II.25. Potential barrier in a retarding potential analyzer.

——— through a grid wire.

----- between a pair of grid wires.

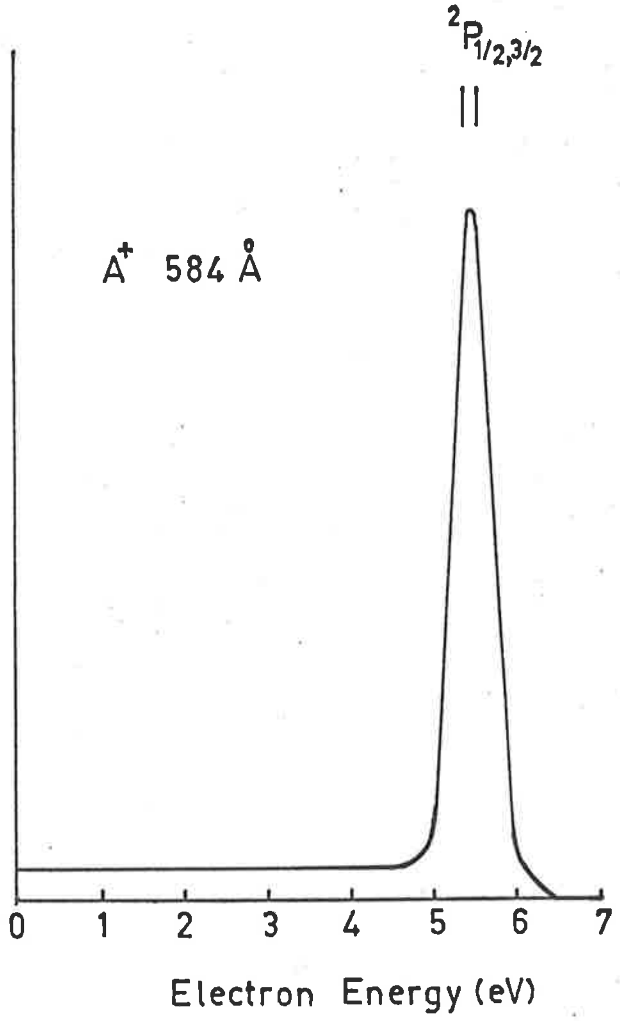

Fig.II.26. Photoelectron spectrum for argon at 584 Å, showing the effect on the resoluti of the spectrometer with the fine mesh grids removed.

inside the spectrometer and around the analyzing grid and the collecting grid (see Fig. II.2). This shielding did not have any noticeable effects on the resolution of the spectrometer, so a pair of Helmholtz coils were placed around the spectrometer as a means of producing a cancellation field. By a trial and error method it was found that the resolution was slightly improved if the horizontal component of the stray magnetic field (∿300 mGauss) was cancelled with the Helmholtz coils. The result of the cancellation is shown in Fig. II.27, which is a spectrum of argon at 774 Å, (a) without any cancellation, and (b) with the cancellation mentioned above. The argon doublet is better separated in the latter case.

Most of the spectra in this thesis were recorded using a resolution of 0.15 - 0.20 eV, and although this was not as good as that which could be obtained at some wavelengths, it was the best obtainable under the adverse conditions (eg. low light levels) which were encountered at many wavelengths.

II.7.4 Calibration of the energy scale.

The energy scale of the spectra was calibrated using the position of the argon and xenon peaks at a variety of wavelengths as a standard. The $^2P_{\frac{3}{2}}$ and $P_{\frac{1}{2}}$ levels of argon were taken to be at 15.76 eV and 15.94 eV respectively, and the $^2P_{\frac{3}{2}}$ and $^2P_{\frac{1}{2}}$ levels of xenon at 12.08 eV and 13.44 eV respectively (METZGER 1965).

The wavelength scale of the monochromator was calibrated by

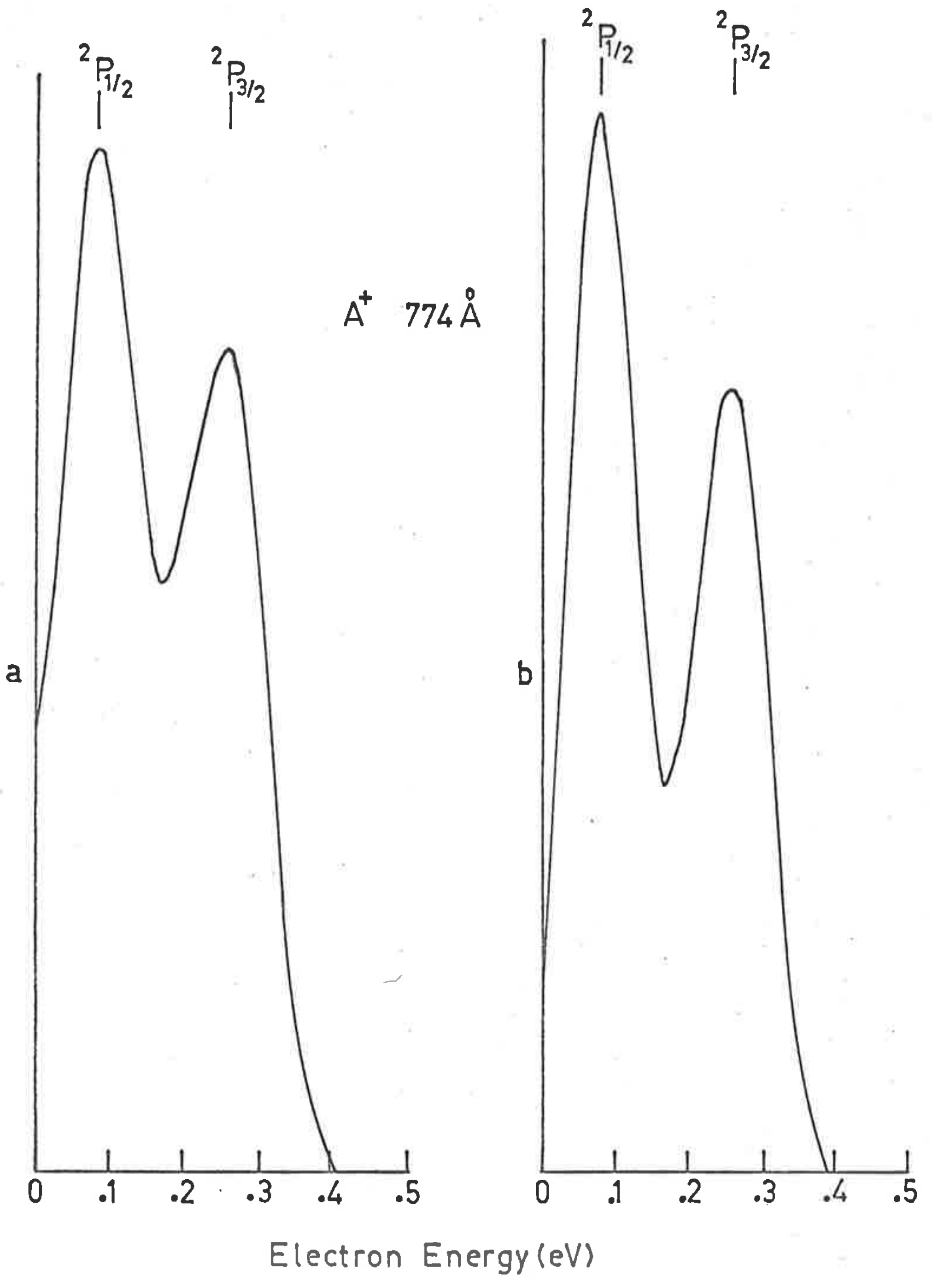

Fig.II.27. Photoelectron spectra for argon at 774 Å.
(a) no cancellation of magnetic field
(b) cancellation of horizontal component of stray magnetic field.

using the 584 Å and 744 Å lines (He and Ne respectively) which were present in the helium continuum, as standards. The peak energy for the states in argon and xenon were measured at a number of wavelengths, and the results were plotted against the expected peak energy, Fig. II. 28. The line in this diagram is a best fit to the data points by the least squares method, and the broken line is the ideal case. The curve indicates that the apparent energy scale is displaced by about 0.2 eV from the true scale.

The energy scale was linear to at least 0.1 eV peak energy which allowed confidence to be placed in peaks which were measured at low energies.

II.7.5 Electron collecting efficiency.

One possible source of error in the spectra was the variation of the electron collecting efficiency with the electron energy. The electron collecting efficiency was measured as a function of electron energy using argon as a source of monoenergetic electrons, whose energy could be varied by changing the wavelength of the incident beam.

The ratio of the total electron current detected to the intensity of the transmitted radiation (n_e/I_t) is proportional to the total photoionization cross-section (k) provided the gas pressure is sufficiently low that there is no significant attenuation of the incident beam (SAMSON 1968b). This ratio was measured in the wavelength range 584-780 Å (i.e. to the $^2P_{\frac{1}{2}}$ edge) while the pressure was

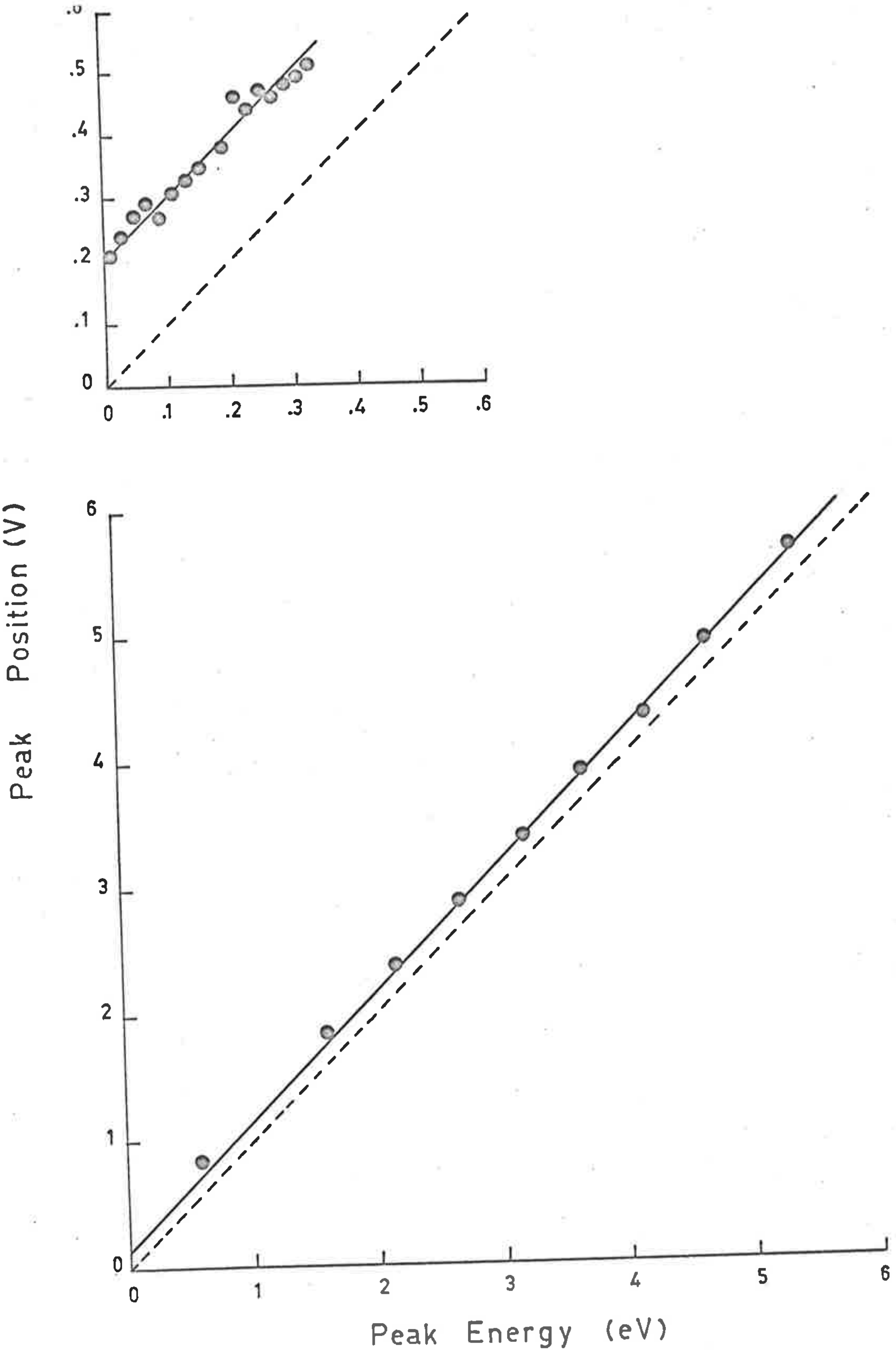

Fig.II.28. Calibration of the energy scale obtained from argon and xenon spectra at various wlths.

kept at a constant value. The ratio was then divided by the absorption coefficient giving

$$y(E) = \frac{n_e(E)}{I_t(E)\ k(E)} \tag{37}$$

where E is the electron energy, so that any deviations from a constant value in y would give a measure of the discrimination in the electron collecting efficiency. The value of y was plotted as a function of the energy of the $^2P_{\frac{1}{2}}$ electron and this curve is shown in Fig. II.29. There was a slow variation in y over the energy range 0.2 - 3.0 eV, with the value flattening out above 4.0 eV. In the region 0 - 0.2 eV the electron collecting efficiency displayed a sharp increase so that electrons of 0.01 eV were collected about four times as efficiently as 1.0 eV electrons. Thus for most of the electron energy region the collecting efficiency was a constant value, only increasing significantly for electrons of very low energy.

There were several possible reasons for this energy discrimination. Electron collisional cross-sections with residual gases in the system could have contributed to the effect; the cross-section for electron-gas interactions is a strong function of the electron energy (BRODE 1933). The large contact potential (∿0.7 volts) between the aluminium honeycomb and its brass envelope in the electron trap could also have caused a discrimination favouring low energy electrons. The

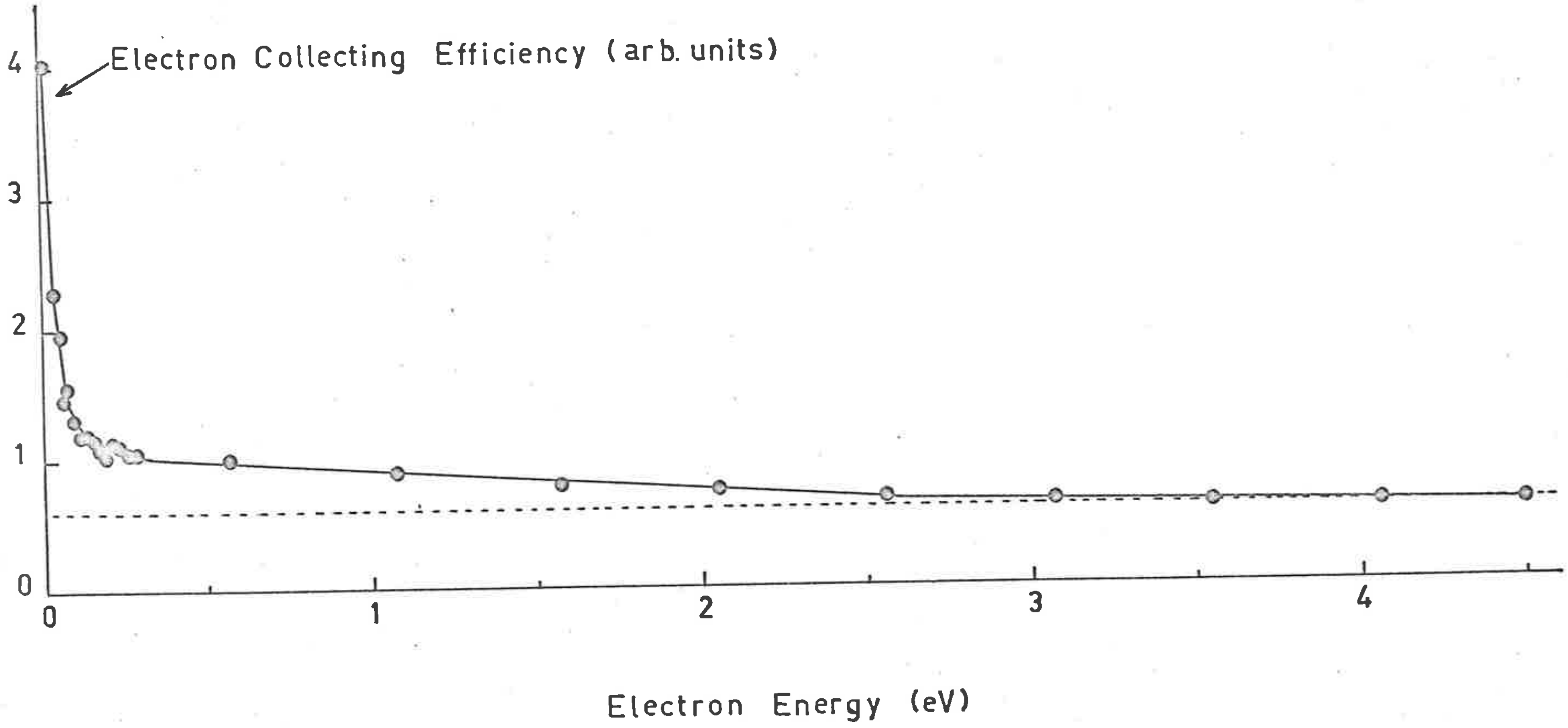

Fig.II.29. Electron collecting efficiency of the spectrometer as a function of the electron energy.

discrimination did not occur unless electrons of low energy were actually formed by the photon-gas interaction. Thus the low energy tail of the argon spectrum in Fig. II.19 was quite level, indicating that these low energy electrons were probably formed by scattering from the grid wires and hence were not affected by the discrimination process. This fact seemed to indicate that the problem originated around the source of the electrons and not elsewhere in the spectrometer.

The effect that this discrimination had on the spectra is illustrated in Fig. II.27 for argon at 774 Å, where the $^2P_{\frac{3}{2}}$ and $^2P_{\frac{1}{2}}$ peaks of A^+ are of about the same magnitude. Samson and Cairns (SAMSON 1968b) have shown that the ratio of ions formed in these two states is a constant value (1.98) for electrons with energies over the range 0-6 eV.

Therefore, the spectra needed to be corrected in some cases for this energy discrimination, where low energy electrons were present. However, the correction was only an important one at very low energies.

CHAPTER III

PARTIAL PHOTOIONIZATION CROSS-SECTIONS

III.1 Carbon monoxide.

It was shown in Chapter II that the photoelectron spectrometer described could be used to record photoelectron spectra with fairly well known characteristics. The molecular spectra generally contained several peaks, corresponding to the different ionic states of the molecule. These spectra were analyzed to give partial photoionization cross-sections for the production of ions in particular states and the variation of the partial cross-sections with the incident wavelength was studied by recording spectra over a range of wavelengths.

III.1.1 Carbon monoxide photoelectron energy spectra.

Photoelectron spectra for carbon monoxide were recorded at 584 Å and over the wavelength range 600-860 Å at 5 Å intervals. Since identification of the electronic states only was needed in these spectra some of the resolution was sacrificed in order to obtain good statistics in regions (of the helium continuum) where the light intensity was low; the incident beam resolution was 8 Å and the energy resolution was ∿0.3 eV for most of the spectra. The carbon monoxide was obtained from AUSTRALIAN LIQUID AIR LTD. and was used without further purification. The photoelectron spectrum from carbon monoxide obtained at 584 Å is shown in Fig. III.1 and may be compared with the similar spectrum of carbon monoxide due to Turner and May (TURNER 1966), shown in the inset of Fig. III.1. The latter result was obtained using a 180° magnetic-field electron velocity analyzer, whose resolution was considerably better than that of the present work.

III.1.2 Identification of the ionic states.

Each peak in a spectrum could be identified with one of the states of the molecular ion, excepting spectra below 605 Å which showed a peak corresponding to an appearance potential of ∿20.7 eV. This peak was thought to be associated with the phenomenon of dissociative ionization by a process like:

$$CO(X^1\Sigma^+) + h\nu \rightarrow C^+(^2P) + O(^3P) + e^-$$

Weissler et al (WEISSLER 1959) reported the appearance potential of C^+ (^2P) as 22.3 ± 0.4 eV. A similar process is thought to explain the peak at 20.7 eV observed in these spectra. The different processes which lead to ionization of carbon monoxide are summarised in Table III.1. There is good agreement between the present results and previous values for the appearance potentials of the three electronic states of CO^+.

The photoelectron spectrum 584 Å showed that the $X^2\Sigma^+$ state had a width comparable to the resolution of the instrument, indicating

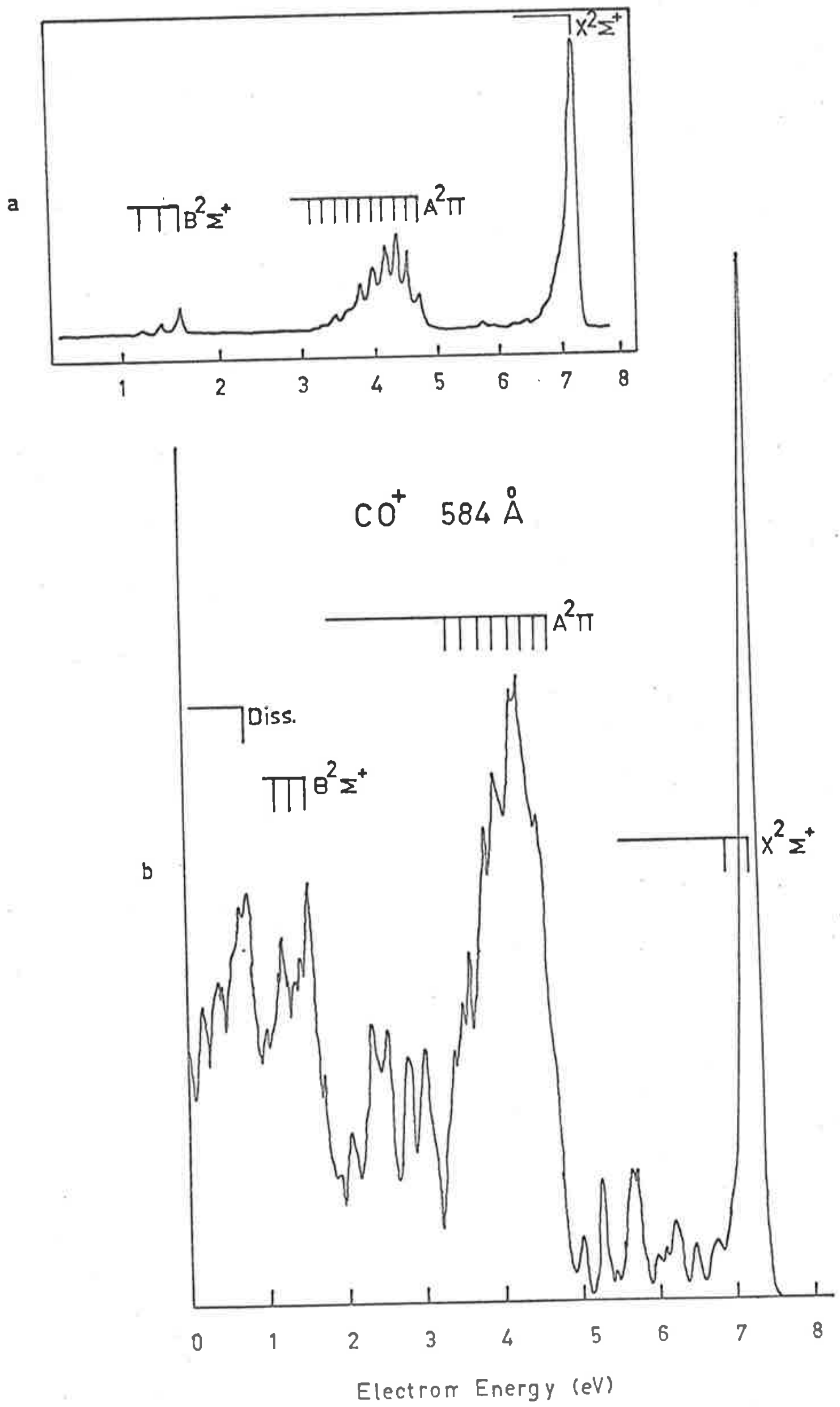

Fig.III.1. Photoelectron spectrum for CO at 584 Å.
(a) TURNER 1966 (b) Present work.

TABLE III.1

Carbon Monoxide Photodisintegration Processes

Process	Appearance Potential (eV)			
	TURNER 1966	COLLIN 1969	Spectroscopic(a)	Present Work
$CO(X^1\Sigma^+) + h\nu \rightarrow$				
$CO^+(X^2\Sigma^+) + e^-$	14.00	14.01	14.013	14.0
$CO^+(A^2\Pi) + e^-$	16.54	16.55	16.536	16.5
$CO^+(B^2\Sigma^+) + e^-$	19.65	19.69	19.674	19.7

(a) TANAKA 1942, TAKAMINE 1943, LINDHOLM 1954a.

that only the v'=0 level of this state was present with any significant intensity. Both the $A^2\Pi$ and the $B^2\Sigma^+$ states contained partially resolved vibrational structure. The photoelectron spectrum of the isoelectronic molecule nitrogen, recorded at 584 Å, is shown in Fig. II.21. The close resemblance of this spectrum to that of carbon monoxide can be seen, apart from the peak which has been attributed to dissociation in the latter.

Fig. III.2 shows photoelectron spectra recorded at 625, 640, 675 and 730 Å. At 625 Å there are three main peaks which can be attributed to the three electronic states as shown, while the

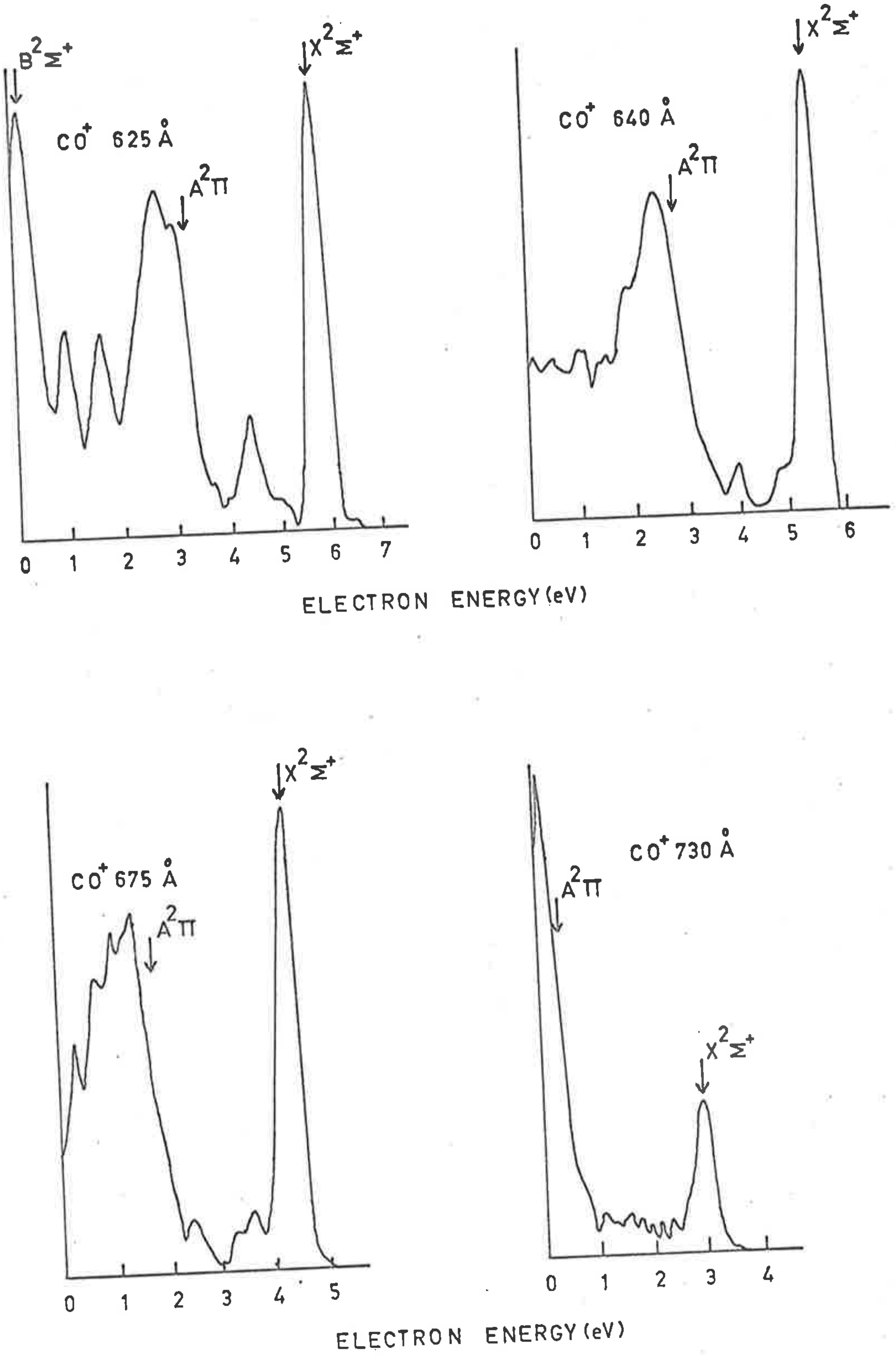

Fig. III.2. Photoelectron spectra for CO at 625, 640, 675, and 730 Å.

structure between the $X^2\Sigma^+$ and $A^2\Pi$ states, and between the $A^2\Pi$ and $B^2\Sigma^+$ states has been attributed to enhancement of the higher vibrational levels of the $X^2\Sigma^+$ and $A^2\Pi$ states respectively. This effect which has been attributed to preionization of the molecule, will be discussed further in Sec. III.1.5 and in Chapter IV. For the determination of the partial photoionization cross-sections for the electronic states, this "anomalous" structure was included as part of the appropriate electronic state. The spectrum at 730 Å shows only a few of the vibrational levels of the $A^2\Pi$ state as well as the $X^2\Sigma^+$ state.

III.1.3 Unfolding the spectra.

In order to obtain the relative transition probabilities for each of the states from the photoelectron energy spectra, the area associated with each state in the spectrum had to be determined.

This was done with the help of the argon and xenon spectra, and the A_1/A_2 versus peak energy curve of Fig. II.23. The spectra were unfolded by the following procedure. The most energetic peak was completed to form a symmetrical shape, unless it was obviously not symmetrical, and the area (A_1) contained by this shape was measured with a planimeter. The area of the low energy tail, which was lost under the less energetic peaks, was then found by reference to the curve shown in Fig. II.23. The complete area associated with the state was then drawn in as shown in Fig. III.3. Each successive peak was treated in the same way, the self-consistency of the

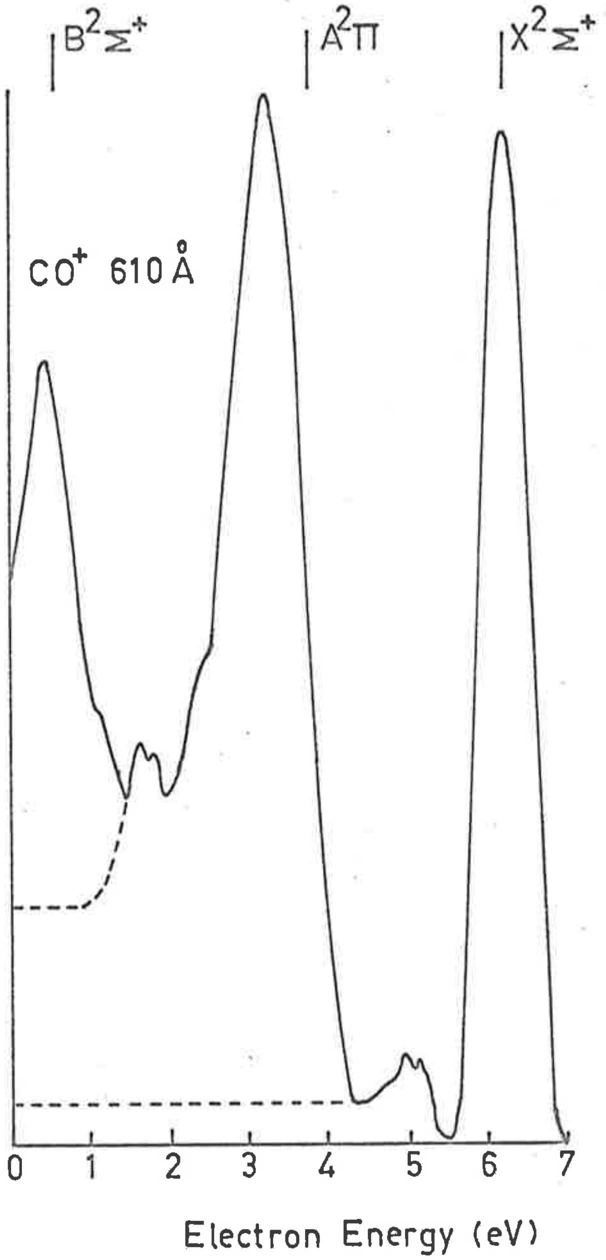

Fig. III.3. Photoelectron spectrum for CO at 610 Å illustrating the unfolding procedure.

unfolding process being indicated by the area which remained for the last peak.

III.1.4 Partial Photoionization cross-sections for carbon monoxide.

The number of ions produced in each state was assumed to be directly proportional to the area associated with that state in the spectrum. Thus the measurement of this area allowed the percentage of ions formed in a particular state to be found. This percentage was defined as the branching ratio of the state concerned. The branching ratios of carbon monoxide are tabled in TABLE III.2 and are shown as a function of the incident wavelength in Fig. III.4; the solid lines are the values given by Schoen (SCHOEN 1964). Schoen used a retarding potential analyzer of cylindrical geometry, and although his results do not contain the detail of the present results they are in reasonable agreement if the detailed structure is averaged out. The most noticeable difference is in the $B^2\Sigma^+$ state where his value is slightly lower than the present one. The branching ratios of the $X^2\Sigma^+$ and the $A^2\Pi$ states are relatively constant over the wavelength range considered, except at the threshold for the $B^2\Sigma^+$ state where the ratio for this state increases at the expense of the $A^2\Pi$ state. The ratio for the $A^2\Pi$ state increases slowly from its threshold, an effect due to the broad nature of this peak which can be attributed to the transition probability distribution among the vibrational levels. Thus as the photon energy is increased from

TABLE III.2

Branching Ratios for Carbon Monoxide

Wavelength		Branching Ratios (%)			Dissociation
(Å)	(eV)	$X^2\Sigma^+$	$A^2\Pi$	$B^2\Sigma^+$	
584	21.21	25	55	15	5
600	20.66	39	45	11	5
605	20.49	40	46	14	
610	20.32	32	59	9	
615	20.16	33	55	12	
620	20.00	34	57	9	
625	19.84	35	54	11	
630	19.68	34	59	7	
635	19.52	39	61		
640	19.37	34	66		
645	19.22	42	58		
650	19.07	37	63		
655	18.93	40	60		
660	18.78	41	59		
665	18.64	40	60		
670	18.50	45	55		
675	18.37	39	61		
680	18.23	34	66		
685	18.10	39	61		
690	17.97	39	61		
695	17.84	38	62		
700	17.71	37	63		
705	17.59	42	58		
710	17.46	37	63		
715	17.34	37	63		
720	17.22	40	60		
725	17.10	46	54		
730	16.98	43	57		
735	16.87	58	42		
740	16.75	67	33		
745	16.64	75	25		
750	16.53	81	19		
755	16.42	100			

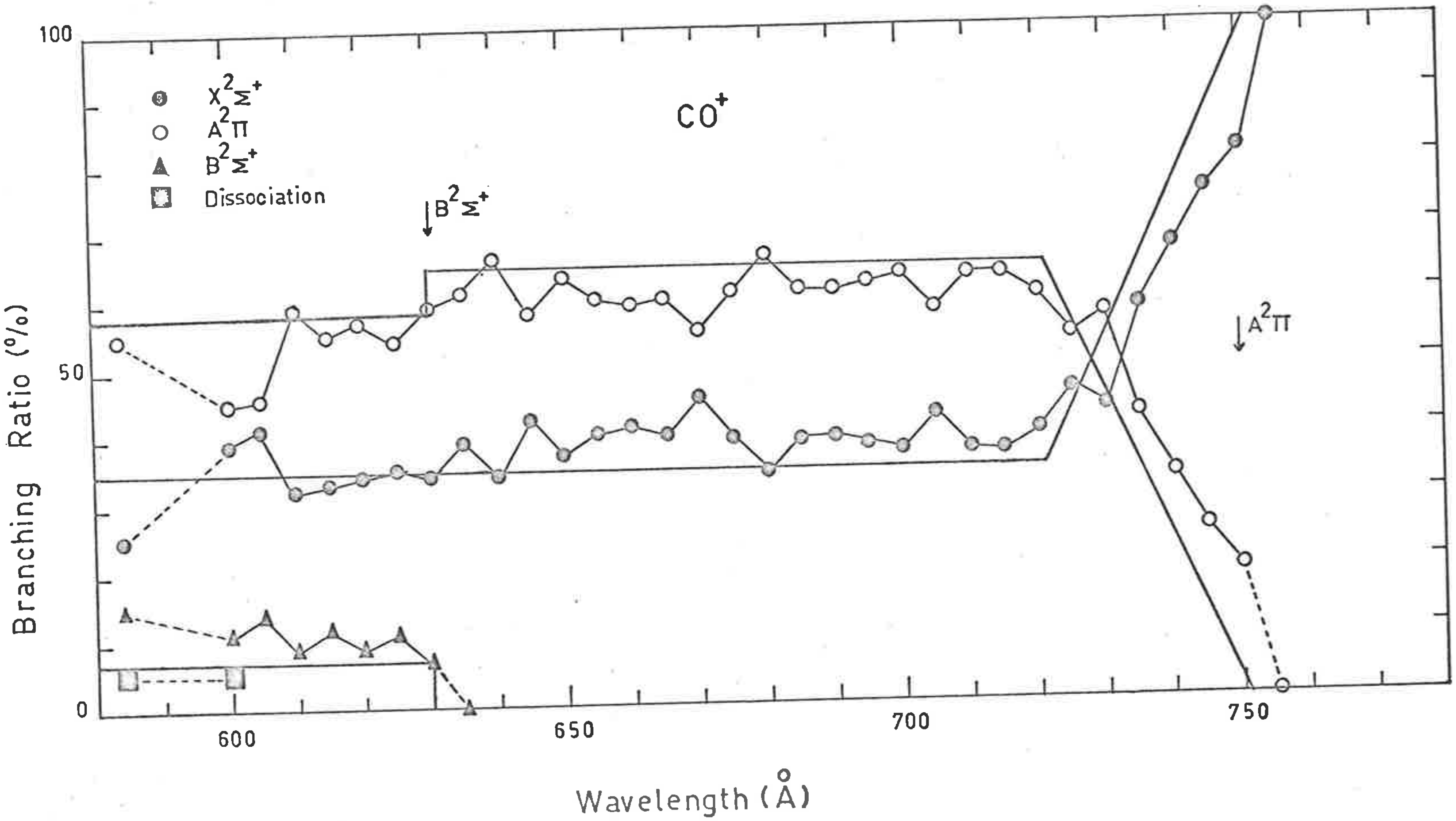

Fig.III.4. Branching ratios for the various photoionizing processes in CO

——— SCHOEN 1964.

16.5 eV more vibrational states become available for ionization, and so the relative cross-section for the whole state increases, ideally in a step-like manner.

The results shown in Fig. III.4 were combined with the total photoionization cross-section results of Cook et al (COOK 1965), which were averaged over 8 Å intervals to produce an effective resolution equivalent to the present experiment; the resulting partial photoionization cross-sections are shown in Fig. III.5.

III.1.5 Preionization processes.

The total photoionization results of Cook et al (COOK 1965) for carbon monoxide show much preionized structure in the wavelength range 600-900 Å. This structure has been divided into many series and progressions, where the series converge to one of the excited states of the CO^+ ion: eg. the $CO(X) \rightarrow CO^+(A)$ and $CO(X) \rightarrow CO^+(B)$ Rydberg series which cover the range 720-820 Å and 630-700 Å respectively.

The photoelectron spectra which have been recorded in these regions often show "extra" structure for the $X^2\Sigma^+$ and $A^2\Pi$ states, for which, it is suggested, the preionization states of the molecule are responsible. This effect has been noticed previously (see Sec. I.7.3). For incident wavelengths above 760 Å the effect of the preionized states on the vibrational distribution of the $X^2\Sigma^+$ state was particularly noticeable, and these spectra will be discussed in more detail in the next Chapter.

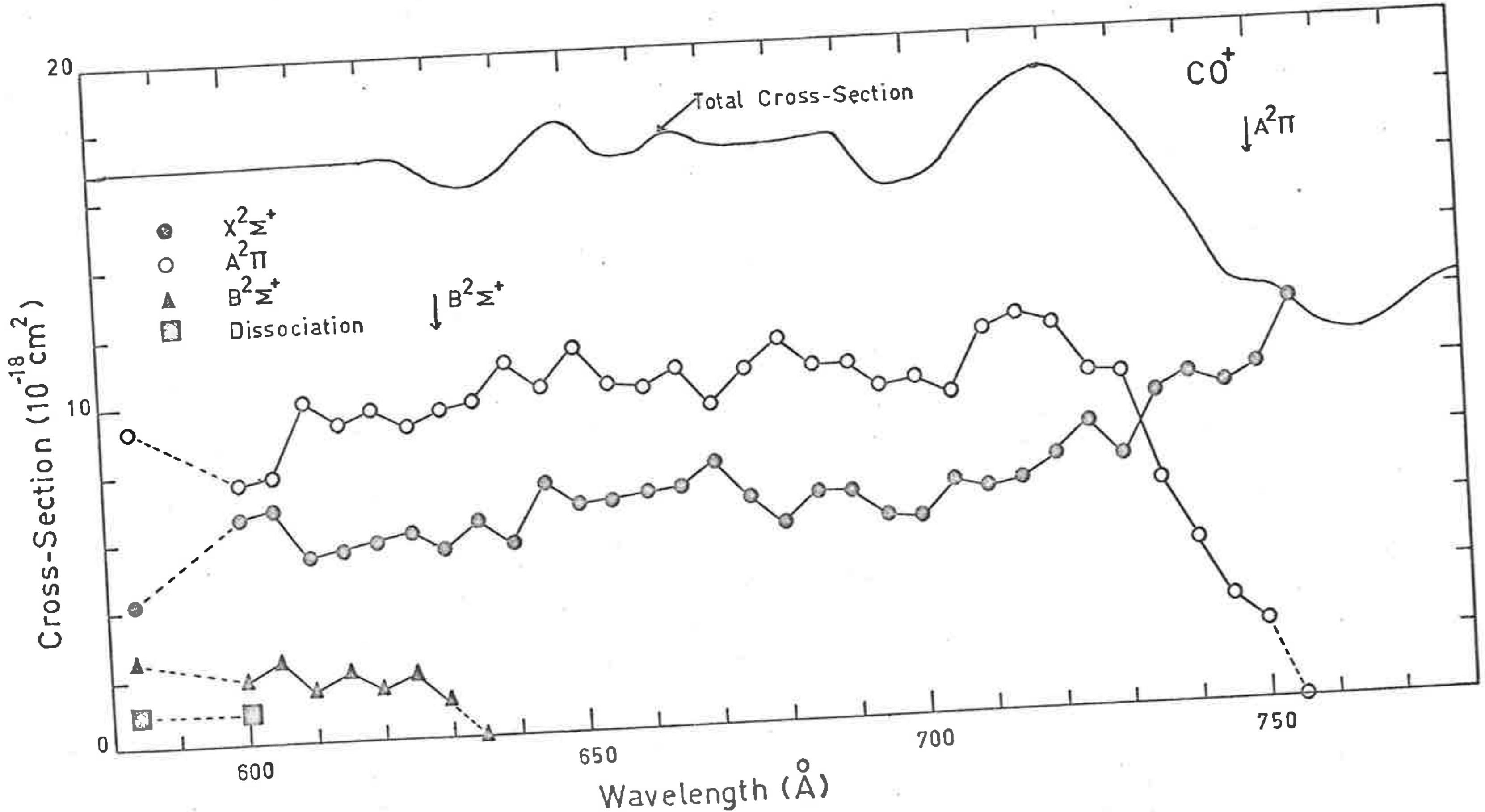

Fig.III.5. Partial photoionization cross-sections for carbon monoxide.

For those spectra which showed vibrational distribution anomalies in the $A^2\Pi$ state, no attempt was made to analyze the structure in more detail and the structure was included in the partial cross-section analysis as an integral part of the $A^2\Pi$ state.

III.2 Nitric oxide.

Nitric oxide is known to be an important constituent of the D and E regions of the ionosphere (NICOLET 1965), and so a study of the photon interactions with this gas is of considerable importance.

III.2.1 The electronic states of NO^+.

The ionization potentials of NO^+ have been a matter of some controversy over recent years, especially in regard to the first excited state of the ion. Only recently does it appear that the energy levels of the ion have been interpreted unambiguously (EDQVIST 1969).

Theoretically, the ionization of NO leads to electronic states which can be classified by use of the Wigner-Witmer rules (HERZBERG 1950). Thus the predicted electronic states of NO^+ are $^1\Sigma^+$ (removal of a $\Pi_g 2p$ electron), $^1\Sigma^+, ^1\Sigma^-, ^1\Delta$, $^3\Sigma^+, ^3\Delta$ (removal of a $\Pi_u 2p$ electron) and $^1\Pi$, $^3\Pi$ (removal of a $\sigma_g 2p$ electron). The above energy levels have been further classified with regard to their energy by Lefebre-Brion and Moser (LEFEBRE 1966), who used LCAO-MO-SCF wavefunctions. They have listed the electronic states in order of increasing energy as:

$X^1\Sigma^+$, $a^3\Sigma^+$, $^3\Delta$, $^3\Pi$, $^3\Sigma^-$, $^1\Sigma^-$, $^1\Delta$ and $A^1\Pi$.

However, the experimental data has presented difficulties in assigning these states, especially the $a^3\Sigma^+$ state. Spectroscopic results (TANAKA 1942, HUBER 1961) have shown a Rydberg series (α-series) which converges to an energy of 14.22 eV, but the photoelectron spectrum of NO^+ at 584 Å shows no state at this energy, except for the rather slim evidence of Collin and Natalis (COLLIN 1968a), which is outweighed by the higher resolution spectra of Price (PRICE 1968) and Edqvist et al (EDQVIST 1969). Samson (SAMSON 1968a) also finds no evidence for a state at this energy in spectra recorded at various wavelengths shorter than 834 Å (14.87 eV). This conclusion is also supported by the present work (Sec. III.2.2). The interpretation of the α-series as a Rydberg series leading to an excited electronic state of NO^+ is now thought to be incorrect by some groups (SJÖGREN 1968, HUBER 1968) and so there is rather strong evidence against the existence of a state in NO^+ at 14.22 eV.

The most recent example of a photoelectron spectrum of NO^+ is that of Edqvist et al (EDQVIST 1969). This high resolution spectrum (Fig. III.6) shows all the electronic states predicted by theory, although the relative order of the energies of the states is slightly different to the predicted order. The classification of states given by Edqvist et al has been adopted for the present work.

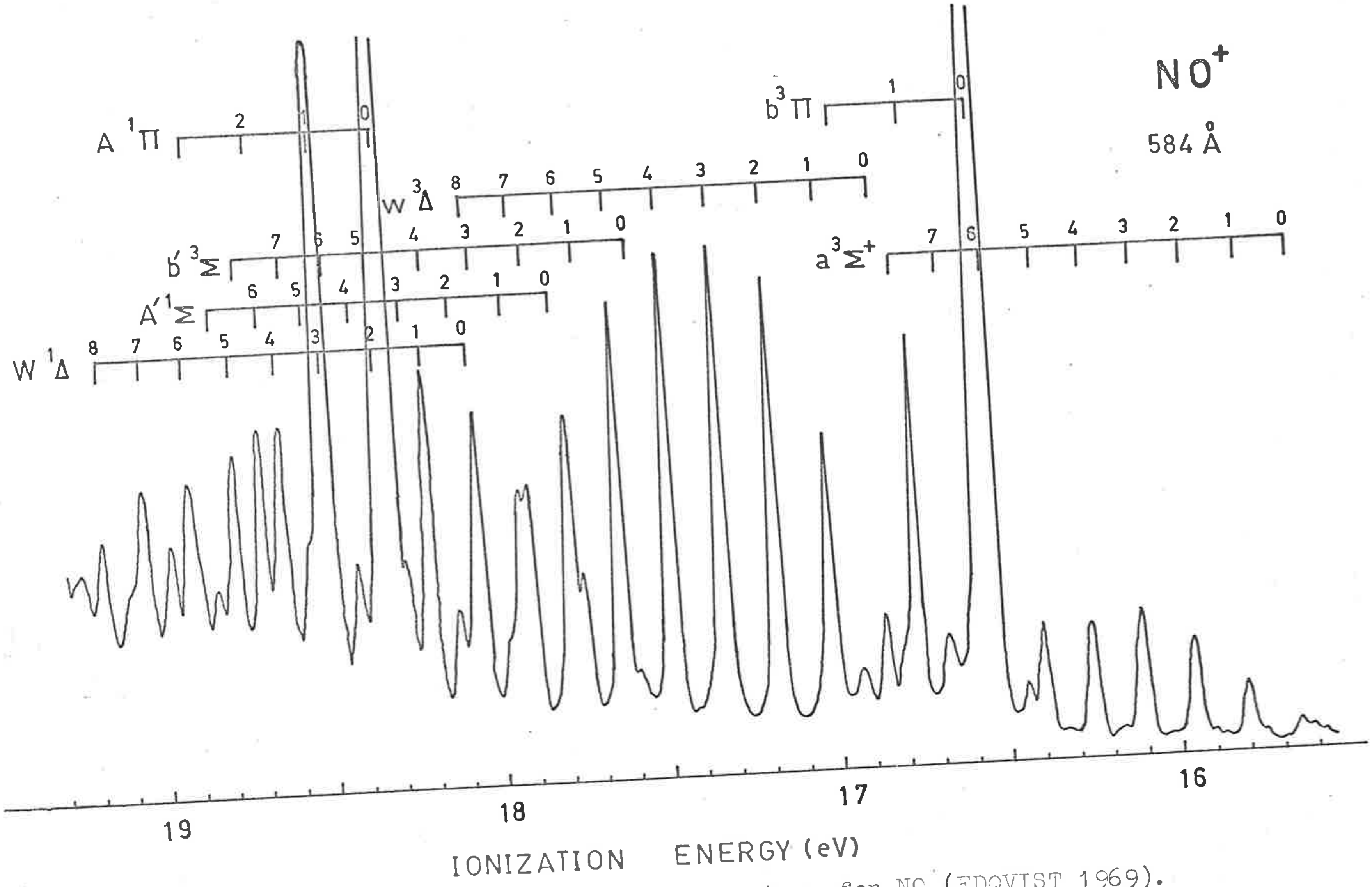

Fig.III.6. Photoelectron spectrum for NO (EDQVIST 1969).

The available experimental data on the ionization potentials of NO^+ is presented in Table III.3.

A potential energy diagram of NO^+, due to Edqvist et al is shown in Fig. III.7. All but the last two states listed in Table III.3. were energetically available in the present experiment.

III.2.2. Nitric Oxide Photoelectron Spectra

Photoelectron energy spectra were recorded at 584 Å and at 5 Å intervals from 590 Å to 850 Å. These spectra were obtained under the same conditions as the carbon monoxide spectra. The nitric oxide was obtained from the Matheson Co. and was used without further purification.

Spectra of nitric oxide at incident wavelengths of 584 Å, 645 Å and 705 Å are shown in Figs. III.8,9. These three spectra were recorded at a higher resolution than the rest of the spectra which were used to determine the partial photoionization cross-sections of nitric oxide. The 584 Å spectrum (Fig. III.8.) shows the $X\,^1\Sigma^+$, $a\,^3\Sigma^+$, $b\,^3\Pi$, $w\,^3\Delta$, and $A\,^1\Pi$ states of NO^+; the other states are not resolved and the positions of these states have been marked on the diagram for completeness. The spectra at 645 Å and 705 Å (Fig. III.9.) show how the number of states available for ionization becomes less as the wavelength of the incident light is increased.

For wavelengths above the threshold for the $a\,^3\Sigma^+$ state (792 Å) the photoelectron spectra showed anomalous intensity

Table III.3.

Nitric Oxide Photodisintegration Processes

	Appearance Potential (eV)										
Process	(1)	(2)	(3)	(4)	(5)	(6)	(7)	(8)	(9)	(10)	(11)
$NO(X\,^2\Pi) + h\nu \rightarrow$											
$NO^+(X\,^1\Sigma^+) + e^-$	9.266	9.23	9.24	9.32	9.25	9.25	9.262	9.3		9.267	9.3
$NO^+(a\,^3\Sigma^+) + e^-$		15.4	15.65	15.72	15.5		15.68	15.6	15.67	15.649	15.7
$NO^+(b\,^3\Pi) + e^-$	16.55	16.53	16.52	16.62	16.5	16.5	16.56	16.6		16.558	16.6
$NO^+(w\,^3\Delta) + e^-$				17.18			17.17	17.2		16.860	
$NO^+(b'\,^3\Sigma^-) + e^-$							17.31	17.5		17.585	
$NO^+(A'\,^1\Sigma^-) + e^-$										17.820	
$NO^+(W\,^1\Delta) + e^-$										(18.07)	
$NO^+(A\,^1\Pi) + e^-$	18.33	18.24	18.26	18.24		18.25	18.33	18.3		18.322	18.3
$NO^+(c\,^3\Pi) + e^-$										20.41	
$NO^+(B\,^1\Pi) + e^-$									21.72	21.72	
$NO^+(B'\,^1\Sigma^+) + e^-$									23.1	22.5	

(1) HUBER 1961, DRESSLER 1965, (2) AL-JOBOURY 1964, (3) TURNER 1966, (4) VROOM 1966, (5) SCHOEN 1965, (6) BERKOWITZ 1967, (7) COLLIN 1968, (8) PRICE 1968, (9) SAMSON 1968a, (10) EDQVIST 1969, (11) Present Work.

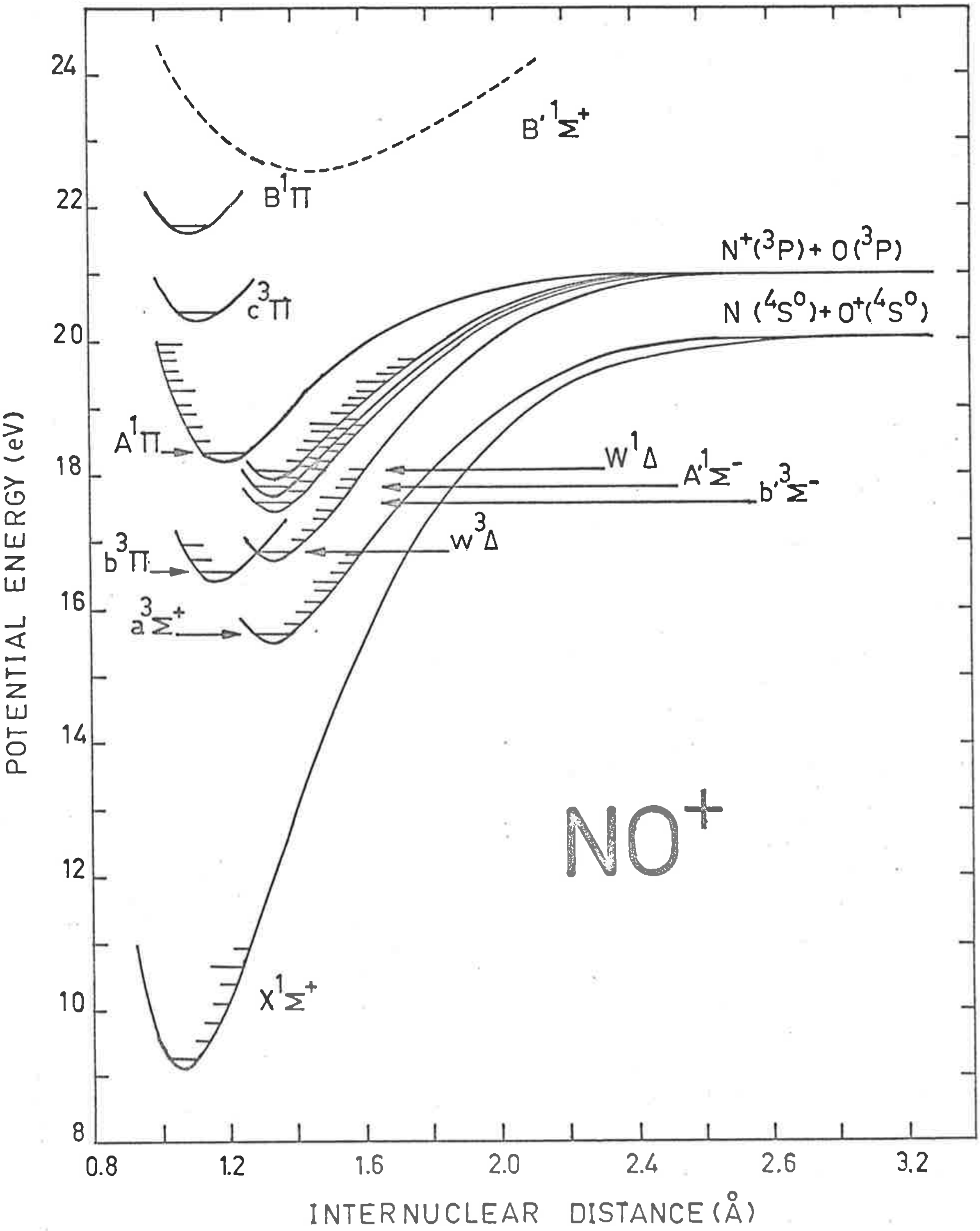

Fig.III.7. Potential energy curves for NO^+.
(EDQVIST 1969)

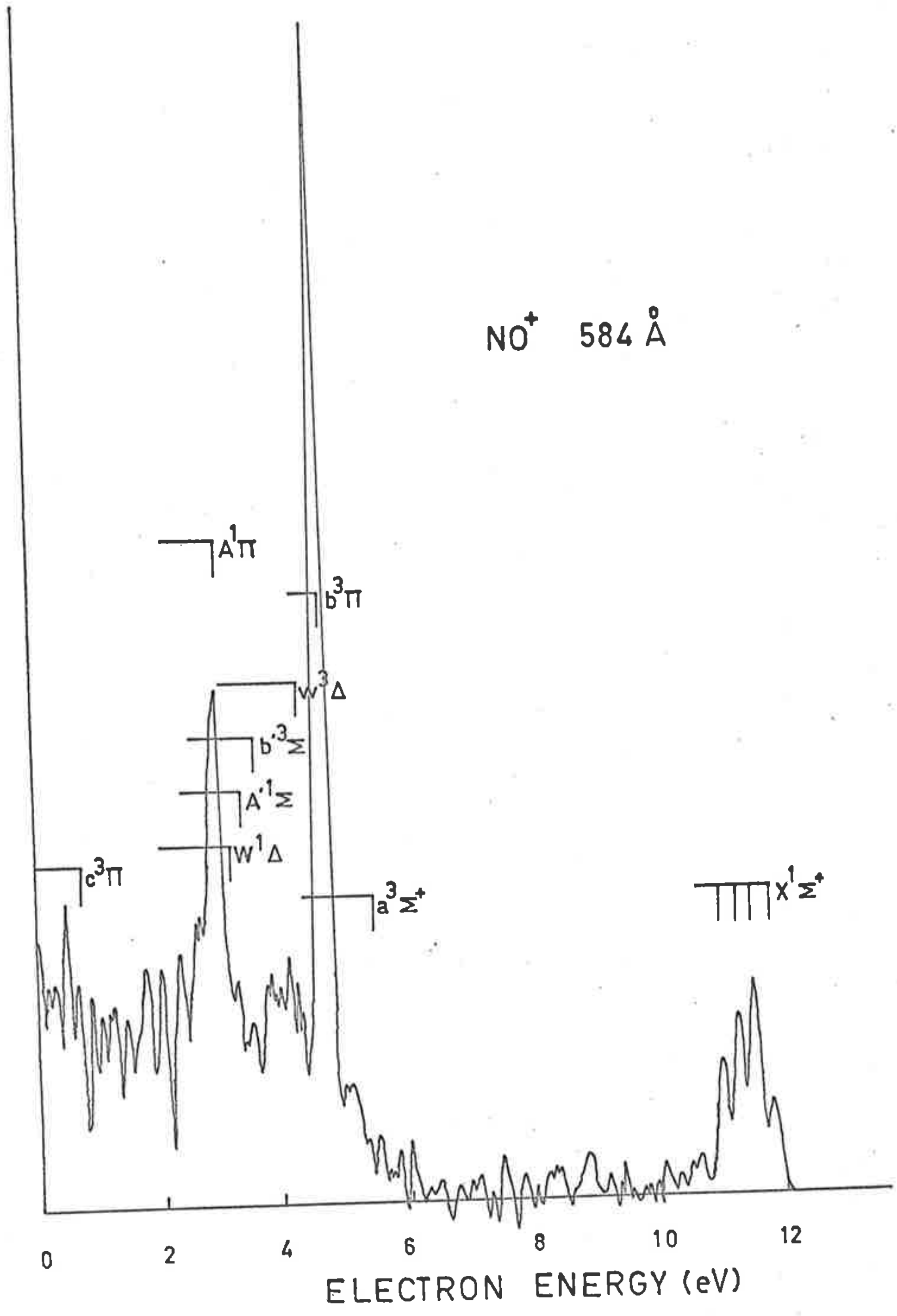

Fig.III.8. Photoelectron spectrum for NO at 584 Å.

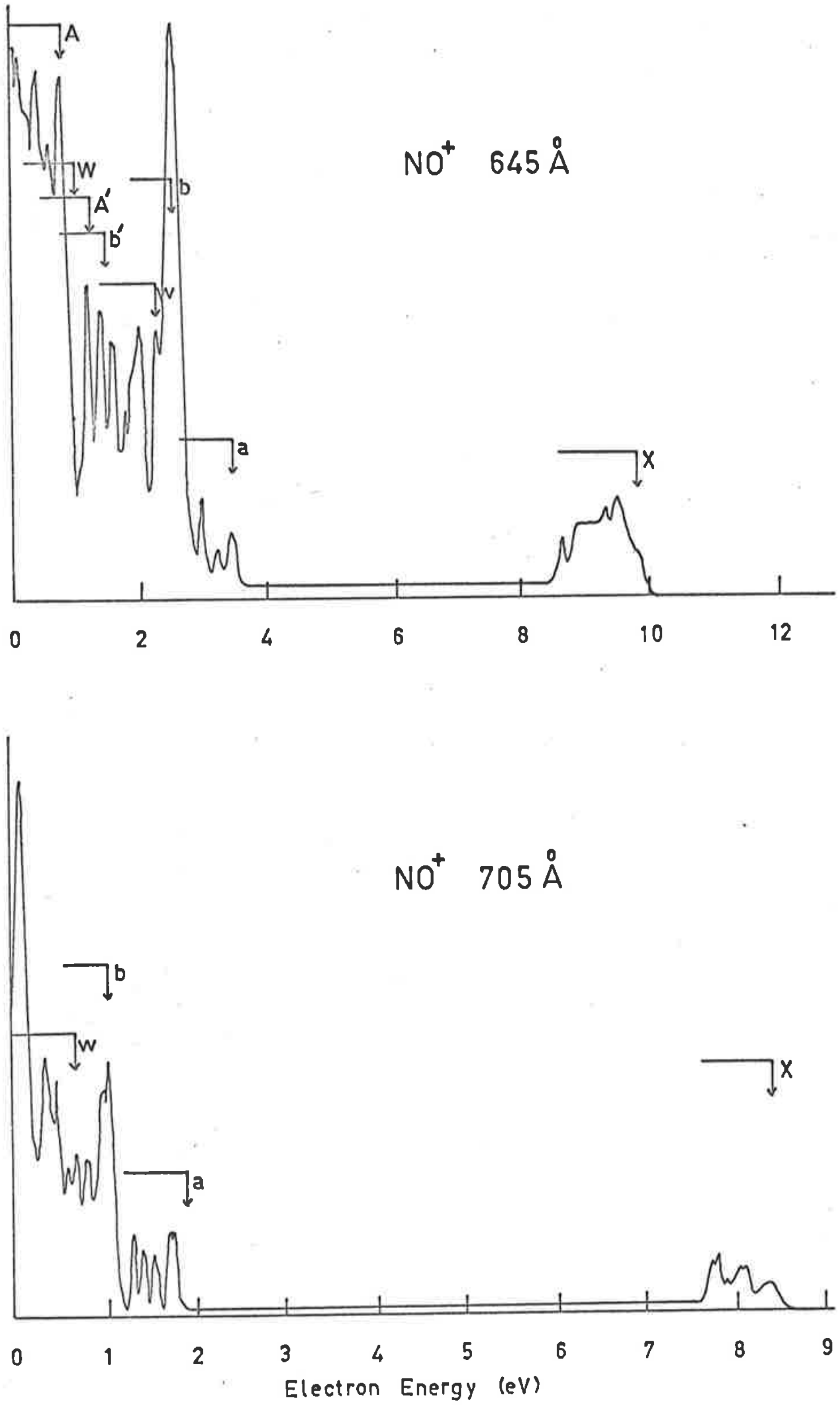

Fig. III. 9. Photoelectron spectra for NO at 645 and 705 Å.

distributions among the vibrational levels of the $X\,^1\Sigma^+$ ground ionic state. This effect has been attributed to preionization of the molecule in the region above 790 Å, and as it only affected the $X\,^1\Sigma^+$ state, the partial cross-sections for the electronic states of NO^+ are unchanged. This effect will be dealt with in more detail in Chapter IV.

III.2.3. Partial Cross-Sections of Nitric Oxide

The branching ratios for the states of NO^+ could only be obtained individually for the $X\,^1\Sigma^+$ states over the entire range. It was possible to measure the branching ratios for the $a\,^3\Sigma^+$ state in the range 750-800 Å, and for the $c\,^3\Pi$ state at wavelengths of 584 Å, 590 Å and 600 Å. The considerable overlapping of the electronic states (see Fig. III.6.) made it impossible at the present resolution to unfold the spectra into individual states, except as mentioned above. Thus the branching ratios have been measured for combinations of several states where those states could not be resolved. The combinations were as follows:

584-675 Å	$X\,^1\Sigma^+$, $(a\,^3\Sigma^+ + b\,^3\Pi)$, $(w\,^3\Delta + b'\,^3\Sigma^- + A'\,^1\Sigma^- + W\,^1\Delta + A\,^1\Pi)$, $c\,^3\Pi$
680-685 Å	$X\,^1\Sigma^+$, $(a\,^3\Sigma^+ + b\,^3\Pi)$, $(w\,^3\Delta + b'\,^3\Sigma^- + A'\,^1\Sigma^- + W\,^1\Delta)$
690-695 Å	$X\,^1\Sigma^+$, $(a\,^3\Sigma^+ + b\,^3\Pi)$, $(w\,^3\Delta + b'\,^3\Sigma^- + A'\,^1\Sigma^-)$
700-705 Å	$X\,^1\Sigma^+$, $(a\,^3\Sigma^+ + b\,^3\Pi)$, $(w\,^3\Delta + b'\,^3\Sigma^-)$
710-735 Å	$X\,^1\Sigma^+$, $(a\,^3\Sigma^+ + b\,^3\Pi)$, $w\,^3\Delta$
740-745 Å	$X\,^1\Sigma^+$, $(a\,^3\Sigma^+ + b\,^3\Pi)$
750-795 Å	$X\,^1\Sigma^+$, $a\,^3\Sigma^+$

The branching ratios for photoionization of nitric oxide are presented in Table III.4., and are plotted as a function of the incident wavelength in Fig. III.10. These branching ratios were combined with the total photoionization cross-section results of Cook et al (COOK 1965), which were averaged over 8 Å intervals to produce an effective resolution equivalent to the present experiment. The partial photoionization cross-sections for nitric oxide are shown in Fig. III.11. as a function of the incident wavelength.

The cross-section for the ground ionic state of $NO^+(X\,^1\Sigma^+)$ is fairly constant over the range 584-750 Å, varying only between 2 and 3 Mbn. (1Mbn = 10^{-18} cm^2). The cross-section for the combination of states ($w\,^3\Delta + b'\,^3\Sigma^- + A'\,^1\Sigma^- + W\,^1\Delta + A\,^1\Pi$) varies between 5 and 7 Mbn from 584 Å to the threshold of the $A\,^1\Pi$ state (677 Å), and as the wavelength increases further, the cross-section gradually falls to zero at 735 Å, indicating that the $A\,^1\Pi$ state accounts for most of the ionization in these states when it is energetically available. The cross-section for the ($a\,^3\Sigma^+ + b\,^3\Pi$) states passes through a maximum just before the $b\,^3\Pi$ threshold at 750 Å, which is caused by the disappearance of the higher excited states (i.e. those above 17 eV). This maximum is evident in the total cross-section curve. The peak in the total cross-section near 780 Å is also reflected in the partial cross-section of the $X\,^1\Sigma^+$ and $a\,^3\Sigma^+$ states, although with the low resolution used this maximum cannot be uniqly attributed to either state. The peak is due to preionized structure

Table II.4.

Branching Ratios for Nitric Oxide

Wavelength Å	eV	$X\,^1\Sigma^+$	$a\,^3\Sigma^+$	$b\,^3\Pi$	$w\,^3\Delta$	$b'\,^3\Sigma^-$	$A'\,^1\Sigma^-$	$W\,^1\Delta$	$A\,^1\Pi$	$c\,^3\Pi$
584	21.21	15		43			34			8
590	21.01	14		42			35			9
600	20.66	13		45			35			7
610	20.32	20		33			47			
615	20.16	19		38			43			
625	19.84	19		40			41			
630	19.68	17		43			40			
635	19.52	16		36			48			
640	19.37	14		36			50			
645	19.22	15		41			44			
650	19.07	17		37			46			
655	18.93	14		44			42			
660	18.78	21		36			43			
665	18.65	20		33			47			
670	18.50	17		35			48			
675	18.37	20		40			40			
680	18.23	16		41			43			
685	18.10	18		43			39			
690	17.97	22		42		38				
695	17.84	21		44		35				
700	17.71	18		51		31				
705	17.59	23		52		25				
710	17.46	23		46	31					
715	17.34	28		43	29					
720	17.22	21		51	28					
725	17.10	24		61	15					
730	16.98	25		57	18					
735	16.87	27		73	0					
740	16.75	24		76						
745	16.64	26		74						
750	16.53	43	57							
755	16.42	44	56							
760	16.31	53	47							
765	16.21	47	53							
770	16.10	53	47							
775	16.00	54	46							
780	15.89	62	38							
790	15.69	70	30							
795	15.59	100								

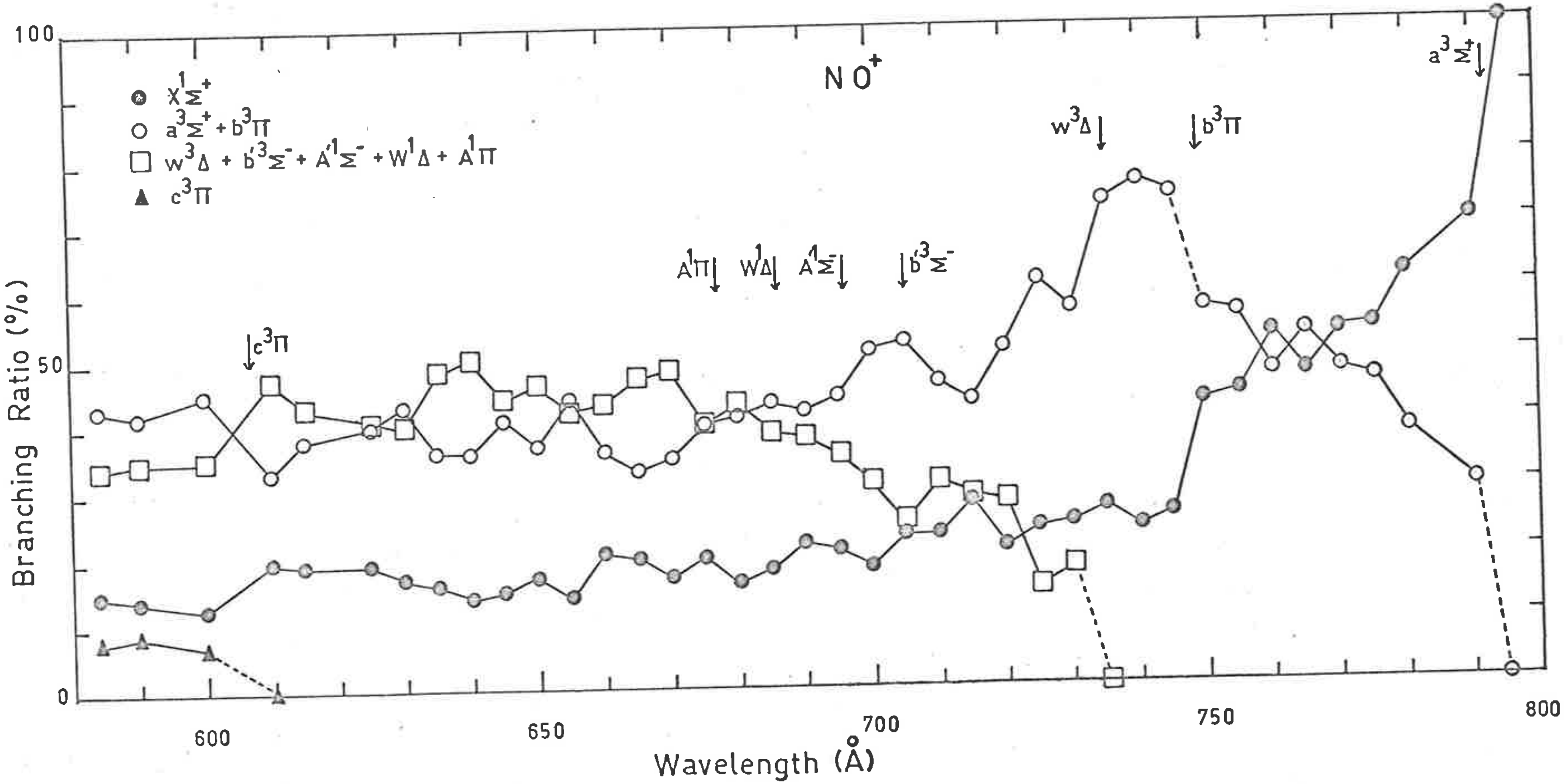

Fig.III.10. Branching ratios for the various photoionizing processes in NO.

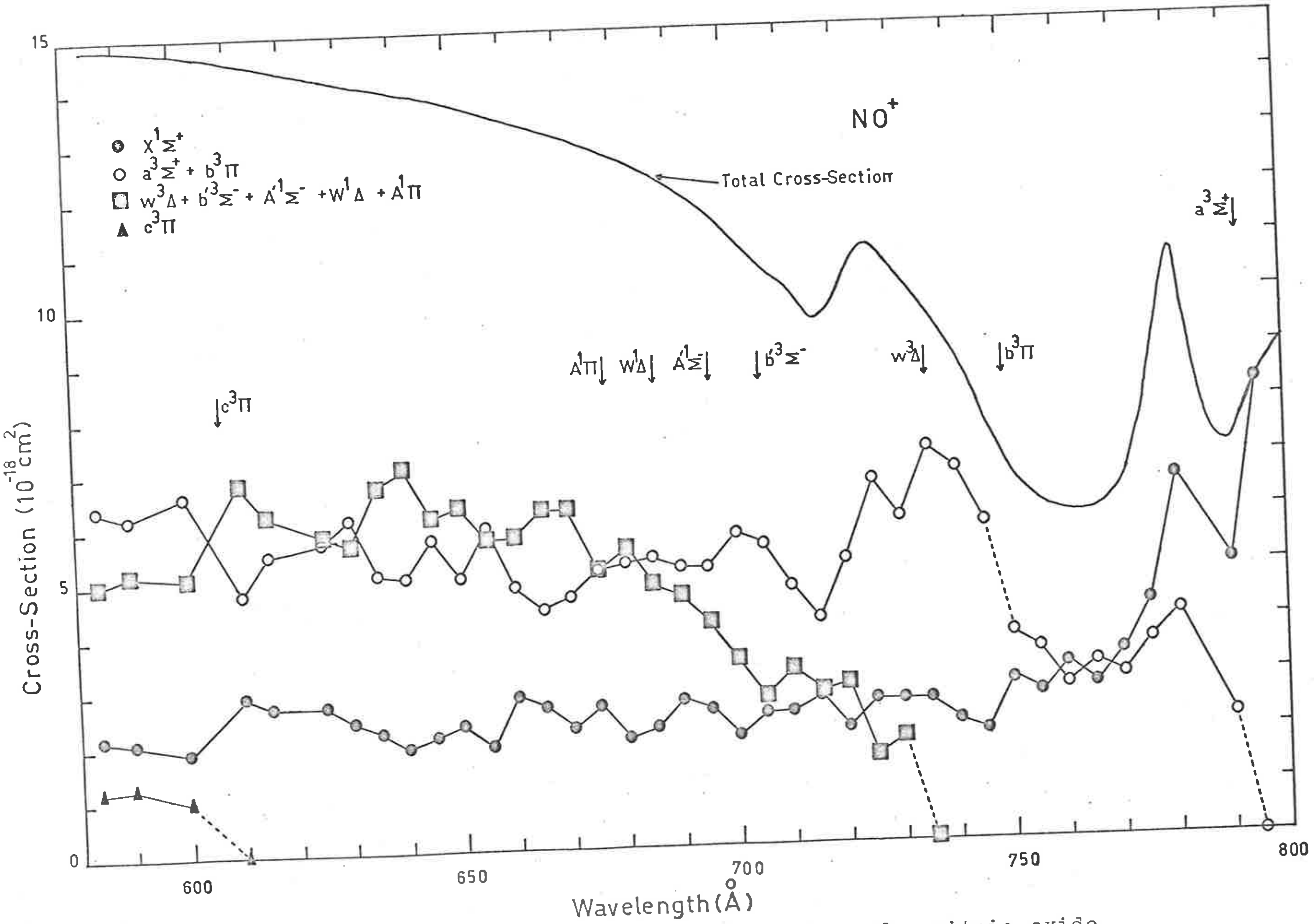

Fig.III.11. Partial photoionization cross-sections for nitric oxide.

in the total cross-section curve ($\beta(0,0)$ series and P_3 progression), and in Chapter IV it will be shown that transitions to the a $^3\Sigma^+$ state are greatly enhanced by the intermediatory transition to the preionized level of the molecule.

III.3. Accuracy of the Partial Cross-Sections

The greatest factor limiting the accuracy of the partial photoionization cross-sections was the uncertainty involved in the unfolding of the spectra. This uncertainty was in the determination of the low energy tail associated with each peak in the spectrum. Partial over-lapping of peaks in some spectra, due to the low resolution, prevented an accurate estimate of the area associated with each state. In cases like this the shape of the individual peaks had to be estimated from spectra at other wavelengths where the peaks were better resolved.

The area under a given peak could be found to an accuracy of 10%, but the absolute error accumulated during the unfolding of the spectra. This meant that the error was greater for peaks of lower energy; this effect was reduced by demanding that the unfolding should be self-consistent.

Thus the accuracy of the partial cross-sections varied greatly, depending on the peak energy, the peak size, and its separation from other peaks. The error was estimated to be between 10%

and 20% in most cases, except near the threshold for each state where the peak and the peak energy were both small, leading to a greater error.

CHAPTER IV

PHOTOELECTRON SPECTROSCOPY AND PREIONIZATION IN NITROGEN, CARBON MONOXIDE AND NITRIC OXIDE.

IV.1. Introduction

In 1964 Schoen (SCHOEN 1964) reported anomalous structure in the photoelectron retarding potential curves for molecular oxygen and carbon monoxide which he attributed to preionization phenomena in those gases. Blake and Carver (BLAKE 1967) also observed structure in the photoelectron spectra of oxygen for wavelengths longer than 680 Å, which they attributed to a process of "fluorescent autoionization" involving quasi-stable states of the neutral molecule. In this process, a photon is absorbed forming a super-excited state in the neutral molecule. In ordinary preionization the molecule would then ionize, finishing in one of the discrete ionic states. It was suggested that in fluorescent autoionization, part of the excitation energy is dissipated in the form of a photon, or photons, thus producing an electron of different energy to that produced by the normal ionizing process. The process of fluorescent autoionization is shown schematically in Fig.IV.1.

The results quoted above were not obtained at sufficient energy resolution to enable a more detailed analysis of the effect. However, in 1965 Doolittle and Schoen (DOOLITTLE 1965) investigated the effects of preionized levels on the photoelectron spectra of

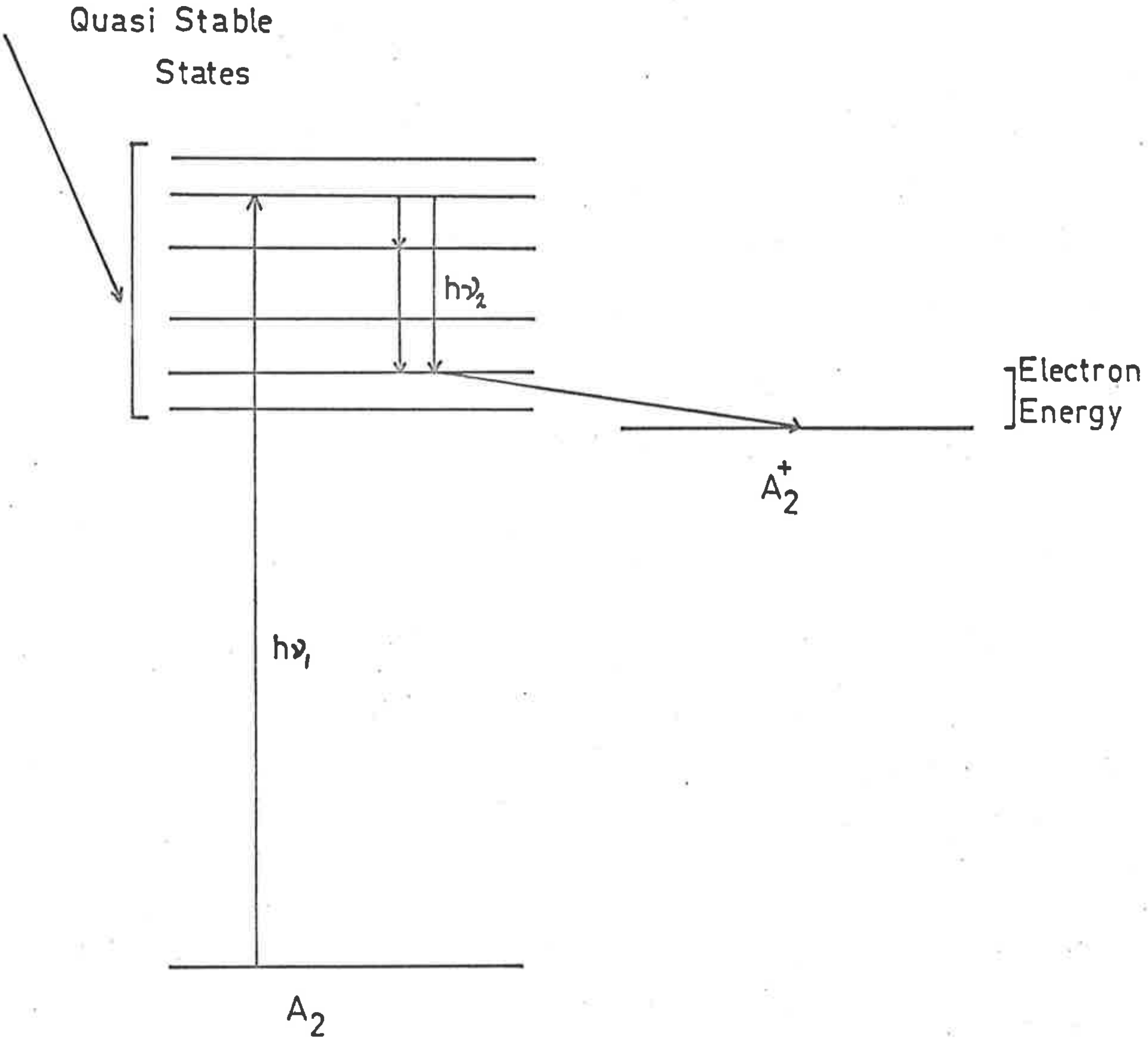

Fig.IV.1. Energy level diagram of a hypothetical molecule A_2, illustrating a fluorescent autoionizing transition.

hydrogen. They recorded retarding potential curves at wavelengths of 772 Å, 780 Å, and 790 Å with an incident beam resolution of 4 Å. The wavelength of 780 Å corresponded to a preionized band in the total cross-section curve for hydrogen, and at this wavelength a strong enhancement of the v' = 1 level of H_2^+ can be seen, (Fig.IV.2(a)). It was assumed that this enhancement was due to ionization taking place via the preionized level. More recently (SCHOEN 1968) the above authors have investigated the difference in the vibrational distribution of the $X\,^2\Sigma_g^+$ state of N_2^+ at two preionized bands within a few angstroms of each other: 771 Å and 765 Å (Fig.IV.2(b)).

Some photoelectron spectroscopists who normally use only 584 Å incident radiation have recently taken spectra of several gases using the light from the neon doublet at 736 - 744 Å and the argon doublet at 1048 - 1067 Å to excite the target gas (COLLIN 1968, PRICE 1968). Both groups have found marked differences in the vibrational distribution of the $X\,^2\Pi_g$ state of O_2^+ at incident wavelengths of 584 Å and 736 - 744 Å. The two results are shown in Fig.IV.3(a),(b). For the 584 Å spectrum both experimenters report the usual five vibrational levels of the $X\,^2\Pi_g$ state which are normally observed in the photoelectron spectrum of O_2 at this wavelength, and whose intensity distribution is in good agreement with the calculated F-C factors, but for the spectrum using the neon light Price observed up to 15 vibrational levels and Collin and Natalis observed 21 levels.

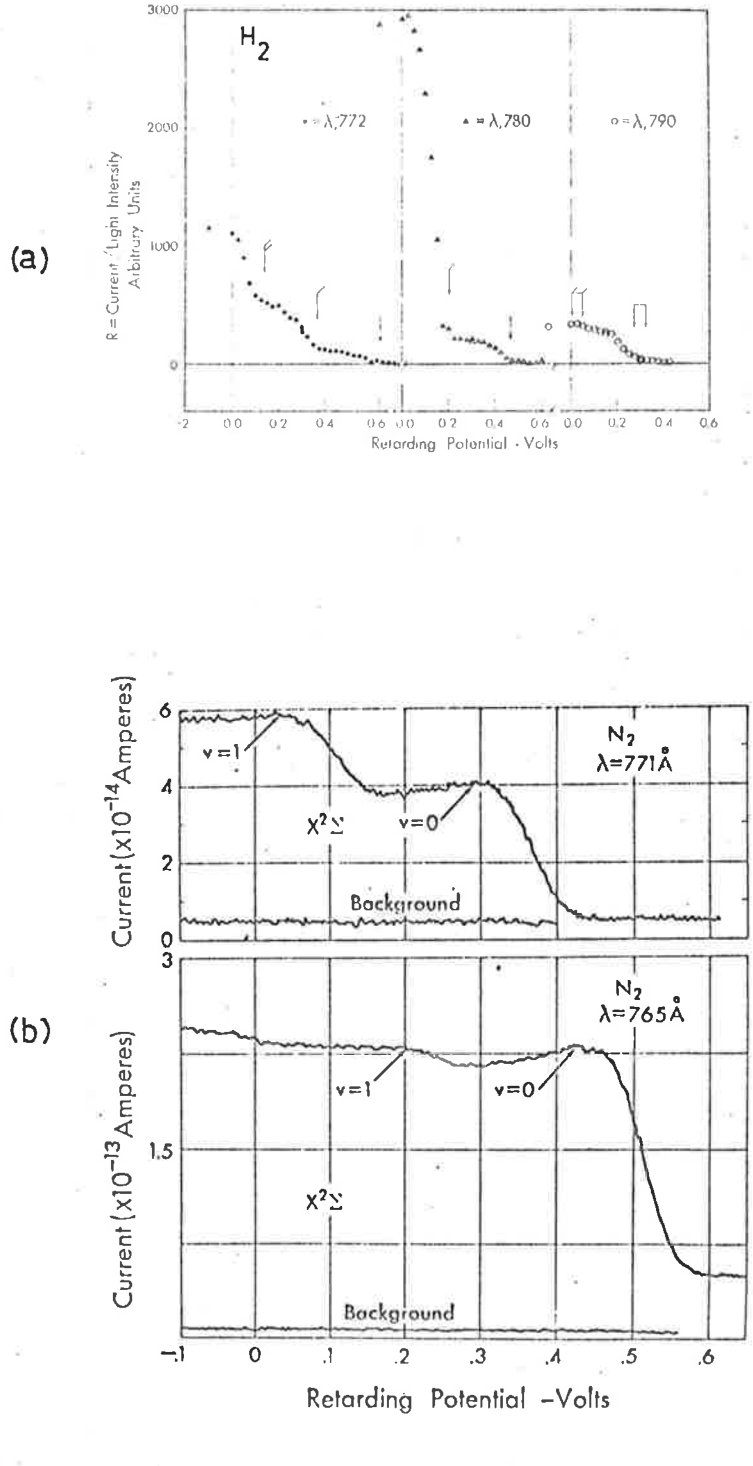

Fig. IV. 2. Photoelectron retarding potential curves for (a) H_2, and (b) N_2, by Schoen and Doolittle, (DOOLITTLE 1965, SCHOEN 1968).

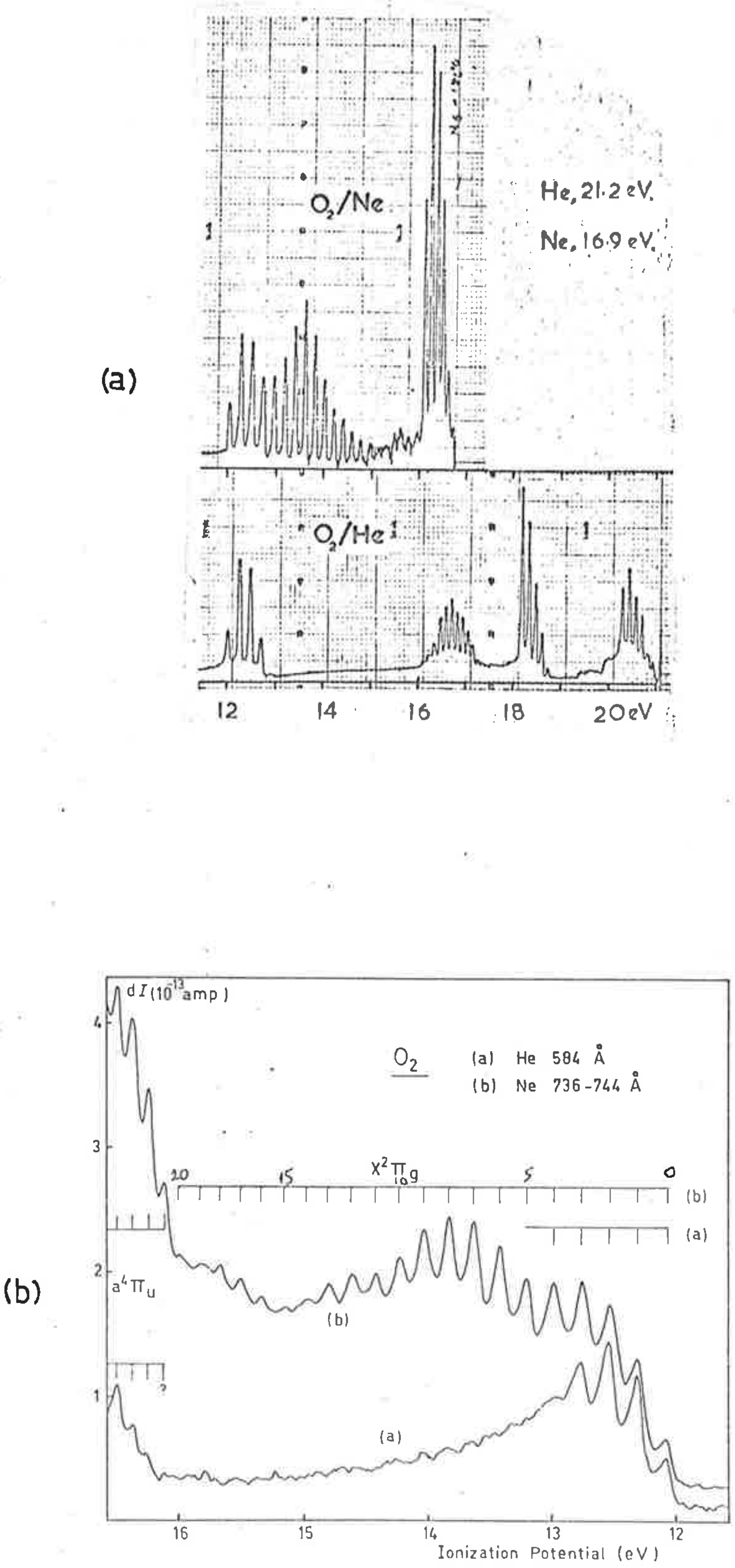

Fig. IV. 3. Photoelectron spectra for O_2 at 584 Å and 736-744 Å by (a) PRICE 1968, and (b) COLLIN 1968b.

Similar effects have also been reported by these authors for carbon monoxide, nitric oxide and molecular nitrogen. For carbon monoxide, Collin and Natalis reported vibrational structure of the $X\,^2\Sigma^+$ state of CO^+ up to v' = 9 at 736 - 744 Å, and in nitric oxide they observed up to v' = 9 of the $X\,^1\Sigma^+$ state of NO^+ using an argon light source (COLLIN 1968a). The 584 Å spectrum of carbon monoxide revealed only the first four vibrational levels and the 584 Å nitric oxide spectrum showed only up to v' = 4 (c.f. also Chapter III of this thesis). The wavelength of 736 - 744 Å corresponds to regions in the photoionization cross-section curves of O_2, CO and NO where preionization structure is clearly evident (COOK 1965). Collin and Natalis offered several suggestions to explain the effects observed in O_2 and CO. They considered the interaction times for direct photoionization and for preionization (10^{-15} sec and 10^{-11} sec respectively) and indicated that the lifetime of the excited molecule may be of the order of, or greater than, the time for a vibrational motion, so that the Born-Oppenheimer and Franck-Condon approximations no longer hold (see Sec.I.2.4.). They have also suggested that the approximation of equation (23) of Sec.I.2.4. may not hold for non-resonance phenomena such as photoionization; i.e. that the electronic transition moment varies with the excess energy of the exciting radiation.

Probably the most significant feature of the O_2 spectrum at 736 - 744 Å is the appearance of a second maximum in the intensity distribution in the v' = 7 region (Fig.IV.3(a) and (b)). Collin and Natalis have suggested that this effect is due to the combination of two sets of F-C distributions, one from the direct ionization process, and the other from the preionized transition. This mechanism has also been proposed in the present work and will be dealt with more fully in Sec.IV.5.

Price has proposed a somewhat different idea to explain the effects that he observed in O_2, NO and N_2. Although preionization is a resonant process in that the energy of the incident photon must be equal to the excitation energy of the preionized level, he suggests that even if the energy of the incident photon is greater than that of the preionized level, virtual transitions of the inner electrons may still occur before the outer electron is ejected. This would result, according to Price, in a very large increase in the photoionization cross-section of those vibrational levels of the ionic state which lie near the preionized levels. This would arise because the interaction of the preionizing bound state wavefunction with the final state wavefunction is very dependant on the velocity of the photoelectron, and is only large when the photoelectron velocity is small (so that there is appreciable time for the interaction to occur).

The main criticism which can be made with the above theory lies in the fact that the preionized transitions are very much a resonant process, and thus only the preionized level whose energy corresponds exactly to the energy of the incident photon will be excited with a given monochromatic light source. This "resonant" effect in the photoelectron spectra will be shown in the following sections, where spectra recorded at wavelengths corresponding to definite preionized levels in CO, NO and O_2 are presented and compared to spectra recorded at wavelengths removed by only a few Angstroms from these resonance levels.

From the results cited above, it is evident that there is a need for a detailed investigation of the photoelectron spectrum in regions of preionization in gases as the existing data does not give information on the photoelectron energy distribution as a function of the incident wavelength where the total photoionization cross-section varies rapidly. In Sec.IV.2. and in Chapter V. photoelectron spectra are presented which have been recorded at wavelengths corresponding to preionized resonances in N_2, CO, NO and O_2.

IV.2. Photoelectron Spectra for Preionized States in Nitrogen, Carbon Monoxide and Nitric Oxide.

IV.2.1. Nitrogen

The total photoionization cross-section measurements of nitrogen indicate positions of many sharp peaks (COOK 1965, OGAWA 1962), which can be seen in Fig.IV.4. This curve shows the photoionization coefficient, k_i, as a function of wavelength over the wavelength region

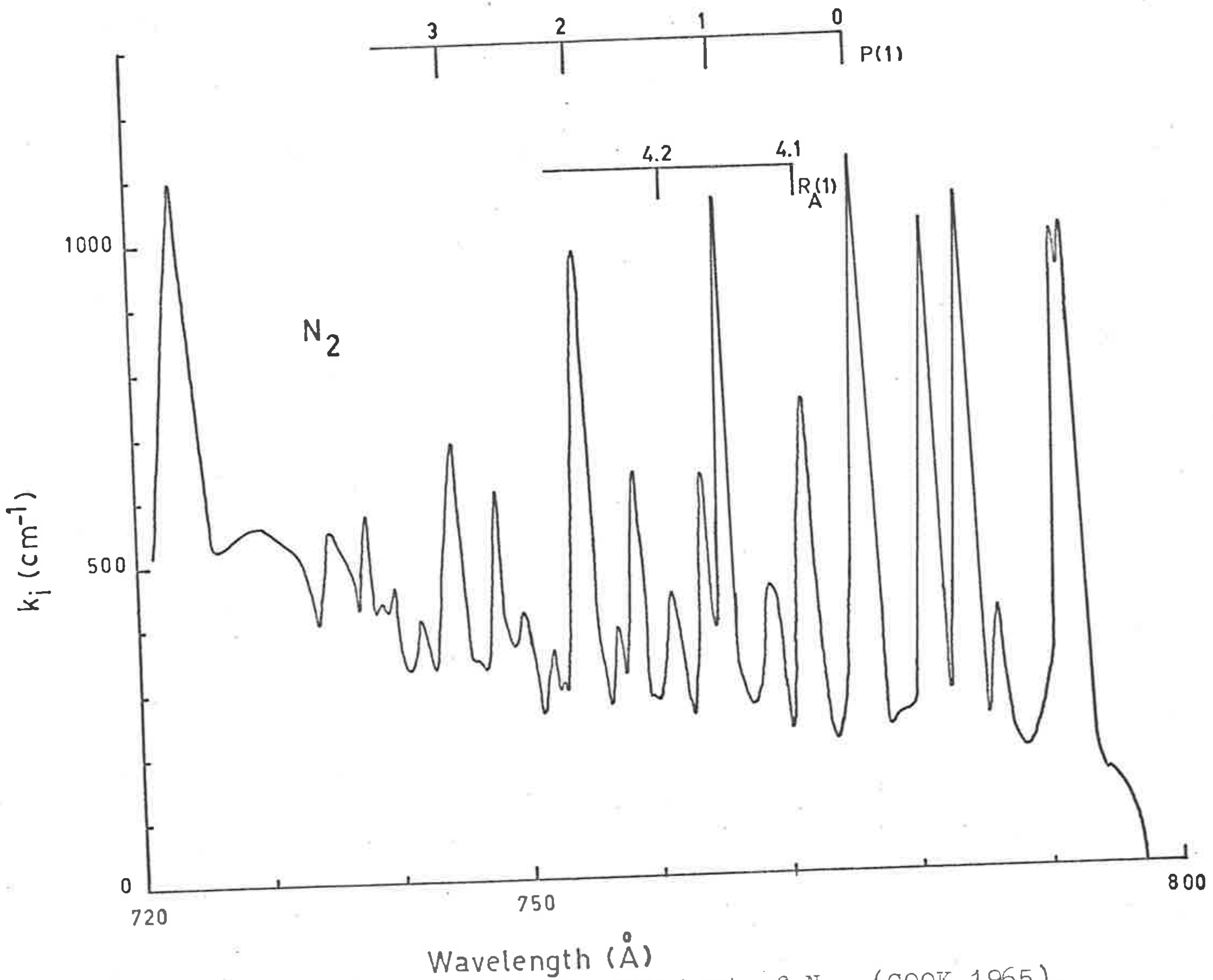

Fig.IV.4. Photoionization coefficient of N_2, (COOK 1965).

720 - 800 Å (after COOK 1965). In the present experiment photoelectron spectra were recorded at the following well-defined wavelengths:

Table IV.1.

Progression or Series	v	λ (Å)	k_i (cm^{-1})
P(1) 0-0	0	775.7	1110
P(1) 1-0	1	765.2	1050
P(1) 2-0	2	754.3	975
P(1) 3-0	3	744.5	685
R_A(1),4.1	1	771.6	740
R_A(1),4.2; R_A(2),6.0	2,0	761.2	440

P(1) 2-0 is the third member of the P(1) progression with vibrational number 2, and R_A(1),4.1 refers to Rydberg bands with m = 4, v = 1, converging to the $A\,^2\Pi_u$ state of N_2^+.

The v numbers listed in Table IV.1. are those given by Cook et al. For a Rydberg series the vibrational quantum number is usually obtained from the series' convergence to a definite vibrational level of an ionic state. For the R_A(1),m.1 series, for example, the convergence is to the v' = 1 level of the $A\,^2\Pi_u$ state of N_2^+, and so all the members of this series have a vibrational quantum number of 1. The vibrational numbering of progressions is, on the other hand, not so precise. In most cases the zero vibrational level is tentatively assigned to the longest wavelength member of a progression. This is probably usually correct, unless the lower members (i.e. the longer wavelength members) of a progression are not observed experimentally, indicating an error in the vibrational numbering of the progression. For the P(1) progression in N_2 the vibrational numbers were assigned by Ogawa (OGAWA 1964).

The wavelength on the monochromator used in the present work could be set accurately to ±0.5 Å and the resonance peak was found by manually driving the grating near the desired wavelength until the electron count rate was a maximum. The wavelengths quoted above are those given by Cook et al (COOK 1965). The experimental arrangements were essentially the same as those used to obtain partial photoionization cross-sections (Chapter III) except that the incident beam resolution for the present spectra was 1.6 Å. This of course meant that the light flux was considerably less than before and the spectra typically took one to two hours to record, making repeated scans of the electron retarding potential as described in Chapter II.

The spectra are shown in Fig. IV.5. It is interesting to compare the spectra recorded at 771.6 Å and 765.2 Å with those of Schoen and Doolittle (Fig.IV.2(b)). There is good agreement between the two sets of results, both showing a marked difference in the vibrational intensity distribution for the $v' = 0$ and 1 levels of the

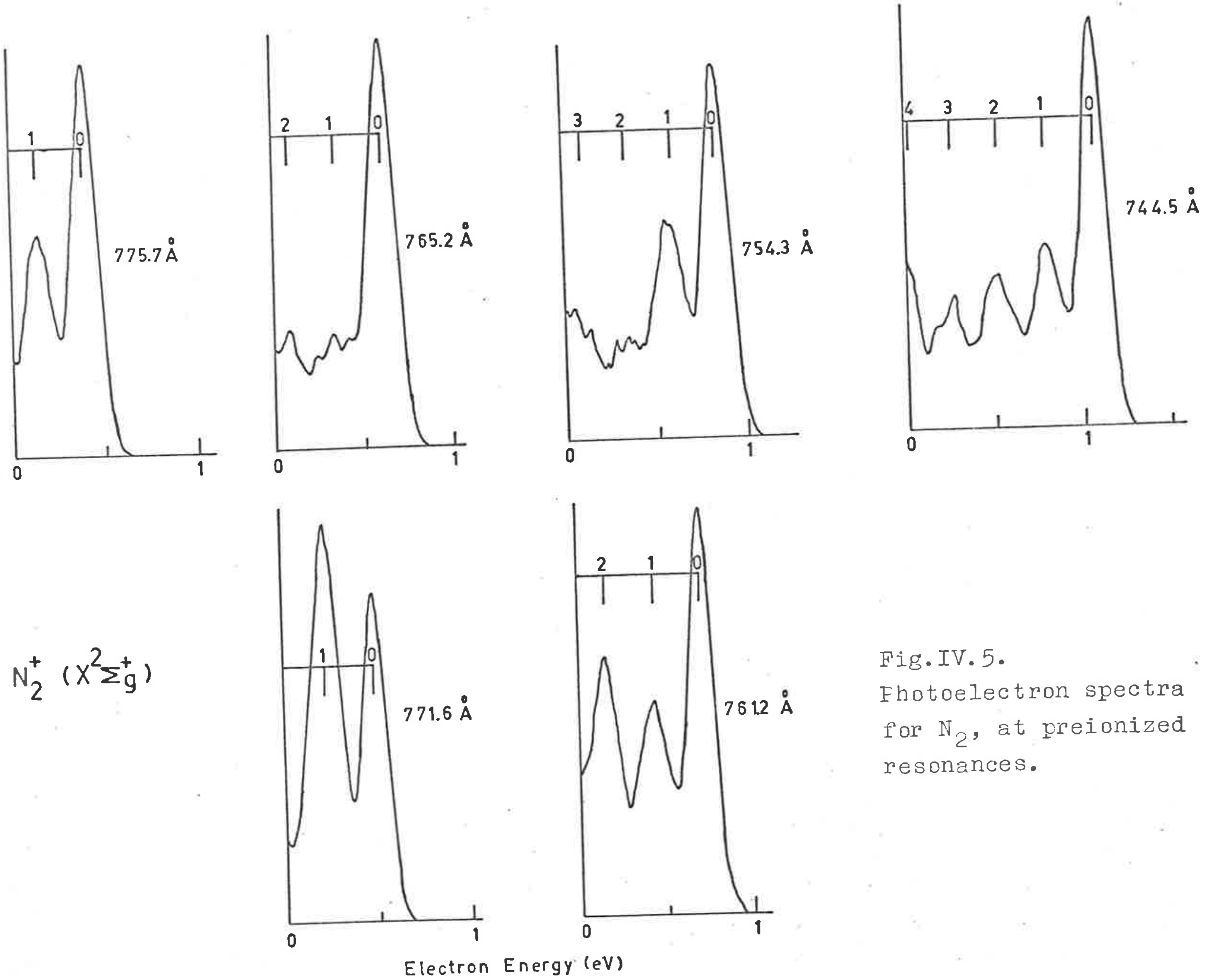

Fig.IV.5.
Photoelectron spectra for N_2, at preionized resonances.

$X\,^2\Sigma_g^+$ state of N_2^+, at the two wavelengths. The most interesting aspect of all the spectra is that the vibrational intensity distribution for the ground ionic state of N_2^+ is different to the calculated F-C factor distribution for the transition $N_2\ (X\,^1\Sigma_g^+,\ v'' = 0) \rightarrow N_2^+\ (X\,^2\Sigma_g^+,\ v')$, i.e. direct photoionization, which is listed in Table IV.5, (see Sec. IV.3.) and which is normally observed at 584 Å. For direct ionization, then, it is expected that the v' = 0 level would appear about nine times as strong as the v' = 1 level (the rest of the v' intensities being insignificant.)

In order to examine the anomalies in these spectra, the peaks were unfolded to give experimental vibrational intensity distributions in the manner described in Sec.III.1.3., using the xenon spectra as standards for the peak width and low energy tail. These experimental values are shown in Fig.IV.6., corrected for the electron collecting efficiency of the spectrometer and normalized to v' = 0. The thick vertical lines in Fig.IV.6. represent the measured vibrational intensities, and have been plotted on the ionization energy scale, which is shown at the bottom of the figure.

IV.2.2. Carbon Monoxide

Preionization in carbon monoxide is evident in the total photoionization cross-section measurements of Cook et al (COOK 1965). The effect that these resonance states have on the photoelectron spectra in the 630 - 700 Å range has already been discussed briefly

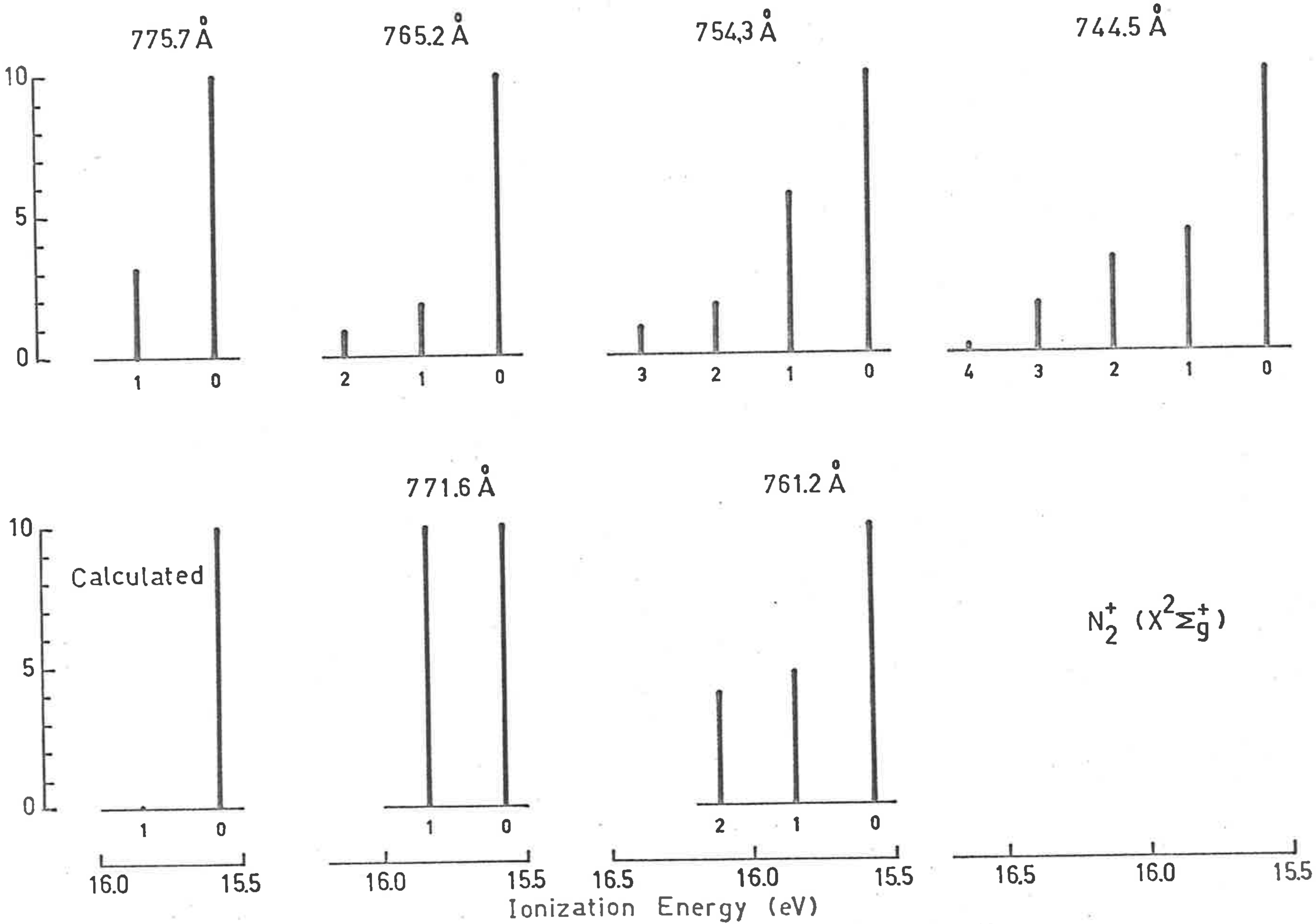

Fig.IV.6. Vibrational intensity distributions for N_2.

in Sec.III.1.5. It was noted that anomalous structure appeared between $A\ ^2\Pi$ and $B\ ^2\Sigma^+$ states of CO^+, and between the $X\ ^2\Sigma^+$ and $A\ ^2\Pi$ states in many of the spectra used to determine partial photoionization cross-sections. This structure was assumed to be vibrational structure of the corresponding states and due to preionized resonances in that wavelength region.

The photoionization coefficient, k_1, as a function of wavelength, is shown in Fig.IV.7 for the region 790 - 850 Å (from COOK 1965). Photoelectron spectra were recorded at the following resonance and off-resonance wavelengths:

Table IV.2.

Progression	v	λ(A)	k_1
H_1	0	838.5	560
H_1	1	827.8	540
H_1	3	807.1	650
H_1	4	796.8	695
Off-resonance		831	345
"		813	290
"		795	260

The wavelengths are those given by Cook, and the v numbering is assumed to start with v = o for the longest wavelength member.

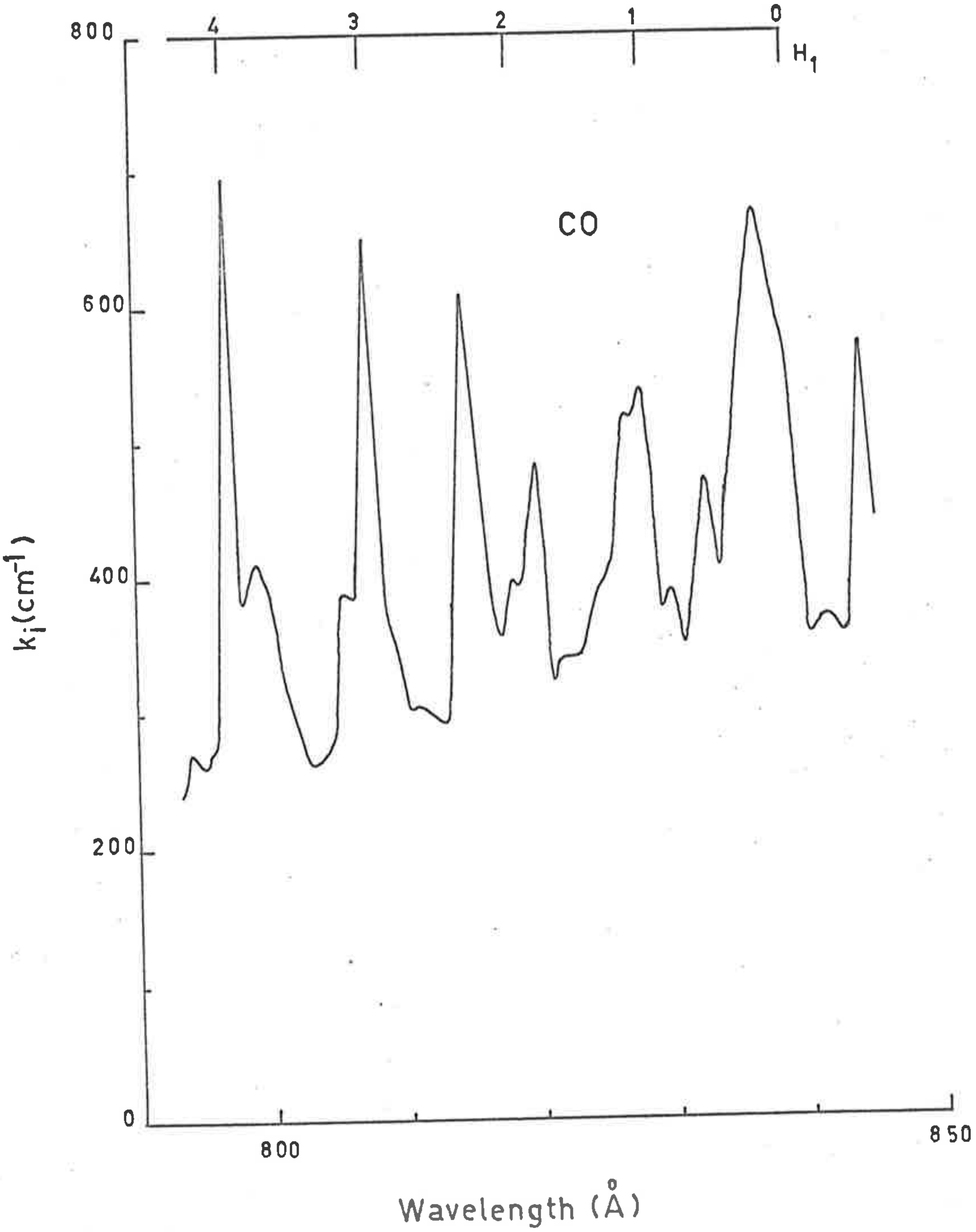

Fig.IV.7. Photoionization coefficient for CO, (COOK 1965).

The spectra are shown in Fig.IV.8. The resonance spectra show enhancement of the vibrational levels v' = 0, while the off-resonance spectra show that at non-resonance wavelengths the CO^+ $(X\,^2\Sigma^+)$ ion is left predominantly in the v' = 0 state.

Vibrational intensity distributions for each of the above spectra were obtained by unfolding the spectra in the same manner as the nitrogen spectra. The distributions were normalized to v' = 0 for each spectrum and are presented schematically in Fig.IV.9. The calculated F-C factors for the transition $CO\ (X\,^1\Sigma^+,\ v'' = 0) \rightarrow CO^+\ (X\,^2\Sigma^+, v')$, i.e. direct photoionization, Fig.IV.9(a), show that 96% of the transitions would favour the v' = 0 level, with the remainding 4% to the v' = 1 level. The only two spectra which approach this distribution are those at 831 Å and 813 Å, which were recorded at wavelengths as near as possible to minima in the total cross-section. One of the most interesting features of the CO spectra is the second maximum which appears at v' = 2 in the 796.8 Å spectrum, and which doesn't show in the 795 Å spectrum.

IV.2.3. Nitric Oxide

The total photoionization cross-section measurements for nitric oxide by Cook et al (COOK 1965) and Watanabe et al (WATANABE 1967) indicate the presence of many preionized levels. Fig.IV.10. illustrates the nature of the photoionization coefficient, k_1, for nitric oxide as a function of wavelength in the region 750 - 850 Å (WATANABE 1967).

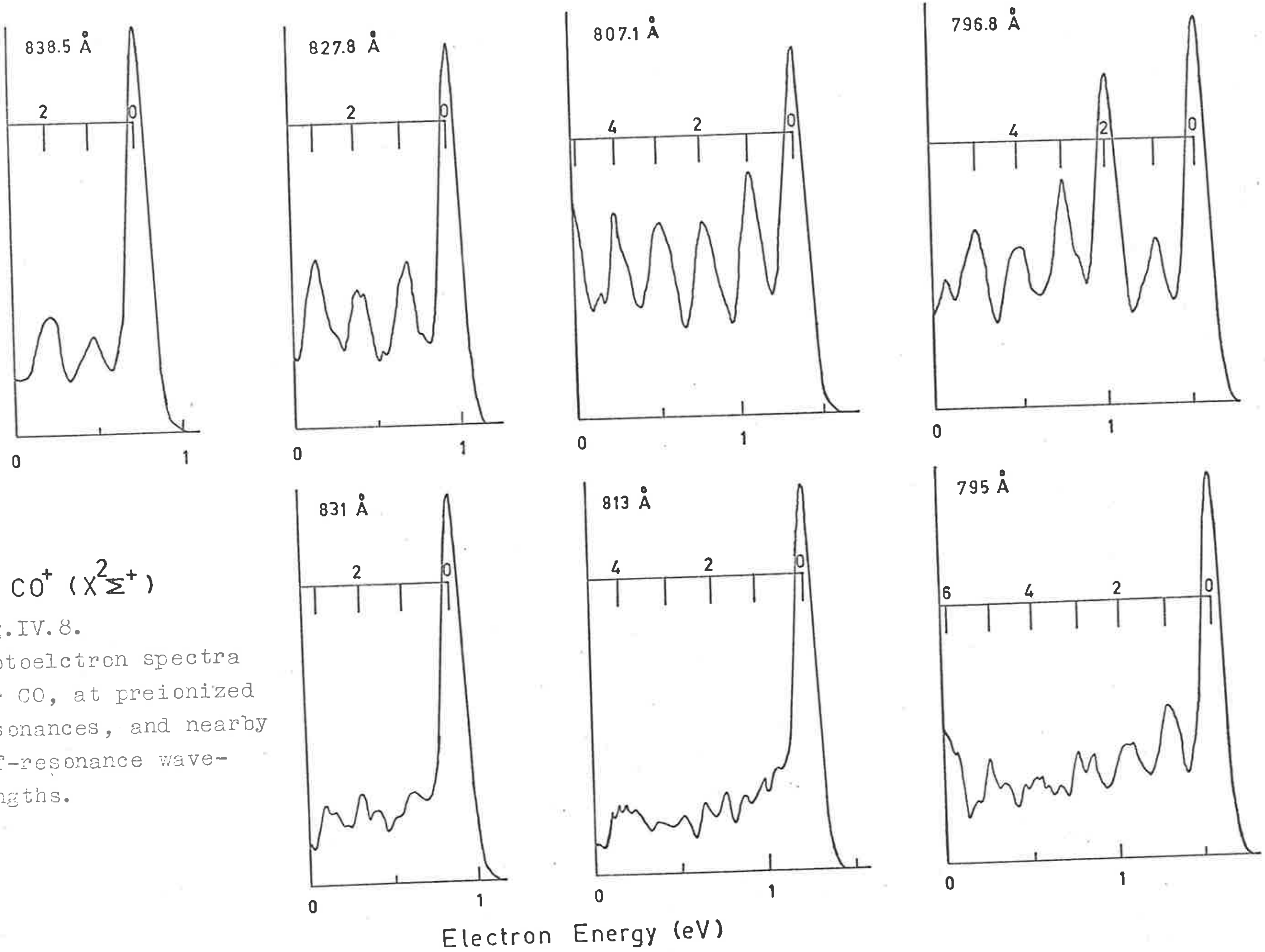

Fig.IV.8.
Photoelctron spectra for CO, at preionized resonances, and nearby off-resonance wave-lengths.

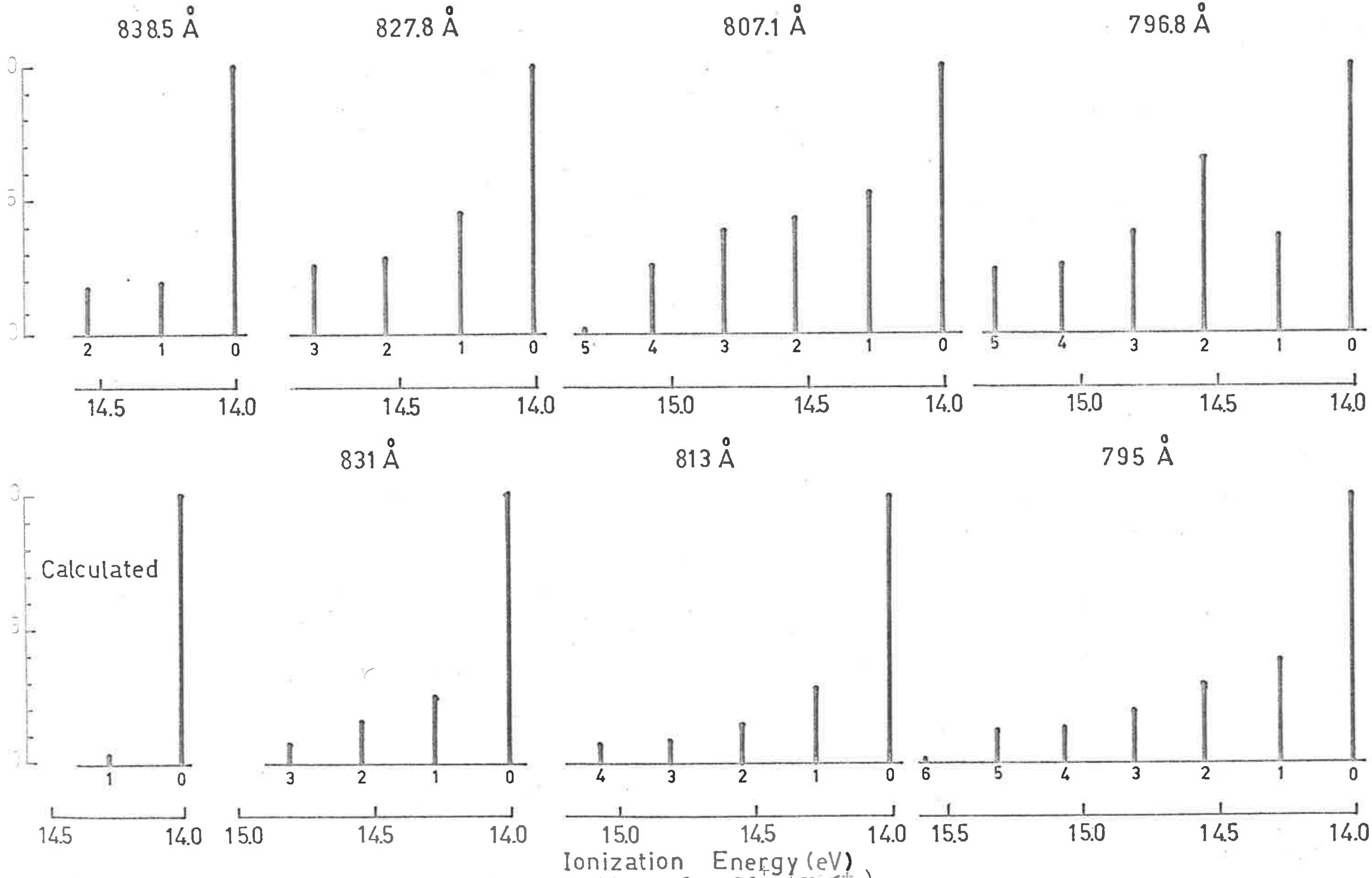

Fig. IV.9. Vibrational distributions for CO^+ ($X^2\Sigma^+$)

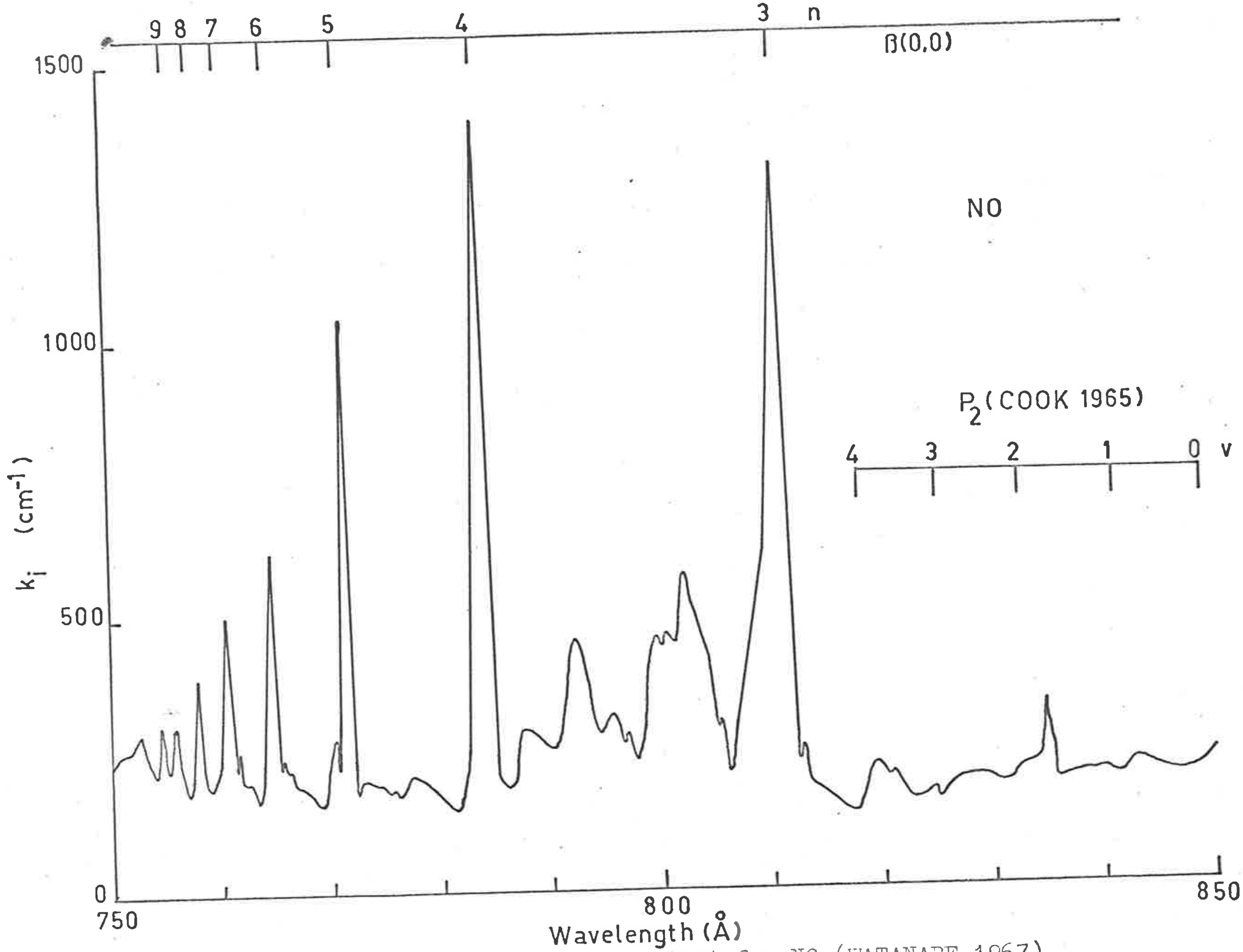

Fig.IV.10 Photoionization coefficient for NO,(WATANABE 1967).

Photoelectron spectra were recorded at the following preionized resonance wavelengths, and off-resonance wavelength:

Table IV.3.

Progression or Series	n	v	$\lambda(\mathring{A})$	$k_1(cm^{-1})$	
Unclassified			941.6	599	
P_2		2	832.5	215	........(a)
P_2		3	825.0	172	........(a)
$\beta(0,0)$	2	0	897.3	3776	
$\beta(0,0)$	3	0	810.6	1310	
$\beta(0,0)$	4	0	783.6	1397	
$\beta(0,0)$	5	0	771.3	1040	
Off-resonance			780	230	

The wavelengths are those given by Watanabe et al except for the two marked (a) which are given by Cook et al; n is the principle quantum number for the $\beta(0,0)$ series which converges to v' = 0 of the $b\,^3\Pi$ state of NO^+, and v is the vibrational quantum number for the preionized state, which, for the P_2 progression is again numbered from the longest wavelength member.

The photoelectron spectra are shown in Figs.IV.11,12. Spectra were also recorded at the argon doublet wavelengths of 1048 Å

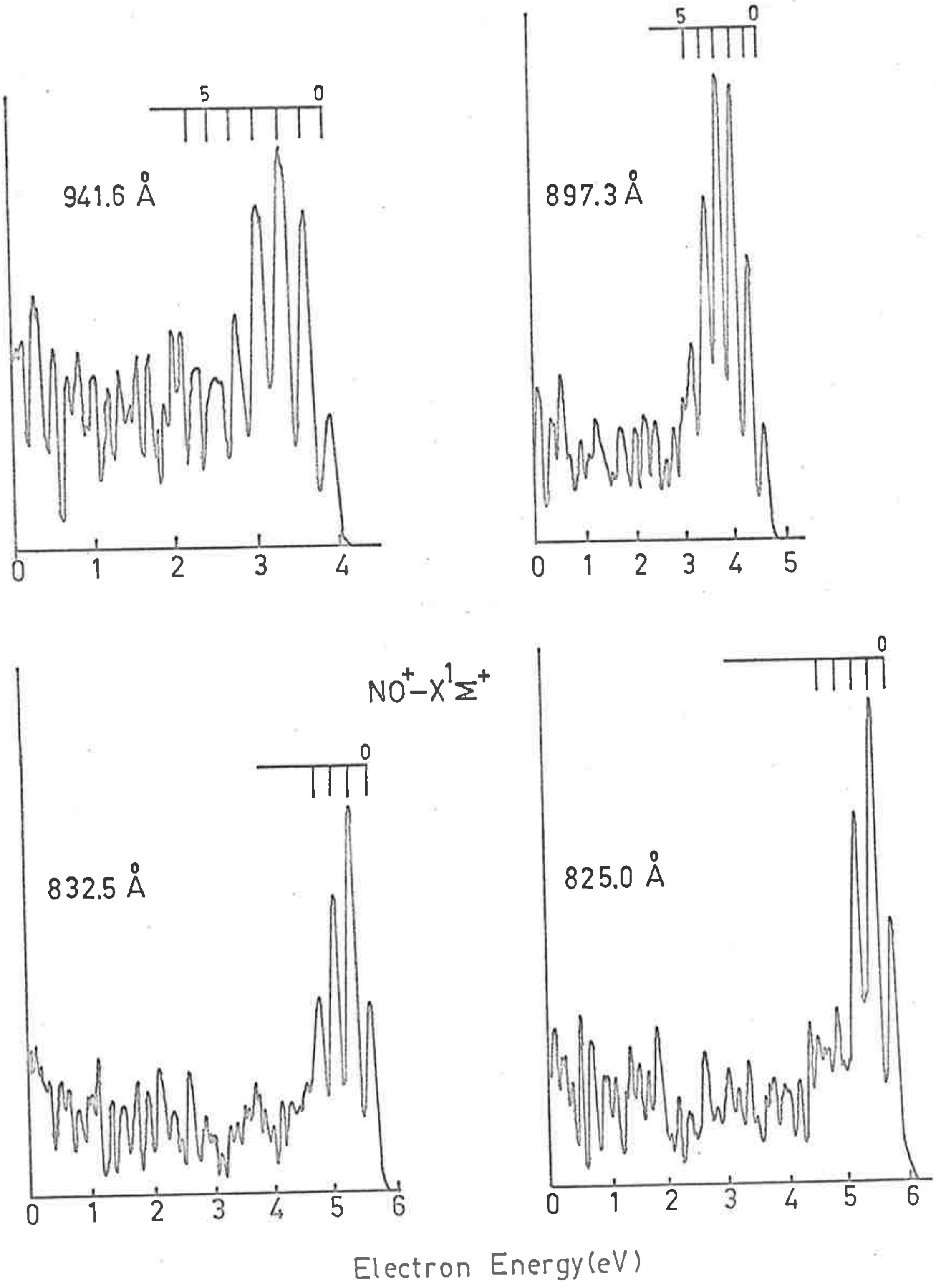

Fig.IV.11. Photoelectron spectra for NO.

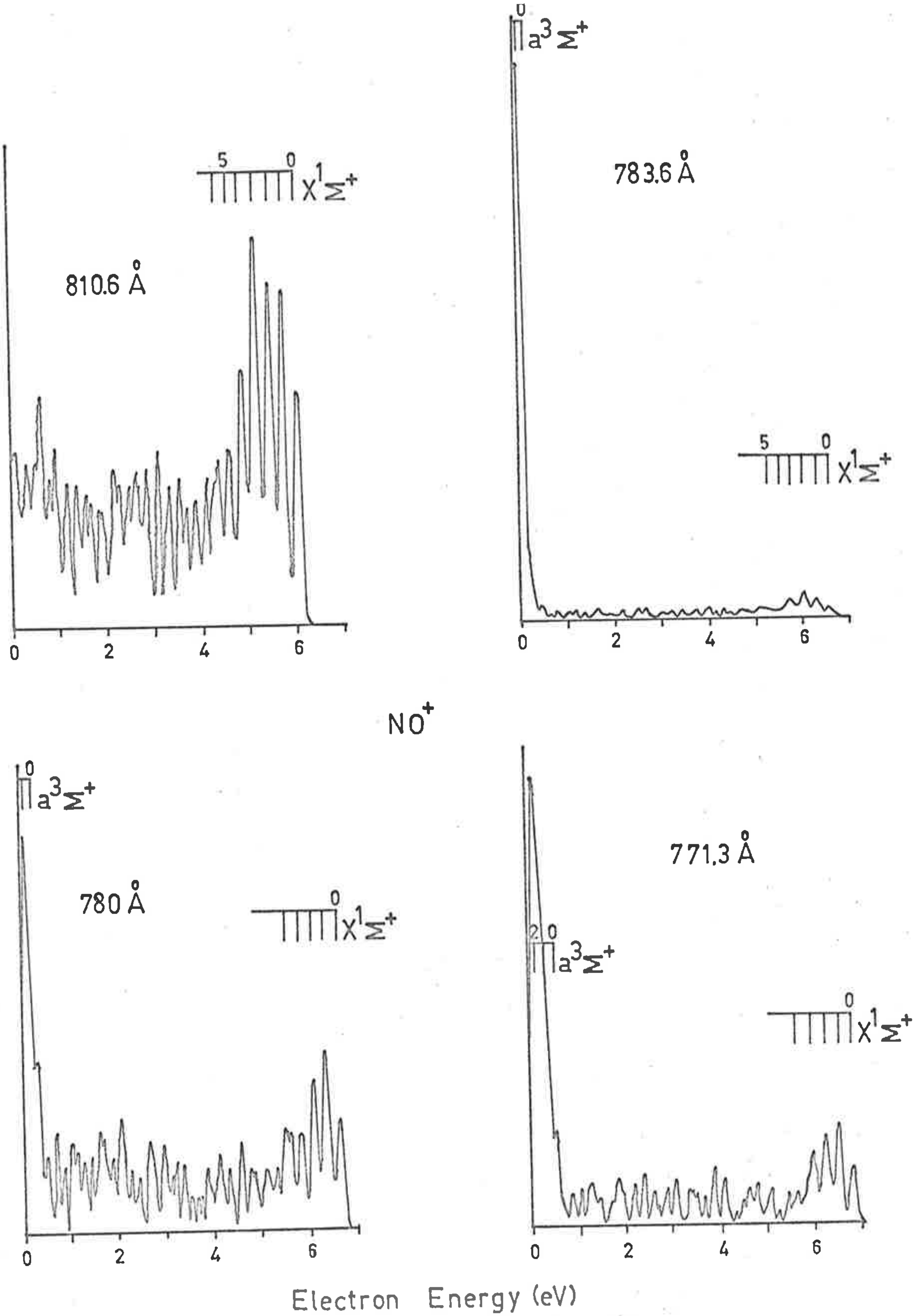

Fig.IV.12. Photoelectron spectra for NO.

and 1067 Å (using an argon light source) and these two spectra are shown in Fig.IV.13. Experimental vibrational intensity distributions were obtained for the spectra by unfolding the curves in the same manner as the nitrogen and carbon monoxide spectra were analyzed. These distributions are shown in Figs.IV.14,15 and 16. Fig.IV.14(a). shows the calculated distribution of F-C factors for the direct photoionization transition $NO(X\,^2\Pi,\ v'' = 0) \rightarrow NO^+\ (X\,^1\Sigma^+,\ v')$, from Table IV.5. The unresolved structure which appeared in the spectra between the $X\,^1\Sigma^+$ state and the $a\,^3\Sigma^+$ state (I.P. = 11 eV to I.P. = 15 eV) was not analyzed because of the large amount of scatter in the data. However, it can be seen from the spectra, especially the 810.6 Å spectrum, that there is more than one maximum in the distribution. For the 810.6 Å spectrum these extra maxima occurred near 0.5 eV and 3 eV (electron energies). Similar effects can be seen in some of the other spectra (941.6 Å, 832.5 Å and 825.0 Å).

The spectra recorded with the argon light source are interesting in that the total cross-section measurements (WATANABE 1967) do not reveal any strong structure in this region. The vibrational intensities of both spectra show secondary maxima, at v = 7-8 for 1067 Å, and at v = 6 and 9 for 1048 Å. Collin and Natalis (COLLIN 1968) reported an asymmetry of the vibrational peaks in their NO spectrum at 1048 - 1067 Å, which they attributed to the rotational envelope of the bands. This type of asymmetry was not observed in the present work,

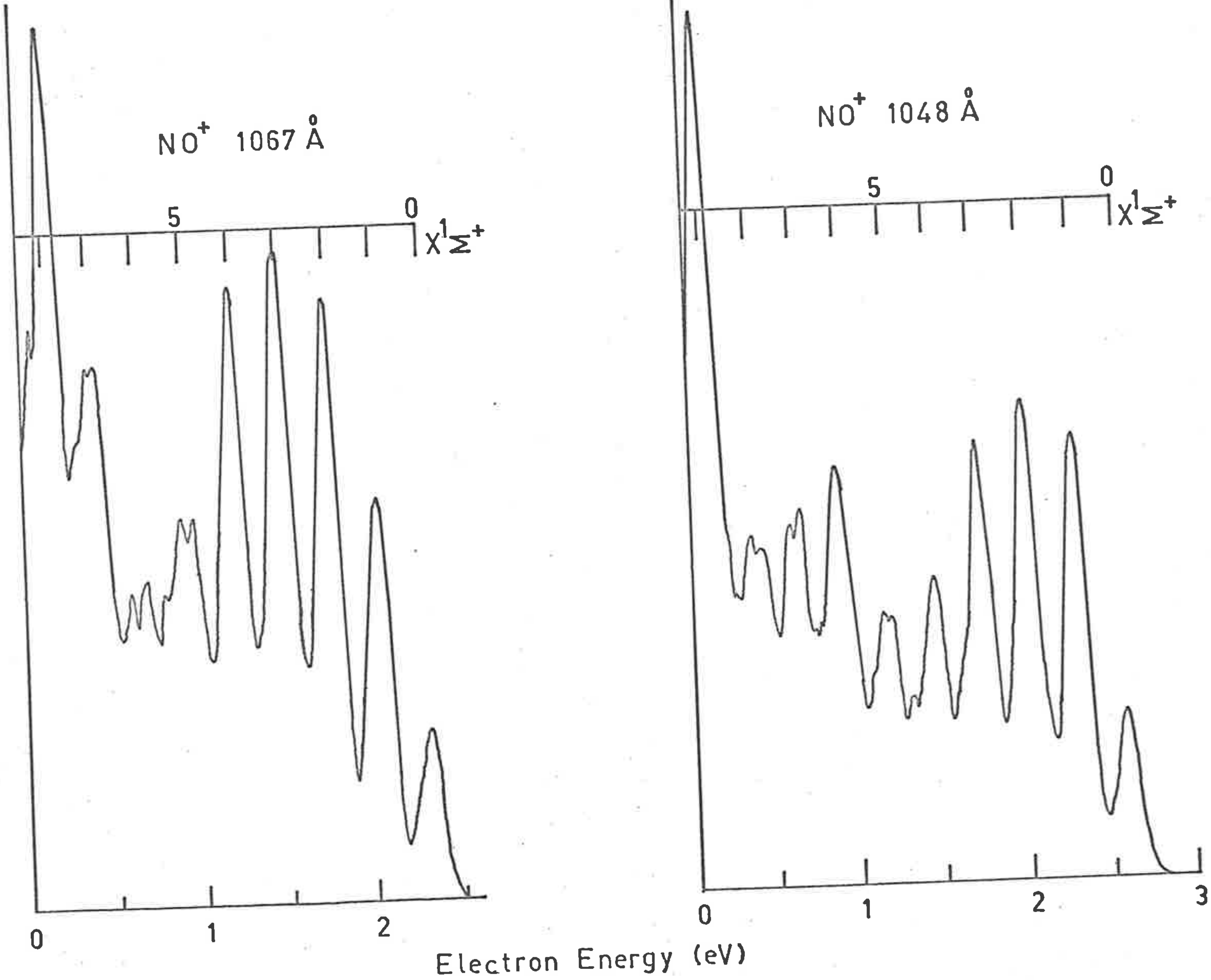

Fig.IV.13. Photoelectron spectra for NO at 1067 and 1048 Å.

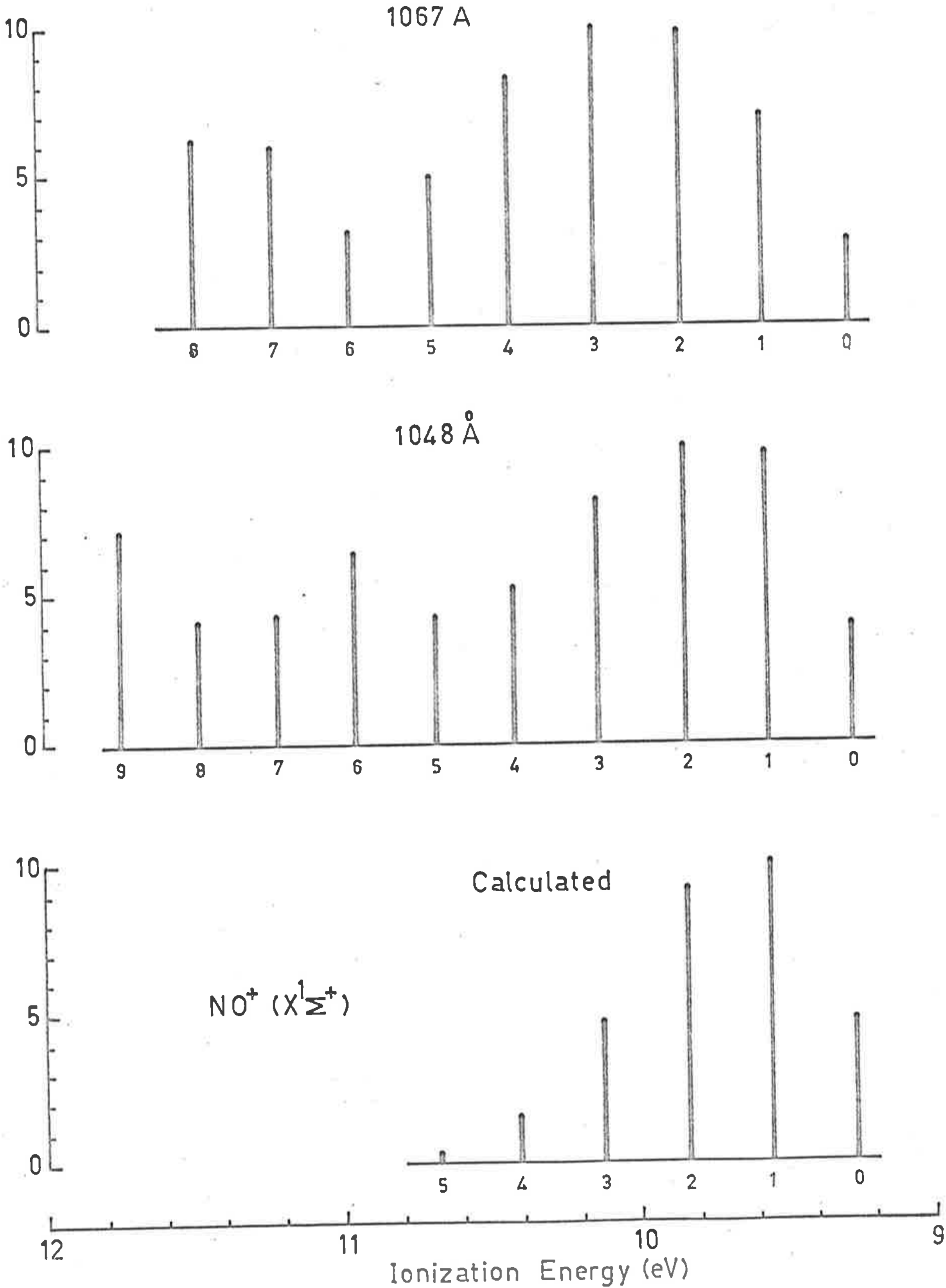

Fig.IV.14. Vibrational intensity distributions for NO$^+$($X^1\Sigma^+$).

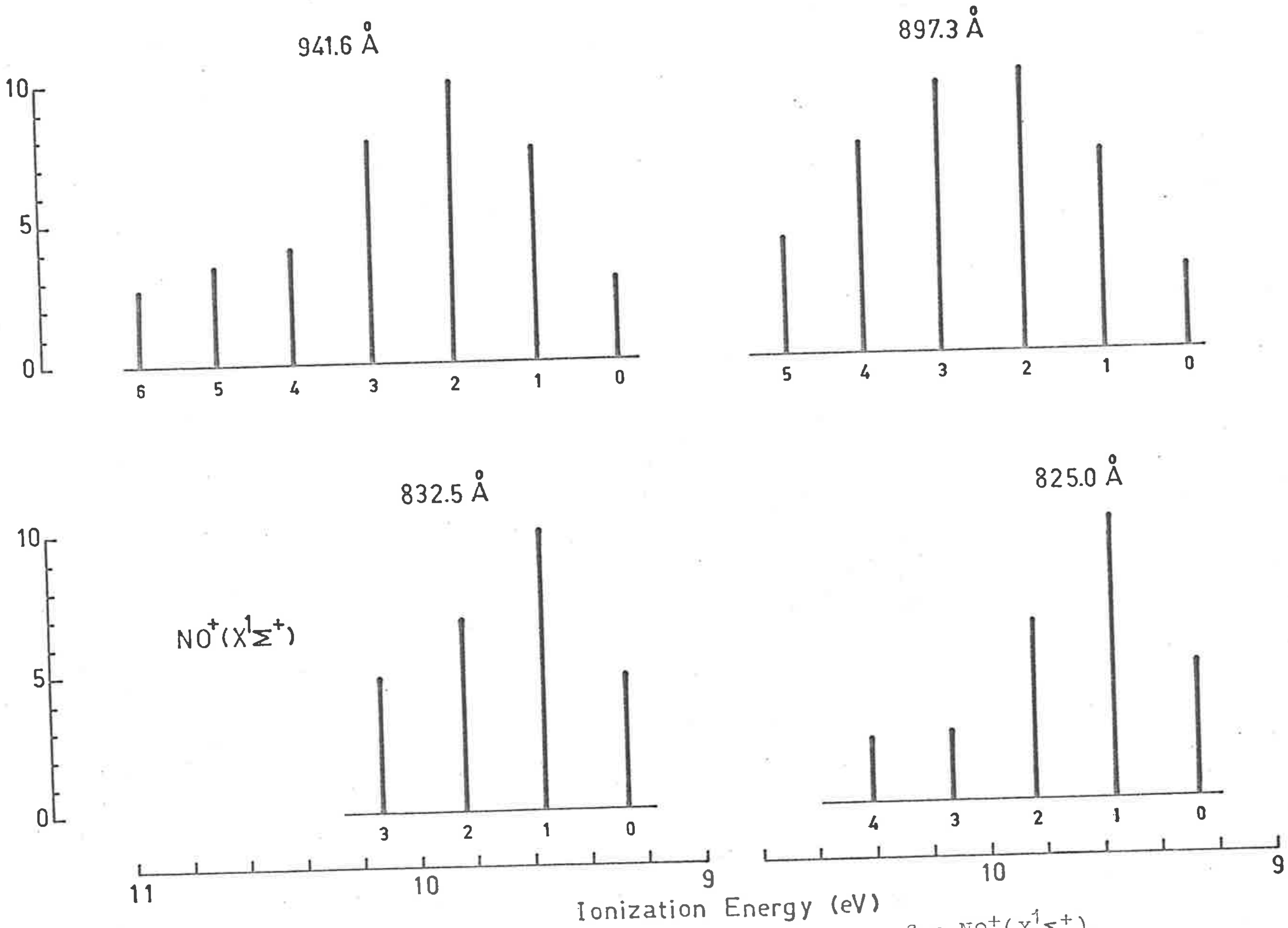

Fig.IV.15. Vibrational intensity distributions for $NO^+(X^1\Sigma^+)$.

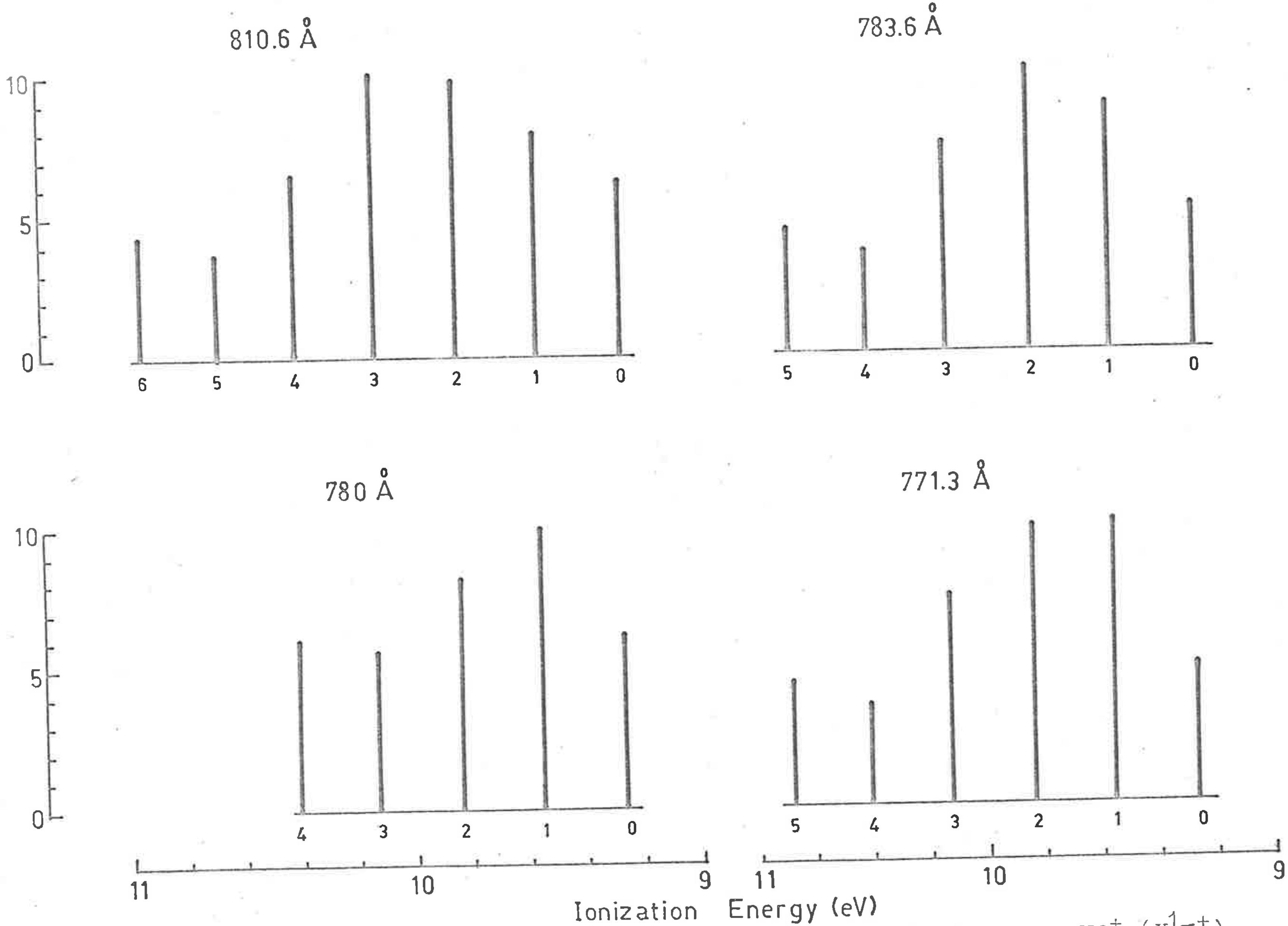

Fig.IV.16. Vibrational intensity distributions for NO$^+$ ($X^1\Sigma^+$).

although the instrument resolution would probably smooth any such effect in the present results. It must also be remembered that Collin and Natalis used undispersed radiation to excite the gas, whereas in the present work a monochromator was used to disperse the radiation.

The three spectra which show the $a\,^3\Sigma^+$ state (783.6 Å, 780 Å, and 771.3 Å) revealed that transitions to this state are enhanced by preionization in the $\beta(0,0)$ series. The branching ratios for these spectra were measured and are shown in Table IV.4.

Table IV.4.

Branching Ratio (%)

λ(Å)	$X\,^1\Sigma^+$	$a\,^3\Sigma^+$	
783.6	78	22	$\beta(0,0)$ n = 4
780	91	9	Off-resonance
771.3	72	28	$\beta(0,0)$ n = 5

Thus there is a substantial increase in the percentage of transitions to the $a\,^3\Sigma^+$ state, at the expense of the $X\,^1\Sigma^+$ state, when the molecule is ionized via the preionized level.

IV.3. Preionization and Franck-Condon Factors in the Photoelectron Spectra of Diatomic Molecules.

The photoelectron spectra of diatomic molecules consist, in general, of several bands which are resolved into a number of peaks, each of which corresponds to a transition from the initial state of the molecule to a particular electronic and vibrational state of the ion. The extent of the vibrational structure depends on the bonding character of the electron which is removed, and in many cases it has been found that the intensity distribution of the peaks in a band is closely related to the calculated Franck-Condon (F-C) factors (e.g. TURNER 1966, FROST 1967).

IV.3.1. Franck-Condon Factors for Ionization

It was shown in Sec.1.2.4. that the probability of photoionization of a diatomic molecule is given by:

$$I_{v'v''} = K_{el}\ \nu\ q_{v'v''} \qquad (38)$$

where

$$K_{el} = I_o \frac{8\Pi^3}{3hc} \Delta x\ N_{v''}\ \overline{R}_e \qquad (39)$$

and

$$q_{v'v''} = \left[\int \Psi_{v'} \Psi_{v''} dr\right]^2 \qquad (24)$$

Thus $I_{v'v''}$ is the probability of a transition between the v'' vibrational level of the initial state and the v' vibrational level of the final state (ionic in this case), and K_{el} is a factor which depends on the electronic transition probability and the statistical weight of the final state. It is assumed that K_{el} varies slowly with the internucelar distance r.

Franck-Condon factors for ionization have been calculated in the past from Morse potential wavefunctions (WACKS 1964 , NICHOLLS 1968, HALMANN 1968). In the present work a method for computing F-C factors using Morse-Pekeris potential functions and wavefunctions was programmed for a CDC 6400 computer. The method, which was basically similar to that used by Halmann and Laulicht (HALMANN 1968), is given in Appendix I.

The quality of the calculations is best seen by comparison with previously published data, and in Table IV.5. the F-C factors for the transitions N_2 $(X\ {}^1\Sigma_g^+,\ v'' = 0) \rightarrow N_2^+$ $(X\ {}^2\Sigma_g^+,\ v')$, CO $(X\ {}^1\Sigma^+,\ v'' = 0) \rightarrow$ CO^+ $(A\ {}^2\Pi,\ v')$ and NO $(X\ {}^2\Pi,\ v'' = 0) \rightarrow NO^+$ $(X\ {}^1\Sigma^+,\ v')$ by Wacks, Halmann and Laulicht, and Nicholls are tabulated with the present results. The agreement between the results is excellent.

In general $q_{v'v''}$ has a significant value for several values of v' for a given v'' and the form of this distribution of $q_{v'v''}$ depends largely on the value of v'' and the change in the equilibrium internuclear distance (r_e) which occurs when the electron is removed. Several

TABLE IV.5

Franck-Condon Factors for Ionization

N_2 $(X^1\Sigma_g^+)\rightarrow N_2^+$ $(X^2\Sigma_g^+)$

$q_{v'v''}$

v''-v'	NICHOLLS	HALMANN	Present Work
0 - 0	0.90236	0.90236	0.90150
1	0.09064	0.09064	0.09135
2	0.00651	0.00651	0.00662
3	0.00045	0.00046	0.00047
4	0.00004	0.00004	0.00004
5	0.00000	0.00000	0.00000

CO $(X^1\Sigma^+)\rightarrow CO^+$ $(A^2\Pi)$

$q_{v'v''}$

v''-v'	NICHOLLS	WACKS	HALMANN	Present Work
0 - 0	0.07906	0.07937	0.07929	0.07938
1	0.17572	0.17618	0.17606	0.17619
2	0.21490	0.21517	0.21510	0.21518
3	0.19213	0.19212	0.19212	0.19211
4	0.14082	0.14062	0.14068	0.14061
5	0.08999	0.08979	0.08981	0.08972
6	0.05208	0.05187	0.05193	0.05184
7	0.02801	0.02786	0.02800	0.02784
8	0.01425	0.01416	0.01420	0.01414
9	0.00696	0.00690	0.00688	0.00689
10	0.00329	0.00326	0.00341	0.00326
11	0.			0.00150
12				0.00068
13				0.00031
14				0.00013
15				0.00004

NO $(X^2\Pi)\rightarrow NO^+$ $(X^1\Sigma^+)$

$q_{v'v''}$

v''-v'	NICHOLLS	WACKS	HALMANN	Present Work
0 - 0	0.15501	0.15500	0.15498	0.15506
1	0.32416	0.32417	0.32415	0.32421
2	0.29723	0.29725	0.29725	0.29723
3	0.15702	0.15702	0.15703	0.15699
4	0.05282	0.05281	0.05282	0.05280
5	0.01181	0.01180	0.01181	0.01180
6	0.00178	0.00178	0.00178	0.00177
7	0.00018	0.00018	0.00018	0.00018
8		0.00001	0.00002	0.00001

distributions of calculated F-C factors are shown in Fig.IV.17. for ionizing transitions between typical electronic states whose potential energy curves have minima separated by an amount Δr_e. The height of each vertical line represents the $q_{v'v''}$ value for the transition from the vibrational level v" of the molecule to the level v' of the ionic state, and v' increases from right to left. Each distribution may be considered as a photoelectron spectrum, with the electron energy increasing from left to right.

For the case of direct ionization from the ground electronic state of the molecule at room temperature the value of v" is restricted to zero. When Δr_e is very small there is almost total overlap between the wavefunctions $\Psi_{v''=0}$ and $\Psi_{v'=0}$ and the v' = 0 level is excited strongly to the exclusion of the others as is shown in Fig.IV.17(a). As Δr_e increases $\Psi_{v''=0}$ begins to have significant overlap with other wavefunctions $\Psi_{v'}$, and the transition probability is shared among several levels v' (Fig.IV.17(b)). For large values of Δr_e it may be expected that the discrete spectrum is joined by a continuous distribution corresponding to dissociative ionization, as shown in Fig.IV.17(c). The form of most observed photoelectron spectra does in fact behave in this manner.

However, if the gas is excited by radiation of a wavelength which coincides with a preionized resonance in the photoionization cross-section then there is a large probability that the molecule is

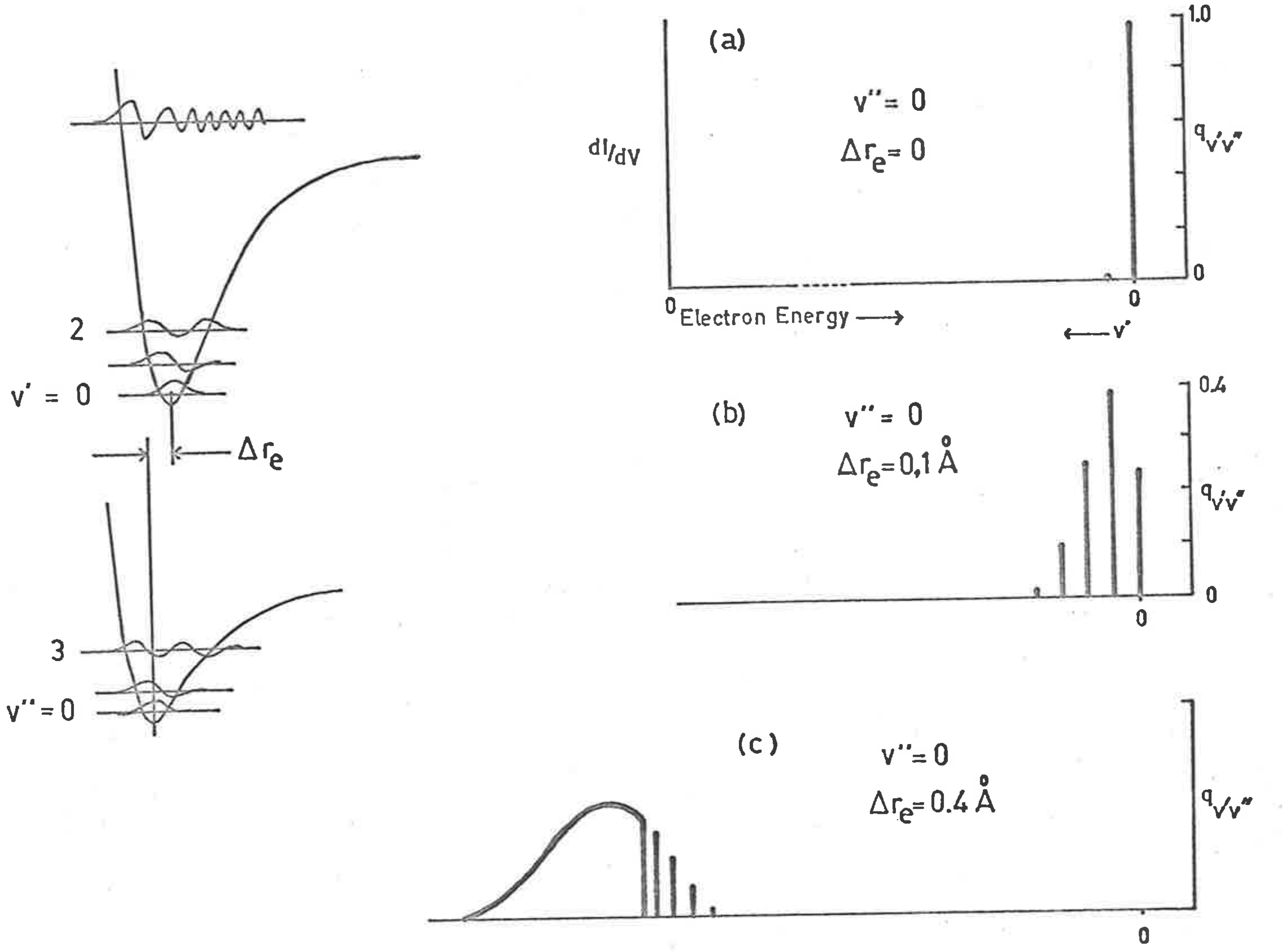

Fig.IV.17. (a), (b), and (c).

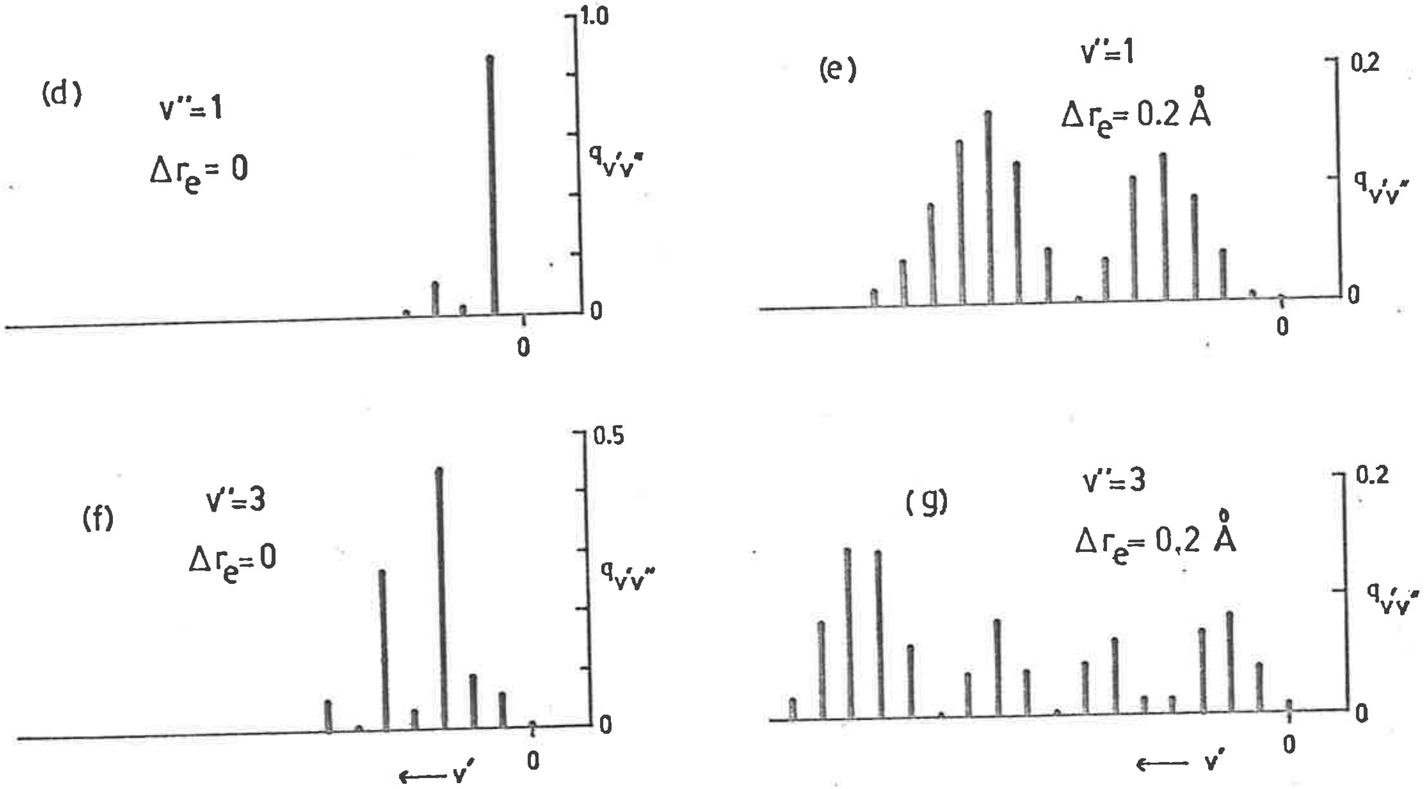

Fig.IV.17. (d), (e), (f), and (g).

excited to the discrete super-excited state, which is a well defined vibrational level, and it then decays to the ionization continuum. It is reasonable to expect that the photoelectron spectrum resulting from preionization is described by the F-C factor distribution for the decay of the preionizing state, and since the value of v'' is no longer restricted to zero, more complex distributions of the F-C factors occur. For small values of v'' it is found that the distribution of $q_{v'v''}$ has $(v'' + 1)$ maxima, corresponding to overlap of the $\Psi_{v'}$ with successive maxima of the function $\Psi_{v''}$. This situation is illustrated schematically in Fig.IV.18. for the case $v'' = 3$ where four broad maxima are expected in the distribution. The vibrational quantum number at which these maxima occur (i.e. the values of v' for which the overlap integral has its maximum values) can be seen from Fig.IV.18. to depend sensitively on the difference between the r_e values for the preionized state of the molecule and the final ionic state. Typical calculated distributions for $v'' = 1$ and $v'' = 3$ are shown in Figs.IV.17(d) to (g). They illustrate the way in which vibrational structure in photoelectron spectra may be dramatically extended in a way that is characteristic of the preionizing level.

It is interesting to note that in some cases the distribution of $q_{v'v''}$ may extend below the zero of the electron energy scale as a result of preionization and the whole distribution will not be seen in the photoelectron spectrum.

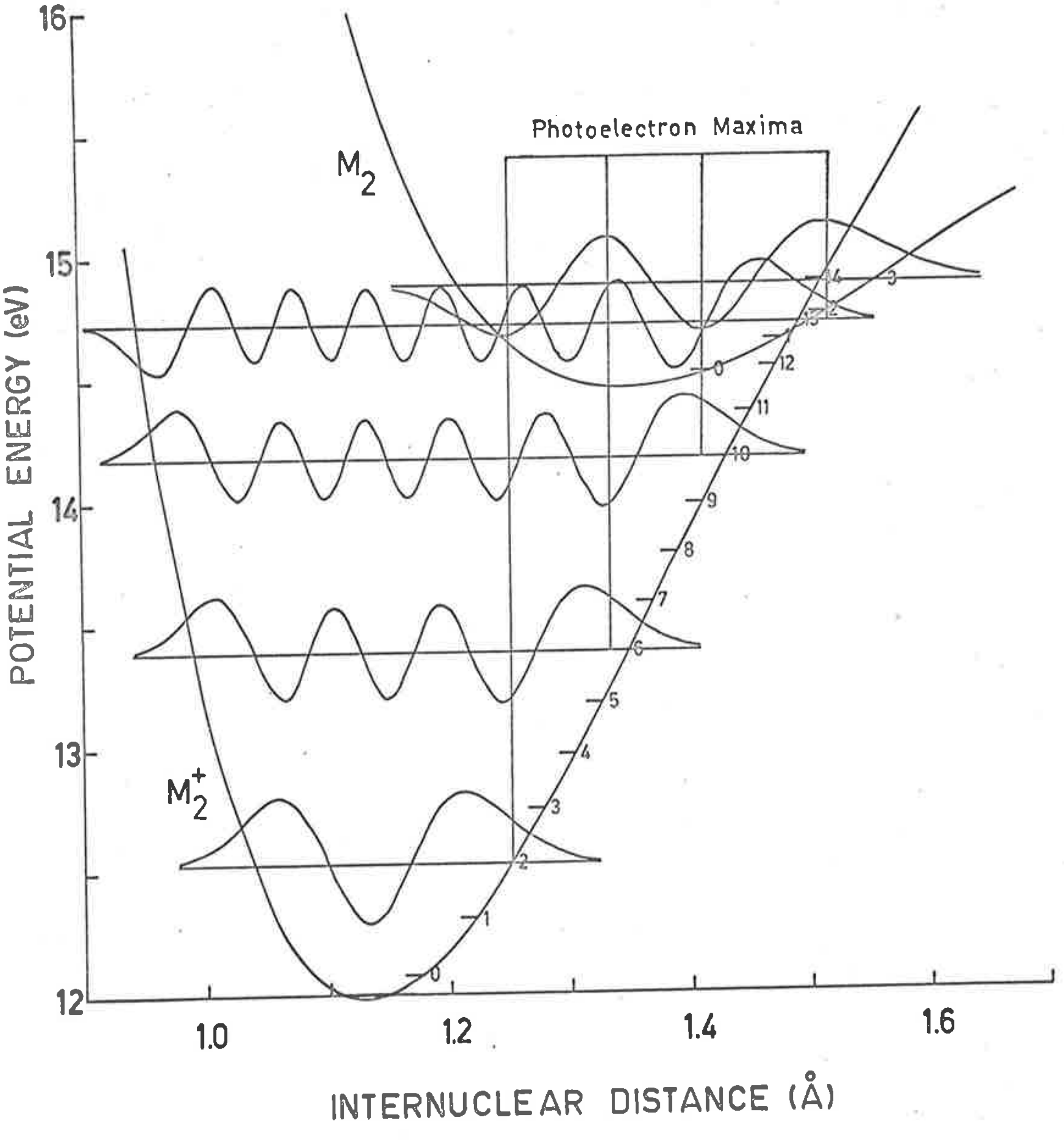

Fig.IV.18. Potential energy diagram illustrating the overlap between the vibrational wavefunctions of a molecule M_2 and its ion M_2^+.

Thus spectra recorded at resonance wavelengths can be reconstructed by combining the relevant F-C distributions for the direct ionization and for preionization, each weighted by a factor K_{el}. Using the vibrational sum rule:

$$\sum_{v'} q_{v'v''} = 1 \qquad (40)$$

the sum of the strengths of the peaks in a band is proportional to K_{el} for a given photon energy, and to the partial photoionization cross-section corresponding to the particular electronic state of the ion.

IV.4. Discussion

The spectra presented in Sec.IV.2. show, in general, that preionization of a diatomic molecule can have a marked effect on the photoelectron energy distribution.

The carbon monoxide spectra provide the best examples of the resonant characteristic of preionization. The three off-resonance spectra show that the anomalous vibrational distributions in the $X\,^2\Sigma^+$ state of CO^+ are uniquely associated with the preionized levels of the H1 progression. The small anomalies which do occur in the off-resonance spectra are assumed to be due to a combination of the broadness of the preionized resonance levels in the molecule and the incident beam resolution (1.6 Å). Thus it is improbable that spectra recorded anywhere in this region (790 - 850 Å) with this beam resolution would show the calculated distribution of F-C factors for direct ionization.

The resonance spectra in carbon monoxide show that the vibrational distributions are quite extended due to preionization, as was suggested in Sec.IV.3.1. The spectrum at 798.6 Å in particular shows two broad maxima (at v' = 0,2) indicating a transition from a level with a vibrational quantum number which is probably non-zero.

The nitrogen spectra do not have enough vibrational levels in the ground ionic state to enable observation of the broad maxima which might be expected from the considerations of Sec.IV.3.1. This occurs because of the onset of the $A\,^2\Pi_u$ state of N_2^+ at 16.69 eV (743 Å) which allows only five vibrational levels at the most to be observed in the spectrum. However, there are definite vibrational distribution anomalies in the spectra presented in Sec.IV.2.1. The spectrum recorded at 771.6 Å shows in particular that the expected distribution of vibrational intensities can be greatly modified by preionization.

The β(0,0) series in nitric oxide, which converges to the $b\,^3\Pi$ state of NO^+ at 16.56 eV (749 Å), has a vibrational quantum number of zero, and hence the spectra recorded at the resonance wavelengths would be expected to show the same vibrational distribution in the $X\,^1\Sigma^+$ state of NO^+, provided the r_e value for all the states is the same. Figs.IV.15,16 indicate that slight variations do occur in the distribution among the first 6 levels, which may be attributed to a variation in the r_e value of the preionized states of the β(0,0) series.

The 810.6 Å spectrum (Fig.IV.11.) does, however, show three broad (but weak) maxima. These maxima are not expected from the theory proposed in Sec.IV.3. if the preionized level is assumed to be a pure $v = 0$ state (since the maximum number of broad peaks possible in this case is two), so it is suggested that as the effect is weak it may be attributed to another overlapping preionized state in nitric oxide with a different vibrational number. Cook et al (COOK 1965) reported a maximum in the total cross-section at 812.2 Å which may be the level producing these maxima in the distribution.

CHAPTER V

V. Photoelectron Spectroscopy for some Preionized States of Molecular Oxygen

Apart from its intrinsic interest, oxygen is one of the most important constituents of the atmosphere, and for this reason it has perhaps been subject to more investigation than any gases other than nitrogen and hydrogen.

It was mentioned in Chapter IV that whilst measuring the partial photoionization cross-sections for oxygen, Blake and Carver (BLAKE 1967) observed anomalous structure in the photoelectron spectra of the gas between the $X^2\Pi_g$ and the $a^4\Pi_u$ states of O_2^+ for wavelengths longer than 680 Å. In particular, for wavelengths longer than 775 Å ($a^4\Pi_u$ threshold) only the $X^2\Pi_g$ ground state of the ion is accessible, and the oxygen photoelectron spectra at these wavelengths might be expected to show but a single band such as is observed at 584 Å, (see Fig. V.4). However, they observed a low energy peak in the spectra which appeared to remain constant at an energy of $\sim$0.5 eV when the photon energy was varied over a large range of values. They attributed this phenomenon to a process of fluorescent autoionization, which is shown schematically in Fig. IV.1.

V.1 The Total Photoionization Cross-section of Oxygen

The region between 800-1000 Å in the total photoionization cross-section for oxygen contains a wealth of preionization structure (see Fig. I.13 for part of this region). Much of this structure has been classified into vibrational progressions as indicated in Fig. I.13. For the present work, a detailed investigation of the photoelectron energy spectrum in this region was achieved by recording spectra at 13 preionized resonance wavelengths and 3 off-resonance wavelengths in the region. The wavelengths, and the values of the photoionization coefficient at those wavelengths, as given by Matsunaga and Watanabe (MATSUNAGA 1967), are listed in Table V.1.

TABLE V.1

Progression	v	λ(Å)	k_i (cm^{-1})
H	3	972.9	800
M	0	957.0	730
M	1	947.7	1060
M	2	939.3	630
M'	3	910.5	300
J	0	894.0	200
J	1	885.8	310
J	2	878.1	230
J	3	870.0	160
I	0	853.2	150
I	1	845.9	140
I	2	839.1	290
I	3	832.5	260
Off-resonance		970	55
"		920	57
"		889	82

Again, the v=o member has been assumed to be the longest wavelength member of the progression, where v is the vibrational quantum number of the preionized state.

In order to know how well resolved the preionized levels were with the present monochromator and detecting system, the total electron current from the photoelectron spectrometer with zero retarding volts was measured as a function of wavelength over the range 800-1000 Å. (The multichannel analyzer was used as a multichannel store, where each channel corresponded to a wavelength interval of 0.25 Å). The resulting curve is shown in Fig. V.1 for the range 800-900 Å. It must be remembered that this curve represents the product of the photoionization cross-section with the incident light intensity (to a good approximation) and should not be interpreted as the photoionization cross-section. Comparing this curve with Fig. I.13 it can be seen that all of the peaks were well defined in the present work, and each preionized resonance could be easily located.

V.2 The Photoelectron Spectra for Incident Wavelengths between 900-1000 Å

The photoelectron spectra for oxygen between 900 and 1000 Å are shown in Fig. V.2. The spectrum for the $X^2\Pi_g$ state of O_2^+ at 584 Å was also recorded and is shown in Fig. V.4(a).

Fig. V.2(a,b) shows the spectra for the strong preionized

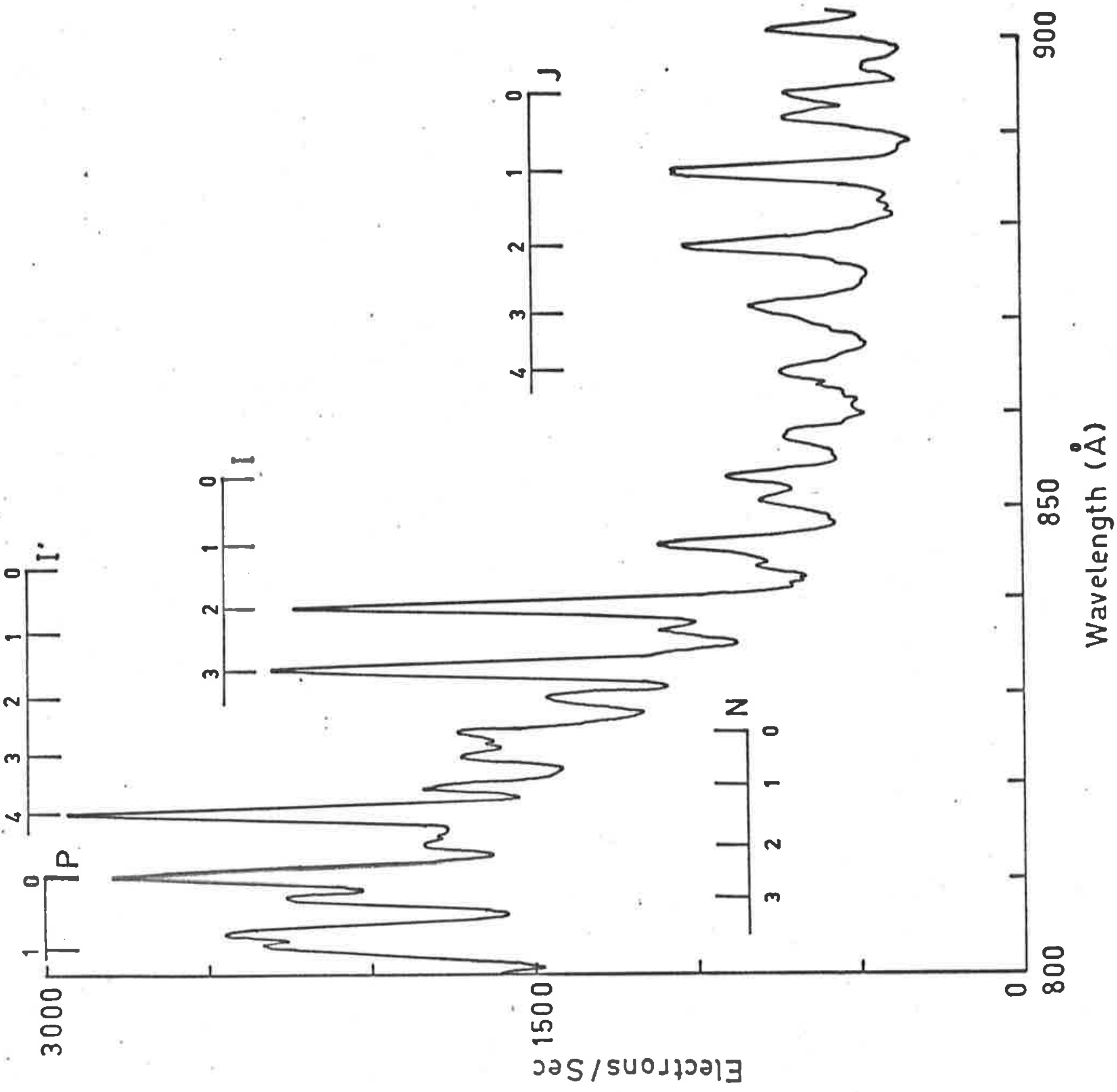

Fig.V.1. Total electron current versus wavelength for O_2 measured at zero retarding volts.

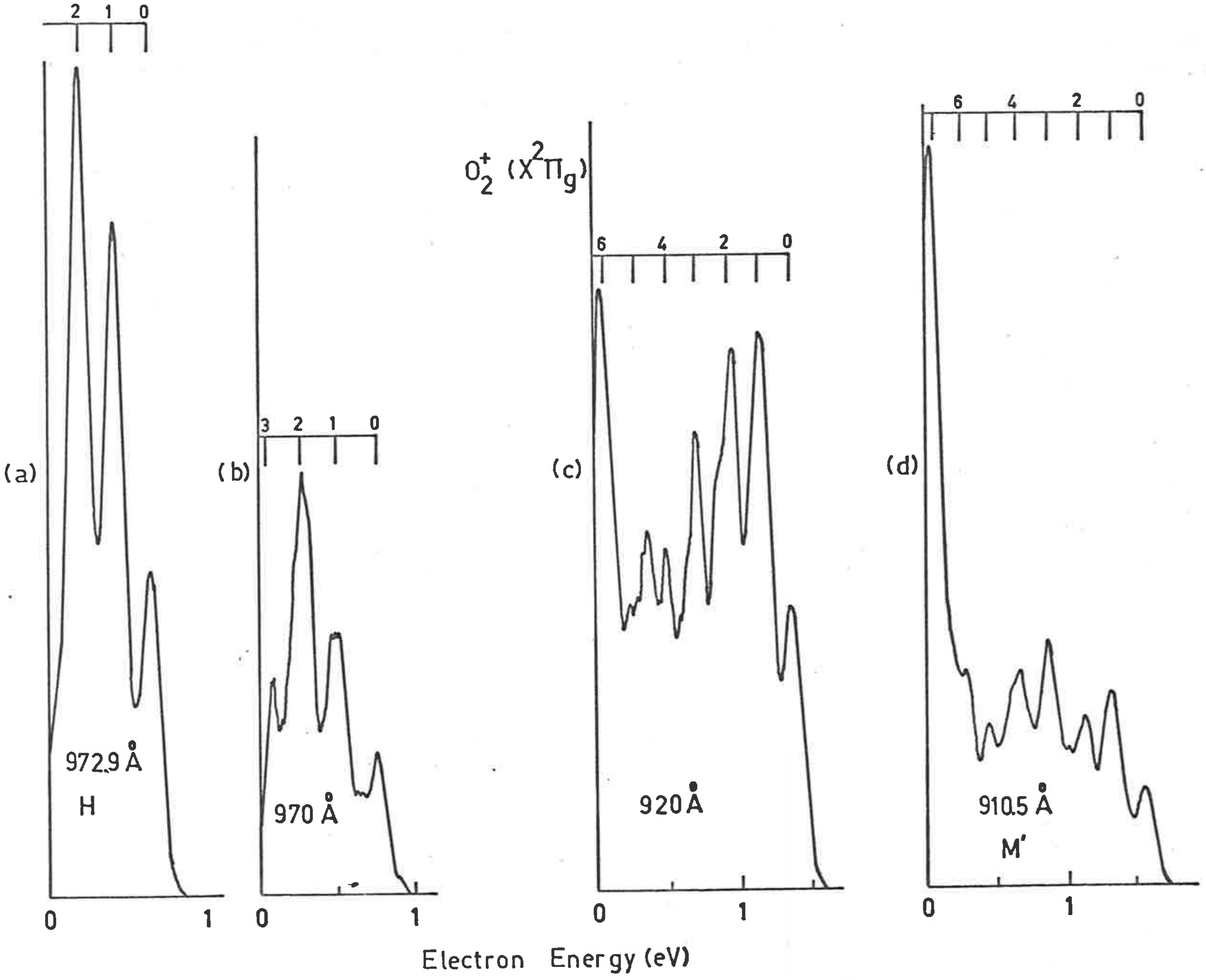

Fig.V.2. Photoelectron spectra for O_2 at 972.9, 970, 920 and 910.5 Å.

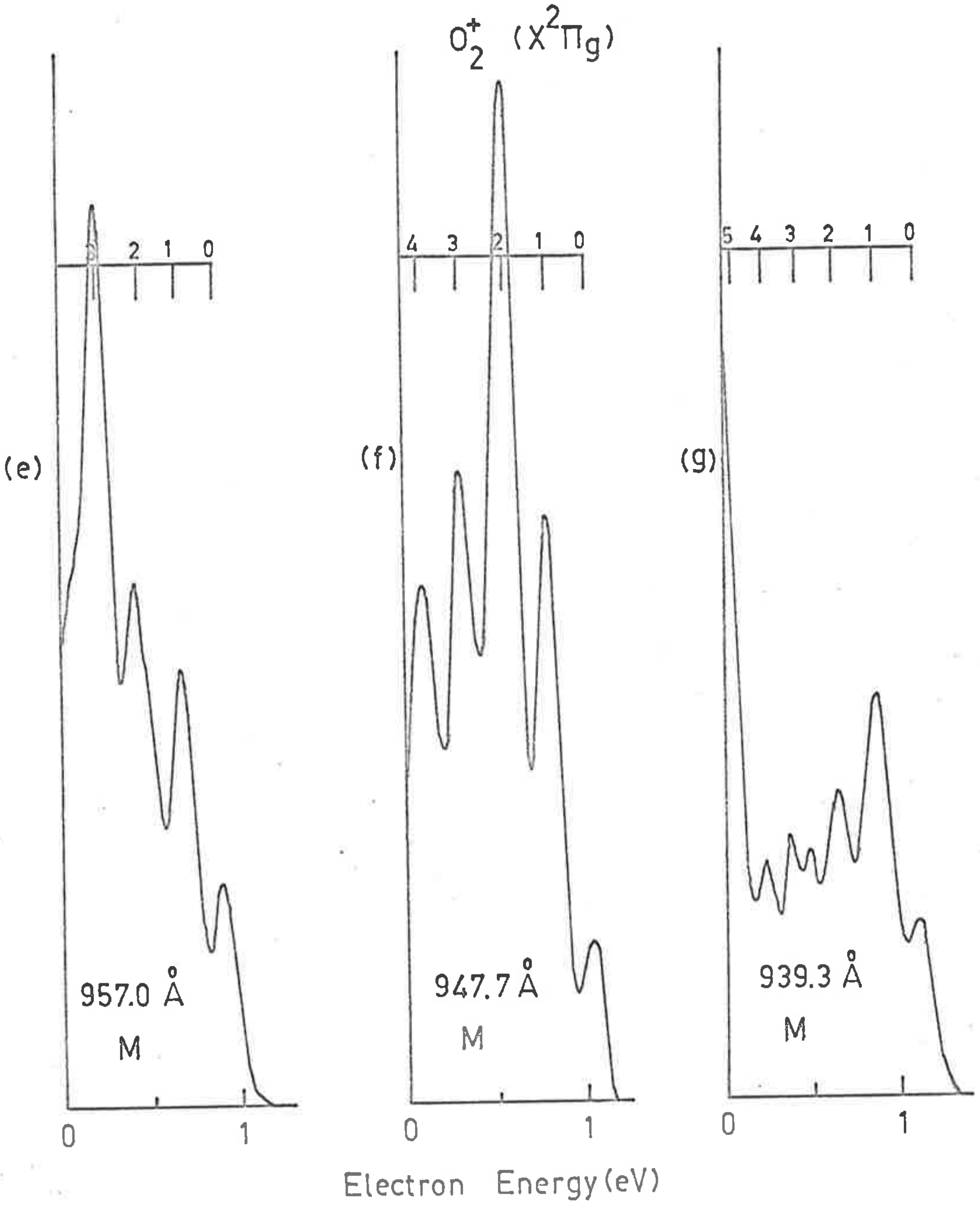

Fig. V. 2. (cont) Photoelectron spectra for O_2 at 957.0, 947.7 and 939.3 Å.

resonance at 972.9 Å (H progression, v=3) and the spectrum recorded at a nearby minimum (970 Å). There is little difference between the spectra. This is probably the result of the broad resonance at 965.5 Å (MATSUNAGA 1967), which is very assymetric in shape when compared with the 972.9 Å resonance and does not allow the minimum at 970 Å to be well defined. Fig. V.2(c,d) shows the spectra on resonance at 910.5 Å (M' progression, v=3) and off resonance at 920 Å. These two spectra show a marked difference in the vibrational distribution of the $X^2\Pi_g$ state of O_2^+. The vibrational distributions for these four wavelengths, obtained by unfolding the spectra as was done previously (Sec. IV.2.1), are presented in Fig. V.3(a,b,c,d). The 920 Å spectrum has a distribution similar to that at 584 Å (Fig. V.4), while the 910.5 Å spectrum has a distribution with maxima at v'=1, 3 and 6, indicating that transitions to the $X^2\Pi_g$ state of O_2^+, at this wavelength, originate at a state with a non-zero vibrational quantum number, as was proposed in Chapter IV.

The spectra corresponding to the M progression, at 957.0 Å, 947.7 Å and 939.3 Å, are shown in Fig. V.2(e,f,g). The experimental vibrational intensity distributions for these spectra are shown in Fig. V.3(e,f,g). The 957.0 Å (v=0) and 947.7 Å (v=1) spectra show marked differences in their vibrational distributions, and both are well removed from the 584 Å distribution of Fig. V.4(b). The 939.3 Å (v=2) spectrum shows a distribution which is closer to the distribution

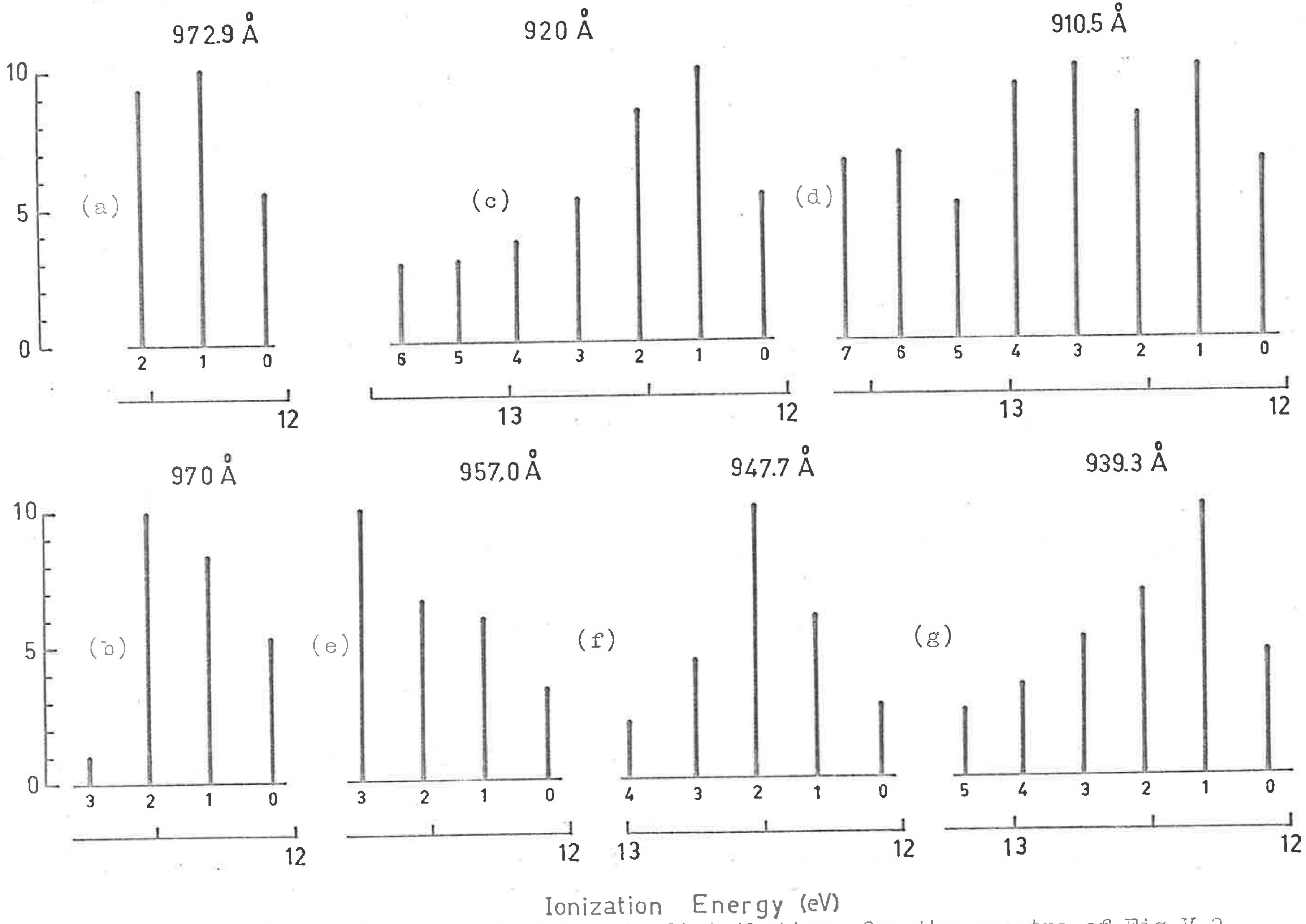

Fig.V.3. Vibrational intensity distributions for the spectra of Fig.V.2.

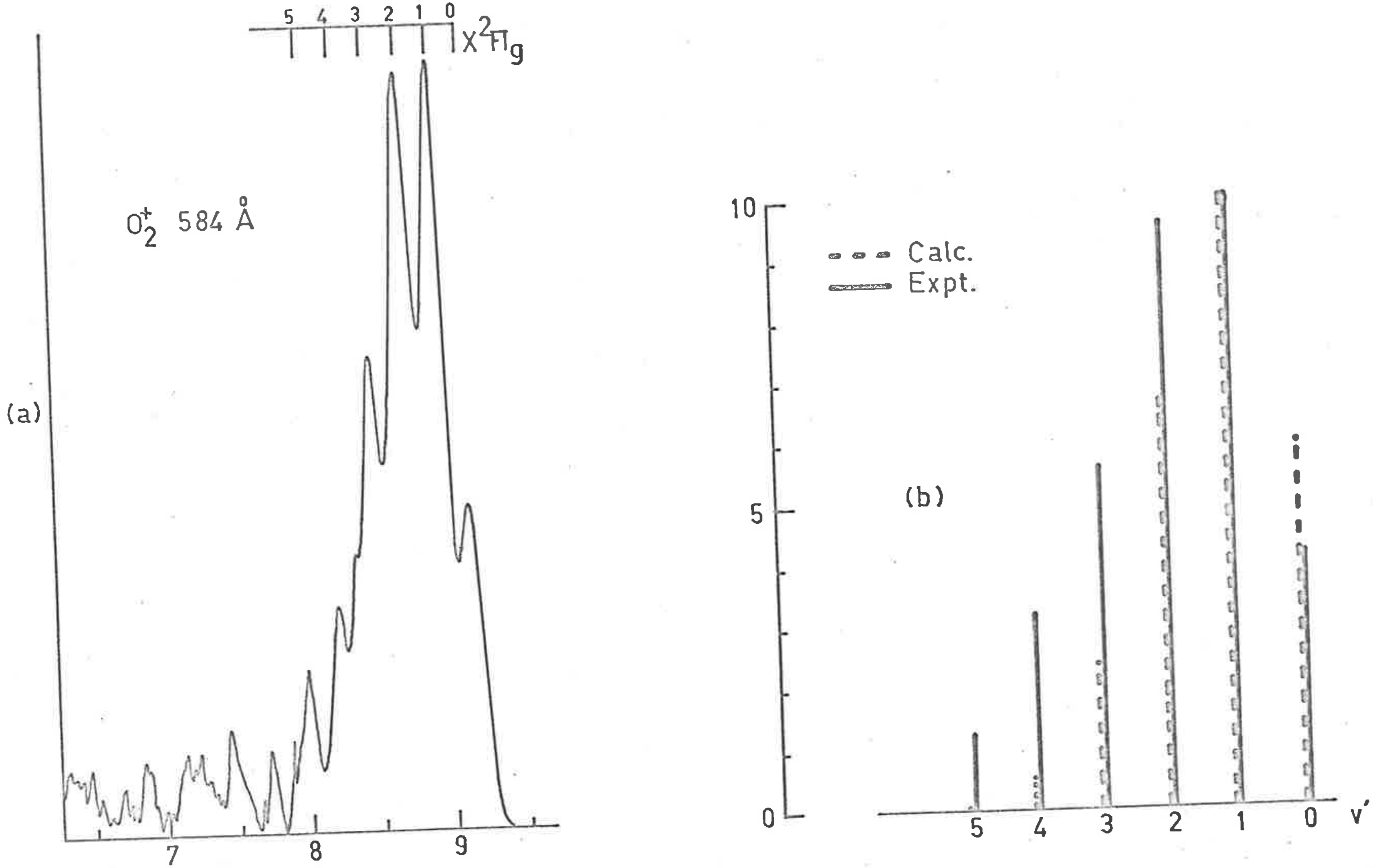

Fig.V.4. (a) Photoelectron spectrum for O_2 at 584 Å
(b) Vibrational distribution for the 584 Å spectrum(solid line), and the calculated F-C distribution (broken line).

calculated for direct ionization, (i.e. for the transition O_2 ($X^3\Sigma_g^-$, v"=0)→O_2^+ ($X^2\Pi_g$, v'), which is given in Appendix I), than those of the other two members of this progression. The reason for this probably lies in the large vibrational quantum number of this state combined with the relatively few vibrational levels of the $X^2\Pi_g$ state which are accessible at this photon energy (13.20 eV). Thus it is possible that vibrational anomalies occur beyond the zero energy point on the electron energy axis of the spectrum, i.e. for large v' numbers of the $X^2\Pi_g$ state.

V.3 The I and J Progressions of Oxygen

The photoelectron spectra recorded for the J and I progressions listed in Table V.1 and for the off-resonance spectrum at 889 Å are shown in Figs. V.5,6. The vibrational distributions from these spectra are shown in Figs. V.7,8.

Inspection of the spectra and distributions reveals that only the off-resonance spectrum at 889 Å has a vibrational distribution which is similar to the calculated direct ionization distribution, or the distribution which is obtained from the 584 Å spectrum of oxygen. All the other spectra, recorded at wavelengths corresponding to members of the I and J progressions, have distributions which are markedly different to the off-resonance distribution, and in fact the I progression members show vibrational structure up to v'=13. In particular the distributions all show more than one maximum.

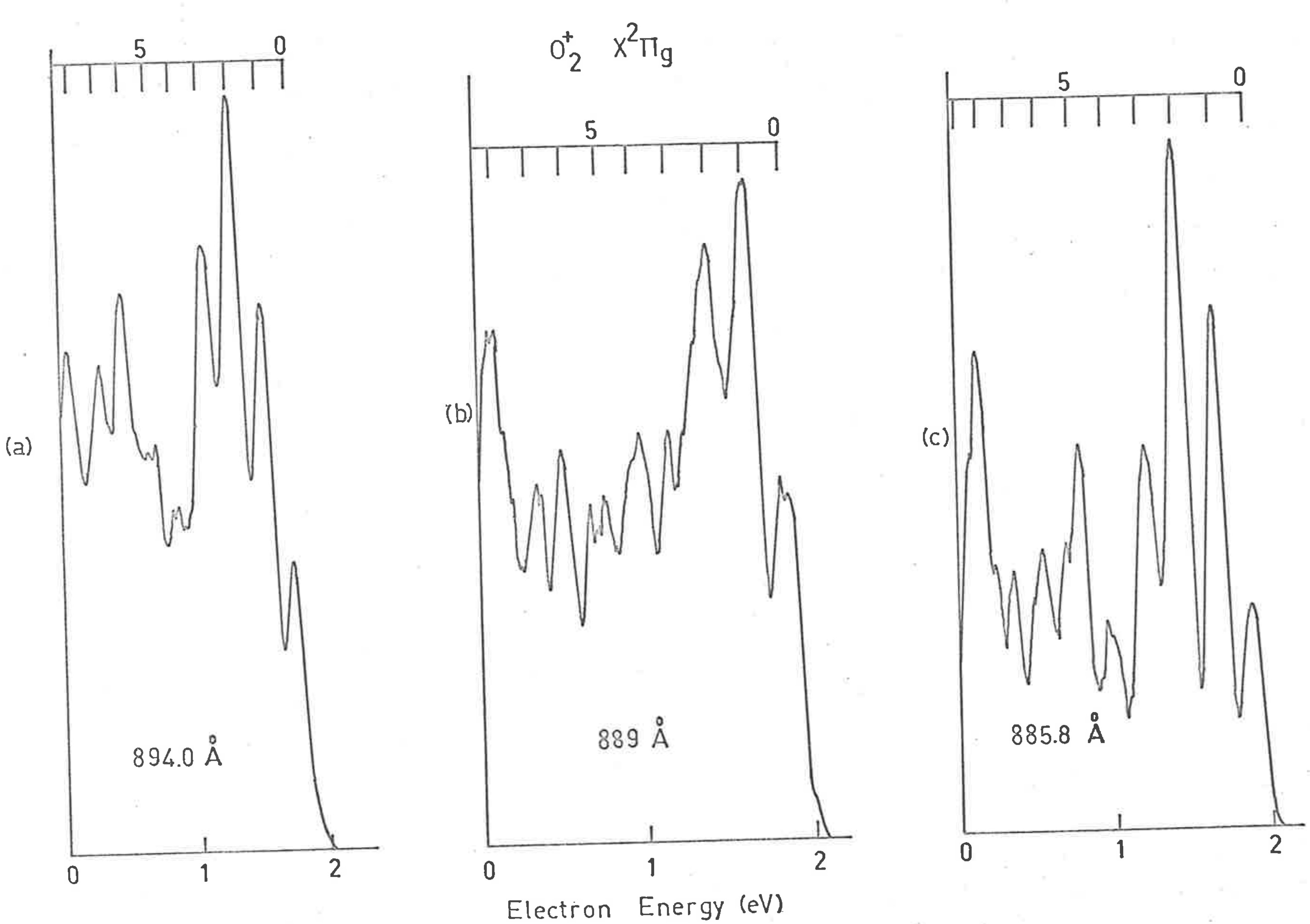

Fig.V.5. Photoelectron spectra for O_2 at 894.0, 889 and 885.8 Å.

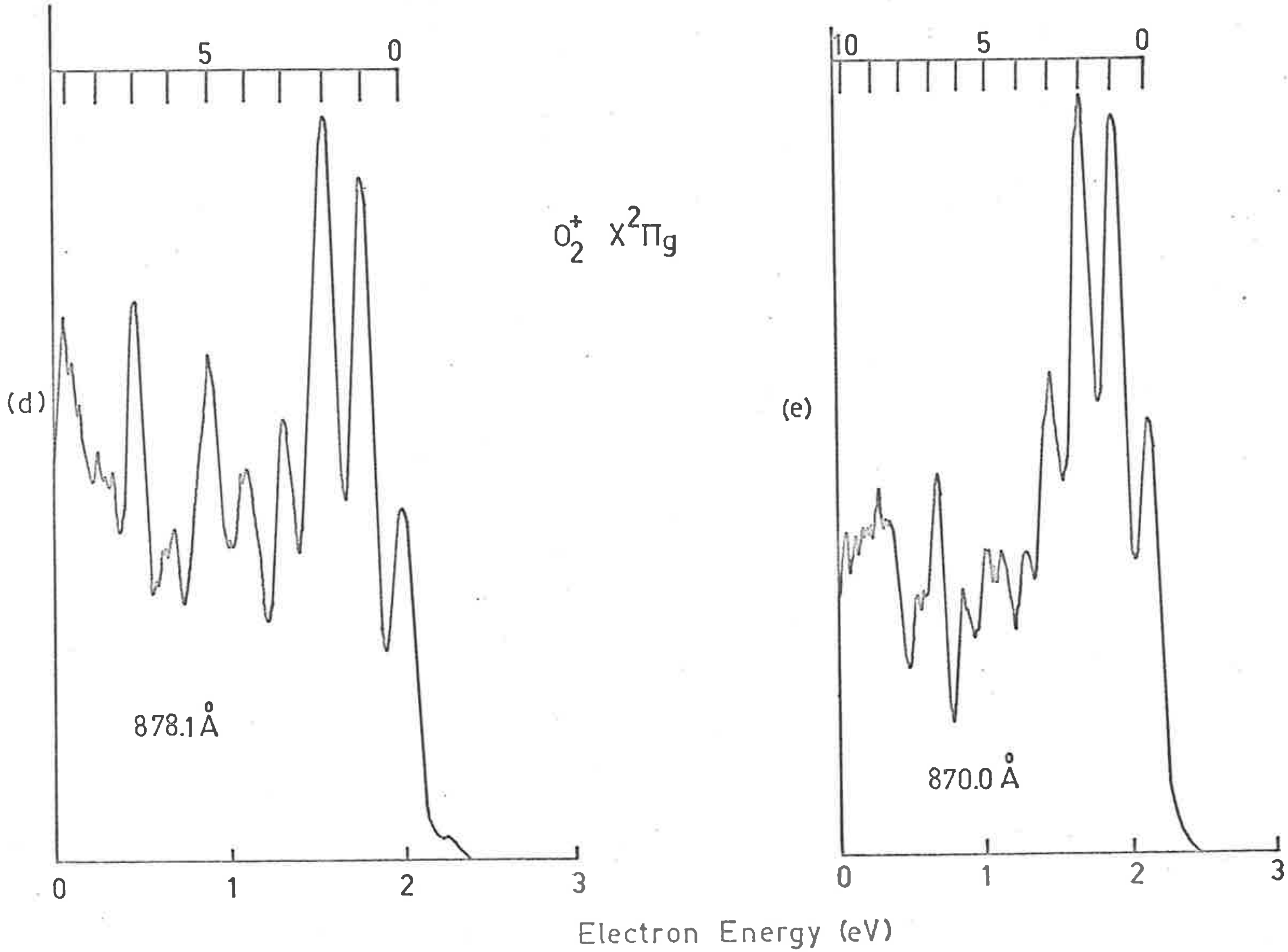

Fig.V.5.(cont) Photolectron spectra for O_2 at 878.1 and 870.0 Å.

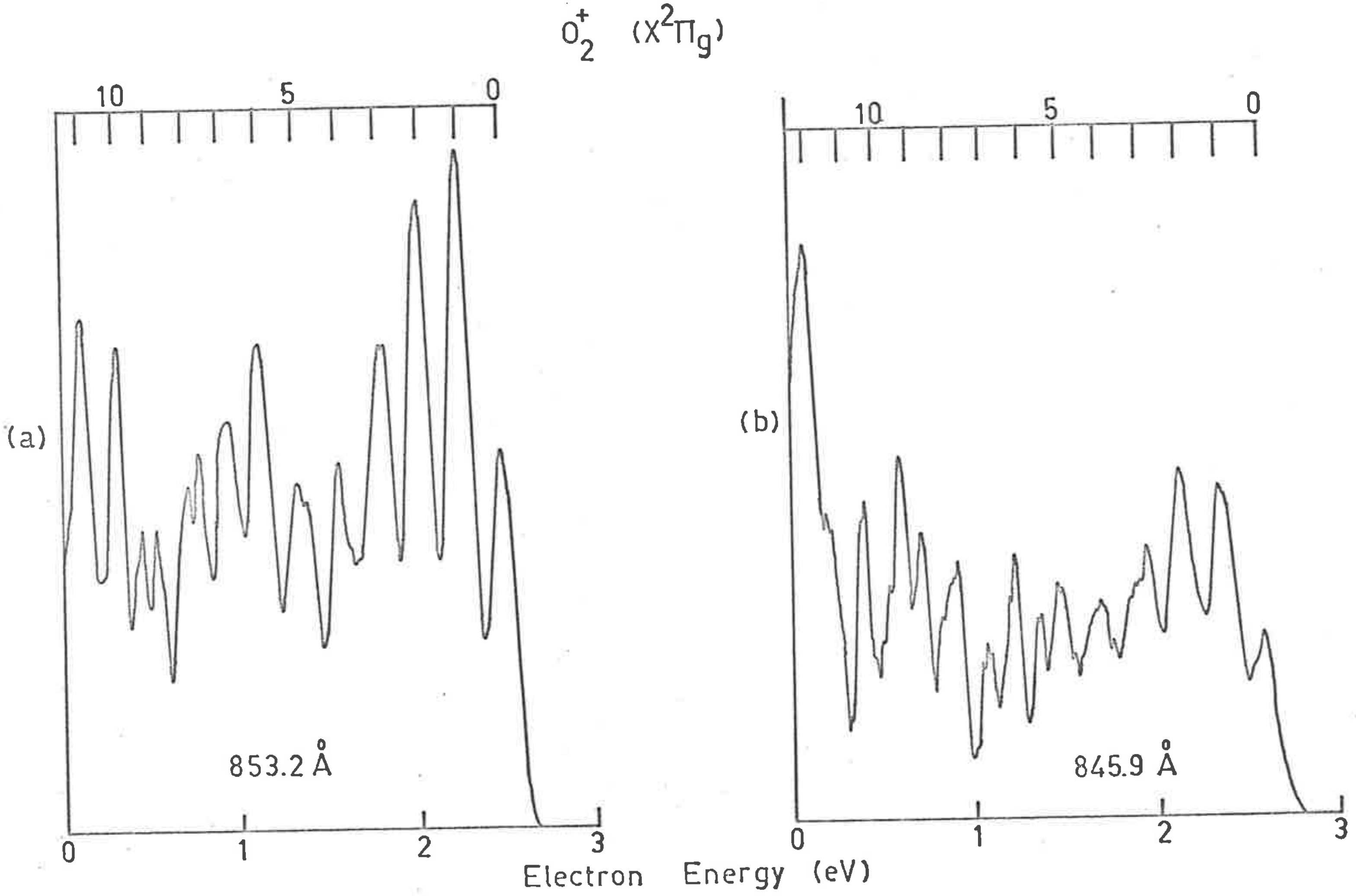

Fig.V.6. Photoelectron spectra for O_2 at 853.2 and 845.9 Å.

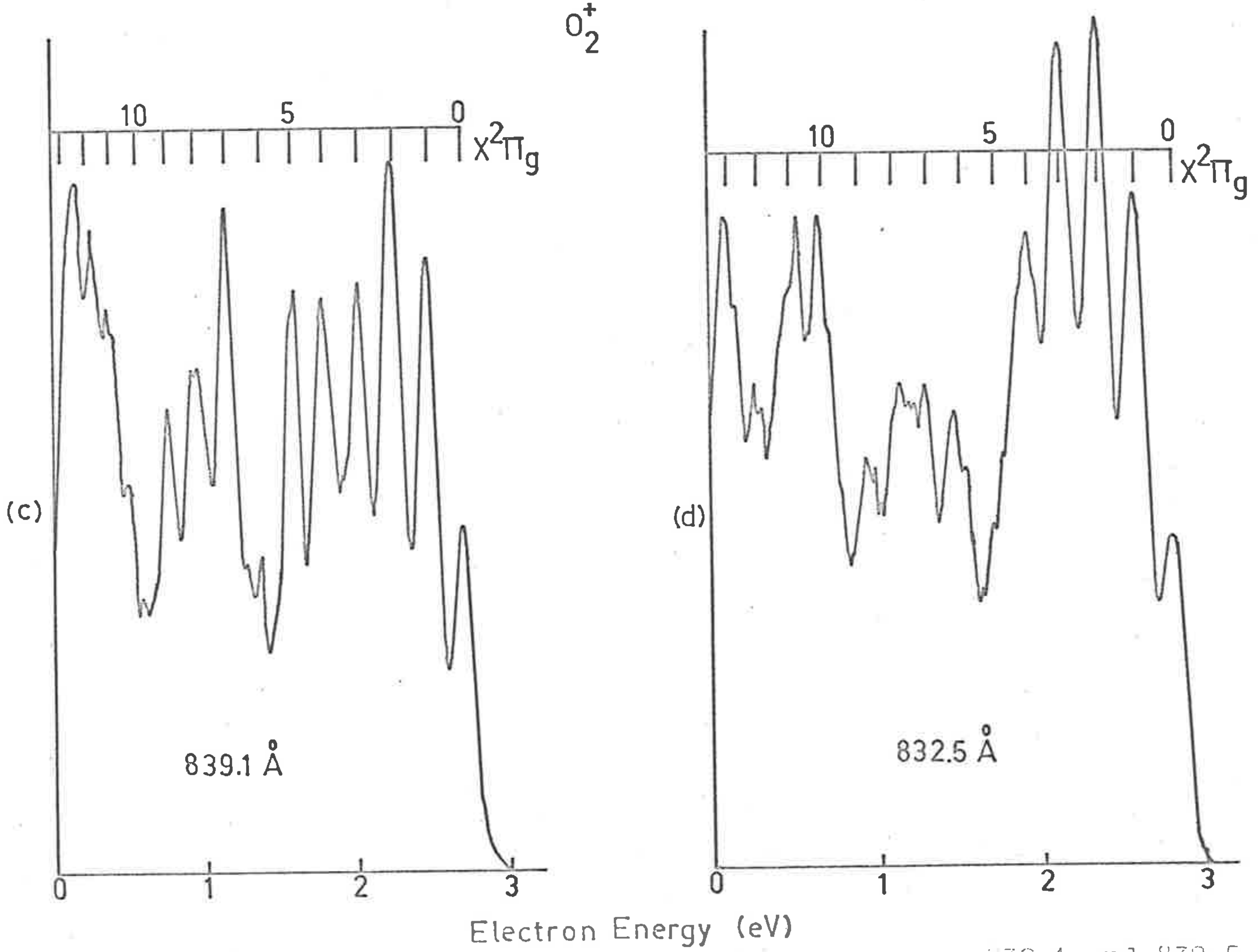

Fig.V.6.(cont) Photelectron spectra for O_2 at 839.1 and 832.5 Å.

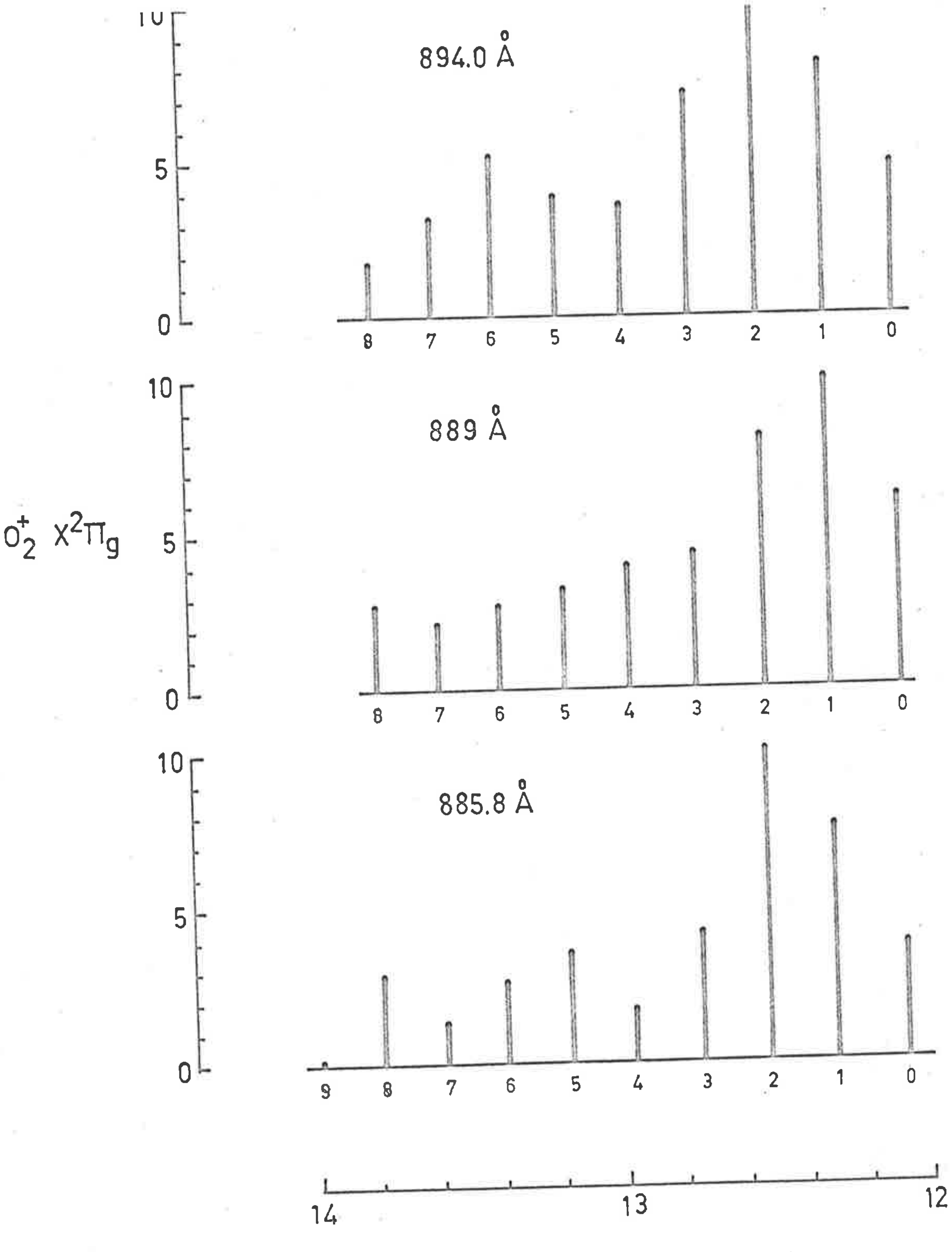

Fig.V.7. Vibrational intensity distributions for the spectra of Fig.V.5.

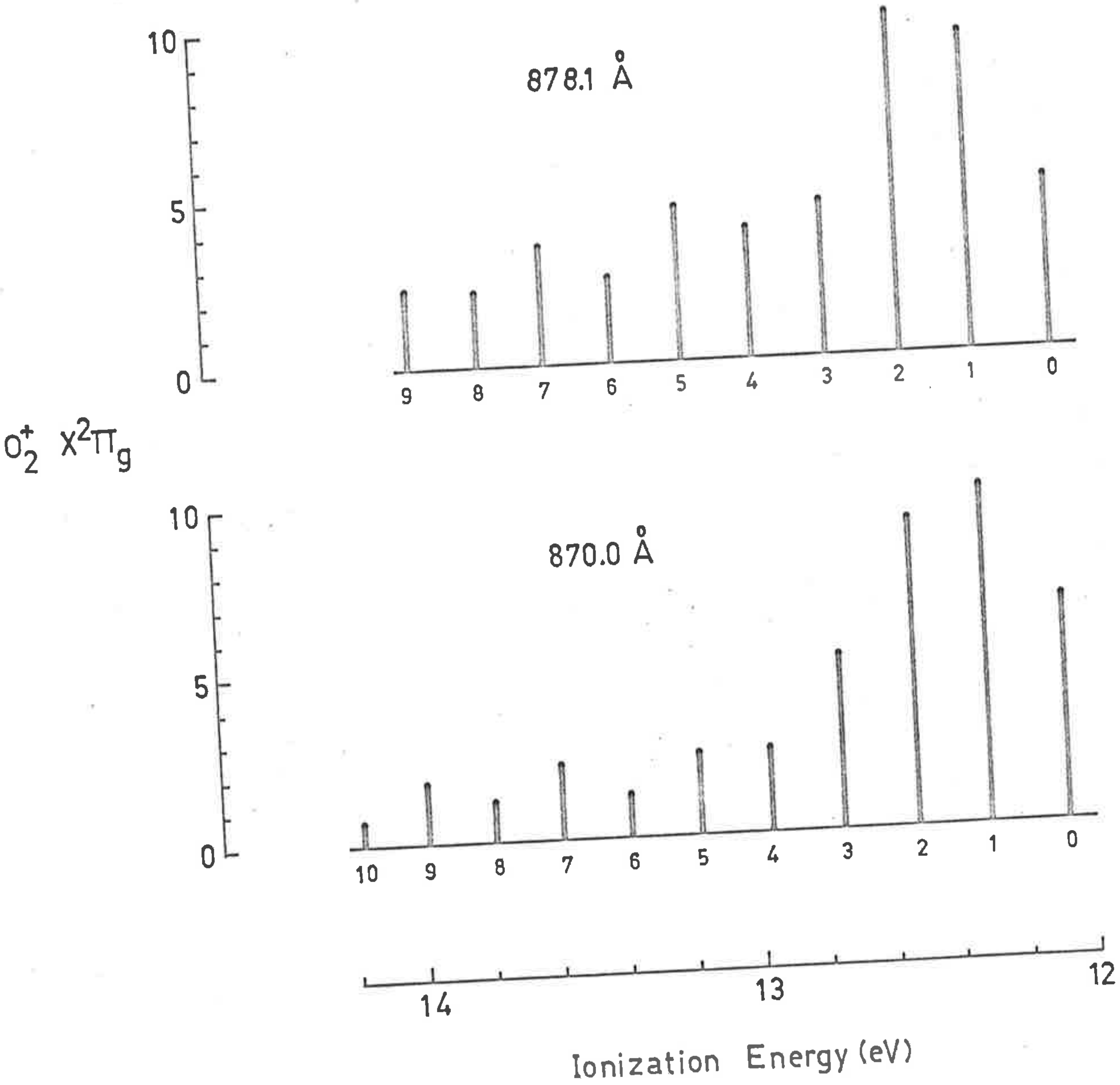

Fig.V.7.(cont) Vibrational intensity distributions for the spectra of Fig.V.5.

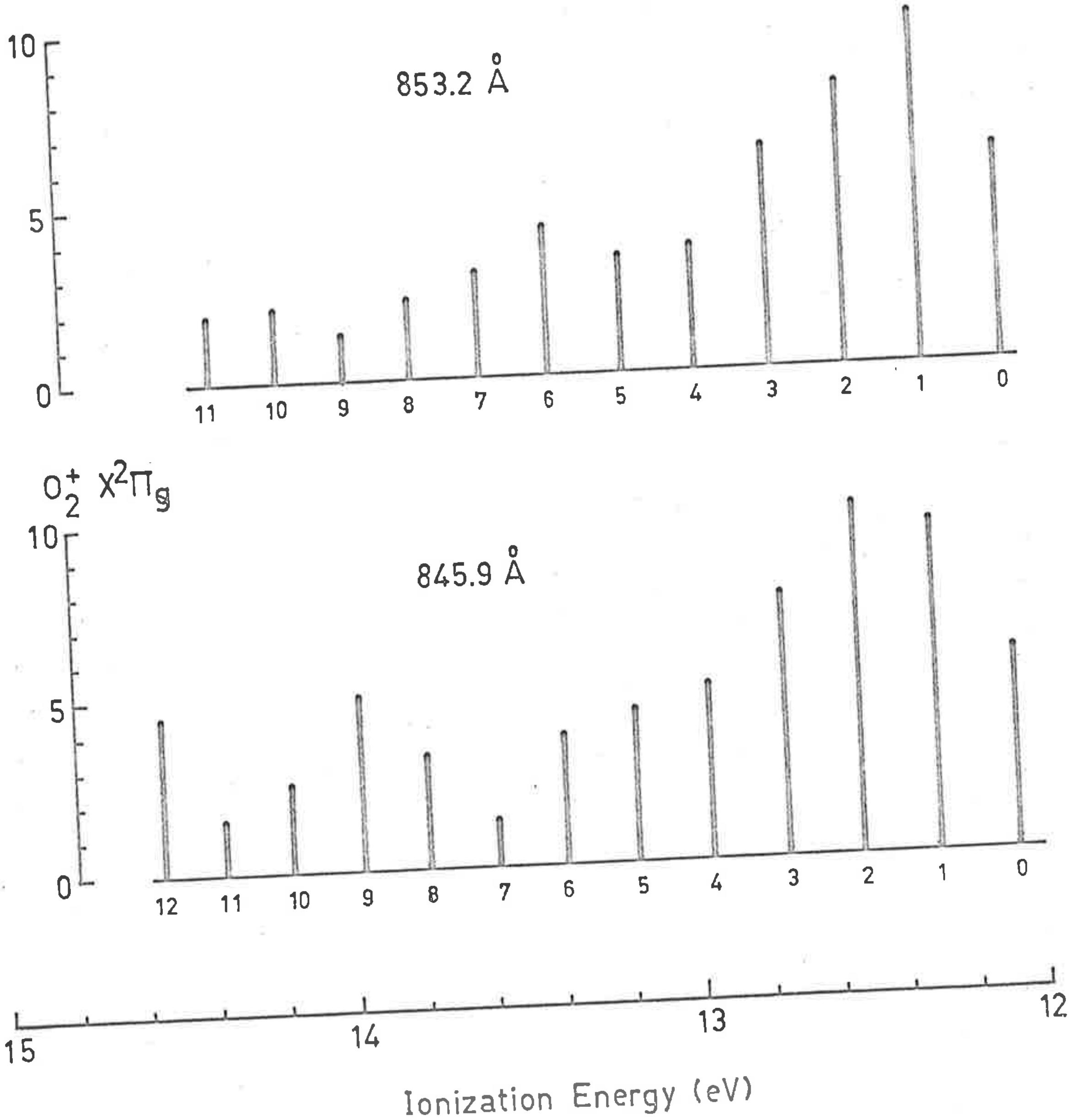

Fig.V.8. Vibrational intensity distributions for the spectra of Fig.V.6.

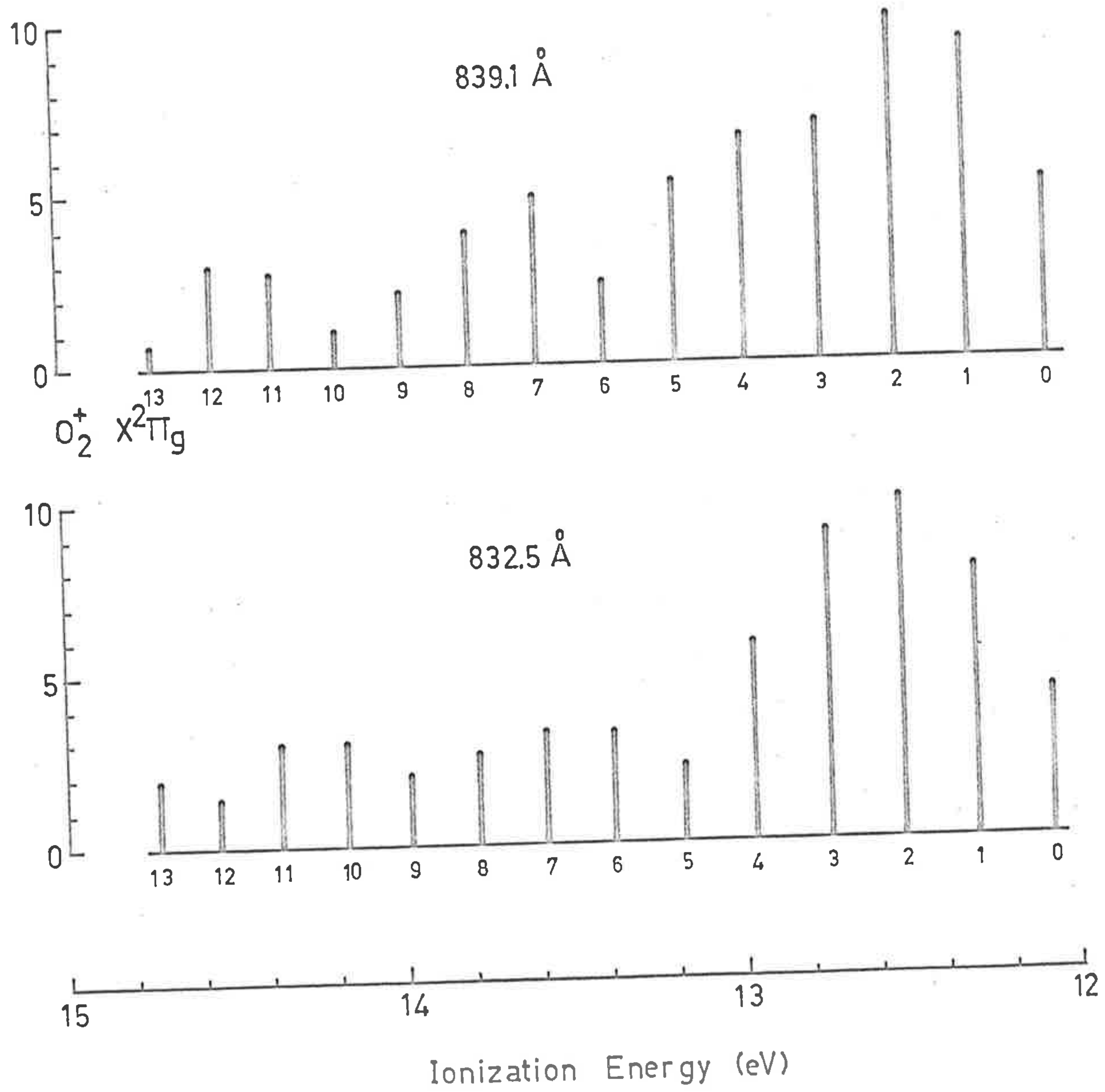

Fig.V.8.(cont) Vibrational intensity distributions for the spectra of Fig.V.6.

If the photoelectron spectra obtained at resonance wavelengths represent the sum of continuum and preionized components corresponding to direct transitions to the ground state of the ion and transitions via the preionizing state respectively, then the off-resonance spectrum contains the continuum component but only a small preionized contribution. Thus the difference between an on-resonance and an off-resonance distribution represents preionizing transitions only. The differences for the 894.0-889 Å and the 885.8-889 Å distributions are shown in Fig. V.9. The differences for the 894.0-584 Å and 885.8-584 Å distributions were also obtained and are represented in Fig. V.9 by the broken vertical lines. In obtaining these differences, each distribution was first normalized to the value of the total electron count rate at the appropriate wavelength, as obtained from Fig. V.1. For the 584 Å distribution, the normalization was the same as for the 889 Å distribution.

It is seen that there is little difference between the two methods of obtaining the difference distributions, and the general shape is the same in each case. If the 584 Å values are used for the off-resonance distribution, the higher vibrational members of the resulting difference distribution are more enhanced than when the 889 Å values are used. This is to be expected, since the 889 Å spectrum contains a small contribution due to preionization, and so has a more extended distribution than the 584 Å spectrum. Thus, again,

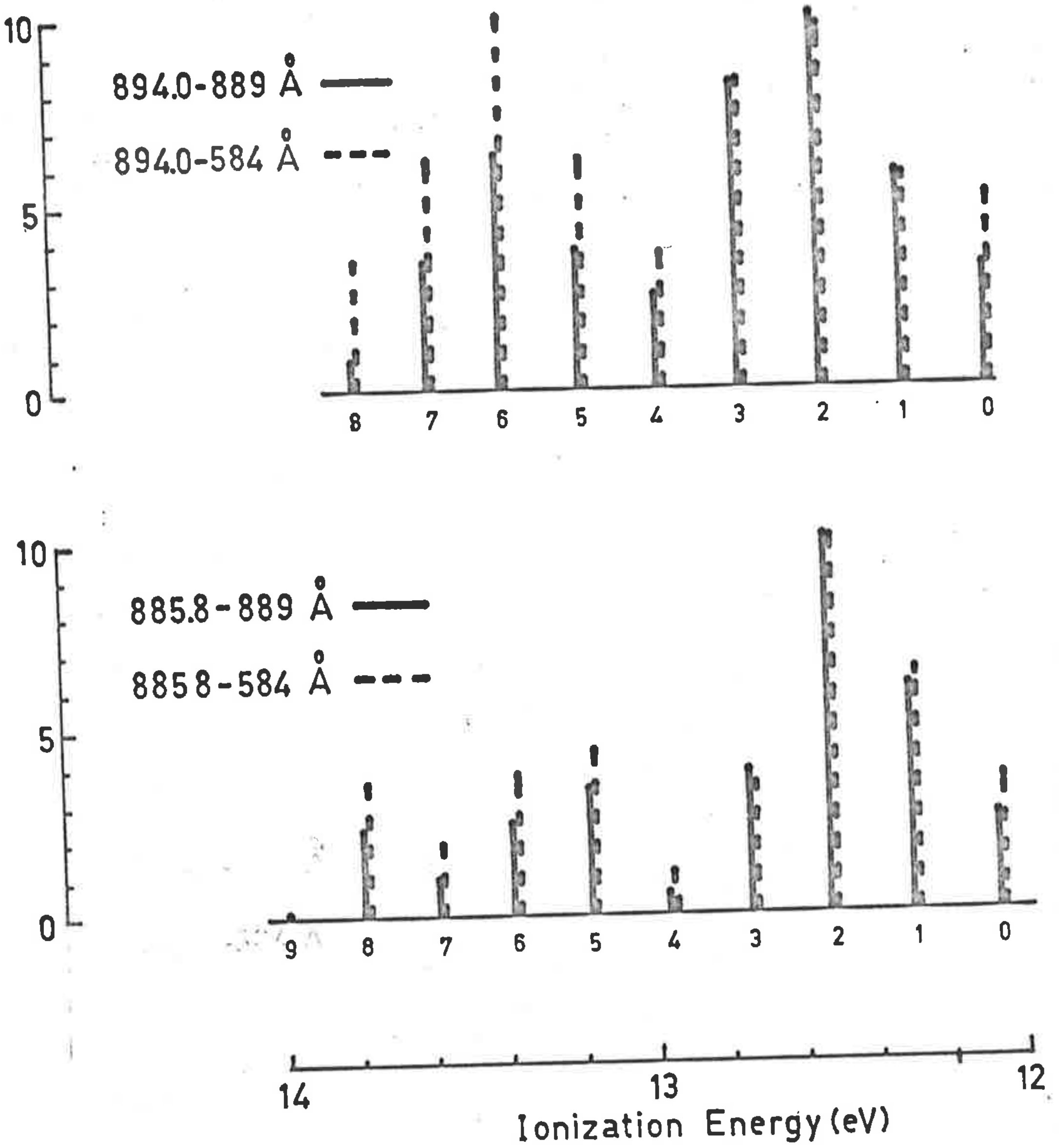

Fig. V. 9. Experimental vibrational distributions for preionizing transitions only.

the photoelectron spectra recorded at preionized resonances show that the preionization of the molecule uniquely changes the vibrational distributions in the spectra.

The differences for the J progression members, namely: 894.0-584 Å, 885.8-584 Å, 878.1-584 Å, and 870.0-584 Å distributions, suitably normalized, are shown in Fig. V.10. The 894.0-584 Å difference distribution shows two maxima, at v'=2 and 6, and the 885.8-584 Å distribution shows three maxima, at v'=2, 5 and 8. The 878.1-584 Å distribution shows three definite maxima at v'=2, 5 and 7, with an indication of another at v' = 9; the 870.0-584 Å distribution shows four maxima at v'=1, 5, 7 and 9.

It was mentioned in Chapter IV that the F-C distribution of vibrational intensities may extend below the zero of the electron energy scale, or above the energy of the incident photon, if only a few levels are available energetically. Thus it is quite possible that the number of maxima observed in the distribution of a photoelectron spectrum is less than the number which is expected on the basis of the theory proposed in Chapter IV, i.e. v+1, where v is the vibrational quantum number of the preionized state. If allowance is made for the possibility that a fourth maximum in the 878.1-584 Å distribution, and a fifth maximum in the 870.0-584 Å distribution are not seen experimentally because they appear below the zero on the electron energy scale, then the four difference distributions

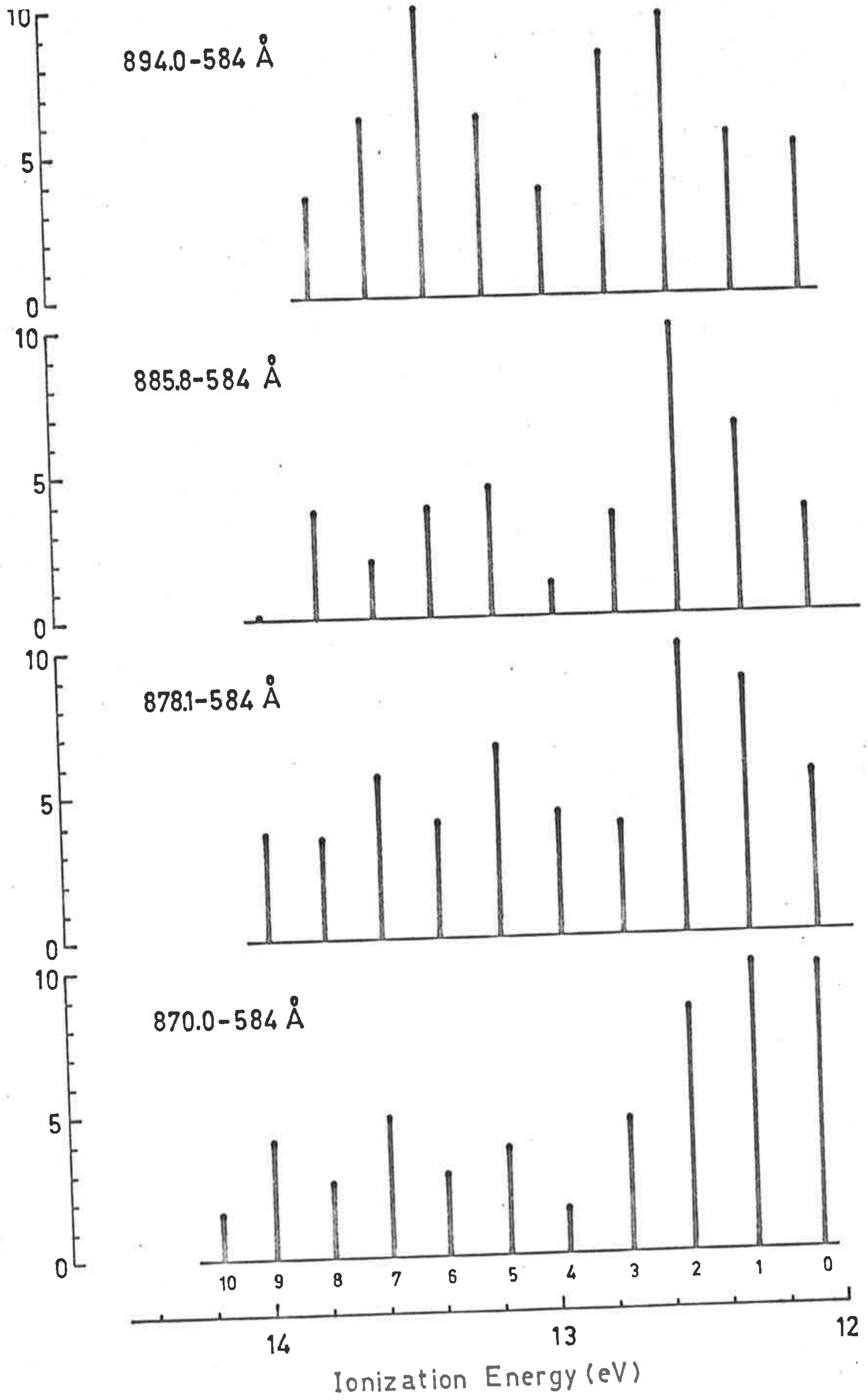

Fig. V. 10. Difference distributions for the J progression members.

clearly show that the total number of maxima in each distribution is equal to v+1 where v is the vibrational quantum number of the preionizing level. This indicates that the 894.0 Å resonance corresponds to v=1, and not v=0 as was assumed in Table V.1, and similarly the resonances at 885.8. Å, 878.1 Å, and 870.0 Å correspond to v = 2, 3 and 4 respectively. Thus the member of the J progression with v=0 is unidentified in the total photoionization cross-sections of oxygen.

The differences for the I progression members, namely: 853.2-584 Å, 845.9-584 Å, 839.1-584 Å, and 832.5-584 Å distributions were similarly obtained and are shown in Fig. V.11. There are no apparent trends in the broad maxima which can be seen in these distributions, especially since the 853.2-584 Å distribution should have only one maximum if the 853.2 Å resonance corresponds to v=0 (Table V.1). From Fig. V.11 it can be seen that this distribution has at least three maxima and possibly four.

The total cross-section values for the 853.2 Å and 845.9 Å resonances are relatively low (Table V.1) and this wavelength region in oxygen is considerably overlapped by the I' and K progressions and other unidentified resonances; these facts probably account for the discrepancies mentioned above. The 839.1 Å and 832.5 Å resonances are much stronger and thus produce comparitively well defined distributions. The 839.1 Å resonance lies quite close to another unidentified resonance at 838.6 Å (MATSUNAGA 1967) which may account for the

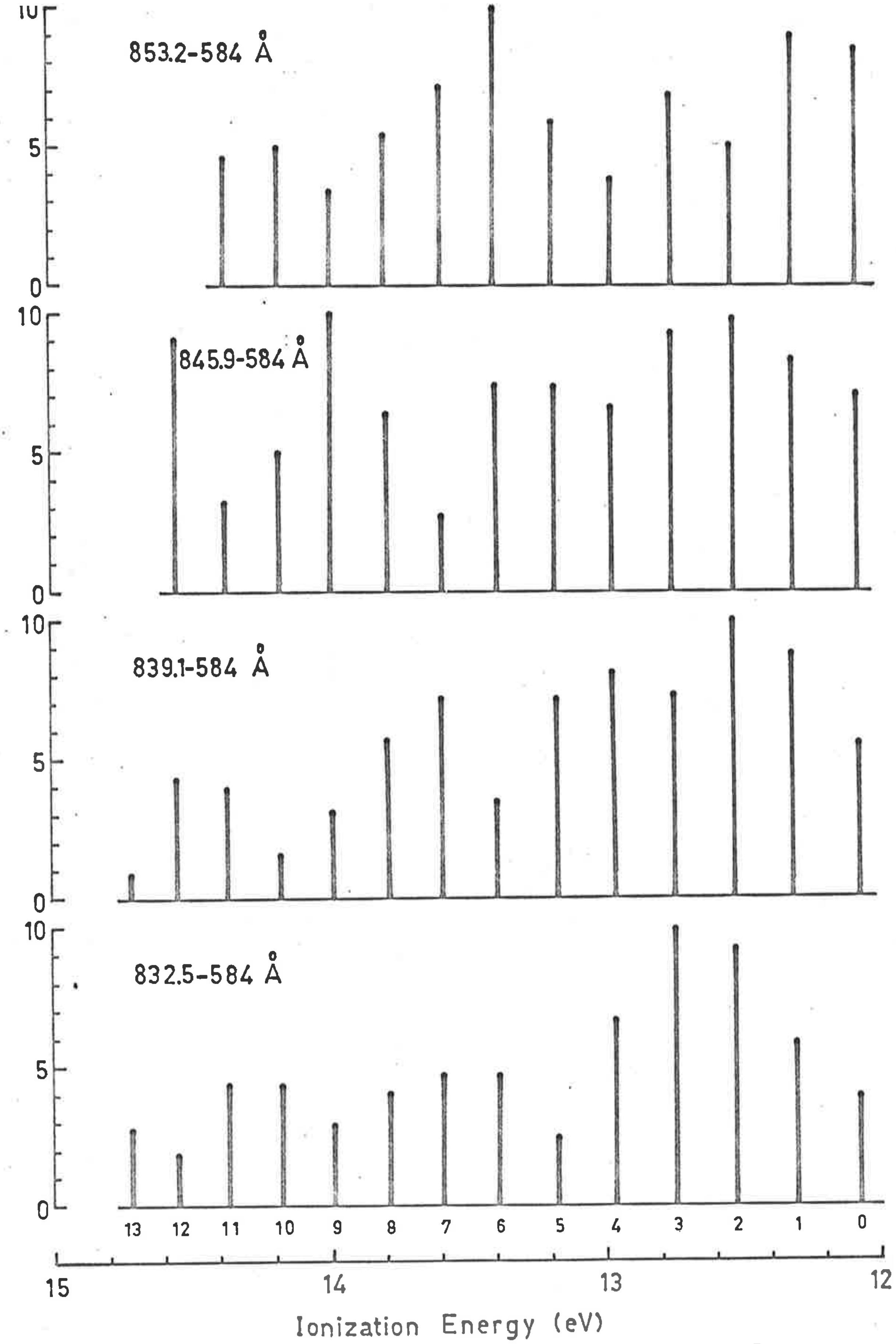

Fig. V. 11. Difference distributions for the I progression members.

extra maximum which is observed in the difference distribution (Table V.1 shows that at 839.1 Å, v=2, and so there should only be three maxima in the distribution by the theory of Chapter IV, and not four).

V.4 Comparison of Calculated and Experimental F-C Factors for the I and J Progressions of Oxygen

Calculations of Franck-Condon factors for preionization have been few in the past because of a lack of knowledge of the molecular constants, especially of r_e, the equilibrium internuclear distance.

For the I and J progressions, the values for ω_e and $\omega_e x_e$ were obtained by fitting the quadratic function

$$G(v) = \omega_e(v+\tfrac{1}{2}) - \omega_e x_e(v+\tfrac{1}{2})^2 \tag{11}$$

to the experimental data of Matsunaga and Watanabe (MATSUNAGA 1967), by the least squares method. The value of r_e for the preionized state was introduced as a parameter which was adjusted to give the distribution of F-C factors in best agreement with the difference distributions of Figs. V.10 and 11. The values for the molecular constants used in the calculations are listed in Table V.2.

TABLE V.2

	μ_a (amu)	ω_e (cm^{-1})	$\omega_e x_e$ (cm^{-1})	r_e (Å)
O_2 I	8.00000	1036	16.5	
O_2 J	8.00000	1110	27.1	
O_2^+ $X^2\Pi_g$	7.99986	1876.4	16.53	1.1227

The calculated vibrational distributions for the transitions O_2 (J, v=1,2,3,4)$\rightarrow O_2^+$ ($X^2\Pi_g$, v') are shown in Fig. V.12, with the corresponding value for r_e of the initial state, which was used in the calculation in each case. It is seen that the calculations have reproduced the general form of the distributions of Fig. V.10 for the four cases. One of the most interesting features that is brought out in Fig. V.12 is that the r_e value required to obtain the best fit in each case must be increased as the v number of the progression is increased. Thus for the 894.0 Å resonance, an r_e value of 1.27 Å is needed, and for the 870.0 Å resonance r_e is 1.32 Å. The accuracy of this fitting procedure was about ±0.01 Å for each r_e value; i.e. the values of r_e which were 0.01 Å above and below the quoted value provided distributions which were not as well matched to the experimental difference distribution. From these results it is possible to say that the J state in oxygen has an equilibrium internuclear distance of 1.30 ± 0.03 Å.

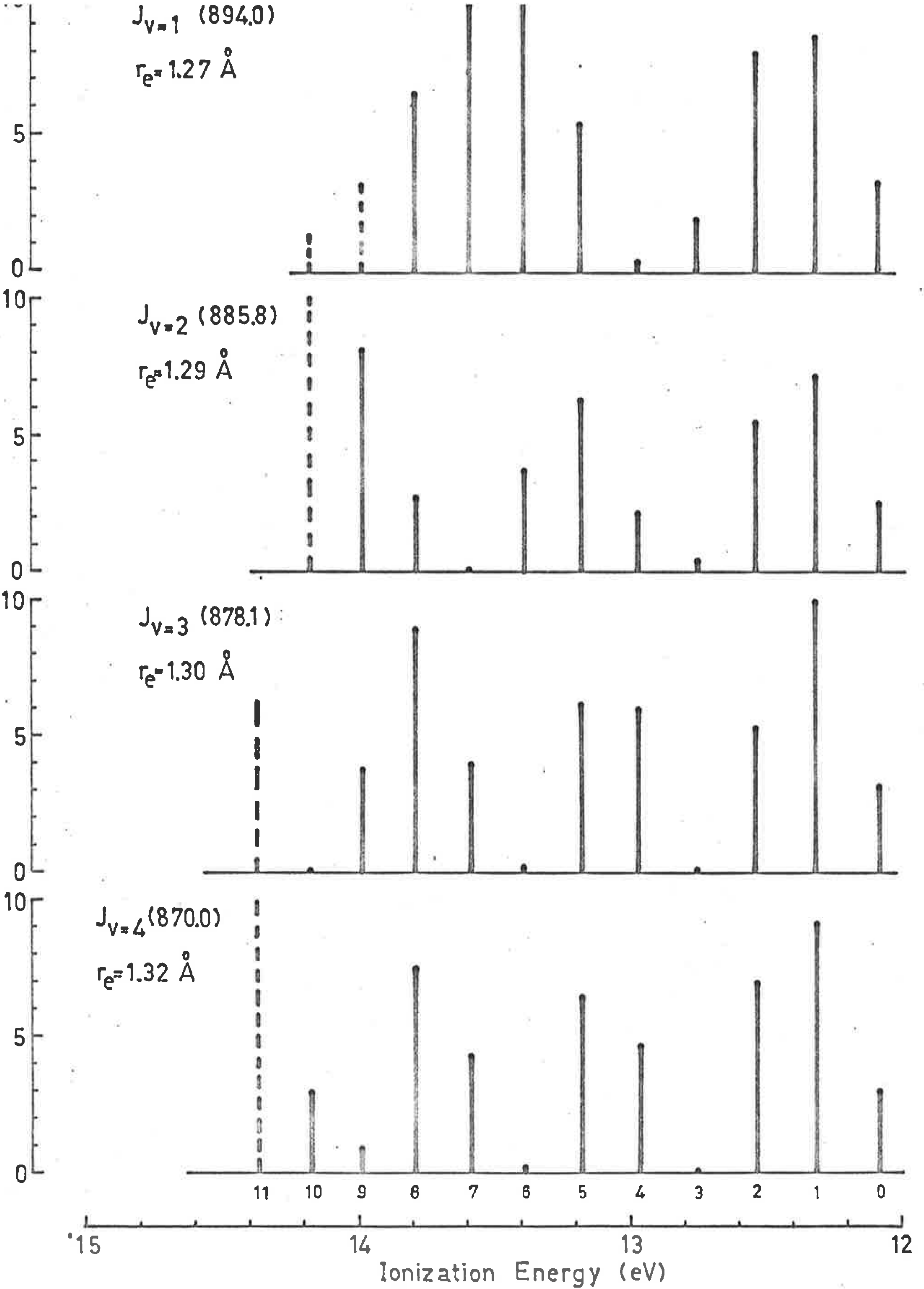

Fig.V.12.Calculated F-C factors for the transitions O_2 (J) ⟶ O_2^+ ($X^2\Pi_g$).

The calculated vibrational distributions for the transitions O_2 (I, v=2,3)→O_2^+ ($X^2\Pi_g$, v') are shown in Fig. V.13. In these two cases the same r_e value (1.36 Å) was used in the calculations. The 832.5 Å F-C factors, in particular, closely resemble the difference distribution for 832.5-584 Å in Fig. V.11.

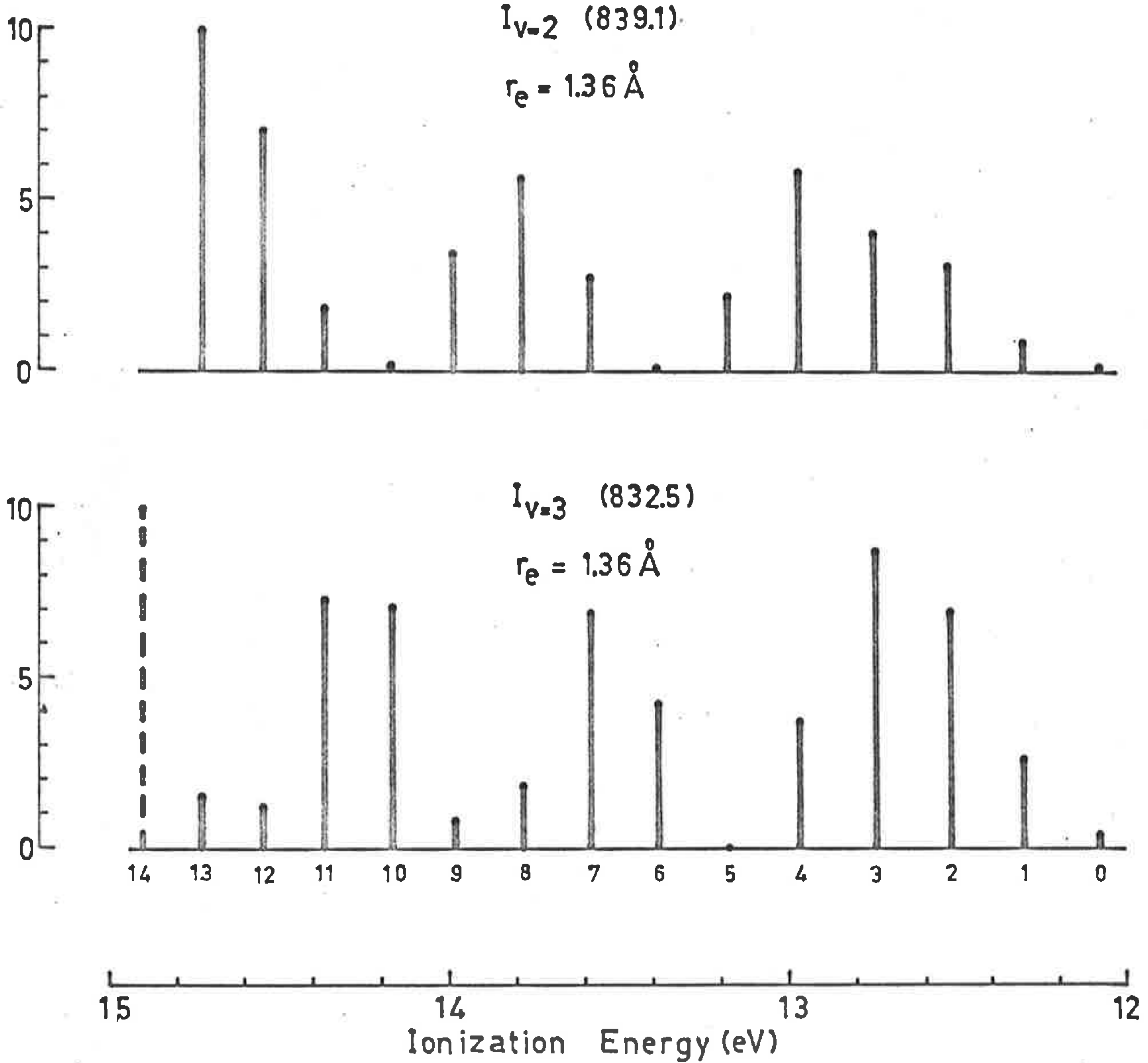

Fig.V.13. Calculated F-C factors for the transitions O_2 (I) $\longrightarrow$ O_2^+ ($X^2\Pi_g$).

APPENDIX I

Calculations of Franck-Condon Factors

The Franck-Condon principle was outlined in Chapter I, where it was shown that the most probable vibrational transition in a diatomic molecule is the one corresponding to the two states whose eigenfunctions have the maximum "overlap". The distribution of F-C factors is represented by:

$$q_{v'v''} = \left[\int \Psi'_v \, \Psi''_v \, dr \right]^2 \qquad \text{(A1)}$$

The form of Ψ_v was taken from Pekeris (PEKERIS 1934) and Learner (LEARNER 1962) with J=0, thus giving:

$$\Psi_v = N \exp(-Z/2) \, Z^{b/2} \, F(-v,b+1,Z) \qquad \text{(A2)}$$

where N is the normalization constant such that

$$N = \left[\frac{\beta}{\Gamma(b)} \binom{v+b}{v} \right]^{\frac{1}{2}} \qquad \text{(A3)}$$

$$\beta = 1.2177 \times 10^7 \; 4\mu_a \omega_e x_e \qquad \text{(A4)}$$

$$b = \frac{4\Pi}{\beta h} \sqrt{2\mu_a(-W)} \qquad \text{(A5)}$$

$$W = E - T_e - D_e = \text{energy measured from the dissociation limit.} \tag{A6}$$

$$D_e = \frac{\omega_e^2}{4\omega_e x_e} \tag{A7}$$

$$Z = \frac{4\Pi}{\beta h} \sqrt{2\mu_a D_e} \exp(-\beta(r-r_e)) \tag{A8}$$

and r_e, ω_e, and $\omega_e x_e$ are the equilibrium internuclear distance, the harmonic vibrational frequency and the anharmonicity constant respectively.

$$F(\alpha,\gamma,x) = 1 + \frac{\alpha}{\gamma} x + \frac{\alpha(\alpha+1)}{2!\gamma(\gamma+1)} x^2 + \ldots \tag{A9}$$

is the confluent hypergeometric function, which is a form of the Laguerre polynomial. μ_a is the reduced mass in atomic mass units.

The calculations consisted of calculating Ψ_v' and Ψ_v'' for a range of values of r (0.5 Å to 2.0 Å in 300 intervals), and then integrating the product of the two functions over the range of r by Simson's method. This integral was then squared to obtain the value for $q_{v'v''}$. The resulting F-C factors were printed as an array of dimensions v' by v''. Table A1 is the array of F-C factors for the transition O_2 ($X^3\Sigma_g^-$, v''=0-5)→O_2^+ ($X^2\Pi_g$, v'=0-15):

TABLE A1

v''	0	1	2	3	4	5
v'						
0	.23544	.29802	.22320	.12945	.06448	.02909
1	.39021	.04404	.02852	.12550	.15017	.11648
2	.26279	.09826	.16261	.01907	.01763	.08315
3	.09199	.29578	.00000	.12169	.08679	.00483
4	.01772	.19901	.19132	.04705	.03869	.10454
5	.00182	.05692	.26443	.07793	.10705	.00089
6	.00009	.00759	.11013	.27512	.01338	.12467
7	.00000	.00042	.01864	.16656	.24382	.00084
8		.00001	.00119	.03512	.21723	.19078
9		.00000	.00001	.00253	.05628	.25686
10			.00000	.00003	.00448	.08087
11				.00000	.00004	.00699
12					.00000	.00005
13						.00001
14						.00000
15						.00000
Sum	1.00006	1.00005	1.00005	1.00005	1.00004	1.00005

The program used to compute the F-C factors is listed below. The input data consisted of: ω_e, $\omega_e x_e$, r_e, μ_a for each state involved in the transition.

```
      PROGRAM FCFACT (INPUT,OUTPUT)
      COMPUTES MORSE POTENTIAL CURVES,VIBRATIONAL ENERGIES AND
      FRANCK-CONDON FACTORS.
      DIMENSION R(301),WFUNCT1(6,301),WFUNCT2(21,301),Q(6,21),QSUM(10)
      COMMON R,WFUNCT1,WFUNCT2
      INTEGER V1,V2
      REAL INT
      READ 100,G1,B1,S1,WE1,WEXE1,RE1,UA1,TE1
      CALL MORSE (G1,B1,S1,WE1,WEXE1,RE1,UA1,TE1)
    1 READ 100,G2,B2,S2,WE2,WEXE2,RE2,UA2,TE2
      IF(WE2.EQ.0.) 7,2
    2 CALL MORSE (G2,B2,S2,WE2,WEXE2,RE2,UA2,TE2)
      WAVEFUNCTION FOR FINAL STATE V2
      DO  3 V2 = 0,15
      K = 2
      CALL WAVEFN (K,V2,WE2,WEXE2,RE2,UA2)
    3 CONTINUE
      DO  6 V1 = 0,5
      QSUM(V1) = 0.
      WAVEFUNCTION FOR INITIAL STATE V1
      K = 1
      CALL WAVEFN (K,V1,WE1,WEXE1,RE1,UA1)
      CALCULATE INTEGRAL BY SIMPSONS RULE

      DO  5 V2 = 0,15
      SUM = 0.               $ H = 0.005*1.E-8
      DO 4 I = 2,301,2
      SUM = SUM + 2.*WFUNCT1(V1,I)*WFUNCT2(V2,I)+4.*WFUNCT1(V1,I-1)*
     $WFUNCT2(V2,I-1)
    4 CONTINUE
      INT = SUM*H/3.
      Q(V1,V2) = INT**2
      QSUM(V1) = QSUM(V1)  + Q(V1,V2)
    5 CONTINUE
    6 CONTINUE
      PRINT 108, S1,G1,B1,S2,G2,B2,S1,WE1,WEXE1,RE1,UA1,TE1,S2,WE2,WEXE2
     $,RE2,UA2,TE2
      PRINT 107,(V2,(Q(V1,V2), V1=0,5), V2=0,15)
      PRINT 109, (QSUM(V1),V1 = 0,5)
      GO TO 1
    7 CONTINUE
  100 FORMAT(  3A10,F10.2,F10.3,F10.4,F10.5,F10.2  )
  101 FORMAT(1H1/,5X,*FRANCK-CONDON FACTORS FOR TRANSITIONS FROM THE V≠≠
     $=*I3* LEVEL OF THE *A10,* STATE OF *A10,A10,/* TO THE *A10,* STATE
     $OF *A10,A10,//,1X,A10,*  WE =*F10.2,*  WEXE =*F10.3,*  RE =*F10.4,
     $*UA =*F10.5,*  TE =*F10.2,/,1X,A10,*  WE =*F10.2,*  WEXE =*F10.3,*
     $  RE =*F10.4,*  UA =*F10.5,*  TE =*F10.2,//)
  102 FORMAT(10X,* V≠≠  V≠        Q*/)
  103 FORMAT(//,10X,*  SUM = *,2X,E12.5,2X,F7.5)
  104 FORMAT( 6(F10.3,E10.2))
  105 FORMAT(10X, I3, I5,2X,E12.5,2X,F7.5)
  106 FORMAT(11(2X,F5.2)/)
  107 FORMAT(8X,*V1          0          1          2          3          4
     $     5*/,5X,*V2*/,  (5X,I2,4X,6F10.5))
  108 FORMAT(1H1/,5X,*FRANCK-CONDON FACTORS FOR TRANSITIONS FROM THE *A1
     $0,*STATE OF *A10,A10,/* TO THE *A10,* STATE OF *A10,A10,//,1X,A10,
     $*  WE =*F10.2,*  WEXE =*F10.3,*  RE =*F10.4,*  UA =*F10.5,*  TE =*
```

```
   $F10.2,/,1X,A10,*  WE =*F10.2,*  WEXE =*F10.3,*  RE =*F10.4,*  UA =
   $*F10.5,*  TE =*F10.2,//)
109 FORMAT (//,2X,*SUM*,4X,6F10.5)
    STOP
    END
```

```
    SUBROUTINE MORSE (GAS,B,STATE,WE,WEXE,RE,UA,TE)
    DIMENSION E(301),U(301),VIB( 21),G(21)
    COMMON R(301)
    INTEGER V
    PRINT 101,STATE,GAS,B,WE,WEXE,RE,UA,TE
    HC = 12397.639722
    DE = WE**2/(4*WEXE)
    BETA = 1.2177E07*SQRT(4*UA*WEXE)
    R(0) = 0.495
    DO 1 I = 1,301
    R(I) = R(I-1) + 0.005
    X = (R(I) - RE)*1.E-8
    E(I) = DE*(1-EXP(-BETA*X))**2 + TE - 0.5*WE + 0.25*WEXE
  1 U(I) = HC*E(I)*1.E-8
    PRINT 102,(R(I),U(I),I = 1,301,2)
    DO 2 V = 0,20
    G(V) = WE*(V+0.5) - WEXE*(V+0.5)**2 + TE - 0.5*WE + 0.25*WEXE
  2 VIB(V) = HC*G(V)*1.E-8
    PRINT 103,(V,G(V),VIB(V),V = 0,20)
101 FORMAT(1H1/30X,20H MORSE POTENTIAL FOR,1X,A10,2X,9H STATE OF 1X,
   $A10,A10,2/5X,5H WE =F10.2,5X,7H WEXE =F10.3,5X,5H RE =F10.4,5X,
   $15H REDUCED MASS =F10.5,5X,5H TE =F10.2,2/)
102 FORMAT(5(F9.2,F6.2))
103 FORMAT(     5X,*V*,6X,*VIBRATIONAL ENERGY*/,14X,*CM-1*,8X,*EV*/
   $(4X,I2,4X,F10.1,4X,F6.2))
    RETURN
    END
```

```
    SUBROUTINE WAVEFN (K,V,WE,WEXE,RE,UA)
    COMMON R(301),WFUNCT1(6,301),WFUNCT2(21,301)
    INTEGER V
    DE = WE**2/(4.*WEXE)
    BETA = 1.2177E07*SQRT(4.*UA*WEXE)
    A = SQRT((0.9995/WEXE)*DE)
    W = WE*(V+0.5)-WEXE*(V+0.5)**2-DE
    B = SQRT(-4.*(0.9995/WEXE)*W)
    GB = GAMMA(B)
    E13 = 0.5*(ALOG(BETA)-ALOG(GB))
    ALN = E13
```

```
    IF(V.EQ.0) GO TO 3
    E12 = 1.
     L = V+1
    DO  1 N = 2,L
    P = N-2
 1  E12 = E12*(V+B-P)
    E12 = FACTORIAL (V+B)/FACTORIAL (B)
    E14 = 1.
    DO  2 N = 2,L
    P = N-1
 2  E14 = E14*P
    E14 = FACTORIAL(V)
    ALN = E13+0.5*ALOG(E12/E14)
    ALN = LOG(NORMALIZATION CONSTANT)
 3  R(0) = 0.495
    DO 15 N = 1,301
    R(N) = R(N-1)+0.005
    DR = (RE-R(N))*1.E-8
    Y = EXP(BETA*DR)
    Z = 2.*A*Y
    E09 = 0.5*B*ALOG(Z)

    F = 1.
    IF(V.EQ.0) GO TO 5
    TERM = 1.
    M = V+1
    DO 4 J = 1,M
    TERM = TERM*Z*(J-V-1)/(J*(B+J))
 4  F = F+TERM
 5  CONTINUE
    IF(F-0.) 6,7,8
 6  SIGN = -1.
    GO TO 9
 7  SIGN =  0.
    GO TO 9
 8  SIGN = +1.
 9  E29 = ABS(F)
    E30 = ALOG(E29)
    EX = E30+ALN-Z/2.+E09
    IF(EX.LT.-88) 10,11
10  WF = 0.
    GO TO 12
11  WF = SIGN*EXP(EX)
12  IF (K.EQ.1) 13,14
13  WFUNCT1(V,N) = WF
    GO TO 15
14  WFUNCT2(V,N) = WF
15  CONTINUE
    RETURN
    END

    FUNCTION GAMMA(Z)
    GAMMA FUNCTION --- FOR +VE Z ONLY
    A = (Z-1/2)*ALOG(Z)-Z+0.5*ALOG(6.2831853)+ALOG(1+1/(12*Z)+1/(288*Z
   $**2)-139/(51840*Z**3)-571/(2488320*Z**4))
    GAMMA = EXP(A)
    RETURN
    END
```

APPENDIX II

Publications

The following papers have been written in conjunction with the work described in this thesis:

"Photoelectron Spectra and Partial Photoionization Cross-Sections for Carbon Dioxide", J.L. Bahr, A.J. Blake, J.H. Carver and Vijay Kumar, (1969). J.Q.S.R.T., 9, 1359.

"Franck-Condon Factors and Autoionization in the Photoelectron Spectra of Diatomic Molecules", A.J. Blake, J.L. Bahr, J.H. Carver and Vijay Kumar, (1969). To be published in Proc. Roy. Soc. (Lon.).

"Photoelectron Spectroscopy for some Autoionized States of Molecular Oxygen", J.L. Bahr, A.J. Blake, J.H. Carver and Vijay Kumar. In preparation.

BIBLIOGRAPHY

Al-Joboury, M.I., and Turner, D.W., (1963). J. Chem. Soc., p.5141.

Al-Joboury, M.I., and Turner, D.W., (1964). J. Chem. Soc., p.4434.

Al-Joboury, M.I., May, D.P., and Turner, D.W., (1965a). J. Chem. Soc., p.616.

Al-Joboury, M.I., May, D.P., and Turner, D.W., (1965b). J. Chem. Soc., p.6350.

Armstrong, B.H., (1959). Proc. Phys. Soc. (Lon), A74, 136.

Baker, A.D., Brundle, C.R., and Turner, D.W., (1968). J. Mass Spectr. and Ion Phys., 1, 443.

Bates, D.R., and Massey, H.S.W., (1943). Phil. Trans. Roy. Soc. (Lon), A239, 269.

Bates, D.R., (1946). Monthly Notices Roy. Astron. Soc., 106, 432.

Bates, D.R., Opic, U., and Poots, G., (1953). Proc. Phys. Soc. (Lon), A66, 1113.

Berkowitz, J., Ehrhardt, H., and Tekaat, T., (1967). Z. fur Physik, 200, 69.

Bethe, H.A., and Salpeter, E.E., (1956). Handbuch der Physik, Vol. 35, Ed. S. Flugge (Berlin: Springer-Verlag).

Bethe, H.A., and Salpeter, E.E., (1957). "Quantum Mechanics of One and Two Electron Atoms". (Berlin: Springer).

Beutler, H., (1935). Z. Phys., 93, 177.

Beutler, H., (1936). Z. Phys., 98, 181.

Blake, A.J., and Carver, J.H., (1965). Phys. Lett., 19, 387.

Blake, A.J., and Carver, J.H., (1967). J. Chem. Phys., 47, 1038.

Blake, A.J., (1966). Ph.D. Thesis, University of Adelaide.

Blake, A.J., Bahr, J.L., Carver, J.H., and Kumar, V., (1969). To be published, Proc. Roy. Soc. (Lon).

Born, M., and Oppenheimer, R., (1927). Ann. Physik, 84, 457.

Brode, R.B., (1933). Rev. Mod. Phys., 5, 257.

Brundle, C.R., and Turner, D.W., (1969). J. Mass Spectr. and Ion Phys., 2, 195.

Bunemann, O., Cranshaw, T.E., and Harvey, J.A., (1949). Can. J. Res., 27, A191.

Burgess, A., and Seaton, M.J., (1960). Monthly Notices Roy. Astron. Soc., 120, 121.

Codling, K., and Madden, R.P., (1965). J. Chem. Phys., 42, 3935.

Collin, J.E., and Natalis, P., (1968a). J. Mass Spectr. and Ion Phys., 1, 121.

Collin, J.E., and Natalis, P., (1968b). J. Mass Spectr. and Ion Phys., 1, 483.

Collin, J.E., and Natalis, P., (1969). J. Mass Spectr. and Ion Phys., 2, 231.

Comes, F.J., Elzer, A., and Lessman, W., (1964). Z. Naturforsch, A19, 65, 508, 721.

Condon, E.U., (1928). Phys. Rev., 32, 858.

Cook, G.R., Ching, B.K., Metzner, P.H., Ogawa, M., and Becker, B.A., (1965). Report No. TDR-469(9260-01)-4, Aerospace Corp., El Segundo, California.

Dalgarno, A., (1952). Proc. Phys. Soc. (Lon), A65, 663.

Dalgarno, A., McElroy, M.B., and Moffet, R.J., (1963). Planet. Space Sci., 11, 463.

Dalgarno, A., McElroy, M.B., (1965). Planet. Space Sci., 13, 947.

Detweiler, C.R., Purcell, J.D., and Tousey, R., (1961). Mem. Soc. Roy. Sci. (Liege), 4, 253.

Dibeler, V.H , Walker, J.A., and Rosenstock, H.M., (1966). J. Res. Nat. Bur. Std., A70, 459.

Dibeler, V.H., and Walker, J.A., (1967). J. Opt. Soc. Am., 57, 1007.

Dibeler, V.H., Walker, J.A., and Liston, S.K., (1967). J. Res. Nat. Bur. Std., A71, 371.

Ditchburn, R.W., (1955). Proc. Roy. Soc. (Lon), A229, 44.

Ditchburn, R.W., (1962). J.Q.S.R.T.*, 2, 361.

Ditchburn, R.W., and Opic, U., (1962). In "Atomic and Molecular Processes", Ed. D.R. Bates.

Doolittle, P.H., and Schoen, R.I., (1965). Phys. Rev. Lett. 14, 348.

Dressler, K., and Miescher, E., (1965). Astrophys. J., 141, 1266.

Edqvist, O., Lindholm, E., Selin, L.E., Sjogren, H., and Asbrink, L., (1969). In Press, Arkiv Fysik.

Eland, J.H.D., and Danby, C.J., (1968). J. Mass Spectr. and Ion Phys., 1, 111.

Fano, U., (1961). Phys. Rev., 124, 1866.

Fano, U., and Cooper, J.W., (1965). Phys. Rev., 137, A1364.

Flannery, M.R., and Opic, U., (1965). Proc. Phys. Soc. (Lon), 86, 491.

Franck, J., (1925). Trans. Faraday Soc., 21, 536.

Frost, D.C., McDowell, C.A., and Vroom, D.A., (1965). Phys. Rev. Letts., 15, 612.

Frost, D.C., McDowell, C.A., and Vroom, D.A., (1967a). Proc. Phys. Soc. (Lon), A296, 566.

Frost, D.C., McDowell, C.A., and Vroom, D.A., (1967b). J. Chem. Phys., 46, 4255.

Gardner, J.L., (1969). Private Communication.

Garton, W.R.S., (1950). Nature, 165, 322.

Garton, W.R.S., Parkison, W.H., and Reeves, E.M., (1964). Astrophys. J., 140, 1269.

Garton, W.R.S., Connerade, J.P., Mansfield, M.W.D., and Wheaton, J.E.G., (1969). Applied Optics, 8, 919.

Gilmore, F.R., (1965). J.Q.S.R.T., 5, 369.

Goodrich, G.W., and Wiley, W.C., (1961). Rev. Sci. Inst., 32, 846.

Goodrich, G.W., and Wiley, W.C., (1962). Rev. Sci. Inst., 33, 761.

Gordon, W., (1929). Ann. Phys. (Paris), 5, 1051.

Halmann, M., and Laulicht, I.J., (1968). J. Chem. Phys., 43, 438.

Hartree, J.B., (1957). "The Calculation of Atomic Structures", (New York: Wiley).

Henning, H.J., (1932). Ann. Phys., 13, 599.

Herzberg, G., (1950). "Molecular Spectra and Molecular Structure. I. Spectra of Diatomic Molecules", (New York: Van Nostrand).

Hinteregger, H.E., Hall, L.A., and Schmidtke, G., (1964). Space Research, V, 1175.

Huber, K.P., (1961). Helv. Phys. Acta., 34, 929.

Huber, K.P., (1968). Can. J. Phys., 46, 1691.

Huffman, R.E., Tanaka, Y., and Larrabee, J.E., (1963a). J. Chem. Phys., 39, 902.

Huffman, R.E., Tanaka, Y., and Larrabee, J.E., (1963b). Appl. Optics, 2, 947.

Huffman, R.E., Larrabee, J.E., and Tanaka, Y., (1964). J. Chem. Phys., 40, 356.

Hurzeler, I., and Morrison, J.D., (1957). J. Chem. Phys., 27, 313.

Judge, D.L., Morse, A.L., and Weissler, G.L., (1963). "Sixth International Conference on Ionization Phenomena in Gases", 3, 373.

Judge, D.L., and Weissler, G.L., (1965). Tech. Report USC-VacUV-105, Dept. of Physics, University of Southern California.

Judge, D.L., and Weissler, G.L., (1968). J. Chem. Phys., 48, 4590.

Kramers, H.A., (1923). Phil. Mag., 46, 836.

Kronig, R de L., (1928). Z. Physik, 50, 347.

Learner, R.C.M., (1962). Proc. Roy. Soc. (Lon), A269, 311.

Lefebre-Brion, H., and Moser, C., (1966). J. Chem. Phys., 44, 2951.

Lempka, H.J., and Price, W.C., (1968a). J. Chem. Phys., 48, 1875.

Lempka, H.J., Passmore, T.R., and Price, W.C., (1968b). Proc. Roy. Soc., A304, 53.

Lindholme, E., (1954a). Arkiv Fysik, 8, 433.

Lindholme, E., (1954b). Z. Naturforsch, 9a, 535.

Madden, R.P., and Codling, K., (1963). Phys. Rev. Letts., 10, 516.

Marr, G.V., (1967). "Photoionization Processes in Gases", (New York: Academic Press).

Matsunaga, F.M., and Watanabe, K., (1967). Sci. of Light, 16, 31.

Metzger, P.H., and Cook, G.R., (1965). J. Opt. Soc. Am., 55, 516.

Morrison, J.D., (1962). Institut International de Chemie, Douziemi Conseil de Chemie, Universite Libre de Bruzelles, p.397.

Morse, P.M., (1929). Phys. Rev., 34, 57.

McGuire, E.J., (1965). Tech. Rep. No. 6. ARO(D), Physics Dept., Cornell University.

Natalis, P., Collin, J.E., and Momigny, J., (1968). J. Mass Spectr. and Ion Phys., 1, 327.

Natalis, P., and Collin, J.E., (1969). J. Mass Spectr. and Ion Phys., 2, 221.

Nicholls, R.W., (1968). J. Phys. B. (Proc. Phys. Soc.), 1, 1192.

Nicolet, M., (1965). J. Geophys. Res., 70, 679, 691.

Ogawa, M., and Tanaka, Y., (1962). Can. J. Phys., 40, 1593.

Ogawa, M., (1964). Can. J. Phys., 42, 1087.

Peach, G., (1962). Monthly Notices Roy. Astron. Soc., 124, 371.

Pekeris, C.C., (1934). Phys. Rev., 45, 98.

Price, W.C., and Collins, C., (1935). Phys. Rev., 48, 714.

Price, W.C., (1968). Molecular Spectroscopy, Inst. of Petroleum, 4, 221.

Radwan, T.N., and Turner, D.W., (1966). J. Chem. Soc., p.85.

Samson, J.A.R., (1963). Phys. Rev., 132, 2122.

Samson, J.A.R., (1964a). J. Opt. Soc. Am., 54, 6.

Samson, J.A.R., (1964b). J. Opt. Soc. Am., 54, 420.

Samson, J.A.R., and Cairns, R.B., (1964c). J. Geophys. Res., 69, 4583.

Samson, J.A.R., (1966a). "Advances in Atomic and Molecular Physics", 2, 178, Ed. D.R. Bates.

Samson, J.A.R., (1966b). J. Opt. Soc. Am., 56, 552.

Samson, J.A.R., (1967). Appl. Optics, 6, 403.

Samson, J.A.R., (1968a). Phys. Lett., A28, 391.

Samson, J.A.R., and Cairns, R.B., (1968b). Phys. Rev., 173, 80.

Samson, J.A.R., (1969). Rev. Sci. Instr., 40, 1174.

Schiff, L.I., (1955). "Quantum Mechanics". (McGraw-Hill: London).

Schoen, R.I., (1964). J. Chem. Phys., 40, 1830.

Schoen, R.I., (1965). 13th ASTM Meeting, St. Louis.

Schoen, R.I., (1968). In "Symposium on Laboratory Measurements of Aeronomic Interest", IAGA, York University.

Selvyn, E.W.H., (1929). Proc. Phys. Soc. (Lon), A41, 392.

Sharma, A., (1967). J.Q.R.S.T., 7, 289.

Shimizu, M., (1960). J. Phys. Soc. Japan, 15, 1440.

Simson, J.A., Mielczarek, S.R., and Cooper, J.W., (1964). J. Opt. Soc. Am., 54, 269.

Sjogren, H., and Szabo, I., (1968). Arkiv Fysik, 37, 551.

Slater, J.C., (1960). "Quantum Theory of Atomic Structures", Vols. I & II. (New York: McGraw-Hill).

Sommerfeld, A., (1930). "Wave Mechanics", (London: Methuen).

Spohr, R., and Puttkamer, E., (1967). Z. Naturforsch, A22, 705.

Stewart, A.L., (1954). Proc. Phys. Soc. (Lon), A67, 917.

Stewart, A.L., (1967). "Advances in Atomic and Molecular Physics", 3, 1. Ed. D.R. Bates.

Takamine, T., Tanaka, Y., and Iwata, M., (1943). Sci. Papers Inst. Phys. Chem. Res. (Tokyo), 40, 371.

Tanaka, Y., (1942). Sci. Papers Inst. Phys. Chem. Res. (Tokyo), 39, 456.

Tanaka, Y., Jursa, A.S., and LeBlanc, F.J., (1958). J. Chem. Phys. 28, 350.

Tanaka, Y., and Ogawa, M., (1962). Can. J. Phys., 40, 879.

Tuckwell, H., (1969). M.Sc. Thesis, University of Adelaide.

Turner, D.W., and Al-Joboury, M.I., (1962). J. Chem. Phys., 37, 3007.

Turner, D.W., and May, D.P., (1966). J. Chem. Phys., 45, 471.

Turner, D.W., and May, D.P., (1967). J. Chem. Phys., 46, 1156.

Turner, D.W., (1968a). Molecular Spectroscopy, Inst. of Petroleum, 4, 209.

Turner, D.W., (1968b). Proc. Roy. Soc., A307, 15.

Vilesov, F.I., Kurbatov, B.L., and Terenin, A.N., (1961). Sov. Phys. (Doklady), 6, 490.

Vilesov, F.I., Akopyan, M.E., Lopatin, S.N., and Kleymenov, V.I., (1967). 5th Int. Conf. on the Phys. of Electronic and Atomic Collisions. Leningrad.

Villarejo, D., (1968). J. Chem. Phys., 48, 4014.

Vroom, D.A., (1966). Ph.D. Thesis, University of British Columbia, Vancouver.

Wacks, M.E., (1964). J. Chem. Phys., 41, 930.

Wainfain, N., Walker, W.C., and Weissler, G.L., (1955). Phys. Rev., 99, 542.

Watanabe, K., Matsunaga, F.M., and Sakai, H., (1967). Applied Optics, 6, 391.

Weinbaum, S., (1933). J. Chem. Phys., 1, 593.

Weissler, G.L., (1956). Handbuck der Physik, 21, Ed. S. Flugge, (Berlin: Springer-Verlag).

Weissler, G.L., Samson, J.A.R., Ogawa, M., and Cook, G.R., (1959). J. Opt. Soc. Am., 49, 338.

Worley, R.E., (1953). Phys. Rev., 89, 863.

Zare, R.N., and Cashion, J.K., (1963). U.C.R.L. Report No. 10881.

* J.Q.S.R.T. - Journal of Quantitative Spectroscopy and Radiative Transfer.